Terms and Conditions of Use of Digitised Theses from Trinity College Library Dublin

Copyright statement

All material supplied by Trinity College Library is protected by copyright (under the Copyright and Related Rights Act, 2000 as amended) and other relevant Intellectual Property Rights. By accessing and using a Digitised Thesis from Trinity College Library you acknowledge that all Intellectual Property Rights in any Works supplied are the sole and exclusive property of the copyright and/or other IPR holder. Specific copyright holders may not be explicitly identified. Use of materials from other sources within a thesis should not be construed as a claim over them.

A non-exclusive, non-transferable licence is hereby granted to those using or reproducing, in whole or in part, the material for valid purposes, providing the copyright owners are acknowledged using the normal conventions. Where specific permission to use material is required, this is identified and such permission must be sought from the copyright holder or agency cited.

Liability statement

By using a Digitised Thesis, I accept that Trinity College Dublin bears no legal responsibility for the accuracy, legality or comprehensiveness of materials contained within the thesis, and that Trinity College Dublin accepts no liability for indirect, consequential, or incidental, damages or losses arising from use of the thesis for whatever reason. Information located in a thesis may be subject to specific use constraints, details of which may not be explicitly described. It is the responsibility of potential and actual users to be aware of such constraints and to abide by them. By making use of material from a digitised thesis, you accept these copyright and disclaimer provisions. Where it is brought to the attention of Trinity College Library that there may be a breach of copyright or other restraint, it is the policy to withdraw or take down access to a thesis while the issue is being resolved.

Access Agreement

By using a Digitised Thesis from Trinity College Library you are bound by the following Terms & Conditions. Please read them carefully.

I have read and I understand the following statement: All material supplied via a Digitised Thesis from Trinity College Library is protected by copyright and other intellectual property rights, and duplication or sale of all or part of any of a thesis is not permitted, except that material may be duplicated by you for your research use or for educational purposes in electronic or print form providing the copyright owners are acknowledged using the normal conventions. You must obtain permission for any other use. Electronic or print copies may not be offered, whether for sale or otherwise to anyone. This copy has been supplied on the understanding that it is copyright material and that no quotation from the thesis may be published without proper acknowledgement.

A study on novel pyrazine-substituted dithiolene complexes as synthetic models for molybdenum cofactor and facile molybdenum mediated unexpected formation of pentathiepins

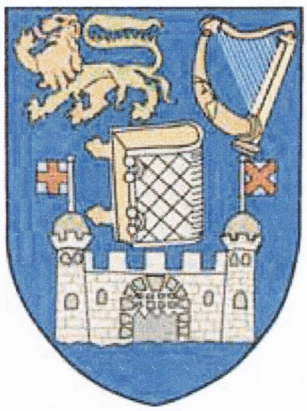

A thesis submitted to the School of Chemistry for award of PhD by

Muhammad Zubair

Under the supervision of

Prof. Carola Schulzke and Prof. Robert Baker

December 2014

Trinity College, University of Dublin

Declaration

I declare that this report details entirely my own work. Due acknowledgements and references are given to the work of others where appropriate.

I agree to deposit this thesis in the University's open access institutional repository or allow the library to do so on my behalf, subject to Irish Copyright Legislation and Trinity College Library conditions of use and acknowledgement.

Signed: _____ Date: 10/02/15

Muhammad Zubair

Acknowledgements

First and foremost, I would like to express my deep and sincere appreciation to my research supervisor: Prof. Carola Schulzke. I consider it a great privilege to have been her student, and I would like to take this opportunity to offer my deepest gratitude for everything she has done for me. I am also deeply grateful to Prof. Robert Baker for his quick and kind guidance and support whenever I needed, more especially for accepting me in his group after Carola move to University of Greifswald. I would like to thank both of them for their endless enthusiasm and knowledge, expert supervision and valued friendship which made this one of the most enjoyable period of my life so far. I wish both of them all the best in the coming year.

I would like to acknowledge COST Action CM1003 funding for STSMs at University of Nottingham. A massive thanks go to Prof. Jonathan McMaster and Dr. Stephen E. Davies for supervising me with spectroelectrochemical studies at University of Nottingham. I wish to say thank to Martin for helping me with the mass spectrometric studies as well as Manuel and John for helping me in NMR spectroscopic studies. Thanking you to Gunther and Alex in helping me to set up the lab in very start. During the period I spent doing this work I have been given opportunity to work with the best colleagues and academic staff at Trinity College as well as University of Greifswald, which makes me feel very lucky and I wish the best of luck to all of these guys in the future career.

I wish to say special and massive thanks to my loved ones mother (Zarina), father (Naseem), sister (Hina) and brothers (Waseem and Umair) in Pakistan for their care for, support and encouragement for my study as I learn how much I love them during my study being far away from them. Sincere and special thanks go to my lovely wife, her continuous support at every stage of life and understanding for what I am doing and what I want to do. I believe that it would have been impossible for me to accomplish my degree without her support, encouragement, and patience, more specially for her unconditional love to me. Also to my lovely piece of my hearts, Siraj and Zain as well as sweet darling Simrah.

Abstract

In the present study, pyrazine (**3** and **12**) and quinoxaline (**4** and **9-11**) based compounds were synthesised as precursors for the synthetic analogues of MPT in MoCo. During the attempts to synthesise target model complexes, an unexpected formation of quinoxaline-derived pentathiepin (**15**) was observed. This by chance invented method for preparation of pentathiepin was optimised and then used to synthesise a series of other pentathiepin derivatives **(16-18)**. Further on, a study has been made with regard to evaluate the influence of different substituents on the biological properties of these compounds. All pentathiepin derivatives (**15-18**) exhibited promising DNA binding properties as a minor groove binding agents and remarkable therapeutic activities.

Further studies were continued at designing the synthetic models of MoCo using dithiolene as scaffold. Towards this, a novel ligand, pyrazine-substituted dithiolene-2-one (**22**), was developed which was used to synthesise its corresponding molybdenum (**23**) and tungsten (**24**) complexes. The spectroelectrochemical properties of molybdenum complex **23** showed a one electron, reversible reduction couple (Mo^{V}-Mo^{IV}) with no structural changes associated with oxidation and reduction processes. EPR spectroscopic and assimilation data concluded that an unpaired electron coupled to the molybdenum nucleus Mo^{V} with no resolvable hyperfine coupling to sulfur. Moreover, attempts were made at exploring and exploiting closed and open alcohol form ligands and their respective molybdenum complexes which resulted in the successful formation of the target open alcohol form molybdenum complex **33**.

Finally, the air stable methoxyphenyl (**37**) and pyrazine (**38**) dithiolene CpCo complexes were synthesised and spectroelectrochemically characterised. The obtained data confirmed a fully reversible, one electron, redox couple for Co^{III}–Co^{II} with no intermediate states involved in both complexes. The CV study on complex **38** in the presence of acid demonstrated a possible electronic effect which communicated from the pyrazine to cobaltadithiolene moiety upon protonation. EPR spectroscopic data for Co^{II} state of both complexes are in consistent with the

presence of unpaired electron which is coupled to the Co (7/2) nucleus. However, reproduction of all the features in the experimental spectra of both complexes require assimilation. The structures of the synthesised all organic compounds and the metal complex were established using spectroscopic techniques (IR, ^{1}H and ^{13}C-NMR, HRMS), as well as X-ray crystallography (where possible).

List of Abbreviations

Å	Angstrom
AIBN	Azobisisobutyronitrile
ACCN	1,1'-Azobis(cyclohexanecarbonitrile)
br	Broad
bdt	Benzene dithiolate
cdt	4-Chromaonone dithiolene
Cp	Cyclopentadienyl
CV	Cyclic voltammetry
d	Doublet
DCM	Dichloromethane
DEE	Diethyl ether
DMSO	Dimethylsulfoxide
DMF	Dimethylformamide
EPR	Electron paramagnetic resonanace
fdt	Flavano-ene dithiolate
hr(s)	Hour(s)
Hz	Hertz
HRMS	High resolution mass spectrometry
IR	Infra Red Spectroscopy
J	Coupling constant
M	Molar
m	Multiplet
m	Meta
min (s)	Minute(s)
mmol	Millimole
MoCo	Molybdenum cofactor
MPT	Molybdopterin
M.P.	Melting point
NMR	Nuclear Magnetic Resonance
o	Ortho
OAT	Oxygen atom transfer

p	Para
PCET	Proton coupled electron transfer
PHT	pyrrolidone hydrotribromide
ppm	Parts per million
pzdt	Pyrazine dithiolate
q	Quartet
s	Singlet
sdt	Phenyl dithiolate
t	Triplet
THF	Tetrahydrofuran
δ	Chemical shift
2-pedt	2-Pyridine dithiolate
3-pedt	3-Pyridine dithiolate
4-pedt	4-Pyridine dithiolate

Chapter 1

Introduction

1.1 Introduction to dithiolene chemistry

Interest in the chemistry of transition metal dithiolene complexes has remained continuously active since its inception in the early 1960's and continues to grow as a significant part of the inorganic chemistry literature.[1,2,3,4,5] The main focus of this introduction is as follows: a) to highlight some interesting properties of transition metal dithiolene complexes; b) to emphasise the significance of dithiolene binding in naturally occurring molybdenum enzymes and c) to underline the background of the work presented in this thesis. Dithiolenes represent a ligand family, in which the donor atoms are sulfur atoms and which can form stable conjugated five membered chelate rings. The dithiolene structural motif consists of two sulfur atoms linked by an ethylene moiety, to which substituents R and R' are attached (alkyl or aryl groups) as shown in Figure 1.1.

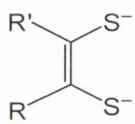

Figure 1.1: Structural representation of the dithiolene motif.

The area of metal related dithiolene chemistry has received increasing attention after pioneering work by the research groups of Gray and Schrauzer.[6,7] Most of the early work is based on exploring the key features of dithiolenes such as geometry, unique electronic structure and versatile redox activity. A dithiolene ligand is considered to be present in one of three possible forms **1A**, **1B** and **1C** (Figure 1.2). These forms include: (i) an ene-1,2-dithiolate form (**1A**), in which two dithiolate sulfurs are bonded to a carbon of an olefinic linkage, to which substituents R and R' are attached; (ii) the oxidation of form **1A** gives rise to form **1C** by a two electron redox process *i.e.* a neutral dithioketone or dithione (**1C**); (iii) the intermediate form **1B**, which is believed to facilitate the conversion of ene-1,2-dithiolate to dithioketone through a monoanionic singly oxidised state (Figure 1.2). Consequently, due to different potential bonding characteristics of the dithiolene ligand around a redox active central metal atom or ion, it is difficult to define the exact electronic nature of the dithiolene complex. Thus, a

dithiolene ligand may be present in a complex in any of these possible forms. As a result of this redox versatility, the oxidation state of a dithiolene ligand in a complex is ambiguous.[8] Because of this uncertainty in the nature of dithiolene ligands in their complexes, these ligands are termed as 'non innocent' and the description 'dithiolene' is generally useful as it avoids the need to specify the ligand as being present in a particular form.

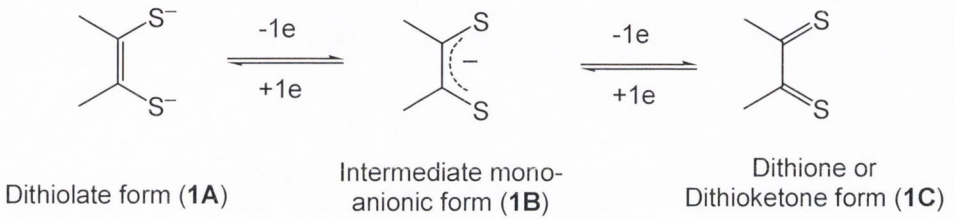

Figure 1.2: Redox related forms of dithiolene ligands, two electrons oxidation of the ene-1,2-dithiolate lead to the oxidised form, *i.e.* a 1,2-dithione.

In 1963, Davison *et al.*[9] explored the specific redox properties of dithiolene complexes after discovering the two electron difference between the neutral complex $[Ni(S_2C_2Ph_2)_2]$ (Figure 1.3 **2A**) of Schrauzer *et al.*[6] and the dianionic species $[Ni(S_2C_2(CN)_2)_2]^{2-}$ (Figure 1.3 **2B**) of Gray *et al.*[7] He demonstrated that it should be possible to reduce the neutral complex **2A** to a dianionic complex or to oxidise the dianionic complex **2B** to the neutral complex. In both cases, conversion from neutral to dianionic or dianionic to neutral may be facilitated through a monoanionic intermediate state.

2A **2B**

Figure 1.3: Structures of neutral $[Ni(S_2C_2Ph_2)_2]$ (**2A**) and the dianionic $[Ni(S_2C_2(CN)_2)_2]^{2-}$ (**2B**) dithiolene based nickel complexes.[9]

This was the first study which suggested that dithiolene ligands can have different potential binding characteristics such as neutral dithioketone or more commonly dianionic dithiolate.

In general, it has been found that different forms of dithiolene ligands have been shown to influence the oxidation state of the metal for a given metal-ligand stiochiometry.[8,9] Therefore, the actual electronic structure of a *bis*-dithiolene complex will be a resonance hybrid and its redox chemistry will consist of a metal-dithiolene system which involves extensive delocalisation, that resulted in extensive electrochemical investigations of such complexes.[4,9,10] Because of this redox chemistry, the oxidation states of the dithiolene ligand and the metal in a complex may be difficult to specify. For example, the nickel atom in dithiolene complex $[Ni(S_2C_2H_2)_2]$ can be considered to be in the formal oxidation states of Ni^0, Ni^{II} or Ni^{IV}, involving the different electronic forms of the metalladithiolene ring system as shown in Figure 1.4.[10]

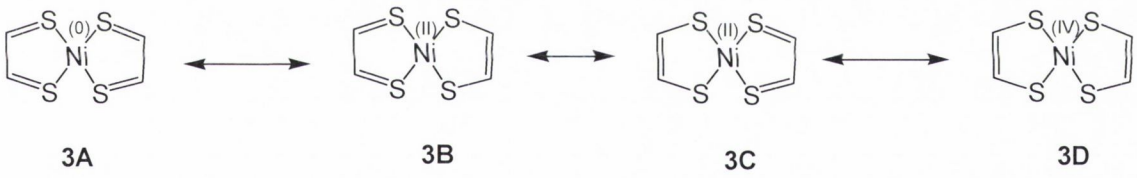

Figure 1.4: Possible oxidation states of the nickel in $[Ni(S_2C_2H_2)_2]$.[10]

In order to understand the electronic structure of dithiolene based metal complexes, Schrauzer *et al.*[11] performed molecular orbital calculations for the $[Ni(S_2C_2H_2)_2]$ complex. He concluded that the ground state of this complex involves extensive π-electron delocalisation. Molecular orbital investigations for metal *bis*-dithiolene complexes were carried out by Alvarez *et al.*[12] They proposed a molecular orbital scheme for the π-electron system of a dithiolene group based on that of 1,3-butadiene as shown in Figure 1.5.

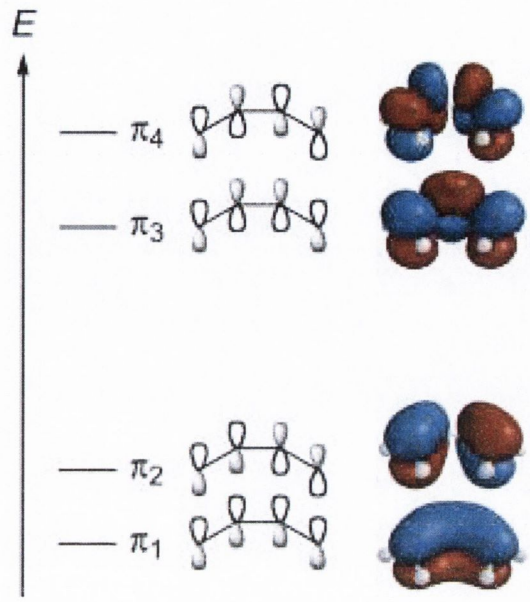

Figure 1.5: Molecular orbital scheme for the π-electron system of a dithiolene corresponding to that of 1,3-butadiene.[12]

This molecular orbital scheme provides a clear basis to understand the electronic structure of the π-electron system of a dithiolene. As described earlier there are two extreme redox states of dithiolenes (Figure 1.2), an ene-1,2-dithiolate (**1A**) bearing six π-electrons, suggesting $(\pi_1)^2$ $(\pi_2)^2$ $(\pi_3)^2$ electronic configuration; and a 1,2-dithioketone (**1C**) state bearing four π-electrons, having $(\pi_1)^2$ $(\pi_2)^2$ electronic configuration. The latter description is in agreement with the valence bond description of a 1,2-dithioketone, involving two electrons in a π-orbital that is the C-C bonding and C-S bonding and two electrons in a π-orbital that is C-C anti-bonding and C-S bonding. In order to form an ene-1,2-dithiolate, two electrons will be added to π_3, which results in a strengthening of the C-C bond and the weakening of the C-S bond, *i.e.* π_3 is C-C bonding and C-S anti-bonding. This agreement between the valence bond and orbital description of the electronic structure of the two extreme forms of a dithiolene is encouraging and highlights the significance of the π-system in the nature and properties of dithiolene complexes.

IR spectral data can provide useful information to predict the various oxidation states of dithiolene ligand in metalladithiolene. A number of studies summarised a key trend in vibrational mode of metalladithiolenes; where υ(C=C) showed a systematic increase and υ(C-S) showed a decrease in frequencies, respectively, from neutral to dianionic states.[13] This general trend in dithiolene ligands suggested the more prevalence of dithiolate (Figure 1.2 **1A**) character upon reduction of metalladithiolene complexes. Moreover, the vibrational frequencies for dithiolate form are markedly different from the vibrations of dithioketone (Figure 1.2 **1C**) due to very little coupling of its vibrational frequencies.[13,14]

Furthermore, in order to confirm electronic structure of a dithiolene metal complex, X-ray structure analysis data also offers practical information. In this respect, it is important to know the bond lengths of the complex as well as its geometry. Therefore, it has been observed that the intra-ligand bond lengths should vary in accordance with the 'oxidation level' of the ligand. These differences in bond lengths may be used as important characteristic for the electronic configuration of dithiolene complexes.[13,15] For example, short C-S distances as low as ~1.64 Å are more characteristics of dithione binding (Figure 1.4 **3A**) whereas, long C-S distances of ~1.77 Å are typical of ligand binding in dithiolate form (Figure 1.4 **3D**). In combination with these determined bond lengths and IR data, the oxidation state of dithiolenes may better be described as present in dithiolate or dithioketone forms where the electron density is distributed over the five ring atoms including the chelated metal.

1.2 Transition metal dithiolene complexes

Transition metal dithiolene complexes have been studied for years as a result of their structural diversity, spectroscopic properties, stability and redox active chemistry.[2,4,15] The dithiolene ligands can bind easily to various metals such as tungsten (W),[4] nickel (Ni),[16] molybdenum (Mo)[17], cobalt (Co)[18] and platinum (Pt)[19], to form their respective metal complexes. Dithiolene based transition metal complexes have been employed for a wide variety of applications, such as opto-electronic devices,[20] building block

materials,[21] dye sensitizers for solar cells,[22] and photocatalysts for water splitting.[23,24] Moreover, transition metal dithiolene complexes containing one or two dithiolene ligands are of special interest because of their versatile redox behaviour as well as their vital role in the majority of living systems. They have been found as an active part of the molybdenum and tungsten cofactors, in which a dithiolene moiety coordinates the metal at the catalytic centre of molybdenum and tungsten oxotransferases. These interesting catalytic activities associated with dithiolene complexes may be due to the presence of its non-innocent character, which is a direct result of a dithiolene's ability to exist as an 1,2-ene-dithiolate, a radical anion or a 1,2-dithioketone (as described in Figure 1.2).[8] A dithiolene ligand binds to a metal through two sulfur atoms and forms a five membered MS_2C_2 chelate ring as shown in Figure 1.6.

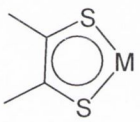

Figure 1.6: Structural representation of the aromatic character in the metalladithiolene ring system.

The aromatic character of the metalladithiolene ring permits substitution reactions that have been observed in conjugated metalladithiolenes.[25]. The molecular geometry of a dithiolene complex depends on the variation and number of bidentate ligands attached to the metal centre. Therefore, the bidentate dithiolene ligand can form *mono*-, *bis*- or *tris*-(1,2-dithiolenes) metal complexes, however, *bis*-dithiolene complexes are quite common. Figure 1.7, for example, shows the homoleptic dithiolene complex *bis*-1,2-diphenyl-1,2-dithiolene nickel(II) (**4A**) complex.[6] Synthesis of this complex was facilitated by the reaction of nickel tetra sulfide (NiS_4) with diphenylacetylene and observed to have square planar geometry. On the other hand, *tris*-dithiolene complexes are unusual, and they have been found to be in a trigonal prismatic geometry. Two examples of homoleptic *tris*-dithiolene complexes are $[Mo(S_2C_2H_2)_3]$ (**4B**) and $[V(S_2C_2Ph_2)_3]$ (**4C**) as shown in Figure 1.7, respectively. These complexes were synthesised from the reaction of metal halides with dithiolates.[26]

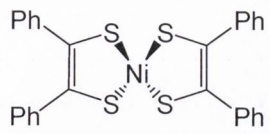

$[Ni(S_2C_2Ph_2)_2]$ (**4A**)

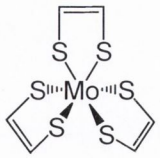

$[Mo(S_2C_2H_2)_3]$ (**4B**)

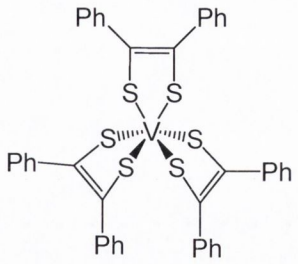

$[V(S_2C_2Ph_2)_3]$ (**4C**)

Figure 1.7: Examples of structurally characterised *bis*-dithiolene (**4A**) and *tris*-dithiolene complexes (**4B** and **4C**).[6,26]

1.3 Dithiolenes in nature

In 1980, it was discovered that some metalloenzymes contain a dithiolene group. These enzymes are prevalent throughout biology where the metals molybdenum or tungsten are chelated by said dithiolene ligands. There are over 50 distinct molybdenum dithiolene enzymes known today, that occur in all classes of living systems and play vital roles in the biochemical cycles of nitrogen and sulfur.[1]

1.3.1 Introduction to molybdenum and tungsten

From early on, the molybdenum and tungsten metals were known to the ancients.[1] In non-living nature, molybdenum is found in the form of its disulfide MoS_2, molybdenite, while the tungsten is mostly found as $CaWO_4$ and $PbWO_4$.[27] The technical use of the former in lubricating materials has grown since the beginning of the 20th century. Both metals have shown nearly equal affinity for hard donor oxo as well as soft donor sulfido ligands due to the availability of various oxidation states with the possibility of different coordination numbers. The current interest in molybdenum (4d) and tungsten (5d), has increased because of their presence in biological systems.[28] Both metals have been found to play an important role as biocatalysts in combination with molybdopterin (MPT, Figure 1.10 **5D**) in several enzymatic reactions. At least one of both metals has

been found in almost all organisms such as bacteria, plants, animals and humans. Due to their chemically related properties, they are found in very similar enzymes, with the exception of nitrogenase, for which no analogue form of tungsten has yet been identified.[29]

1.3.2 Active site structures of molybdenum enzymes

In order to understand the enzymatic catalytic activities, efforts in determining the active site structures of molybdenum and tungsten dependent oxotransferases was initiated in 1982. Rajagopalan and co-workers demonstrated the presence of sulfur atoms in a specific ligand system which they called molybdopterin (MPT).[30,31] They successfully isolated and characterised the di(carboxamidomethyl) derivatives of MPT using fluorescence and mass spectrometry. On the basis of initial results, they first proposed the structure of the active site to have a pterin dithiolene chelation to the molybdenum (Figure 1.10 **5A**). The proposed structure **5A** consists of a bicyclic pterin ring, in which a pyrazine ring is a one side chain of the dithiolene group being coordinated to molybdenum and the other side chain consists of a hydroxyl and phosphate group. However, there is an unidentified group (X) at the second position of the dithiolene moiety. The refined model for the molybdenum cofactor was published in 1987 by the same authors (Figure 1.10 **5B**), they suggested that the molybdenum cofactor carries a alkylpterin with a 4-carbon side chain bearing an dithiolene on C-1 and C-4, a secondary alcohol on C-5 and a phosphorylated primary alcohol on C-6.[30] This proposed structure for the molybdenum cofactor was further supported by Chan *et al.*[31] They reported the crystal structure of an oxotransferase, the tungsten containing aldehyde ferredoxin oxidoreductase (Figure 1.10 **5C**) from *Pyrococcus furiosus*, a hyperthermophilic archaeon. The active site structure of this enzyme was observed to have a MPT that is bound to the metal through dithiolene sulfur atoms, exactly as proposed by the Rajagopalan group. The nature of MPT has been elucidated, through a series of biochemical and several crystallographic studies of these enzymes.[31,32] It was found that MPT itself cannot be studied directly due to its highly unstable nature once liberated from proteins.[1] On the basis of various studies, the commonly agreed chemical structure

of molybdopterin is shown in Figure 1.10 **5D**. In this structure, MPT is identified as a tricyclic pyranopterin, the pyran ring of which carries the dithiolene group and phosphate side chain. In all of the enzymes characterised so far, the dithiolene acts as a bidentate ligand to molybdenum or tungsten. The MPT may exist in either the mononucleotide form (where R = H), as found in many eukaryotic Mo-MPT enzymes, or as dinucleotide form (where R = adenine or cytosine), as found in prokaryotic Mo-MPT enzymes.

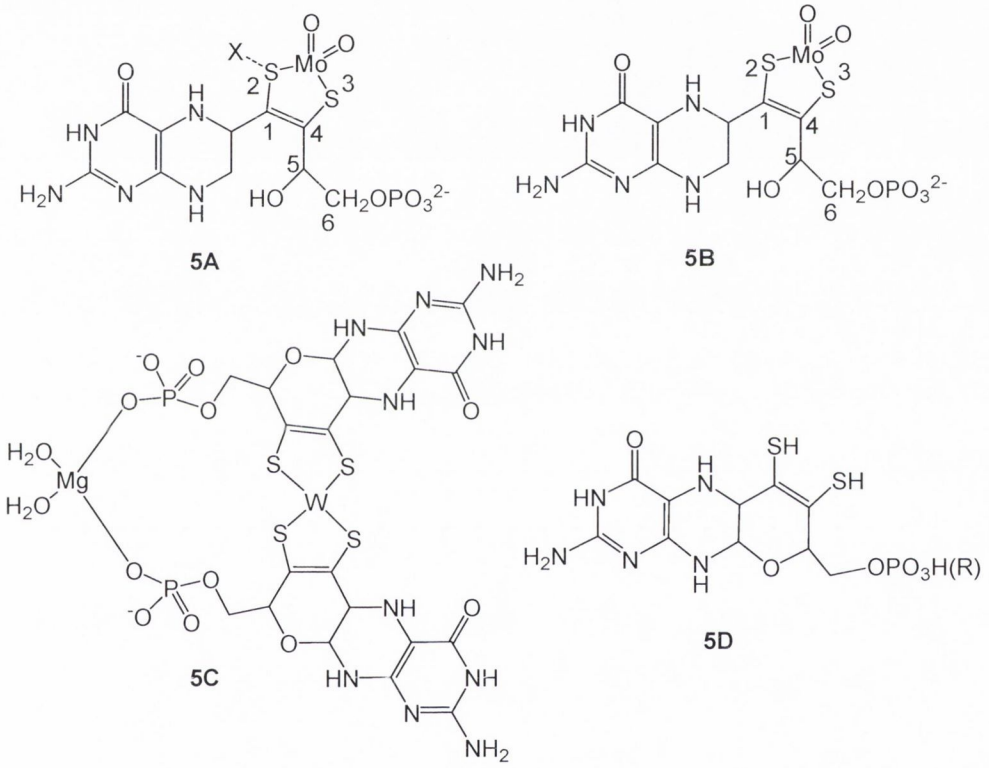

Figure 1.10: 5A) First proposed structure of the MoCo (molybdenum cofactor) active site by Rajagopalan and co-workers; (**5B**) the refined proposed structure of the active site by same authors; (**5C**) the structure of the tungsten containing aldehyde ferredoxin oxidoreductase reported by Chan *et al.*; (**5D**) the commonly agreed chemical structure of MPT.

Current interest in studying the molybdenum cofactor has increased after understanding that at least one, and often several, molybdenum enzymes are essential within every

living organism. Most importantly from a human perspective, these molybdoenzymes, such as sulfite oxidase, xanthine oxidase and aldehyde oxidase are essential for proper human health. In extreme cases, biosynthesis of functional molybdoenzymes is prevented in living systems due to genetic errors. This may result in the absence of the molybdenum cofactor and leads to the accumulation of toxic levels of sulfite which can cause a neurologic deterioration and early death (especially in infants).[33] No treatment for the deficiency of functional molybdoenzymes has been developed yet and research along this direction is still in progress. Due to the versatile functions of the molybdenum cofactor in humans, a large number of groups has conducted synthetic studies, in order to reproduce key spectroscopic, structural, and reactivity properties of the catalytic site of molybdenum enzymes compared to the available active site structures, despite some success the area still remains challenging and key questions remain:

- Can we design and develop exact synthetic models for the molybdenum cofactor active site of molybdenum oxidoreductases?
- Will these synthetic models be able to catalyse oxygen atom transfer reactions *i.e.* oxidation of sulfite to sulfate, in artificial or biologic conditions?

1.3.3 Catalytic activities of molybdenum enzymes

The catalytic activity of molybdenum and tungsten enzymes to promote oxygen atom transfer reactions is now well documented.[28,34,35] These active sites are found to be redox active between the oxidation states (IV) and (VI). In addition, the intermediate oxidation state (V) mediates the two proton coupled electron transfer (PCET) steps as part of the regeneration of these enzymes.[2] PCET describes a reaction in which there is a change in both electron and proton content between reactants and products, and which allows to build up multiple redox components. As a result, PCET is a keystone of many important biological energy conversion processes.[28] The majority of enzymes catalyse two electron redox reactions involving the transfer of an oxygen atom to a substrate X or from a substrate XO. For instance, molybdenum (with the exception of nitrogenase) and

tungsten enzymes catalyse reactions of the general type as shown in equation 1.

$$X + H_2O \longleftrightarrow XO + 2H^+ + 2e^- \quad (1)$$

Here, X and XO are termed as acceptor and donor molecules, respectively. In this type of reactions, water acts as a source of oxygen. Moreover, the difference of substrate and product (X and XO) is only one oxygen atom. Therefore, the process has been termed oxygen atom transfer reaction. All molybdenum and tungsten enzymes belong to this broad class with the only exception of nitrogenase. Table 1.1 shows a selection of substrate transformations by molybdenum and tungsten enzymes such as DMSO reductase which catalyses the reduction of DMSO to DMS, sulfite oxidase which catalyses the oxidation of sulfite to sulfate, xanthine oxidase which catalyses the oxidation of xanthine to uric acid, etc.[1,39] Generally, the enzymes are named according to the specific reactions which they catalyse, for instance sulfite oxidase, DMSO reductase.

Table 1.1: Some examples of molybdenum and tungsten enzyme catalysed reactions

Enzyme	Reaction
Aldehyde oxidoreductase	$RCHO + H_2O \rightleftharpoons RCO_2H + H^+ + 2e^-$
Arsenite oxidase	$H_2AsO_3^- + H_2O \rightleftharpoons HAsO_4^{2-} + 3H^+ + 2e^-$
Dimethyl sulfoxide reductase	$Me_2SO + 2H^+ + 2e^- \rightleftharpoons Me_2S + H_2O$
Nitrate reductase	$NO_3^- + 2H^+ + 2e^- \rightleftharpoons NO_2^- + H_2O$
Sulfite oxidase	$SO_3^{2-} + H_2O \rightleftharpoons SO_4^{2-} + 2H^+ + 2e^-$
Xanthine oxidase	$Xanthine + H_2O \rightleftharpoons Uric\ acid + 2H^+ + 2e^-$

Molybdenum enzymes have been well documented as a cycle between molybdenum(IV) and molybdenum(VI) states through an intermediate molybdenum(V) being part of the catalysis. During the catalytic activity, the molybdenum enzymes catalyse the oxidative oxygen atom transfer from water and/or its backward reaction as earlier described in equation 1.[13,28,36] This reaction utilises water as a source of oxygen, coupled with proton and electron transfer (PCET) to generate *bis*-oxomolybdenum(VI) centre which then gives one oxygen atom to the substrate, regenerating *mono*-oxomolybdenum(IV) centre. Scheme 1.1 illustrates how a combination of PCET and OAT describes catalytic reaction of arsenite oxidase (an oxidative class of molybdenum enzyme), yielding arsenate and the corresponding *mono*-oxomolybdenum(IV) centre.

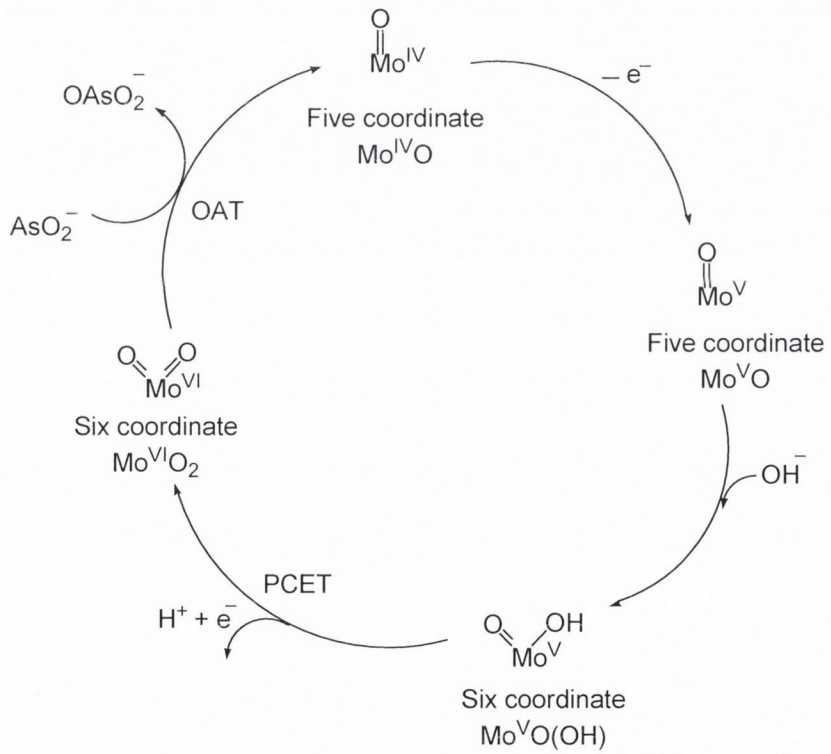

Scheme 1.1: The combination of PCET and OAT reactions in the active site of molybdenum enzymes, with the catalytic *bis*-oxomolybdenum(IV) and *mono*-oxomolybdenum(VI) couple[36]

1.3.4 Nature and classification of molybdenum and tungsten enzymes

Molybdenum and tungsten have always attracted bioinorganic chemists because of their presence in a large number of enzymes.[1,4] All of the molybdenum and tungsten enzymes are mononuclear and associated with MPT, with the exception of nitrogenase.[37] The name of MPT only refers to the tricyclic organic part and does not include coordinated molybdenum. Therefore, MPT may be associated with both molybdenum and tungsten enzymes. To avoid this potentially confusing name, different terms have been used throughout the literature such as pyranopterin-dithiolate, pterin-dithiolate, pterin-ene-dithiolate and in some cases tungstopterin when coordinated to tungsten.[38] However, the acronym MPT is still commonly used today. The number of coordinated MPT ligands can be one or two, depending on the type of enzymes. Hille has classified the molybdenum oxotransferases into different families, based on their chemical structures and reactivities.[39,40] This classification comprises the xanthine oxidase family, sulfite oxidase family and DMSO reductase family and is described as below;

- Members of the xanthine oxidase family have a single MPT coordinated to a $Mo^{VI}OX$ (H_2O) centre (X = S or O) with no bound amino acids.
- Members of the sulfite oxidase family involve one MPT bound to a $Mo^{VI}O_2$ centre and ligated by an additional S of a cysteinyl residue (S-cys).
- Members of the DMSO reductase family involve two MPTs coordinated to the molybdenum atom, bearing a terminal oxo group (Mo=O), and additional donor atom from the side chain of an amino acid residue such as S of cysteine (S-cys), O of serine (ser) or Se of selenocysteine (Se-cys).

All of the known tungsten oxotransferases were found to have two MPTs coordinated to the metal centre, *i.e.* they are most closely related to the DMSO reductase family. Each family is named after their best known member and the active site structures for each molybdenum family are presented in Figure 1.12.

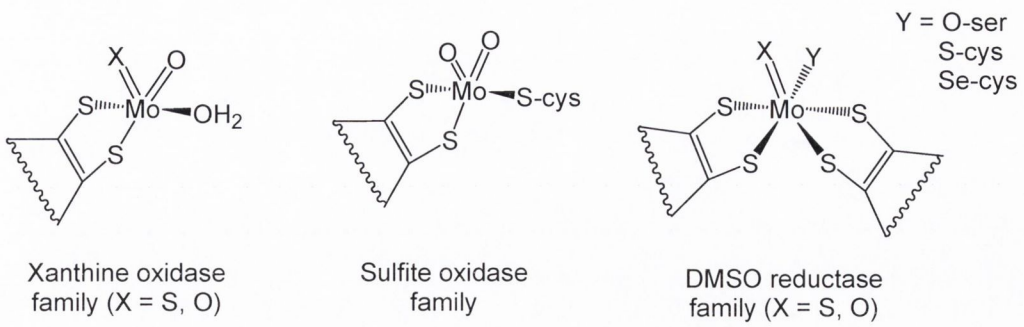

Figure 1.12: The structural classification of the catalytic centres of the molybdenum oxotransferases.[39,40]

1.3.5 Key roles of molybdopterin (MPT) in catalysis

The ubiquitous presence of MPT in all of the molybdenum and tungsten oxotransferases and the remarkable conservation of its nature suggest that this moiety must play an important role in the catalytic process.[5] It was suggested that the presence of the dithiolene in MPT could act as a route for electronic communication between the metal centre and other components of the pyranopterin ligand. The exact roles of MPT in molybdenum or tungsten oxotransferases is not yet understood; however, few possible roles for MPT in the catalysis of oxygen atom transfer have been suggested which include:[5]

- To allow electronic communication between the metal centre and other components of MPT.
- To provide a route for one or two electron transfer processes required to re-oxidise, or re-reduce, the metal centre back to the catalytically active state.

There are several other possible roles of MPT in the catalysis of oxygen atom transfer reactions, when considering the composition of MPT. Firstly, one contribution to this process could be the provision of basic sites to handle the protons that are an integral part of the regenerating oxidation or reduction processes.

Secondly, the pterin moiety is also considerable itself, since both pyrimidine and pyrazine rings, can serve to anchor MPT to the surrounding protein through a series of hydrogen bonds. In addition, the pterin part is redox active on its own and can exist in one of three oxidation levels. These three oxidation forms can be interconnected *via* two proton, two electron processes as shown in Figure 1.13.

(i) Fully oxidised form

(ii) Dihydro form (or semi-reduced state)

(iii) Tetrahydro form

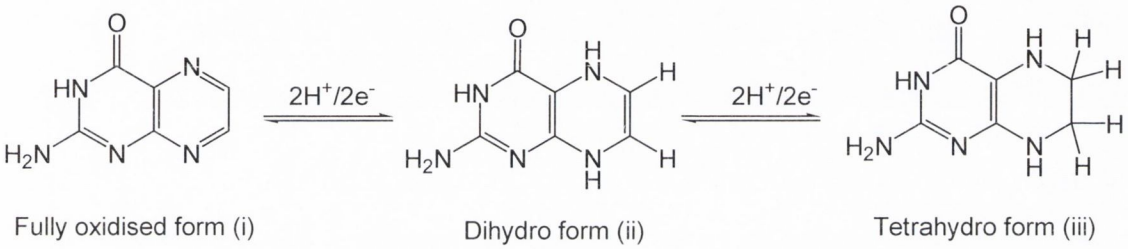

Figure 1.13: Different oxidation levels of a pyrazine ring as part of pterin.

Another interesting role MPT might play is to change the sterics of the active site *via* opening of the pyran ring being part of the catalytic process. The presence of an open alcohol and closed forms has been further supported by X-ray crystallographic study of the molybdenum enzyme, from *Escherichia coli* as described in Figure 1.14.[41]

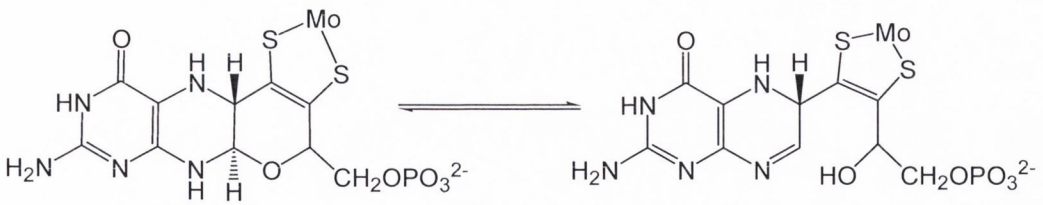

Figure 1.14: The interconversion of open and closed forms of MoCo.[41]

When the oxidation levels of the pyrazine and ring opening of the pyran ring are considered together, it becomes clear that the oxidation levels of the pyrazine ring determine a potential conjuction between the pyrazine ring and the metal centre. Studies

revealed that only when the pyrazine ring is in its dihydro or semi-reduced state, the pyran ring can open and lead to the conjuction between the pyrazine ring and the metal centre.[5] Here, a problem arises when considering the dihydro form of the pterin moiety to exist in three tautomeric forms (Figure 1.15). Which tautomeric form will be more favourable when considering the pyrazine ring promoted ring opening of the pyran ring?

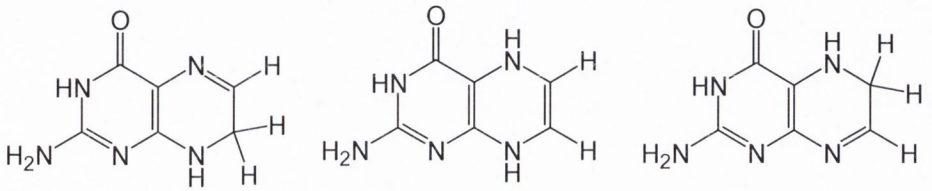

Figure 1.15: Different tautomeric forms of a pyrazine ring being part of pterin.

To shed light on this problem, Greatbanks *et al.*[42] carried out theoretical calculations and discovered that the 7,8-dihydro form of MPT is the most thermodynamically stable of all three tautomers. This form of MPT allows electronic communication between the pyrazine ring of MPT, the metal centre and the opening of the pyran ring. The presence of the 7,8-dihydro oxidation state of MPT was further supported by a crystal structure of an oxotransferases, where the pterin functionality in MPT is present in the dihydro state.[27]

The entire role of the pterin and pyran rings in the MPT structure has not been clarified yet even though its participation in fine tuning the redox nature of the active site is beyond doubt.[1,5] It has already mentioned earlier (Section 1.3.2) that the bicyclic MPT structure was originally proposed by Rajagopalan and the tricyclic form found in X-ray crystal structures of MPT in the following years where both forms were different only by two hydrogen atoms. In another study, the X-ray crystal structure of molybdenum cofactor showed the presence of two MPTs at the metal centre, one with a bicyclic open alcohol structure and the other with a tricyclic closed pyrane ring structure.[41] Therefore, it proposes the possibility of pyran ring opening and closing during the catalytic

turnover due to the redox activity of adjacent pterin moiety which is conjugated to the metal-dithiolene aromatic system. The pyrazine ring present in the tricyclic form of MPT is in its reduced tetrahydro form as supported by crystallographic structures, whereas the opening of the pyran ring may result in a dihydropyrazine structure and therefore the loss of two protons coupled to an oxidation of this ring. The reversal of this process is a two proton reduction (addition of protons) combined with the pyran ring closing and restoration of the reduced tetrahydro pyrazine. Therefore, it can be argued that MPT have a considerable role in handling the two protons which are involved in the catalytic PCET reaction. A simple proton catalysed process (Scheme 1.2) illustrating the ring opening and closing of the pyran ring in the MPT structure have been suggested by Enemark and Garner.[43]

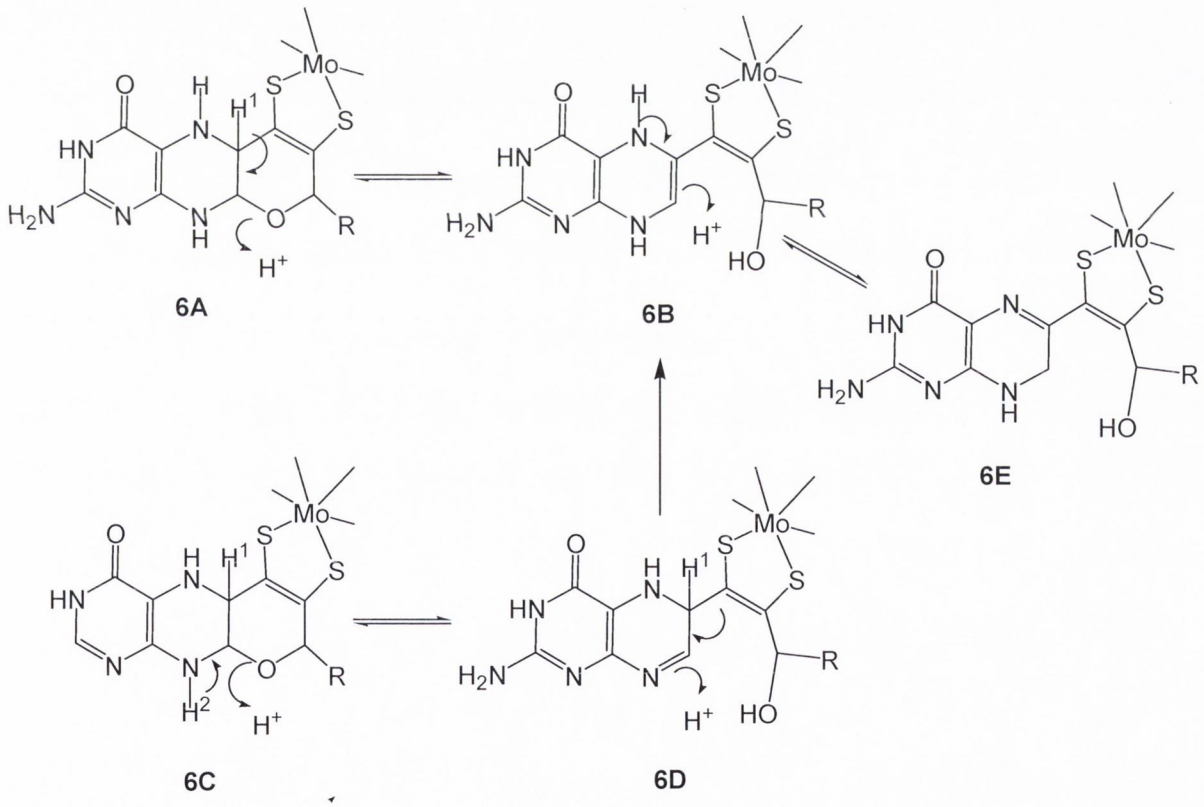

Scheme 1.2: The proposed mechanism for the proton catalysed scission/condensation of the pyran ring of MPT to produce dihydropterin.[43]

This proposed mechanism shows that the proton (H_1) of closed form **6A** may interact with MPT to facilitate the oxygen atom transfer and results in the formation of open alcohol form **6B**. Another possibility is that proton (H_2) of closed form **6C** may also initiate the oxygen atom transfer reaction to form open alcohol form **6D**. Similar to form **6A**, proton (H_1) of form **6D** can interact with MPT resulting in the formation of open alcohol form **6B**. As discussed earlier, the 6,7-dihydro open alcohol form **6B** is not thermodynamically stable, so then this form rearranges to a more stable 7,8-dihydro open alcohol form **6E**. Thus, this mechanism proposes that a proton is involved in the oxygen atom transfer reaction, as ring opening and closing may operate during enzymatic catalytic reactions. Moreover, it was also suggested that the presence of two dithiolene moieties is key to the somewhat unusual *mono*-oxo (Mo^{VI}) and *bis*-oxo (Mo^{IV}) units found in enzymes of the DMSO reductase family.[44,45] In enzymatic catalytic reaction, involvement of open alcohol and closed form due to scission and condensation reaction of pyran ring

1.4 Chemical analogues of catalytic centres of the molybdenum oxotransferases

In the last two decades, the area of molybdenum and tungsten dithiolene chemistry became well established as these compounds serve as model complexes for the molybdenum cofactor (MoCo). Synthesis, structural trends, electronic structure, spectroscopic properties and biological relevance of synthetic chemical analogues of the catalytic centres of MoCo have been systematically and extensively studied.[15] In addition to represent the development of new and interesting chemistry, these studies improved our current understanding to the role of molybdenum or tungsten that is attached to dithiolene moiety in the active sites of MoCo. The structure and reactivity of such synthetic analogues should be of considerable value in interpreting corresponding properties of enzyme active sites. Moreover, there are two general approaches developed so far, to investigate the role of MPT which may be described as follows:[1]

- Biomimetic; to synthesise chemical analogues, where the construction of the ligand system around the metal centre is as close as possible to the active site structures found in nature.
- Bioinspired; where the aim is to study the catalytic activity of synthetic analogues under ambient conditions.

According to the first approach, it is desired to synthesise structural models that should have a very similar donor atom environment around the metal centre compared to that of the active site of the native enzyme and be capable of reproducing general features of the metal coordination sphere in at least one stage of the catalytic cycle. Synthesis of such a model complex will provide useful information to establish key structural and spectroscopic characteristics of molybdenum and tungsten terminal oxo and sulfido complexes. In view of the existence of molybdenum and tungsten iso enzymes, a number of efforts have been made to explore tungsten dithiolene chemistry.[27,28,46,47] A typical example of this type of system is the oxidised xanthine oxidase analogue as shown in Figure 1.16.[48] Comparison of this synthetic analogue and oxidised protein site structures reveals near congruency and indicates that protein interaction does not cause significant perturbation in the coordination sphere of the metal centre.

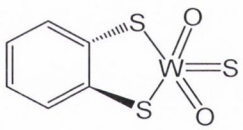

Figure 1.16: The oxidised xanthine oxidase structural analogue.[48]

In the second approach, the reactivity of the synthesised model analogues is studied. It is attempted to reproduce oxygen atom or H^+/e^- reactions of the catalytic centres, which should function in a similar manner as are observed in the native enzymes. In particular, interesting oxygen atom transfer reactions of synthesised molybdenum and tungsten dithiolene complexes have been studied extensively.[49,50] For example, Holm *et al.* synthesised a series of dithiolene complexes of the general type $[Mo(OR')(S_2C_2R_2)_2]^{1-}$ (where R' = Ph, 2-Ad, ^{i}Pr; R = Me or Ph). These complexes were characterised as

possible structural models of reduced sites of the DMSO reductase family.[50] In reactivity modelling studies, these complexes were treated with N or S-oxides, in order to study oxygen atom transfer reactions. Results obtained suggested that these complexes have direct oxygen atom transfer reaction ability (as described in Scheme 1.3). In the first step, these complexes reduce N or S-oxides by an associative transition state and, in the following step removal of an alcohol group as a side product take place due to an internal redox process. This interesting oxygen atom transfer reaction study is the first example of an analogue reaction system transforming biological S-oxide substrates.[50] Furthermore, a number of analogous tungsten complexes have been synthesised and studied for their oxygen atom transfer reactions ability.[51,52]

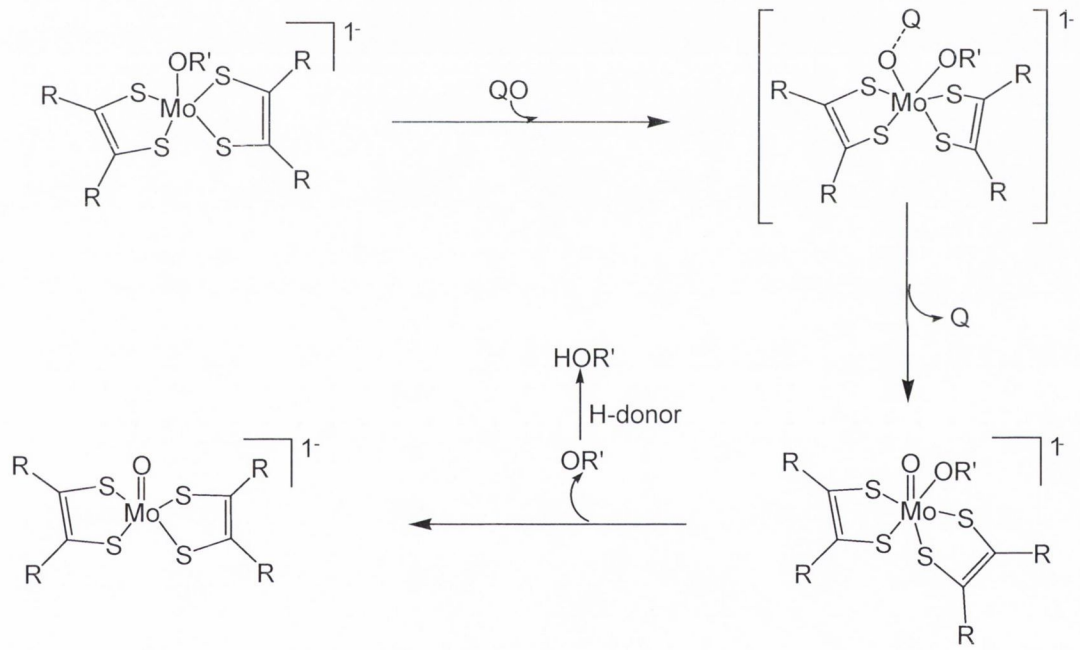

Scheme 1.3: Schematic representation of the oxo transfer reaction studies, employed with a series of dithiolene complexes of the general type $[Mo(OR')(S_2C_2R_2)_2]^{1-}$ (where R' = Ph, 2-Ad, ^{i}Pr; R = Me or Ph; QO = N or S-oxides).

In an effort to synthesise a chemical analogue of the molybdenum cofactor, Garner's group was the first to report the synthesis of a symmetrically substituted dithiolene metal complex *i.e.* $[MoO(bdt)_2]^{2-}$.[53] Following this, a number of groups utilised similar methodology to synthesise a number of symmetrical dithiolene derived ligands and their respective complexes such as $[MoO(bdt)]^{2-}$, $[MoO(bdt(Cl)_2)_2]^{2-}$, $[MoO(S_2C_2H_2)_2]^{2-}$,

$[MoO(S_2C_2(CN)_2)_2]^{2-}$, $[MoO(S_2C_2(Me)_2)_2]^{2-}$ and $[MoO(S_2C_2(Ph)_2)_2]^{2-}$ as shown in Figure 1.17.[54,55,56] Although synthetically easy to obtain, such symmetrical dithiolenes do not represent the natural MPT very well. In order to develop more accurate models of the natural cofactor, first of all the immediate coordination sphere of the central metal needs to be met; *i.e. mono*-oxo Mo(IV). Secondly the unsymmetric nature of MPT requires consideration. As a result, synthetic strategies for the preparation of asymmetrically substituted protected dithiolene's have been developed by Garner's group.[57,58,59]

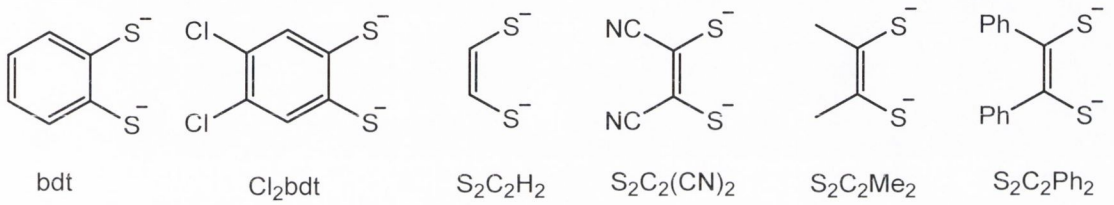

Figure 1.17: Structures of symmetrical dithiolene based ligands as model for molybdopterin (MPT).

Scheme 1.4 illustrates that bromoacetyl compounds react with potassium salts of dithiocarbonic acid to form compound **7A** which can further be cyclised in strong acidic conditions to give a protected 1,3-dithiolene-2-one moiety (**7B**). An alternative route involves the reaction of bromoacetyl compounds with sodium salts of dithiocarbamic acid to yield compound **7C**, followed by cyclisation in strong acidic condition, generating the protected 1,3-dithiolene-2-carbamide (**7D**). Both compounds **7B** and **7D** can be easily hydrolysed using a strong base and can then *in situ* be used for metal complexation reactions. This methodology was then used to construct asymmetrically substituted dithiolene ligands particularly with *N*-heterocyclic compounds in order to make structural analogue of MPT in molybdenum cofactor. These *N*-heterocyclic substituted dithiolene ligands were then used to form the respective molybdenum and tungsten complexes. These model complexes showed similar coordination geometry as was observed in the active sites of the DMSO reductase family. For example, Davies *et al.* reported the synthesis of a series of $[MO(S_2C_2R_2)_2]^{2-}$ [where M = Mo or W; R = sdt (phenyl dithiolene), 2-pedt (2-pyridine dithiolene), 3-pedt (3-pyridine dithiolene), 4-pedt (4-pyridine dithiolene)] complexes as shown in Figure 1.18.[59,60]

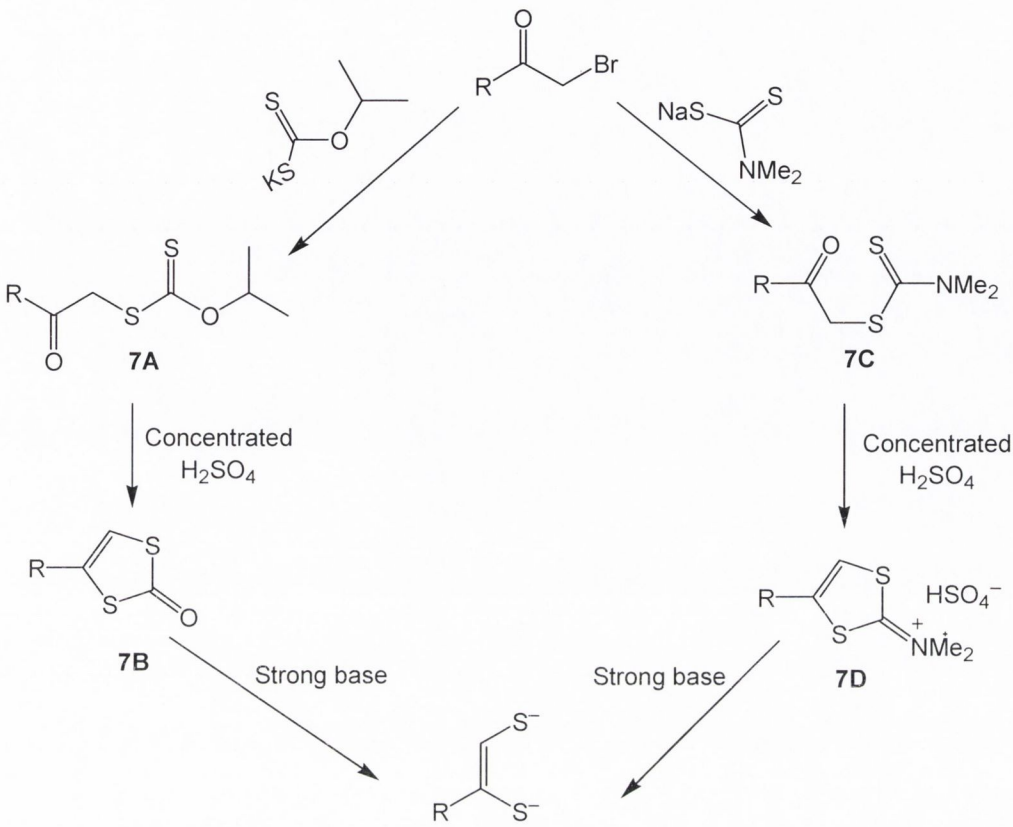

Scheme 1.4: Two strategies for the synthesis of asymmetrically substituted dithiolene ligands.[59,60]

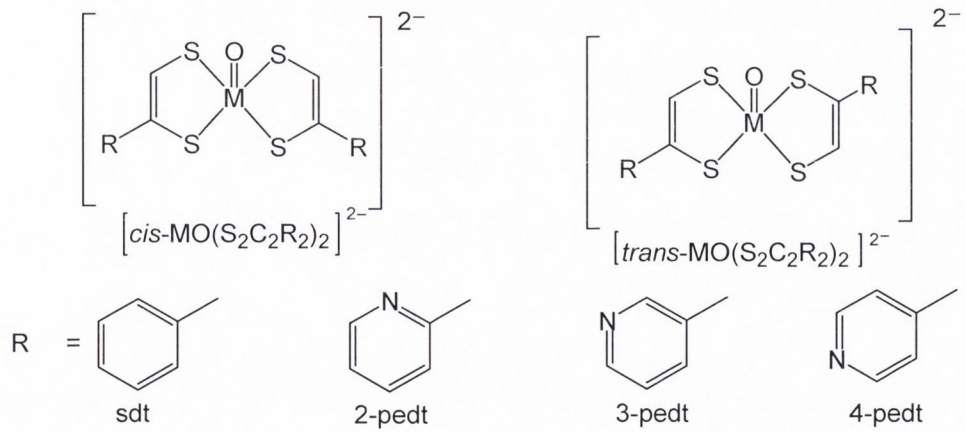

Figure 1.18: The unsymmetrical dithiolene metal complexes (where M = Mo, W) as models including features of MPT.[59,60]

Subsequently, the chemistry of *bis*-dithiolene molybdenum complexes was extended by including a pterin unit (Figure 1.19 **8A**) as a substituent.[61] In the later years, the chemistry of molybdenum and tungsten cofactors has been further developed by Bradshaw *et al.* who synthesised a quinoxaline-enedithiolate open alcohol form ligand (Figure 1.19 **8B**).[62] This ligand show somehow success in order to achieve an open alcohol form synthetic analogue of MPT, however, a true chemical analogue in a molybdenum and tungsten complex for this type of ligand has still to be established.

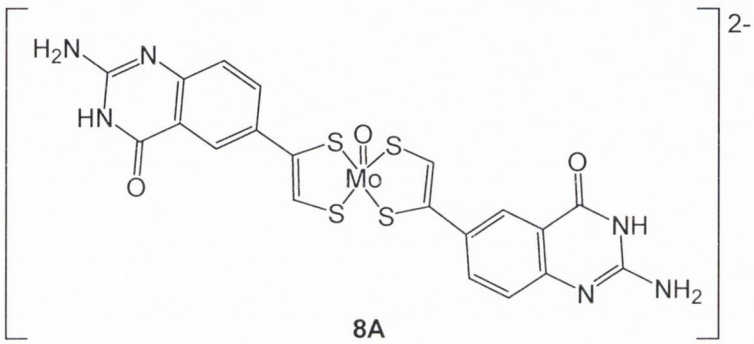

8A

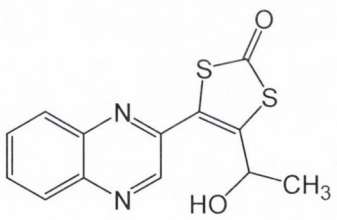

8B

Figure 1.19: Structure of the pterin derived dithiolene molybdenum complex (**8A**); quinoxaline-enedithiolate derived ligand as a structural model of MPT (**8B**).[61,62]

Further methods have been utilised in the development of mixed ligand complexes involving for instance CpCo (cyclopentadienyl cobalt) or a Cp_2M (M = Mo or W) centre bound to one dithiolene ligand. The chemical inertness of these cyclopentadienyl (Cp) centres allows the introduction of substituents on the dithiolene that may have some relevance to MPT. For example, Armstrong *et al.* reported the synthesis and the protonation of the heterocyclic nitrogen atoms of the [η^5-CpCo(dithiolene)] complex (Figure 1.20 **9A**).[63] The protonation of nitrogen atoms results in a shift of the redox potential of the CpCo centre to a more positive value, suggesting that the effect of

protonation is communicated through the dithiolene to the metal centre. The model chemistry of MPT was further developed by Bradshaw *et al.* who included the pyrazine and pyran rings in the [η^5-CpCo(dt)] analogues of MPT as shown in Figure 1.20 **9B**.[62] However, attempts to synthesise molybdenum or tungsten complexes with this ligand still remained unsuccessful.

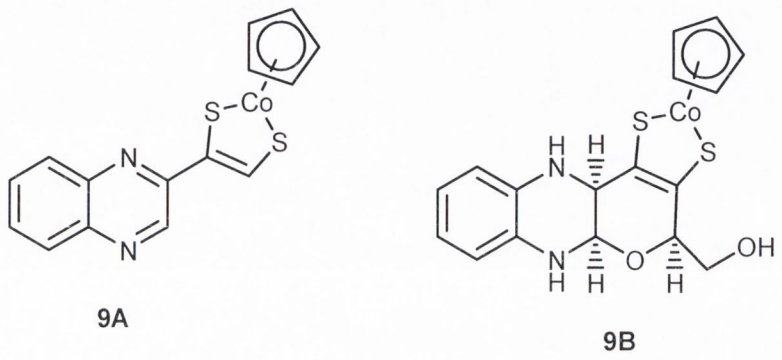

Figure 1.20: Different approaches to chemical analogues of MPT.[62,63]

Coucouvanis *et al.* introduced a new methodology to synthesise dithiolene complexes by the reaction of a transition metal di- or polysulfide complex with a substituted alkyne.[64] However, this type of reaction is only favoured when the alkyne is substituted by at least one electron withdrawing group. Such type of reactions may offer a useful synthetic pathway to produce a variety of substituted dithiolene complexes. For example, a suitable metal precursor, such as [$Cp_2Mo(S_4)$][65] was reacted with substituted-alkynyl quinoxaline to produce the corresponding [$Cp_2Mo(S_2C_2RR')$] complex by the use of a radical initiator (Figure 1.21 **10A**).[66]

Another approach used by Alexandra *et al.* describes the synthesis of molybdenum and tungsten complexes by the reaction of [Cp_2MoCl_2] with a series of dithiolene ligands as shown in Figure 1.21 **10B**.[67] Electrochemical and associated spectroelectrocheimcal investigations of these complexes have demonstrated that the nature of the substituent of a dithiolene ligand modulates the properties of the complex, including the potential at which redox changes occur.

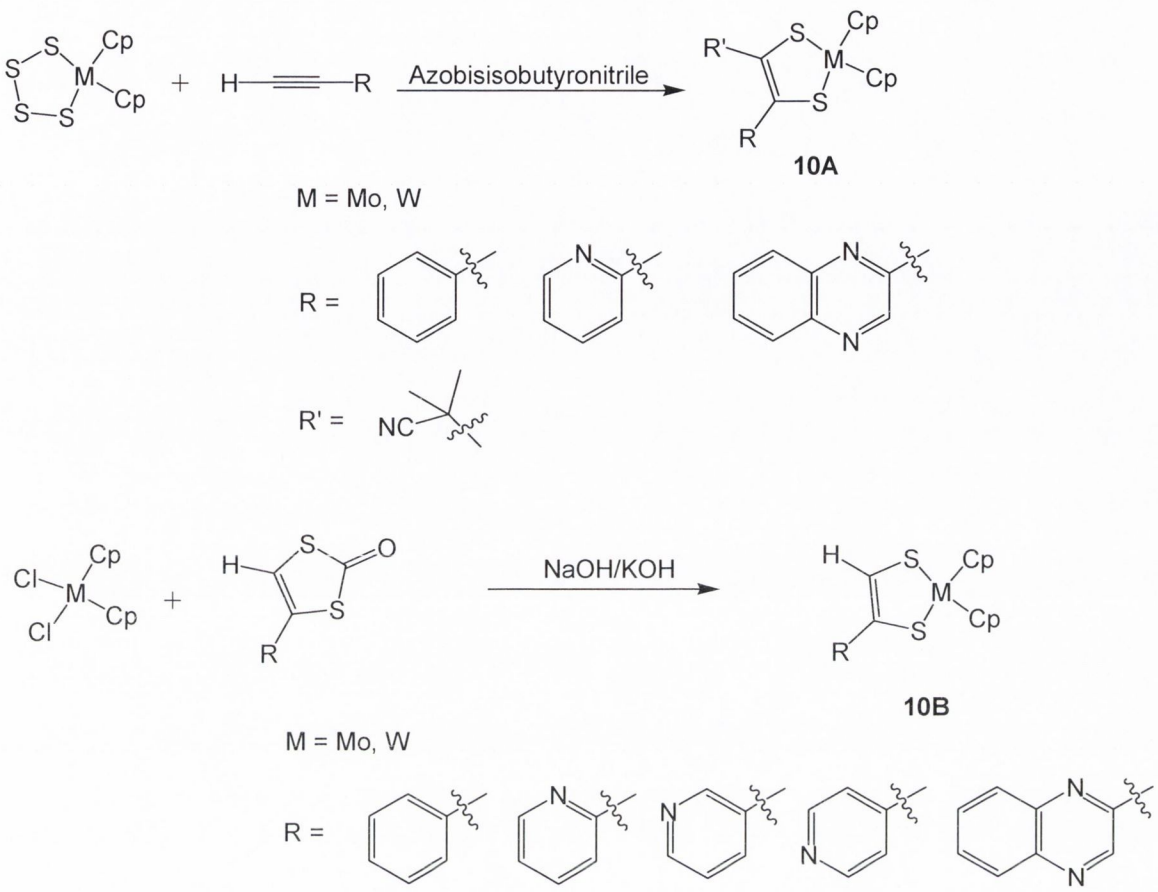

Figure 1.21: Structural representation of $[Cp_2M(S_2C_2RR')]$ (**10A**), and $[Cp_2M(S_2C_2(H)R)]$ (**10B**) complexes.[66,67]

In recent years, the trend has been diverted from employing conventional dithiolene ligands to addressing the different components of MPT. More attention has been paid to understand the influence of all of its functional groups and their individual catalytic properties in detail. In this respect, Schulzke noticed the significance of the pyran ring in MPT and synthesised the first flavanone dithiolene (fdt) derived metal complexes (Figure 1.22), addressing the pyran feature of natural MPT.[68] Studies on these complexes indicated the presence of weak Mo=O bond character due to electron withdrawing nature of pyran ring. This weakened M=O bond has a great interest in the bioinorganic chemistry and was most remarkably exposed by the studies of the oxidised form of arsenite oxidase. The studies suggested that the $Mo^{VI}O_2$ core of arsenite oxidase had one longer $Mo^{VI}O$ bond at 1.83 Å and this undergoes protonation to form

$Mo^{VI}O(OH)$ in the catalytic cycle.[69] Most of the earlier reported $Mo^{VI}O_2$ complexes with electron donating ligands had a strong Mo=O bond and protonation hardly ever occurred.[70,71]

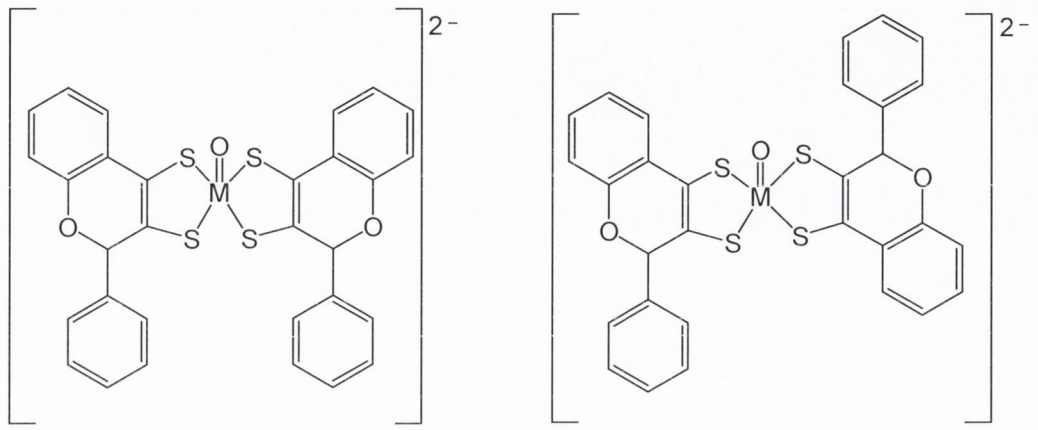

$[cis\text{-}MO(fdt)_2]^{2-}$ $[trans\text{-}MO(fdt)_2]^{2-}$

Figure 1.22: Structures of flavanone dithiolene complexes $[MO(fdt))_2]^{2-}$ (where M = Mo, W).[68]

Unfortunately, crystals of these flavanone derived dithiolene complexes could not be isolated due to the fact that they form *cis* and *trans* (ligand oriented) isomers, which usually result in poor crystallisation behaviour.[68] In an extension to this study, 4-chromanone dithiolene (cdt) derived molybdenum and tungsten complexes *i.e.* $[(MO(cdt)_2]^{2-}$ were also synthesised and structurally characterised.[72] X-ray structural studies revealed that the geometry around the molybdenum centre is square pyramidal (Figure 1.23), with the base of the pyramid constituted of the four sulfur atoms and the apex being the terminal oxygen atom with a weakened M=O character.

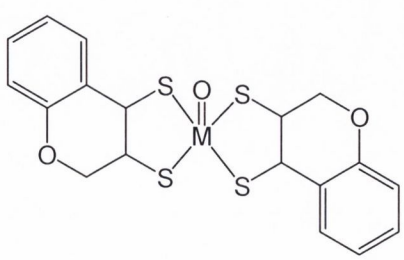

Figure 1.23: Structure of $[MO(cdt))_2]^{2-}$ (where M = Mo, W).[72]

According to the study of our group, pyran derived molybdenum and tungsten shows a weakened Mo=O bond character which clearly shows that the presence of the pyran ring attached to the dithiolene group in molybdopterin is an interesting property of the catalytic activity at the metal centre.

Sugimoto *et al.* have also synthesised a series of dithiolene derived molybdenum and tungsten complexes[73] such as $[MO(cyclohexane)_2]^{2-}$, $[MO(thio\text{-}pyran)_2]^{2-}$, $[MO(pyran)_2]^{2-}$, after similar types of pyran based dithiolene complexes were reported by our group earlier.[68] The structure of the pyran dithiolene derived molybdenum complex (Figure 1.24) showed that the oxo ligand together with the four sulfur atoms from the dithiolene functionality constitute a square pyramidal geometry with weakened Mo=O bond character.

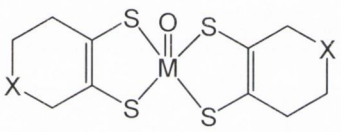

Figure 1.24: General structure of a series of dithiolene derived molybdenum complexes [where X = CH_2, S, O).[73]

Modelling the different components of MPT individually such as pyran based dithiolene, pyrazine based dithiolene and fused pyrazine-pyran based dithiolene as well as the open alcohol and closed pyran forms of molybdenum enzymes, operating a modular model strategy would allow to mimic the active site in a more systematic way. Consequently, data obtained from all of the separately synthesised components together, would give more relevant and comprehensive information for understanding the role of this native enzyme cofactor in the catalytic transformation, which are accomplished at the metal centres of the oxotransferase enzymes.

1.5 Introduction to pentathiepins

Over the past few decades, interest in organic polysulfides has significantly increased because of their special physical properties (chemical resistance and dielectrc strength etc.) as well as their potential for synthetic applications.[74,75,76] For example, pentathiepins have been successfully used to synthesise organic compounds such as dithiols, isothiocyanates and tetrathiepins.[76] The study of unusual five membered ring systems bearing one carbon-carbon double bond and five adjacent sulfur atoms, the 1,2,3,4,5-pentathiepins, is of great interest because of their great stability, occurrence in natural products and their potent biological activities.[77] The formation of stable medium to large rings is due to the unique nature of elemental sulfur among the other elements. For example, the natural existence of the cyclic polysulfides ranges from monocyclic molecules such as lenthionine to the polycyclic molecule sporidesmin E as shown in Figure 1.25.

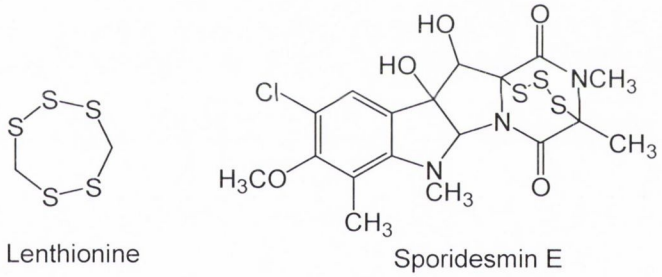

Figure 1.25: Naturally occurring polysulfides, lenthionine and sporidesmin E.[74]

A number of biologically active polysulfides have been isolated from natural sources. For example, the first naturally occurring pentathiepin varacin (Figure 1.26 **11A**) was isolated from the marine ascidian *Lissoclinum vareau* in 1991.[78] Later, another closely related pentathiepin, lissoclinotoxin (Figure 1.26 **11B**) was isolated from *Lissoclinum sp.*[79] The structures of both isolated natural products are distinguishable by their hydroxyl and methoxy groups and have been found to have remarkable stability despite bearing seven-membered rings.

Various naturally isolated and synthetic pentathiepins exhibit potent biological

activities.[76] For example, naturally occurring benzo-pentathiepins, bearing an aminoethyl group such as varacin and lissoclinotoxin, have shown potent anti-bacterial and anti-fungal activities.[78] Moreover, Chatterji *et al.* first reported that varacin was found to have DNA cleaving properties.[80] In addition, varacin was also screened for its cytotoxicity and was found to be highly active in the treatment of human colon cancer HCT116 with an IC_{50} value of 0.05 μg/ml.[75] After establishing the bioactivity of natural pentathiepins, synthesised benzo-pentathiepin[81] (Figure 1.26 **11C**) was tested for its biological activity. In vitro, antimicrobial results proved benzo-pentathiepin to be a potent antimicrobial agent against *Candida albicans* and *Bacillus subtilus*.[78,79,82]

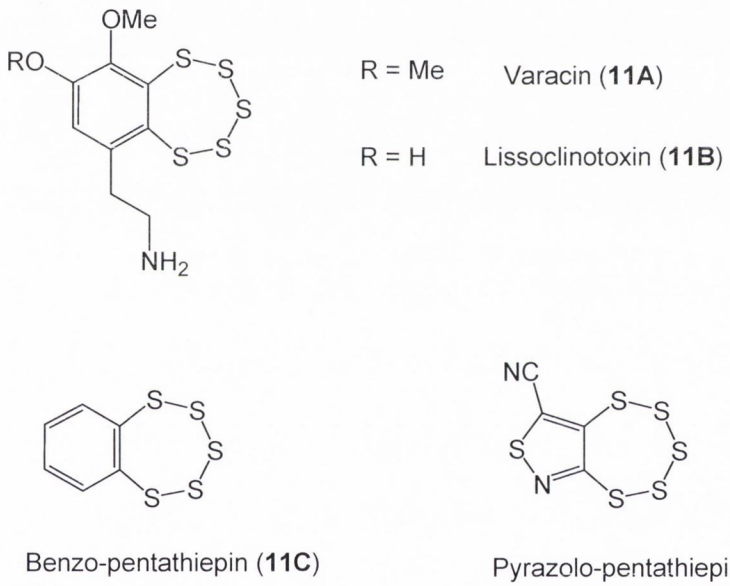

Figure 1.26: Structures of biologically active naturally occurring pentathiepins varacin (**11A**) and lissoclinotoxin (**11B**) and synthetic benzo (**11C**) and pyrazolo (**11D**) pentathiepins.[78,79,81]

Biological activities of these natural and synthetic compounds also suggested that the presence of the pentathiepin ring is crucial for the biological activity of any such compound.[76] Furthermore, fungicidal activity of synthesised pyrazolo-pentathiepin (Figure 1.26 **11D**) has been patented.[83] This compound was found to inhibit the growth of *Phytophthora infestans* in tomatoes[84] as well as *Venturia inaecqualis* infection in

apples.[85] In addition to biological activities, polysulfide aromatics have also shown potential applications in electronics such as cathode active material in batteries.[86] It was suggested that the construction of the pentathiepin moiety makes the whole structure electrochemically active. For example, electrochemically inactive compounds such as 1-methylindole, were electrochemically activated by the introduction of a pentathiepin moiety *i.e.* indole-pentathiepin. The laboratory preparation of stable pentathiepins as well as their discovery in bioactive natural products, has spurred greater interest in pentathiepin chemistry. Therefore, the development of efficient methods for the synthesis of heterocyclic pentathiepins and their biological investigation is a very interesting and relevant topic. So far, there is only a limited number of methods available for the chemical synthesis of pentathiepins and the mechanisms are still not well understood. Surprisingly, most of the synthesised pentatiepins are restricted to benzene and some other simple heterocyclic systems due to synthetic difficulties. For example, there are only very few reports available describing the synthesis of pentathiepins with various heteroatomic compounds such as benzo-pentathiepin (**12A**), naphthalene-penathiepin (**12B**), indole-pentathiepin (**12C**) and thieno-pentathiepin (**12D**) (Figure 1.27).[75,87,88,89]

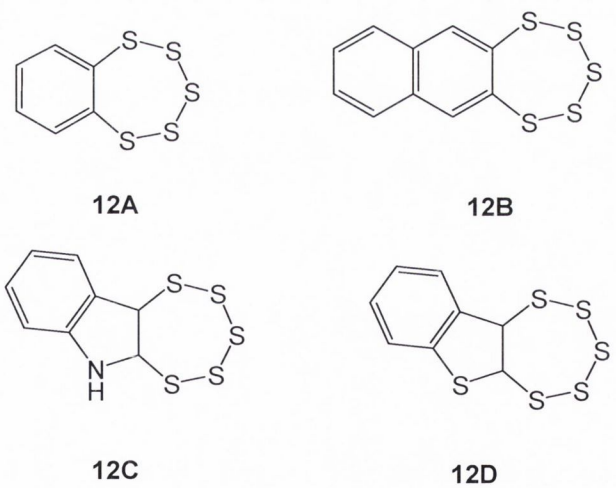

Figure 1.27: Structures of synthesised heterocyclic compounds such as benzo-pentathiepin (**12A**), naphthalene-penathiepin (**12B**), indole-pentathiepin (**12C**) and thieno-pentathiepin (**12D**).

The most commonly used method for the synthesis of benzo-pentathiepins is the treatment of *O*-dithiols with S_2Cl_2, S_3Cl_2 or S_8 in liquid ammonia.[88] Moreover, in connection with attempts to develop a more rational methodology for the preparation of indol-pentathiepins, Bergman *et al.* reported the synthetic strategy using isatin and P_4S_{10} in refluxing pyridine.[89] Therefore, the synthetic methodologies for the preparation of pentathiepins have been somewhat limited by long reaction times, the necessity for a particularly careful handling (harsh conditions and reaction media), the complex isolation of intermediates and purification procedures. Therefore, the development of facile synthetic procedures for fused heterocyclic-pentathiepins is really significant as it will allow us to find potent biologically active compounds in the future.

1.6 Aim of research

The above discussion highlights the significance of functional molybdoenzymes in living systems as well as present synthetic challenges which are involved in the development of dithiolene based molybdenum and tungsten model complexes in comparison to the available active sites. A complete synthetic model for DMSO reductase family that can reproduce key spectroscopic, structural and reactivity properties of the catalytic molybdenum or tungsten centre, despite some successes still remains a challenge for bioinorganic chemists. The fundamental objective of this research is to design and synthesise molybdenum and tungsten based dithiolene complexes bearing a pyrazine ring. The significance of the pyrazine ring has been shown by theoretical methods and it potentially influences and electronically communicates with the coordinated oxo metal centre in the enzymatic active sites. For instance, the existence of pyrazine ring as reduced tetrahydro state in the tricyclic form of MPT, whereas dihydropyrazine structure has been found in open alcohol form. Therefore, it can be postulated that pyrazine ring has a considerable role in handling the protons which are involved in the catalytic reaction. In order to modulate the pyrazine features of MoCo, there is a need to design an oxomolybdenum centre, which is not only coordinated to a *bis*-dithiolene ligand set but also includes the pyrazine feature of enzymatic MPT and therefore will serve as a quite accurate structural model to this

naturally occurring ligand system. In this context, pyrazine derived molybdenum and tungsten complexes will be synthesised, isolated, analysed and structurally characterised. Investigation of the spectroelectrochemical properties on such type of structural models (*i.e.* pyrazine dithiolene molybdenum and tungsten complexes) is the main motivation of this research. The redox properties of these complexes will be studied using cyclic voltammetry, in combination with UV-Vis spectroelectrochemistry as well as electron paramagnetic resonance spectroscopic techniques and the obtained data will be compared with the available studies on DMSO reductase family. Another major aim of this research is to synthesise dithiolene ligands and their respective molybdenum complexes, which bear an alcohol function representing the alcohol side chain features of enzymatic MPT. It has already been suggested (Section 1.3.5) that the fused pyrazine and pyran unit in these enzymes is not simply a part of the ligand, but is actively involved in the mechanism of action of the enzymes. Consequently, the synthesis and spectroelectrochemical characterisation of open form MPT analogues and their respective complexes will provide key information regarding the potential ring opening and closing in the active sites during enzymatic catalytic reactions. Once the pyrazine dithiolene and the alcohol dithiolene synthetic procedures are established individually, both approaches could be combined to generate fused molecule, allowing the direct investigation of ring opening and closing mechanism.

Another objective of this work was to investigate the electronic communication process between pyrazine and metalladithiolene moieties in the presence of acid. It was not possible to modulate this process using already established molybdenum or tungsten based dithiolene complexes due to their unstable nature upon protonation. Towards modelling this electronic communication process, design and synthetic strategies for the construction of novel dithiolene CpCo complexes will be explored. These CpCo complexes are of great interest due to their air stable nature and feasibility for spectroelectrochemical studies in the presence of acid which would possibly allow us to investigate the electronic interaction between pyrazine and cobaltadithiolene moiety. The comparison of redox properties of synthesised dithiolene CpCo complexes in the presence or absence of acid may provide useful information in relevance to the pyrazine

features of naturally occurring enzymes.

In an attempt to synthesise side alcohol form molybdenum dithiolene complexes, an unexpected formation of novel heterocyclic pentathiepino-pyrrollo[1,2-*a*] compound was discovered. Studies have revealed that pentathiepins are present in a large number of natural products which have shown potent biological activities. After learning about the synthetic difficulties and interesting applications of pentathiepin moiety as described in the literature, exploring the unexpected facile synthetic methodologies, their refinement and relevant biological studies have become another aim of this research. In order to investigate whether these novel pentathiepins have biological activities, these compounds have to be screened for their potential DNA binding as well as anti-cancer activities. Data will be collected about the factors affecting the biological activities of pentathiepins by varying the substituents on the heterocyclic ring.

References

[1] P. P. Samuel, C. Schulzke, Handbook of Inorganic Chemistry., Nova Sci. Publ., **2010**.

[2] C. Schulzke, *Eur. J. Chem.*, **2011**, 1189.

[3] P. Chandrasekaran, K. Arumugam, U. Jayarathne, L. M. P. Rez, J. T. Mague, J. P. Donahue, *Inorg. Chem.*, **2009**, 48, 2103.

[4] A. Majumdar, S. Sarkar, *Coord. Chem. Rev.*, **2011**, 255, 1039.

[5] J. Freya, H. J. Adam, C. Taylor, C. D. Garner, *Coord. Chem. Rev.*, **2010**, 254, 1570.

[6] G. N. Schrauzer, V. P. Mayweg, *J. Am. Chem. Soc.*, **1962**, 84, 3221.

[7] H. B. Gray, R. Williams, E. Billing, *J. Am. Chem. Soc.*, **1962**, 84, 3596.

[8] C. K. Jørgensen, *Coord. Chem. Rev.*, **1966**, 1, 164.

[9] (a) A. Davison, N. Edelstein, R. H. Holm, *Inorg. Chem.*, **1963**, 2, 1227. (b) A. Davison, N. Edelstein, R. H. Holm, A. H. Maki, *J. Am. Chem. Soc.*, **1963**, 85, 2029.

[10] S. Soralova, M. Breza, M. Grof, *Polyhedron*, **2011**, 30, 307.

[11] G. N. Schrauzer, V. P. Mayweg, *J. Am. Chem. Soc.*, **1965**, 87, 3585.

[12] S. Alvarez, R. Vincente, R. Hoffmann, *J. Am. Chem. Soc.*, **1985**, 107, 6253.

[13] E. I. Stiefel, K. D. Karlin, Progress in Inorganic Chemistry, Dithiolene Chemistry; Synthesis, Properties, and Applications, Wiley, John & Sons., **2004**, P 52.

[14]E. I. Stiefel, M. K. Johnson, Prog. Inorg. Chem. Vol. 52. John Wiley and Sons, Inc., Hoboken, New Jersey: 2004. p. 213-266.

[15] P. Chaudhuri, C. N. Verani, E. Bill, E. Bothe, T. Weyhermüller, K. Wieghardt, *J. Am. Chem. Soc.*, **2001**, 123, 2213.

[16] B. G. Bonneval, K. I. M. Ching, F. Alary, T. T. Bui, L. Valade, *Coord. Chem. Rev.*, **2010**, 254, 1457.

[17] G. Moula, M. Bose, H. Datta, S. Sarkar, *Polyhedron*, **2013**, 52, 900.

[18] M. Nomura, N. Sakamoto, H. Nakajima, C. Fujita-Takayama, T. Sugiyama, M. Kajitani, *Polyhedron*, **2011**, 30, 2890.

[19] H. Kunkely, A. Vogler, *Inorg. Chim. Acta.*, **2001**, 319, 183.

[20] M. C. Aragoni, M. Arca, F. A. Devillanova, F. Isaia, V. Lippolis, A. Mancini, L. Pala,

G. Verani, T. Agostinelli, M. Caironi, D. Natali, M. Sampietro, *Inorg. Chem. Commun.*, **2007**, 10, 191.

[21] A. Majumdar, J. Mitra, K. Pal, S. Sarkar, *Inorg. Chem.*, **2008**, 47, 5360.

[22] Q. Miao, J. Gao, Z. Wang, H. Yu, Y. Luo, T. Ma, *Inorg. Chim. Acta.*, **2011**, 376, 619.

[23] A. Zarkadoulas, E. Koutsouri, C. A. Mitsopoulou, *Coord. Chem. Rev.*, **2012**, 256, 2424.

[24] W.-F. Mark-Lee, K.-H. Ng, L. J. Minggu, A. A. Umar, M. B. Kassim, *Int. J. Hydrogen Energy.*, **2013**, 9578.

[25] A. Sugimori, T. Akiyama, M. Kajitani, T. Sugiyama, *Bull. Chem. Soc. Jpn.*, **1999**, 72, 879.

[26] R. Eisenberg, J. Ibers, *J. Am. Chem. Soc.*, **1965**, 87, 3776.

[27] I. S. Edward, *J. Chem Soc., Dalton Trans.*, **1997**, 3915.

[28] H. Sugimoto, H. Tsukube, *Chem. Soc. Rev.*, **2008**, 37, 2609.

[29] O. Einsle, F. A. Tezcan, S. L. A. Andrade, J. B. Howard, *Science*, **2002**, 27, 360.

[30] K. V. Rajagoplan, J. L. Johnson, D. S. Millington, *Biol. Chem.*, **1987**, 120, 16357.

[31] M. K. Chan, S. Mukund, M. W. Adams, *Science*, **1995**, 267, 1463.

[32] K. V. Rajagopalan, J. L. Johnson, *Proc. Nat. Acad. Sci.*, **1982**, 79, 6856.

[33] (a) C. R. Scriver, A. L. Deaudet, W. S. Sly, D. Valle, The Metabolic and Molecular Basis of Inherited Disease. 8th edition New York. **1995**, 2271; (b) M. Z. Seidahmed, E. A. Alyamani, M. S. Rashed, A. A. Saadallah, O. B. Abdelbasit, M. M. Shaheed, A. Rasheed, F. A. Hamid, M. A. Sabry, *Am. J. Med. Genet.*, **2005**, 36A, 205.

[34] J. Wang, O. P. Kryatova, E. V. Rybak-Akimova, R. H. Holm, *Inorg. Chem.*, **2004**, 43, 8092.

[35] J. M. Rebelo, J. M. Dias, R. Huber, J. J. G. Moura, M. J. Romão, *J. Biol. Inorg. Chem.*, **2001**, 6, 791.

[36] H. Sugimoto, H. Tano, H. Miyako, S. Itoh, *Dalton Trans.*, **2011**, 40, 2358.

[37] O. Einsle, F. A. Tezcan, S. L. A. Andrade, J. B. Howard, *Science*, **2002**, 297, 1696.

[38] J. H. Enemark, J. J. A. Cooney, R. H. Holm, *Chem. Rev.*, **2004**, 104, 1175.

[39] R. Hille, *Trend. Biochem. Sci.*, **2002**, 27, 360.

[40] R. Hille, *Chem. Rev.*, **1996**, 96, 2757.

[41] . G. Bertero, R. A. Rothery, M. Palak, C. Hou, D. Lim, F. Blasco, J. H. Weiner, N. C. J. Strynadka, *Nat. Struct. Biol.*, **2003**, 10, 681.

[42] S. P. Greatbanks, I. H. Hillier, C. D. Garner, J. A. Joule, *J. Chem. Soc., Perkin Trans.*, **1997**, 2, 1529.

[43] J. H. Enemark, C. D. Garner, *J. Biol. Inorg. Chem.*, **1997**, 2, 817.

[44] B. S. Lim, M. W. Willer, M. Miao, R. H. Holm, *J. Am. Chem. Soc.*, **2001**, 123, 8343.

[45] B. Lim, R. H. Holm, *J. Am. Chem. Soc.*, **2001**, 123, 1920.

[46] C. A. Goddard, R. H. Holm, *Inorg. Chem.*, **1999**, 5389.

[47] K. M. Sung, R. H. Holm, *Inorg. Chem.*, **2000**, 39, 1275.

[48] S. Groysman, J. J. Wang, R. Tagore, S. C. Lee, R. H. Holm, *J. Am. Chem. Soc.*, **2008**, 130, 12794.

[49] K. M. Sung, R. H. Holm, *J. Am. Chem. Soc.*, **2001**, *123*, 1931.

[50] L. S. Booyong, R. H. Holm, *J. Am. Chem. Soc.*, **2001**, *123,* 1920.

[51] J. J. Wang, O. P. Kryatova, E. V. Rybak-Akimova, R. H. Holm, *Inorg. Chem.*, **2004**, 43, 8092.

[52] J. Jiang, R. H. Holm, *Inorg. Chem.*, **2005**, 44, 1068.

[53] S. Boyde, S. R. Ellis, C. D. Garner, W. Clegg, *Chem. Commun.*, **1986**, 1541.

[54] M. A. Ansari, J. Chandrasekaran, S. Sarkar, *Inorg. Chim. Acta.*, **1987**, 133, 133.

[55] D. Coucouvanis, A. Hadjikyriacou, A. Toupadakis, S. M. Koo, O. Ileperuma, M. Draganjac, A. Salifoglou, *Inorg. Chem.*, **1991**, 30, 754.

[56] J. P. Donahue, C. R. Goldsmith, U. Nadiminti, R. H. Holm, *J. Am. Chem. Soc.*, **1998**, 120, 12869.

[57] D. J. Rowe, C. D. Garner, J. A. Joule, *J. Chem. Soc., Perkin Trans. 1.*, **1985**, 1907.

[58] A. Dinsmore, J. H. Birks, C. D. Garner, J. A. Joule, *J. Chem.* Soc., *Perkin Trans. 1.*, **1997**, 801.

[59] E. S. Davies, R. L. Beddoes, D. Collison, A. Dinsmore, A. Docrat, J. A. Joule, C. R. Wilson, C. D. Garner, *J. Chem. Soc., Dalton Trans.* 1., **1997**, 3985.

[60] E. S. Davies, G. M. Aston, R. L. Beddoes, D. Collison, A. Dinsmore, A. Docrat, J. A. Joule, C. R. Wilson, C. D. Garner, *J. Chem. Soc., Dalton Trans.*, **1998**, 3647.

[61] E. S. Davies, G. M. Aston, R. L. Beddoes, D. Collison, J. A. Joule, C. D. Garner, *J. Chem. Soc., Dalton Trans*, **1998**, 3647.

[62] B. Bradshaw, D. Collison, J. A. Joule, *J. Chem. Soc., Perkin Trans.*, **2001**, 1, 3232.

[63] E. M. Armstrong, M. S. Austerberry, H. J. Birks, J. A. Joule, C. D. Garner, *Heterocycles*, **1993**, 35, 563.

[64] D. Coucouvanis, A. Hadjikyriacou, M. Draganjac, M. G. Kanatzidis and O. Ileperuma, *Polyhedron*, **1986**, 5, 349.

[65] H. Ko, *Angew. Chem., Int. Ed. Engl.*, **1969**, 8, 375.

[66] A. L. Tan, A. J. Blake, E. S. Davies, C. Wilson, C. D. Garner *Chem. Commun.*, **2011**, 47, 953.

[67] L. Alexandra, A. J. Blake, D. Collison, E. S. Davies, H. J. Disley, M. Helliwell, F. E. Mabbs, J. McMaster, C. Wilson, C. D. Garner, *Dalton Trans.*, **2011**, 40, 10457.

[68] C. Schulzke, *Dalton Trans.*, **2005**, 713.

[69] T. Conrads, C. Hemann, G. N. George, I. J. Pickering; R. C. Prince, R. Hill, *J. Am. Chem. Soc.*, **2002**, 124, 11276.

[70] J. M. Berg, R. H. Holm, *J. Am. Chem. Soc.*, **1985**, 107, 917.

[71] F. W. Moore, M. L. Larson, *Inorg. Chem.*, **1967**, 6, 998.

[72] P. P. Samuel, Molybdenum and tungsten compounds with dithiolene ligands inspired by molybdopterin as models for the molybdenum and tungsten cofactors, Universität zu Göttingen, PhD thesis, August, **2011**.

[73] H. Sugimoto, M. Harihara, M. Shiro, K. Sugimoto, K. Tanaka, H. Miyake, H. Tsukube, *Inorg. Chem.*, **2005**, 44, 6386.

[74] S. A. Amelichev, S. L. Konstantinova, K. A. Lyssenko, C. W. Rees, *J. Org. Biomol. Chem.*, **2005**, 3, 3496.

[75] A. Alam, M. Kon-no, S. Ogawa, R. Sato, *Tetrahedron*, **2007**, 63, 927.

[76] L. S. Konstantinova, O. A. Rakitin, *Chem. Rev.*, **2004**, *104,* 2617.

[77] F. Compagnone, R. S. John, *Tetrahedron*, **1994**, 50, 12785.

[78] B. S. Davidson, T. F. Molinski, L. R. Barrows, C. M. Ireland, *J. Am. Chem. Soc.*, **1991**, 113, 4709.

[79] P. A. Sarle, T. F. Molinski, *J. Org. Chem.*, **1994**, 59, 6600.

[80] T. Chatterji, K. S. Gates, *Bioorg. Medicinal Chem. Lett.*, **1998**, 8, 535.

[81] F. Feher; M. Langer, *Tetrahedron Lett.*, **1971**, 2125.

[82] T. N. Makarieva; V. A. Stonik, A. S. Dmitrenok, B. B. Grebnev, V. V. Isakov, N. M. Rebachyk, *J. Nat. Prod.*, **1995**, 58, 254.

[83] W. K. Moberg, U.S. Patent 4275073; *Chem. Abstr.*, **1981**, 95, 150654.

[84] E. I. Du Pont de Nemours. NL Patent 7704108; *Chem. Abstr.*, **1979**, 90, 137878.

[85] E. I. Du Pont de Nemours. J. Patent 78127489; *Chem. Abstr.*, **1979**, 90, 82132.

[86] H. Tsutsumi, H. Higashiyama, K. Onimura, T. Oishi, *J. Power Sources.*, **2005**, 146, 345.

[87] L. S. Konstantinova, S. A. Amelichev, B. A. Belyakov, T. S. Pivina, K. A. Lyssenko, O. A. Rakitin, *Tetrahedron*, **2012**. 68, 590.

[88] B. L. Chenard, R. L. Harlow, A. L. Johnson, *J. Am. Chem. Soc.*, **1985**, 107, 3871.

[89] J. Bergman, S. Claes, *Tetrahedron Lett.*, **1994**, 35, 5279.

Chapter 2

Synthesis and characterisation of a series of novel pentathiepino-pyrrolo[1,2-a]-derivatives and their biological activities

2.1 Overview

This chapter describes the discovery of new synthetic pathways to make pentathiepins, their optimisation and work towards understanding the reaction mechanism. This discovery was made purely by chance while working on the synthesis of chemical analogues of molybdenum cofactor (MoCo). This chapter is organised into three parts. The first section describes the synthesis of a series of hydroxyl and ethoxy-substituted pyrazine (**3** and **12**) and quinoxaline derivatives (**4** and **9-11**). These derivatives were prepared by the reaction of chloro-substituted pyrazine (**1**) and quinoxaline compounds (**2**, **6** and **8**) with appropriate-substituted terminal alkynyl derivatives using the Sonogashira coupling reaction.[1,2] In an attempt to synthesise models of MoCo, the hydroxy-substituted alkynyl pyrazine (**3**) was reacted with 4-phenyl-1,3-dithiolane-2-thione (**13**)[3] using cycloaddition reaction to form pyrazine-1,3-dithiolene-2-thione ligand (**14**) and its respective *bis*-dithiolene molybdenum and tungsten complexes. The second part describes attempted strategies to synthesise *bis*-dithiolene complexes by the reaction of hydroxyl and ethoxy-substituted alkynyl pyrazine (**3** and **12**) and quinoxaline derivatives (**4** and **9-11**) with $(Et_4N)_2[MoO(S_4)_2]$[4] (molybdenum oxo *bis*-tetrasulfide). During the course of these attempts, unexpected and novel pentathiepino-pyrrolo[1,2-*a*]-quinoxaline (**15-17**) and pyrazine derivatives (**18**) were isolated. The refined synthetic methodology is discussed in detail. The final part describes the investigation of these novel pentathiepin compounds for their potential biological activities.

2.2 Synthesis and characterisation of varieties of alkynyl pyrazine (3 and 12) and quinoxaline derivatives (4 and 9-11)

Chloro-substituted precursors such as 2-chloro-pyrazine (**1**) and 2-chloro-quinoxaline (**2**) were used as purchased. Other chloro-substituted derivatives of quinoxalines were synthesised according to procedures previously described in the literature.[5] Reactions of 4-methyl-1,2-phenylenediamine or 4,5-dimethyl-1,2-phenylenediamine with ethyl glyoxylate gave 7-methylquinoxalin-2-one (**5**) or 6,7-dimethylquinoxalin-2-one (**7**), respectively. In the next step, compounds **5** and **7** were then heated under reflux in

$POCl_3$ for 6 hrs, to convert chloro into oxo group, yielding the corresponding 2-chloro-7-methylquinoxaline (**6**) and 2-chloro-6,7-dimethylquinoxaline (**8**) The chloro-substituted pyrazine (**1**) and quinoxaline (**2**) derivatives were reacted with propyn-1-ol to generate hydroxy-substituted alkynyl pyrazine (**3**) and quinoxaline (**4**) derivatives using the Sonogashira coupling reaction as shown in Scheme 2.1. Similarly, the chloro-substituted pyrazine (**1**) and quinoxaline (**2**, **6** and **8**) derivatives were further coupled with 3,3-diethoxy-propyne to form ethoxy-substituted alkynyl quinoxaline (**9-11**) and pyrazine (**12**) derivatives (Scheme 2.1).

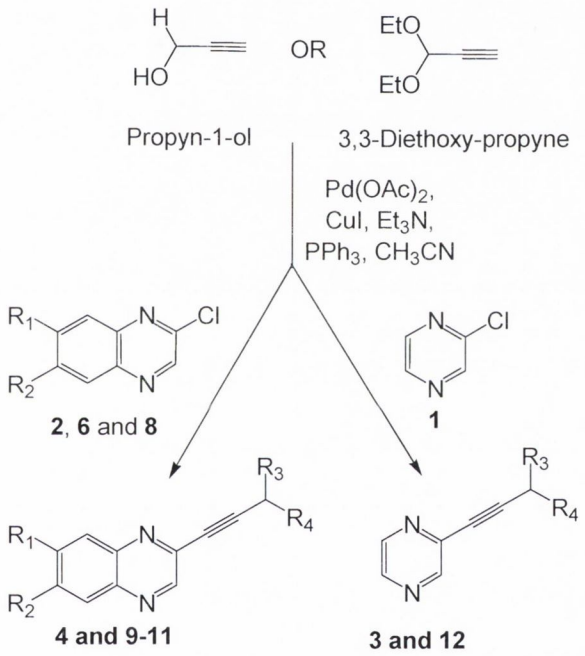

Compound	R_1	R_2	R_3	R_4
2	H	H		
3			OH	H
4	H	H	OH	H
6	CH_3	H		
8	CH_3	CH_3		
9	H	H	OEt	OEt
10	CH_3	H	OEt	OEt
11	CH_3	CH_3	OEt	OEt
12			OEt	OEt

Scheme 2.1: Synthetic pathway for hydroxyl and ethoxy-substituted alkynyl pyrazine (**3** and **12**) and quinoxaline (**4** and **9-11**) compounds.

The general reaction procedure for the synthesis of compounds **3-4** and **9-12** involves 6 hrs reflux of the reaction mixture under a nitrogen atmosphere. Upon cooling, the crude products were obtained after the removal of the solvent which were purified by column chromatography to yield quite stable and pure compounds. Generally, the Sonogashira coupling reaction requires two catalysts such as a zero valent palladium complex and a copper(I) halide.[6] In this reaction, palladium(II) is often used as a pre-catalyst which has

greater stability over palladium(0). The palladium(II) pre-catalyst is reduced to palladium(0) in the reaction mixture by the use of phosphine, allowing the reaction to proceed.[7] In addition, a copper(I) salt is used as a co-catalyst in this reaction. The commonly used copper catalyst is copper(I) iodide, which reacts with the terminal alkyne to produce a copper(I) acetylide. The formed copper(I) acetylide is an activated compound which is required for the coupling reactions to proceed.[8]

Scheme 2.2 shows the mechanistic steps which are involved in the synthesis of the ethoxy-substituted alkynyl pyrazine compound (**12**) using the Sonogashira coupling reaction (which is the same for all other relevant derivatives).

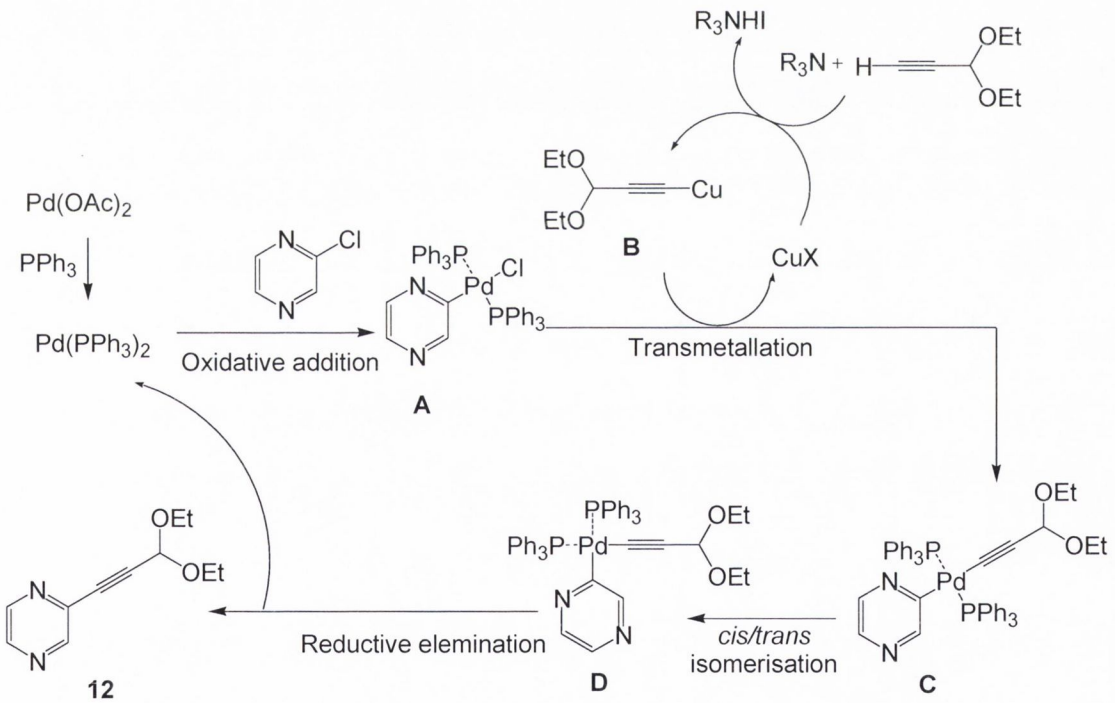

Scheme 2.2: Mechanistic steps for the synthesis of compound **12** by the Sonogashira coupling reaction.

The reduction of the inactive Pd(II) acetate was achieved by the reaction of triphenylphosphine to form the activated palladium catalyst [$(Pd(PPh_3)_2$] which reacts with chloro pyrazine in an oxidative addition to produce a palladium(II) intermediate (**A**). The intermediate (**A**) reacts *via* a transmetallation with copper(I) acetylide (**B**) to form complex (**C**), with the regeneration of copper(I) halide. In the following step, both organic ligands bound *trans* to each other to palladium are converted to the *cis* isomer in a *trans-cis* isomerisation producing complex (**D**). Finally, complex (**D**) undergoes reductive elimination to produce compound **12**, with the regeneration of the palladium catalyst.

All synthesised compounds **3-4** and **9-12** were characterised by standard spectroscopic techniques. The melting point values for compounds **3** and **4** were found to be 112-113 °C and 140-141 °C, respectively. Moreover, all other compounds (**9-10** and **12**) were found to be present as oil at room temperature except compound **11** (M.P = 50-51 °C). The IR spectra of all compounds **3-4** and **9-12** showed two characteristic bands at 1555-1514 cm^{-1} and 2213-2172 cm^{-1} corresponding to the vibrations of the υ(C=N) of the pyrazine ring and acetylene υ(C≡C) functionalities, respectively. Broad bands were observed cantered at 3275 cm^{-1} and 3248 cm^{-1}, respectively, which were attributed to the hydroxyl group (OH) present in compounds **3** and **4**.

The ^{1}H and $^{13}C\{^{1}H\}$-NMR spectra of compounds **3-4** and **9-12** were measured in $CDCl_3$. The signals for the aromatic protons of all compounds **3-4** and **9-12** were observed in the range of 8.91-7.33 ppm. Compounds **3** and **4** showed two characteristic signals at 4.66 and 4.58 ppm, respectively for methylene protons as well as broad singlets at 2.28 and 2.19 ppm, respectively for hydroxyl protons. Compounds **9-12** showed a characteristic singlet in the range of 5.49-5.40 ppm that was attributed to the ether (CH-O) functionality. In addition, two signals in between 3.82-3.49 ppm and 1.22-1.10 ppm were attributed to the methylene and methyl groups of the ethoxy functionalities. The methyl protons (CH_3) on the quinoxaline ring in compounds **10** and **11** appeared at 2.33 ppm as a singlet. The obtained $^{13}C\{^{1}H\}$-NMR spectra for all compounds exhibited the distinctive acetylenic carbons in the range of 91.6-76.4 ppm. The peaks found in

between 147.0-103.5 ppm were assigned to the aromatic carbons. HRMS spectra for compounds **3-4** and **9-12** were recorded and molecular formulae were confirmed through electron spray ionisation (ESI^+) measurements in a positive mode $[M+H]^+$. All obtained values were in good agreement with the calculated molecular formulae of these compounds (see Section 2.7.2 for details).

2.3 Synthesis and characterisation of pyrazine-1,3-dithiolane-2-thione compound (14)

The main purpose for the synthesis of hydroxy-substituted alkynyl pyrazine (**3**) was to develop dithiolene based ligands and their respective model complexes as analogues of the naturally occurring molybdenum cofactor. Several synthetic methodologies have previously been described in the literature for constructing dithiolene moieties using substituted alkynyl derivatives.[9,10] For instance, a straightforward approach was reported by Bradshaw *et al.* in which an electron deficient alkyne can be used to generate a 1,2-dithiolene-2-thione moiety.[11] In this study, it was attempted to synthesise a novel pyrazine-1,3-dithiolene-2-thione by the reaction of compound **3** with 4-phenyl-1,3-dithiolane-2-thione (**13**),[3] but no change in the reaction mixture could be detected by thin layer chromatography (Scheme 2.3). One possible explanation is that the alkynyl functionality in compound **3** is not strongly electron withdrawing enough to promote the cycloaddition reaction. In further attempt, boron trifluoride etherate was added into this reaction mixture to make the alkynyl functionality more electron deficient. It has been suggested that the Lewis acid interacts with the pyrazine ring in order to increase its electron-withdrawing ability and consequently promote the cycloaddition.[10] The mixture was left to stir at 40 °C for 30 mins using THF as a solvent. The presence of boron trifluoride etherate did eventually promote the cycloaddition reaction and a change in colour from light brown to reddish-yellow was observed. After work up, the crude product was purified by column chromatography to give yellow solid which was recrystallised from chloroform to afford needle shaped crystals suitable for X-ray analysis.

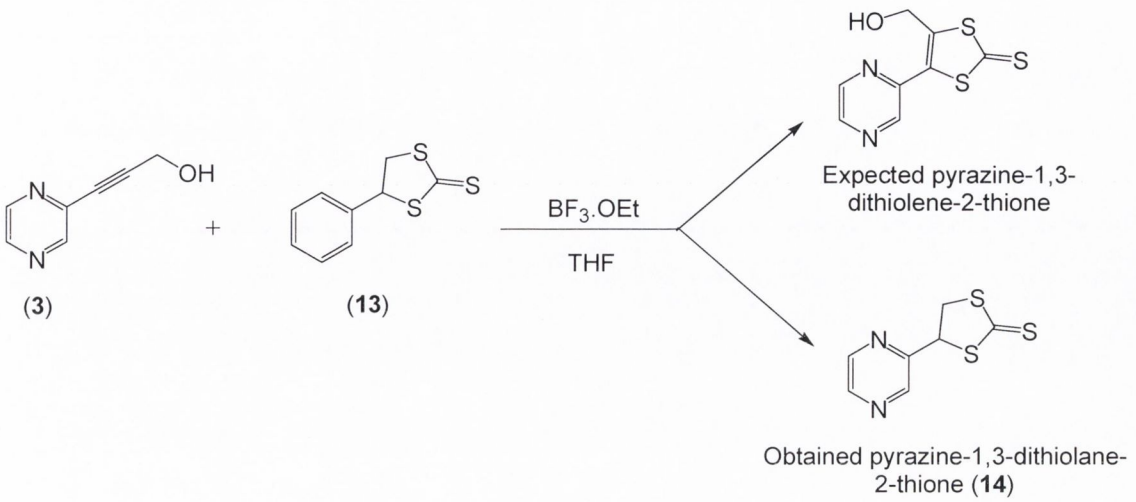

Scheme 2.3: Synthesis of reduced pyrazine-1,3-dithiolane-2-thione (**14**).

The melting point temperature for compound **14** was found to be 135-136 °C. Compound **14** was further characterised by IR spectroscopy. The appearance of the characteristic medium intensity bands at 895 cm^{-1} and 1544 cm^{-1} is due to the stretching vibrations of the carbon-sulfur bond υ(C-S) of the 1,3-dithiole moiety and υ(C=N) of pyrazine ring, respectively. Surprisingly, no distinctive band for the hydroxyl (OH) group of the expected pyrazine-1,3-dithiolene-2-thione was noticed in the obtained IR spectrum, indicating a reduction of the alcohol group possibly due to the interaction with boron trifluoride.

The ^{1}H-NMR spectrum of compound **14** was recorded in d_6-DMSO. Similar to IR data, no alcoholic (CH_2OH) proton signals were seen in the upfield region as expected for the pyrazine-1,3-dithiolene-2-thione. However, two unpredicted downfield signals were observed at 6.88 and 5.41-5.28 ppm, which were attributed to the methine (CH) and methylene (CH_2) protons of a reduced dithiolane moiety. The appearance of these signals suggests the unlikely reduction of dithiolene (alkene, C=C) to dithiolane (alkane, C-C). All of the aromatic protons were observed in the range of 8.73-8.63 ppm. The $^{13}C\{^{1}H\}$-NMR spectrum of **14** further supported the formation of the dithiolane moiety, as the presence of two signals at 64.8 and 49.8 ppm were assigned to the methine (CH) and methylene (CH_2) signals, respectively. The signal at 227.1 ppm corresponds to the

carbodithione group (C=S) of the dithiolane moiety. All signals for the aromatic carbons were observed in the range of 144.8-137.1 ppm. The obtained molecular mass value (212.9973 u) of compound **14** through High Resolution Mass Spectrometry (HRMS) was in good agreement with the calculated value (212.9693 u) based on the revised molecular formula of compound **14**.

The formation of the pyrazine-1,3-dithiolane-2-thione (**14**) was eventually also confirmed by X-ray crystal structure analysis of the yellow single crystals, which were obtained by the slow evaporation of chloroform. The atomic numbering scheme is shown in Figure 2.1 **A**. A summary of the crystallographic data collection and structural refinement parameters along with selected bond lengths and angles is listed in Appendices 6.1 and 6.3, respectively. The structure was solved in the orthorhombic space group *P2(1)2(1)2(1)* and contains four molecules in the unit cell and one independent molecule in the asymmetric unit (Figure 2.1 **B**). The planar pyrazine and dithiolane rings are linked by the C(3)-C(4) bond with a distance of 1.522(5) Å. The length of the C(2)-C(3) bond is 1.530(5) Å, which is consistent with the spectroscopic data and confirmed the reduction of the double bond (dithiolene) to a single bond (dithiolane).

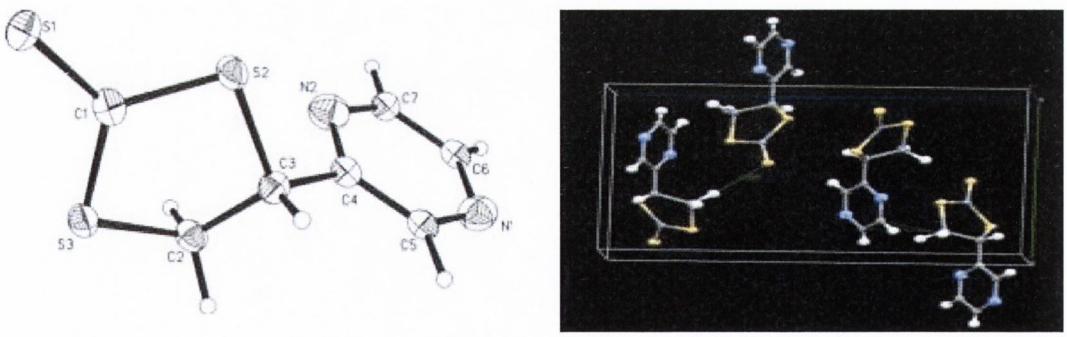

A **B**

Figure 2.1: The X-ray crystal structure of pyrazine-1,3-dithiolane-2-thione (**14**); **A**) the atomic numbering scheme, **B**) the unit cell diagram.

The bonds, which the sulfur atoms form with the doubly bonded carbon atoms are 1.815(4) Å for C(2)-S(3) and 1.838(4) Å for C(3)-S(2). The bond angles around the sulfur atoms are 98.25(19)° for C(2)-S(3)-C(1) and 98.20(19)° for C(3)-S(2)-C(1). These findings are in agreement with reported values for other dithiolene-derived ligands.[12,13] Another interesting feature in the crystal structure of compound **14** is the formation of an intermolecular interaction between the thionyl sulfur S(1) and the hydrogen of the dithiolane ring C(2) with a distance of 2.961(5) Å and an angle (C(1)-S(1)-S(3)) of 124.11(3)°.

The mechanism for the reduction of the double bond (dithiolene) to a single bond (dithiolane) is still not well understood. However, it seems feasible that firstly boron trifluoride etherate (Lewis acid) interacts with the pyrazine ring, in order to increase its electron withdrawing effect and as a result promotes the cycloaddition reaction between compound **13** and hydroxy-substituted alkynyl pyrazine (**3**). Then, boron trifluoride etherate somehow reduces the double bond of dithiolene-2-thione moiety by elimination of the alcoholic (CH_2OH) group, possibly due to interaction with boron trifluoride. In order to synthesise the desired pyrazine-1,3-dithiolene-2-thione, a number of attempts were made by varying the amounts of boron trifluoride etherate to avoid the reduction of the double bond as observed for compound **14**, but remained unsuccessful. Unfortunately, compound **14** could not be employed for further reaction to form *bis*-dithiolene pyrazine derived metal complexes, as the reduced dithiolene moiety would not support the formation of stable conjugated five membered metallacycle.

2.4 Synthesis and characterisation of a series of unexpectedly isolated pentathiepino-pyrrolo[1,2-a]-derivatives (15-18)

After failure of the first methodology for the synthesis of pyrazine-1,3-dithiolene compounds as a synthetic analogues of the MPT (molybdopterin) ligand in MoCo, it was thought to use another approach in which a direct route could be utilised to synthesise *bis*-dithiolene molybdenum complexes as models of MoCo. For instance, one literature report describes the reaction of highly electrophilic (electron deficient) alkynes

such as dicarbomethoxy-substituted alkynyl derivatives with molybdenum oxo *bis*-tetrasulfide, resulting in the formation of *bis*-dithiolene molybdenum complexes as shown in Figure 2.2.[14] Using this approach, the synthesised hydroxy-substituted alkynyl pyrazine (**3**) and quinoxaline (**4**) compounds were reacted with $[(Et_4N)_2[MoO(S_4)_2]$,4 to form their respective *bis*-dithiolene molybdenum complexes **3a** and **4a**.

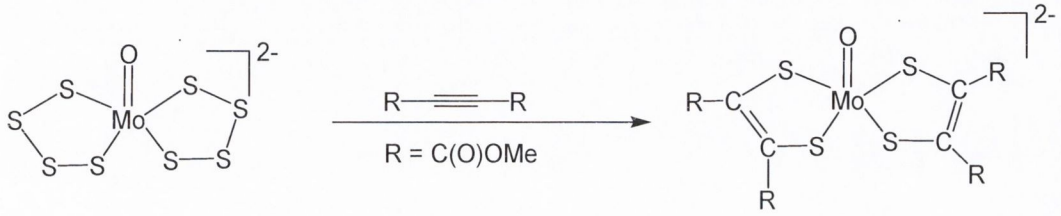

Figure 2.2: Dicarbomethoxy derived *bis*-dithiolene molybdenum complex.[14]

Unfortunately, no reactions could be observed with **3** and **4** (as described in Scheme 2.4), as the isolated red crystals were characterised to be molybdenum precursor, instead of the desired molybdenum complexes **3a** and **4a**. This was not entirely unanticipated as Donahue *et al.* already found that $[(Et_4N)_2[MoO(S_4)_2]$ may not react with weakly activated alkynes or acetylenes itself.[15] It was concluded that hydroxy-substituted alkynes **3** and **4** would not be sufficiently electron deficient to proceed the reaction in a forward direction. In order to obtain more electron deficient alkyne derivatives, the hydroxy-substituents and protons were replaced by ethoxy-groups. Consequently, compounds **9-12** were synthesised and fully characterised (as described earlier in Section 2.2). In a further attempt to develop synthetic models of MoCo, the electron deficient ethoxy-substituted alkynyl compound **9** was then reacted with the molybdenum precursor $[(Et_4N)_2[MoO(S_4)_2]$ in DMF. The reaction mixture was heated to 50-60 °C for 2 hrs to form the respective molybdenum complex but no change in reaction was observed by thin layer chromatography. A number of attempts were made under increasingly harsh reaction conditions such as high temperature, long reaction times and use of excess amount of molybdenum precursor. No change in the reaction between starting materials could be detected. Only in the case when a rather old batch of the molybdenum precursor was used, a transformation of the reaction mixture could be observed and afforded red crystals suitable for single X-ray structural analysis. X-ray

studies revealed the formation of an unexpected heterocyclic pentathiepino-pyrrolo[1,2-*a*]-quinoxaline (**15**) instead of the desired molybdenum complex. Whilst, it was not our intention to synthesise a pentathiepin, to the best of our knowledge a novel and interesting compound was unexpectedly found.[16] After several attempts to reproduce this result, it was concluded that this reaction only proceed in the presence of elemental sulfur, with which the old batch of molybdenum starting precursor had been contaminated. Both molybdenum oxo *bis*-tetrasulfide and elemental sulfur are equally important for the advancement of this reaction. In order to make other pentathiepin derivatives, the ethoxy-substituted alkynyl quinoxaline (**10-11**) and pyrazine (**12**) derivatives were reacted with the molybdenum precursor and elemental sulfur to form their corresponding quinoxaline (**16-17**) and pyrazine (**18**) based novel pentathiepino-pyrrolo[1,2-*a*]-compounds. The overall synthetic route to obtain these novel pentathiepin compounds is shown in Scheme 2.4.

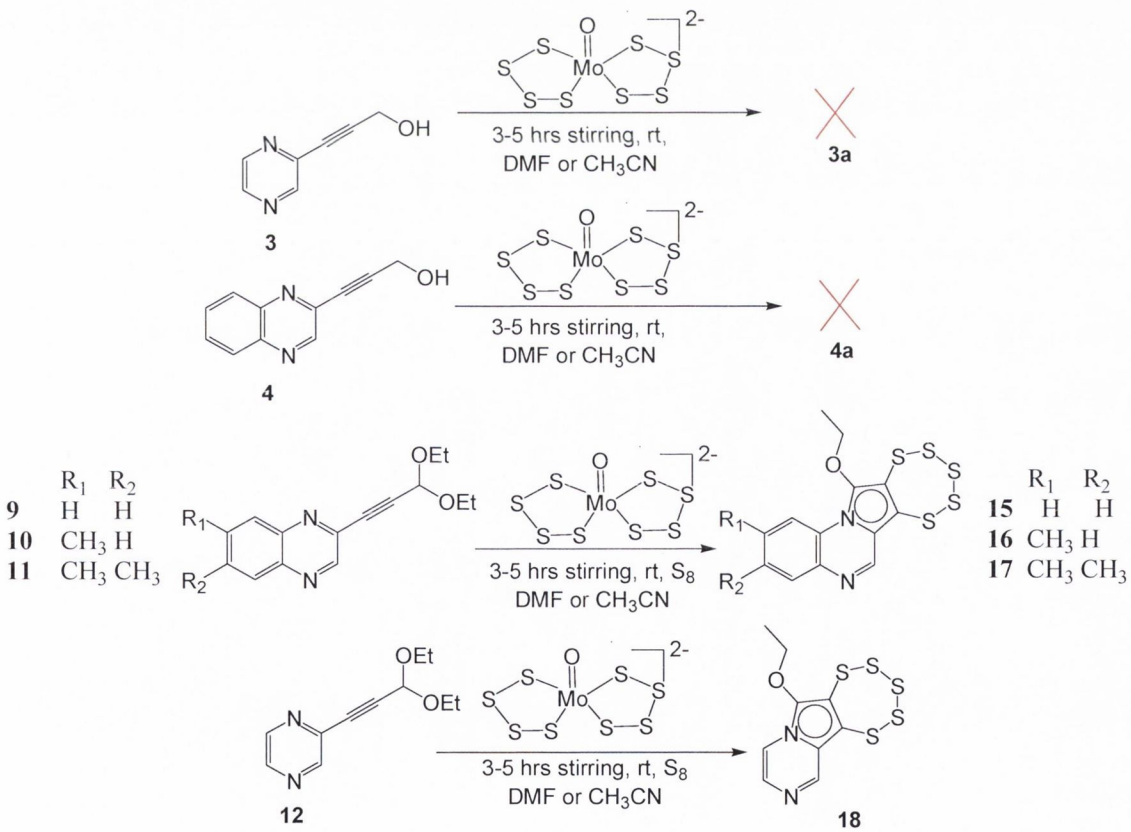

Scheme 2.4: Synthesis of a series of novel pentathiepino-pyrrolo[1,2-*a*]-quinoxaline (**15-17**) and pyrazine (**18**) derivatives.[16]

The suggested mechanism for the synthesis of pentathiepino-pyrrolo[1,2-*a*]-pyrazine (**18**) (which is relevant for all investigated syntheses of pentathiepins) is illustrated in Scheme 2.5. The first step involves the loss of one ethoxy group from the diethoxy functionality promoted by coordination to the molybdenum precursor, to produce an ethoxonium ion (EtO^+). In the next step, a $^-S..S_3..S^+$ zwitterion formed from S_8 (possibly again promoted by molybdenum), adds along the alkynyl moiety which results in the formation of a stable pentathiepin ring adjacent to the pyrazine ring.

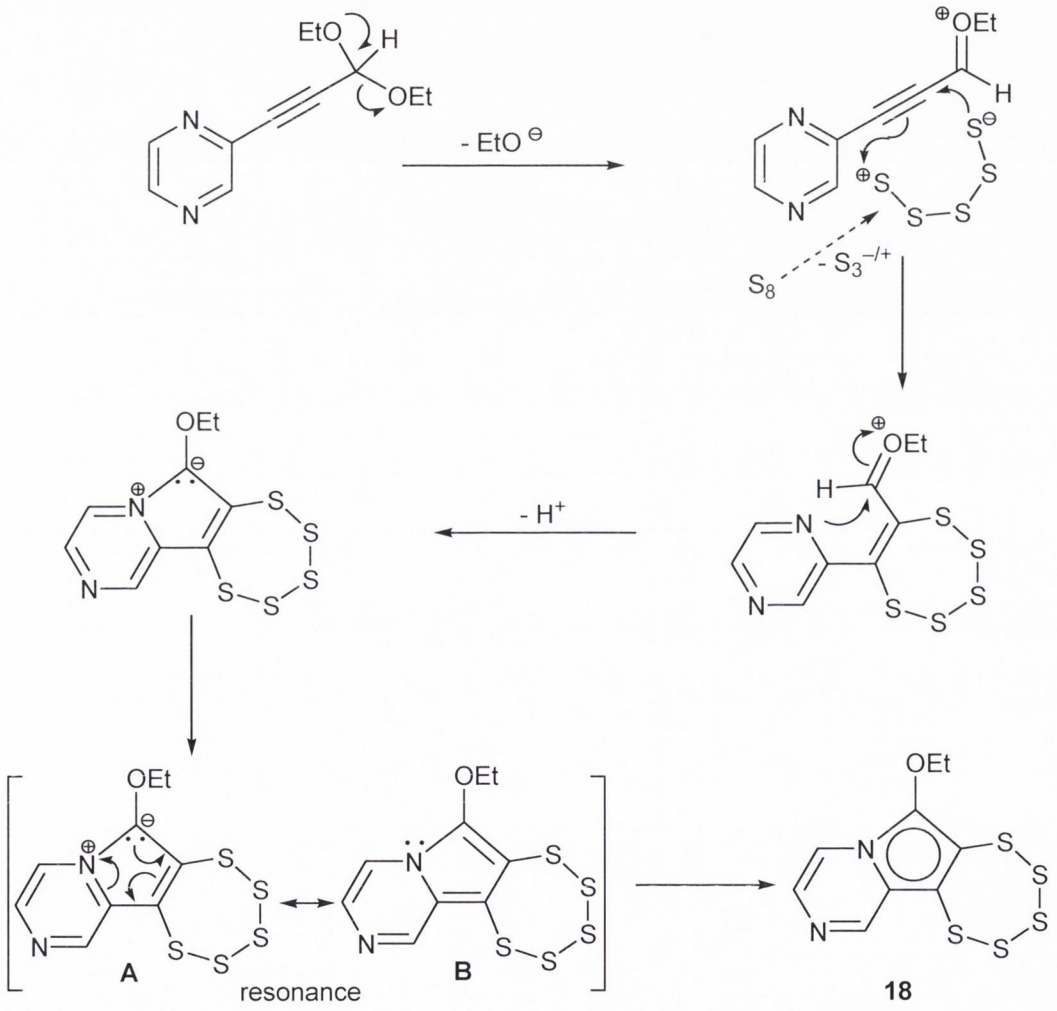

Scheme 2.5: The proposed mechanism for the synthesis of novel pentathiepino-pyrrolo[1,2-*a*]-pyrazine (**18**).[16]

Subsequently, a re-orientation of the pyrazine takes place. When its nitrogen atom is adjacent to the carbon atom (bearing the ethoxonium ion), the nitrogen lone pair attacks this carbon to form the C-N bond. This intramolecular cyclisation generates a five-membered pyrrole-like ring fused to the pyrazine ring. This results in the formation of an ammonium ion, which after deprotonation of the molecule favours the key resonance steps (**A** and **B**) to facilitate the aromatisation of the pyrrole like ring. As a result, the stable pentathiepin compound **18** is generated. The key resonance structures **A** and **B** are shown in Scheme 2.5.

In the deprotonation step, the combination of H^+ and EtO^- results in the formation of ethanol as side product. The initial generation of the ethoxonium ion, which is in fact responsible for the construction of the pyrrole ring fused in between the pyrazine and pentathiepin, describes the lack of ability of compounds **3** and **4** having a hydroxyl (OH) group instead of ethoxy (OEt) group, to react in a similar way. According to the proposed mechanism the hydroxyl (OH) group would not be able to activate the formation of a positively charged oxygen function.

In initial studies, pentathiepino-pyrrolo[1,2-*a*]-quinoxaline (**15-17**) and pyrazine (**18**) derivatives formation reactions were carried out in DMF and the obtained products were precipitated out by iso-propanol with only low yield, when 1:10 ratios of elemental sulfur and alkynyl-substituted pyrazine and quinoxaline derivatives were used. The proposed mechanism, however, requires the key involvement of elemental sulfur in the formation of the pentathiepin ring and the reaction conditions were further refined by employing a number of test reactions.

In order to optimise the reaction conditions, the amounts of molybdenum oxo *bis*-tetrasulfides and elemental sulfur were varied. The reaction conditions and yields for the most significant test reactions are summarised in Table 2.1. For all active alkynes (**9-12**) it was found that 0.5 equivalents of molybdenum oxo *bis*-tetrasulfides gave the best results. No significant reaction could be observed, if less than 0.5 equivalents of molybdenum oxo *bis*-tetrasulfides were used. This is a strong indication that the

molybdenum compound does not act as a catalyst but is in fact used during the reaction. Secondly, the amount of elemental sulfur was optimised. With raised amounts of sulfur the yields increased (27-37%) and the use of approximately 1 equivalent of sulfur gave the best results. However, column chromatography is required to isolate the pure compound. Lastly, changing the solvent from DMF to acetonitrile gave the desired pentathiepins in reliably good overall yields of 57-68%.

Table 1.1: Ratio of ethoxy-substituted alkynyl quinoxaline (**9-11**) and pyrazine (**12**) versus yields of pentathiepino-pyrrolo[1,2-*a*]-quinoxaline (**15-17**) and pyrazine (**18**) derivatives.[16]

Alkyne reactant	No.	Molar Ratio Alkyne:Mo:S_8	Yield(%)		Product
			DMF	CH_3CN	
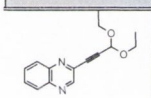 (**9**)	1	1 : 0.5 : 0.1	8	-	 (**15**)
	2	1 : 0.5 : 1	27	-	
	3	1 : 0.5 : 1	-	57	
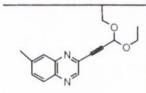 (**10**)	1	1 : 0.5 : 0.1	15	-	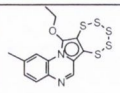 (**16**)
	2	1 : 0.5 : 1	37	-	
	3	1 : 0.5 : 1	-	68	
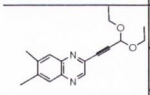 (**11**)	1	1 : 0.5 : 0.1	12	-	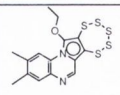 (**17**)
	2	1 : 0.5 : 1	33	-	
	3	1 : 0.5 : 1	-	67	
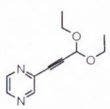 (**12**)	1	1 : 0.5 : 0.1	9	-	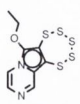 (**18**)
	2	1 : 0.5 : 1	32	-	
	3	1 : 0.5 : 1	-	63	

Once the general reaction conditions were established, then the potential activity of other molybdenum complexes to form pentathiepins was investigated. Different readily available molybdenum precursors such as molybdenum(IV) oxide and molybdic acid were used. No significant reactions could be observed and no traces of the pentathiepins were detected in the reaction mixtures. These findings suggest that the molybdenum oxo

bis-tetrasulfides is not only responsible for abstracting EtO^- from the alkyne precursor but is also involved in processing the sulfur chains and atoms.

The melting point values for compounds **15-18** were found to be in the range of 150-267 °C. Compound **15** has a lower melting point temperature (205-206 °C) compared to that of **16** (245-246 °C) and **17** (266-267 °C), highlighting the effect of methyl substituents present on the quinoxaline ring. Moreover, the replacement of quinoxaline with a pyrazine ring in compound **18** resulted in a decreased melting point temperature (150-151 °C).

In the IR spectra of compounds **15-18**, the appearance of characteristic medium intensity bands in the range of 784-742 cm^{-1} were noticeable and were assigned to the stretching vibrations of the carbon-sulfur bonds υ(C-S) of the fused pyrrole-pentathiepins. Literature reports have indicated that these stretching vibrations υ(C-S) of benzo-pentathiepins are normally in the range of 780-740 cm^{-1}.[17,18] In addition, the disappearance of the υ(C≡C) stretching vibration of alkynyl in the IR spectra of all pentathiepin compounds strongly supported the formation of the pentathiepins. Moreover, the bands around 1017-997 cm^{-1} and 1548-1521 cm^{-1} were ascribed to the ether moiety (C-O) of the ethoxy functionality and υ(C=N) of the pyrazine ring, respectively.

The ^{1}H-NMR spectra of pentathiepin compounds (**15-18**) were recorded in d_6-DMSO as well as $CDCl_3$. The most downfield characteristic sharp singlet in the range of 8.88-8.39 ppm was observed for all pentathiepin compounds which was assigned to the (CH=N) moiety of the aromatic ring, while the multiplets of other aromatic protons were observed in the range of 8.56-7.00 ppm. The most upfield signal around 1.60-1.42 ppm was ascribed to the protons of the methyl group while the downfield multiplets in between 4.80-4.58 ppm were attributed to the methylene (CH_2) protons of the ethoxy moiety. The $^{13}C\{^1H\}$-NMR spectra of pentathiepin compounds (**15-18**) showed all of the aromatic carbons in the range of 146.3-128.8 ppm. The measured molecular mass values for the novel pentathiepin compounds (**15-18**) were consistent with the calculated values based on molecular formulae (see Section 2.7.5 for details).

The formation of the tetracyclic pentathiepino-pyrrolo[1,2-*a*]-quinoxaline compound (**15**) was further confirmed by X-ray crystal structure analysis of dark red single crystals, which were obtained by the addition of an acetonitrile and diethyl ether (1:3) mixture to a DMF solution. The atomic numbering scheme is shown in Figure 2.3. A summary of the crystallographic data collection and structural refinement parameters along with selected bond lengths and angles for compound **15** are listed in Appendices 6.2 and 6.4, respectively. The structure of compound **15** was solved in the monoclinic space group *P* $2_1/n$.

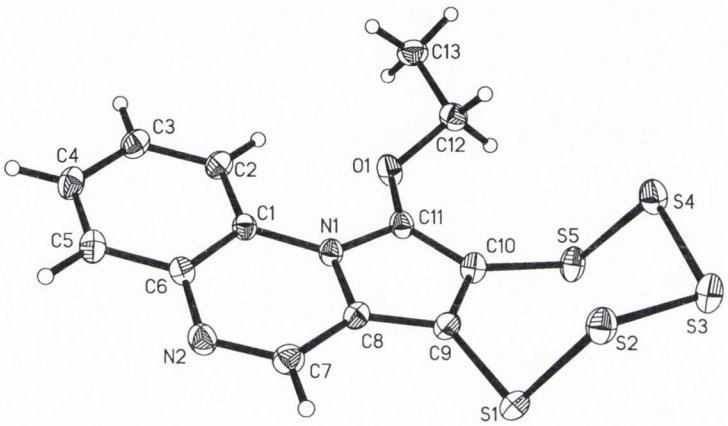

Figure 2.3: X-ray structure and atomic numbering scheme for pentathiepino-pyrrolo[1,2-*a*]-quinoxaline (**15**).[16]

Compound **15** contains four molecules in the unit cell and one independent molecule in the asymmetric unit. The bond lengths and bond angles of S-S bonds in compound **15** were observed as averages of 2.06(10) Å and 104(4)°, respectively. Similar results for the bond lengths and bond angles of S-S bonds for S_6 as well as S_8 were reported as 2.05 Å and 102° as well as 2.05 Å and 108°, respectively.[18] From these observations, it can be concluded that the stability and reactivity of the pentathiepin moiety in compound **15** should be similar to S_8.

The three aromatic rings are almost perfectly planar and, furthermore, are all coplanar throughout the whole crystal lattice. The sulfur atoms are involved in non-classical intermolecular hydrogen bonding with aromatic protons (S···H: 2.87(3) – 3.27Å). N1, the nitrogen atom being part of the pyrazine and the pyrrole rings is weakly hydrogen

bonded to a methyl proton (N···H: 2.85(3) Å). Hydrogen bonding generally takes place between different planes formed by the aromatic ring systems not within a plane. An interesting feature of the crystal structure of compound **15** is the formation of the chair confirmation of the S_5 ring with approximate S-S bond lengths of 2.06(10) Å. The consistency of the S-S (≈ 2.05 Å) bond lengths within benzo-pentathiepins has previously been pointed out by Chenard *et al.*[18] The crystal packing diagram shows that molecules of **15** aggregate in 1-D chains along the *a*-axis *via* π-π stacking interactions, S-S interactions and strong hydrogen bonding S-H interactions (Figure 2.4 **A**). There are two pairs of methylene C-H...π offset interactions which are C(3)-H(3)...π [(N(1)-C(8)-C(9)-C(10)-C(11))] and C(4)-H(4)... π [(N(1)-C(8)-C(9)-C(10)-C(11))]. The distances of H(3) or H(4) to the centre of the adjacent aromatic ring [(N(1)-C(8)-C(9)-C(10)-C(11))] are 3.62(3) Å and 3.36(3) Å, respectively. Figure 2.5 **A** shows the packing of **15** in a 1-D chain being facilitated by strong hydrogen bonds between S(3) and H(13). The distance and angle (C(13)-H(13)-S(3)) of this hydrogen bond are 2.98(5) Å and 119(3)°, respectively. These 1-D chains are packed and arranged in a parallel manner, to form 2-D sheets, through π-π stacking interactions, S-S interactions and strong hydrogen bonding S-H interactions between the adjacent molecules of **15** (Figure 2.4 **B**).

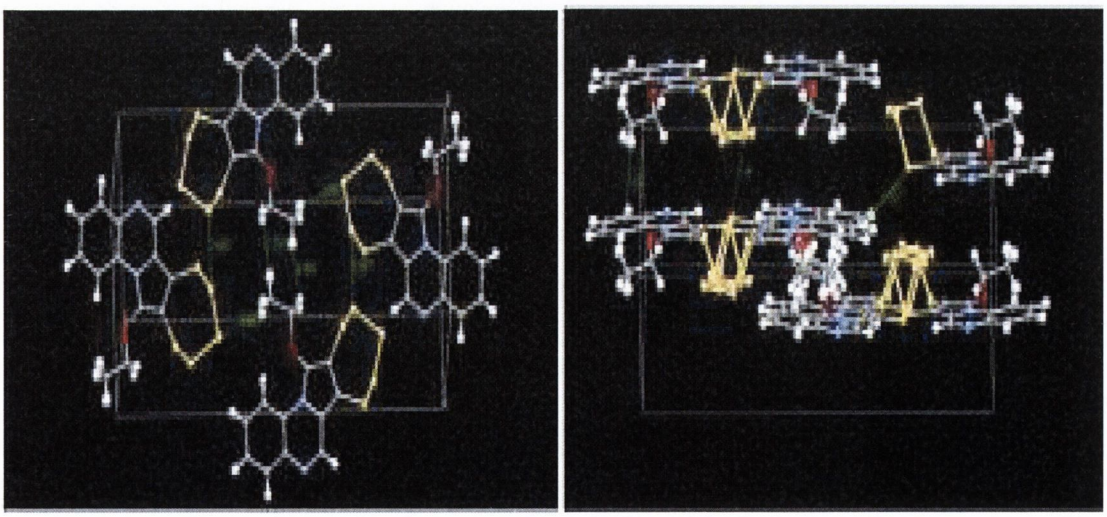

A **B**

Figure 2.4: The crystal packing diagram of the quinoxaline-derived tetracyclic pentathiepin (**15**): (**A**) 1-D chain along the *a*-axis and (**B**) 2-D chain perspective.

In summary, this section details the synthesis and characterisation of hydroxyl (**3-4**) and ethoxy (**9-12**)-substituted alkynyl derivatives. This study also describes the unsuccessful attempt to synthesise the pyrazine-1,3-dithiolene-2-thione ligand, which resulted in the formation of the reduced pyrazine-1,3-dithiolane-2-thione compound (**14**). A number of other methodologies were also described to synthesise the pyrazine derived dithiolene ligand and its respective metal complexes as models for the naturally occurring molybdenum enzymes. During the attempts to synthesise the target model complexes, novel heterocyclic pentathiepino-pyrrolo[1,2-*a*]-derivatives (**15-18**) were isolated unexpectedly and fully characterised. Furthermore, chemical structures for all synthesised compounds were confirmed based on spectroscopic as well as HRMS data obtained along with X-ray structural analysis (where possible). The presence of pentathiepins in natural products and their proven bioactivity prompted us to screen these novel pentathiepin compounds for their potential biological activities which are discussed in Section 2.5.

2.5 Biological evaluation of novel pentathiepino-pyrrolo[1,2-a]-derivatives (15-18)

A broad spectrum of biological activity has been reported for a number of naturally occurring pentathiepins.[19,20,21] Studies have shown that the presence of the S_5 ring is crucial for the biological activity of such pentathiepin derivatives.[21] Moreover, naturally occurring S_5 ring based drugs comprise an important area of research in which interest is rapidly growing because of their enormous pharmacological application potential. In the last few years, a number of pentathiepin based compounds have been reported to possess DNA (deoxyribonucleic acid) binding, anti-microbial and anti-cancer activities.[19,22,23]

In the present study, a series of novel pentathiepino-pyrrolo[1,2-*a*]-quinoxaline (**15-17**) and pyrazine (**18**) derivatives were prepared unexpectedly and fully characterised (described in Section 2.4). After learning about the interesting biological applications of pentathiepins from literature studies, it was decided to investigate the bioactivity of the synthesised pentathiepin compounds. Firstly, DNA binding studies for the pentathiepin derivatives were carried out using ultra pure calf thymus DNA. These studies were performed by Dr. Kellett's group, School of Chemical Sciences, Dublin City University. Secondly, anti-cancer screening for novel pentathiepin derivatives was carried out against various cancer cell lines by Prof. Bednarski's group, at Institute of Pharmaceutical Biology, Ernst-Moritz-Arndt-University Greifswald.

2.5.1 DNA binding studies for novel pentathiepino-pyrrolo[1,2-a]-derivatives (15-18)

2.5.1.1 Introduction to DNA

DNA is present in all small and large living organisms, being the most complex structure which scientists are still trying to understand. The complexity arises due to the fact that the DNA in the human haploid genome (the total genetic message) is made up of $3x10^9$ base pairs.[24] DNA is responsible for the maintenance of the species; it transfers from one generation to the next in germ cells.[25] It also carries the information to enable

all proteins required for the operation of biological systems to be synthesised. A number of different conformations of double helical DNA can be formed by rotating various bonds.[25] The structures of A-DNA, B-DNA and Z-DNA are shown in Figure 2.5. DNA under physiological conditions is generally assumed to be in a B-DNA conformation.[24]

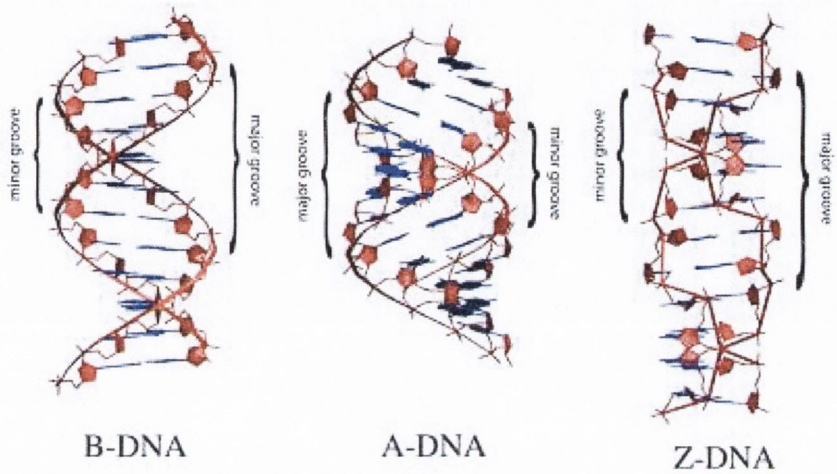

Figure 2.5: Double helical structures of B, A and Z-DNA, showing major and minor grooves.[26]

There are a number of ways in which a compound, can interact with the poly anionic B-DNA, which include;[25,27]

(i) major or minor groove binding: Arrangement of the double helix is such that there are two distinguishable grooves running the length of the DNA: the major and the minor grooves. For B-DNA, the major groove has a width of ~12 Å and a depth of ~80 Å; the minor groove of 6 Å and 8 Å, respectively.[25] This means that only thin molecules, that can twist and interact with the minor groove whereas much larger molecules can interact with the major groove. The difference between binding in the major and minor groove is due to hydrogen bonding characteristics, electrostatic potential, solvation and steric effects of the compound in combination with the DNA. Hydrogen bonding is fundamental in the recognition of target binding sites.

(ii) intercalation: A planar, most often aromatic molecule slips between the base pairs (into a hydrophobic environment) and leads to unwinding of the DNA.

2.5.1.2 Determination of DNA binding properties

In the present study, four different assays were employed to evaluate the interaction of heterocyclic pentathiepino-pyrrolo[1,2-*a*]-quinoxaline (**15-17**) and pyrazine (**18**) compounds with DNA. The DNA binding constant value is determined using a competitive ethidium bromide (EtB) displacement experiment with high-purity calf thymus DNA (CT-DNA). It has been previously reported that EtB is an efficient DNA intercalator and its interaction with DNA makes Et-DNA solution highly fluorescent.[28,29] Thus, the reduction of fluorescence suggests the replacement of Et^+ from the DNA, by the test sample.[30,31] More commonly, the competitive ethidium bromide (EtB) displacement method has been used by a number of groups to calculate the binding constant values for tested compounds, along with commercially available compounds which are highly efficient in the displacement of the Et^+ from the DNA.[28,29,32] In order to establish an apparent DNA binding constant (K_{app}) a sample of high purity CT-DNA was freshly treated with an excess ethidium bromide (EtB) and then this highly fluorescent Et^+-saturated DNA sample was exposed to range of concentrations of tested compounds. Figure 2.6 shows the graphical representation of DNA binding affinities evaluated for commercial drugs (pentamidine and netropsin) and tested pentathiepin compounds (**15-18**). These graphs were plotted in % fluorescence per compound or tested drug concentration and were used to calculate the respective C_{50} values (concentration of the sample that is required to inhibit the initial fluorescence by 50%). DNA binding affinities are reported in terms of the binding constant (K_{app}) values and are calculated based on C_{50} values. The greater the binding constant (K_{app}) value, the greater the interaction the compound has with the DNA. The protocol used in this work is described in Section 2.8.1.[32] The results for the novel pentathiepin compounds (**15-18**) and those for commercial compounds are summarised in Table 2.2. All tested compounds were found to have significant binding constant values (1.98-2.29 x 10^6) towards DNA. The known commercial DNA targeting compounds were also examined in parallel and their relevant binding constant values were calculated as ~1.09 x 10^6 and 2.99 x 10^6 for pentamidine and netropsin, respectively. Comparison reveals that all of tested pentathiepin compounds were found to have stronger binding affinities to DNA

compared to that of the known commercially used compound pentamidine, suggesting stronger electrostatic interactions of pentathiepins towards DNA. However, pentathiepin compounds exhibited lower binding affinities than other commercially known groove binding drug, netropsin (2.99×10^6). Moreover, the binding affinities of pentathiepin derivatives towards DNA give an insight to investigate the potential antitumor activities of these compounds and are discussed in Section 2.5.2.2.

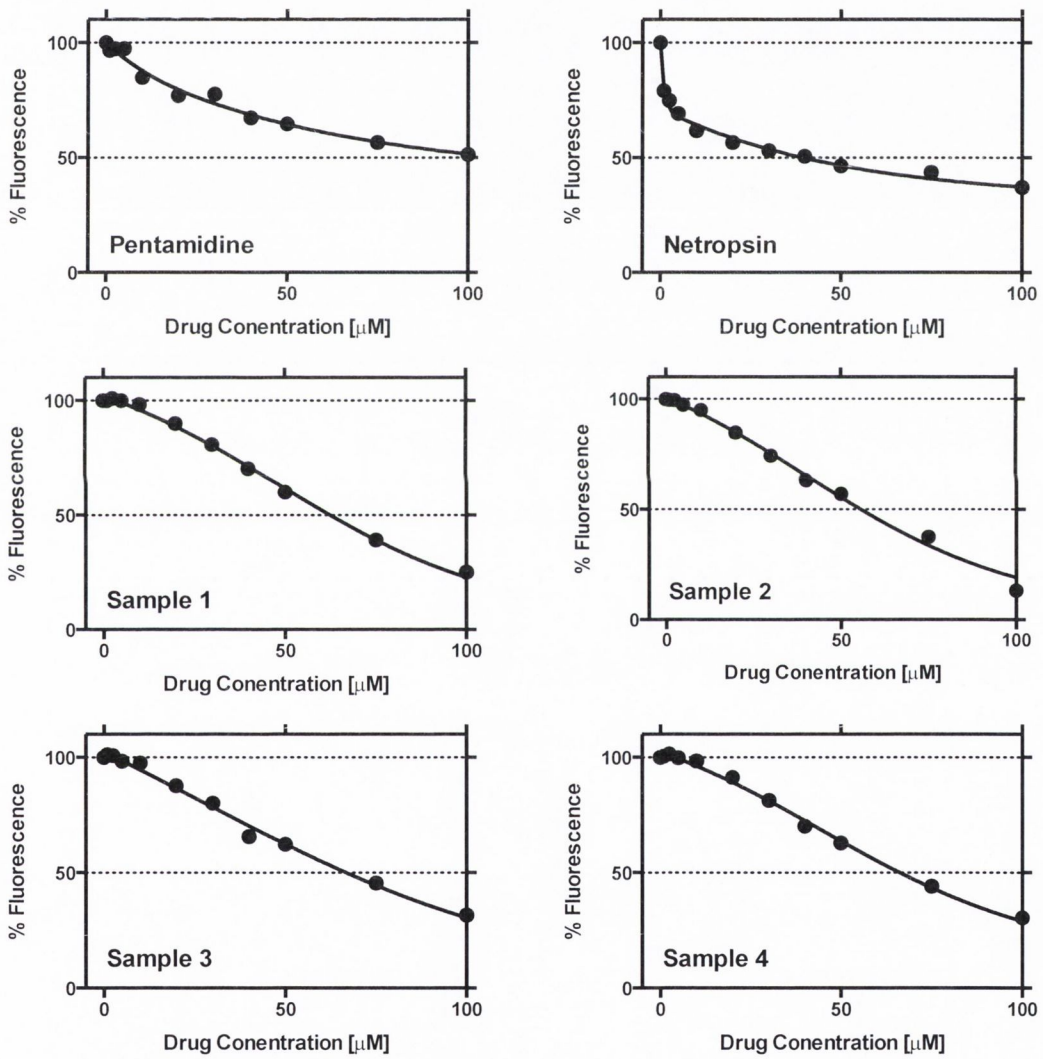

Figure 2.6: Competitive fluorescence quenching of ethidium bromide (12.6 μM) bound to CT-DNA (10 ⌈M in DNA) by DNA binding drugs and pentathiepin compounds **15-18**. Data points are shown as an average of triplicate measurement.

Table 2.2: Determined CT-DNA binding constant (K_{app}) values using competitive ethidium bromide binding for compounds **15-18**, along with commercial drugs pentamidine and netropsin.

Compound Codes	Samples	C_{50} (μM)	K_{app} (M^{-1})
15	1	60.97	1.98×10^6
16	2	57.97	2.06×10^6
17	3	52.24	2.29×10^6
18	4	56.09	2.13×10^6
pentamidine		109.41	1.09×10^6
netropsin		39.99	2.99×10^6

C_{50} = concentration required to reduce fluorescence by 50%; $K_{app} = K_e \times 12.6/C_{50}$ where 12.6 = concentration of EtBr and $K_e = 9.5 \times 10^6\ M^{-1}$.

In an effort to further elucidate the DNA binding mode of pentathiepin compounds **15-18**, fluorescence quenching (Q values) experiments were conducted using competitive displacement of DNA bound Hoechst 33258 (minor groove binder) and ethidium cations (Et^+, intercalator). In this study, the introduction of the tested compound may then displace either Et^+ or Hoechst and can give valuable information regarding the binding mode of the test compound with DNA.[30] Figure 2.7 shows the plot of % fluorescence against drug concentration for all of the tested pentathiepin compounds. These graphs are used to calculate the Q values (displacement of 50% initial fluorescence from DNA-bound dye) for each tested compound along with commercial minor groove binding drugs and are summarised in Table 2.3. All novel pentathiepins **15-18** showed high Q values for Hoechst 33258, compared to those of ethidium cation quenching, suggesting the pentathiepins to be preferential minor groove binders. The Q values towards Hoechst 33258 for all pentathiepin derivatives were in the range of ~ 50.79-57.97 μM, *i.e.* nearly as active as pentamidine (35.6 μM). However, netropsin showed a considerably higher Q value (3.50 μM) than all tested pentathiepin compounds.

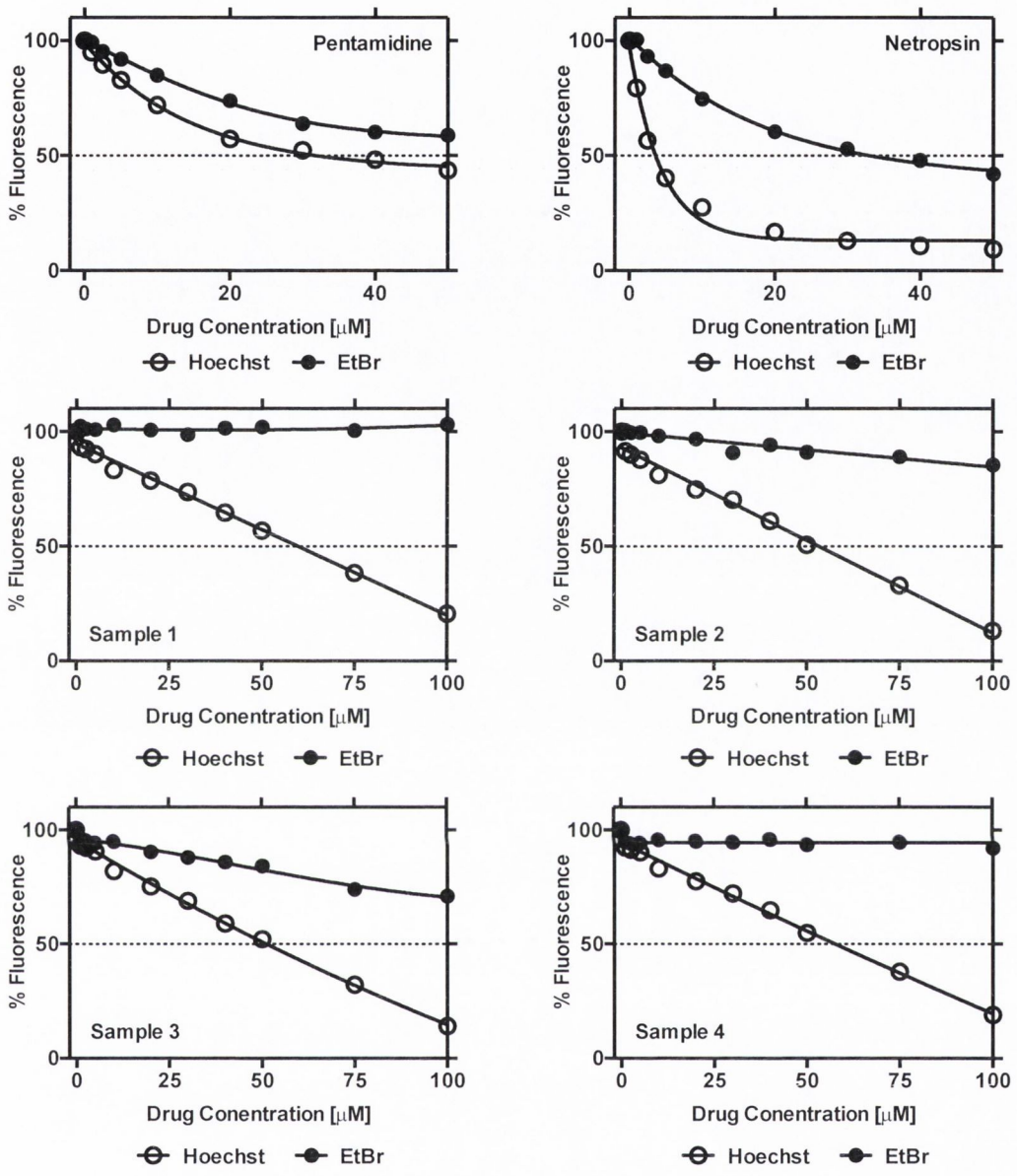

Figure 2.7: Fluorescence quenching of bound intercalator (ethidium) or minor groove binder (Hoechst 33258) (5 μM) on CT-DNA (25 μM in DNA) by DNA binding drugs, pentamidine and netropsin along with tested samples. Data points are shown as an average of triplicate measurement.

Table 2.3: Fluorescence quenching (Q) values obtained against CT-DNA bound by Hoechst 33258 (groove binder) or ethidium bromide (intercalator) for pentathiepin compounds **15-18** along with pentamidine and netropsin.

Compound Codes	Samples	Q [Hoechst 33258 (μM)]	Q [Ethidium Bromide (μM)]	η/η_o
15	1	57.97	>>150	0.98
16	2	50.79	>>150	0.96
17	3	52.24	>>150	0.98
18	4	56.09	>>150	0.95
pentamidine		35.86	>150	0.987
netropsin		3.50	35.98	1.007

Q = displacement of 50% initial fluorescence from DNA-bound dye; η/η_o relative viscosity, where η_o and η refers to viscosity of each DNA working sample in the absence and presence of tested compound and [drug]/[DNA] ratio r = 0.20.

Further confirmation of pentathiepin compounds **15-18** to be minor groove binders was obtained by viscosity experiments. Studies have suggested that intercalating agents can increase the viscosity due to a conformational change of the DNA induced after accommodation of the drug between DNA bases. However, surface binding species have shown very little effect on the viscosity.[32] It can be seen from Figure 2.8 that all of the pentathiepin compounds **15-18** as well as commercially known compounds (*i.e.* pentamidine and netropsin) showed no considerable change in viscosity. These results were consistent with the above mentioned studies and further supported the potential binding mode of the tested pentathiepin compounds and commercially known drugs towards DNA to be minor groove binding species.

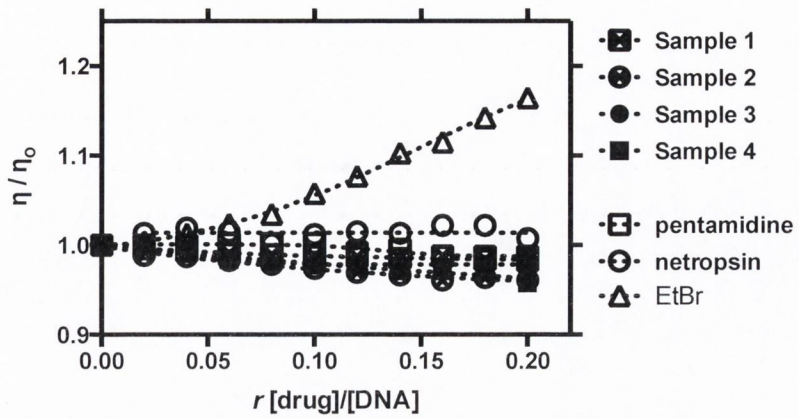

Figure 2.8: Viscosity data from the standard DNA interacting drugs and tested samples on salmon testes dsDNA (Deoxyribonucleic acid sodium salt from Salmon Testes, Sigma-Aldrich, D1626- 1G) from salmon testes).

In summary, three different assays were used to evaluate the pentathiepins DNA binding mode. On the basis of these studies, the data obtained confirmed that these pentathiepin compounds do not intercalate, but bind to the surface of DNA as minor groove binding agents. Consequently, the DNA binding mode results were found to be interesting and further encouraged us to test these compounds for their potential activity against cancer cell lines. The investigation of the activities of these compounds against various cancer cell lines is discussed in Section 2.5.2.

2.5.2 Anti-cancer screening of novel pentathiepino-pyrrolo[1,2-a]-derivatives (15-18)

2.5.2.1 Introduction to cancer

Cancer is one of the most serious health problem worldwide, affecting individuals from different sexes, ages, and races. It comprises a group of diseases, characterised by uncontrolled cellular growth with frequent cancer cells invasion to different body parts and spreading to other organs, a process referred to as Metastasis.[33,34] Metastasis is the major cause of cancer related mortality. Cancer is a heterogeneous illness which can originate from many different organs of the human body. However, some important

frequent types in the world are lung, bladder, ovarian, breast, and cervical cancers *etc*. For example a large cell carcinoma in the lung is shown in Figure 2.9.

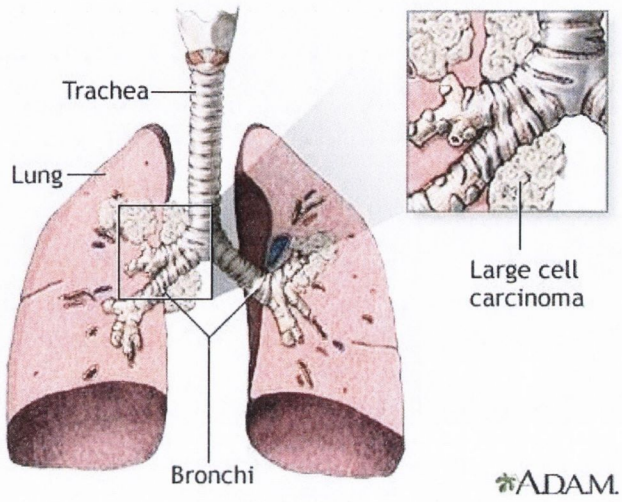

Figure 2.9: An example of lung cell carcinoma.[35]

Several strategies have been developed to cure cancer among which the most common ones are surgery, chemotherapy (drug therapy) and radiotherapy.[36] All of these therapies have undesired side effects, they are usually not available all the time and they are expensive.

One of the main methods of modern cancer treatment is drug therapy (chemotherapy).[37] The majority of drugs used for the treatment of cancer today are cytotoxic (cell-killing) drugs that work by interfering in some way with the operation of the DNA in the cells.[38] Cytotoxic drugs have the potential to be very harmful to the body unless they are very specific to cancer cells. Therefore, it is difficult to reduce side effects because the modifications that change a healthy cell into a cancerous one are very subtle.[38] Conventional drug therapies failed to completely fulfil the criteria for a successful cancer therapy yet. Thus, a major challenge is to design and synthesise more effective and selective anti-cancer agents that should act as an alternative being more selective for cancer cells, safer and low in cost than presently known commercial drugs.

2.5.2.2 Determination of anti-cancer activities of pentathiepino-pyrrolo[1,2-a]-derivatives (15-18)

Potential DNA binding properties of pentathiepin compounds inspired us to investigate these compounds for their possible activities against cancer cells using established protocols by Bednarski *et al.* (Section 2.8.2). This section describes the screening of all pentathiepins **15-18** for their potential activities towards a panel of selected cancer cell lines; ovarian cancer (A2780), bladder carcinoma (5637), cervix carcinoma (SISo) and lung cell carcinoma (LCLC) (obtained from the German Collection of Microorganisms and Cell Cultures). The results were compared with most of the clinically used anti-cancer agents such as carboplatin and cisplatin, highlighting the clinical potential of the novel pentathiepins. In a primary screening, it was found that three of the compounds were active against four cancer cell lines in micromolar concentration, however, compound **15** showed less activity, mainly due to some solubility problems. The activities are illustrated in Figure 2.10. A value of 0 means no change occurred with respect to cell numbers at time 0. A value of 1 means that the number of cells were identical to the number of cells in control experiment after 96 hrs (*i.e.* no activity). A value below 0 indicates that not only growth was inhibited but also the number of cells had declined. It can be clearly seen that the tested compounds showed greater activity against three of the cancer cell lines, but only against the SISo results were less encouraging. The primary tests were then repeated for selected compounds at lower concentrations (5 μM) for all cancer cell lines. As expected the activities were decreased but still apparent.

In the secondary screening, the three promising pentathiepin compounds (**16-18**) were further investigated for their concentration dependent activities. The average GI_{50} values were calculated from the dose-response data curves from three independent experiments as shown in Figure 2.11. Activities are reported in terms of GI_{50} values, which is the concentration that is required to inhibit growth by 50%. The smaller the GI_{50} value, the greater the compound activity. Table 2.4 shows the results of the anti-cancer screening of the pentathiepin compounds (**16-18**) that were compared with widely used anti-cancer

drugs such as cisplatin and carboplatin.

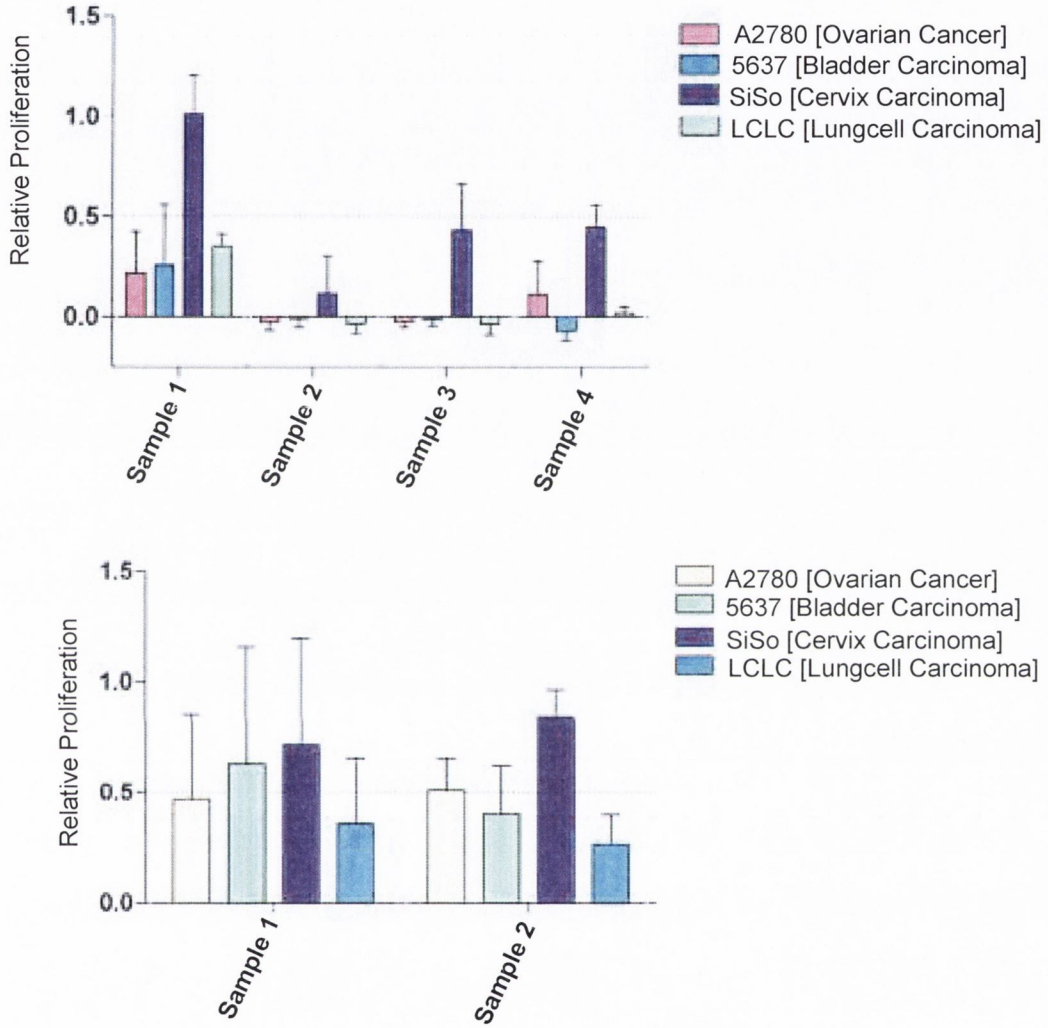

Figure 2.10: The primary screening of the pentathiepin compounds **15-18** at concentration 20 μM (top); repeated primary tests against selected compounds **15-16** at lower concentration (5 μM) (bottom); against panel of four cancer cell lines. Sample 1 (**15**), Sample 2 (**16**), Sample 3 (**17**) and Sample 4 (**18**).

The obtained data show that the tested pentathiepin compounds (**16-18**) exhibit activity against all tested cancer cell lines. The most significant result was obtained against A2780, where the compound with a dimethyl substituent at the quinoxaline ring (**17**) exhibited the greatest activity, 1.70 μM, whereas the presence of only one methyl

substituent at the same ring (**16**) resulted in decreased activity, 2.73 μM. An opposite trend was observed in the case of cancer cell line LCLC, where the compound **16** showed greater activity (2.46 μM), compared to **17** (5.01 μM). Compound **17** was also found to be active, with GI_{50} values of 4.69 μM and 4.44 μM towards 5637 and SISo cell lines, respectively.

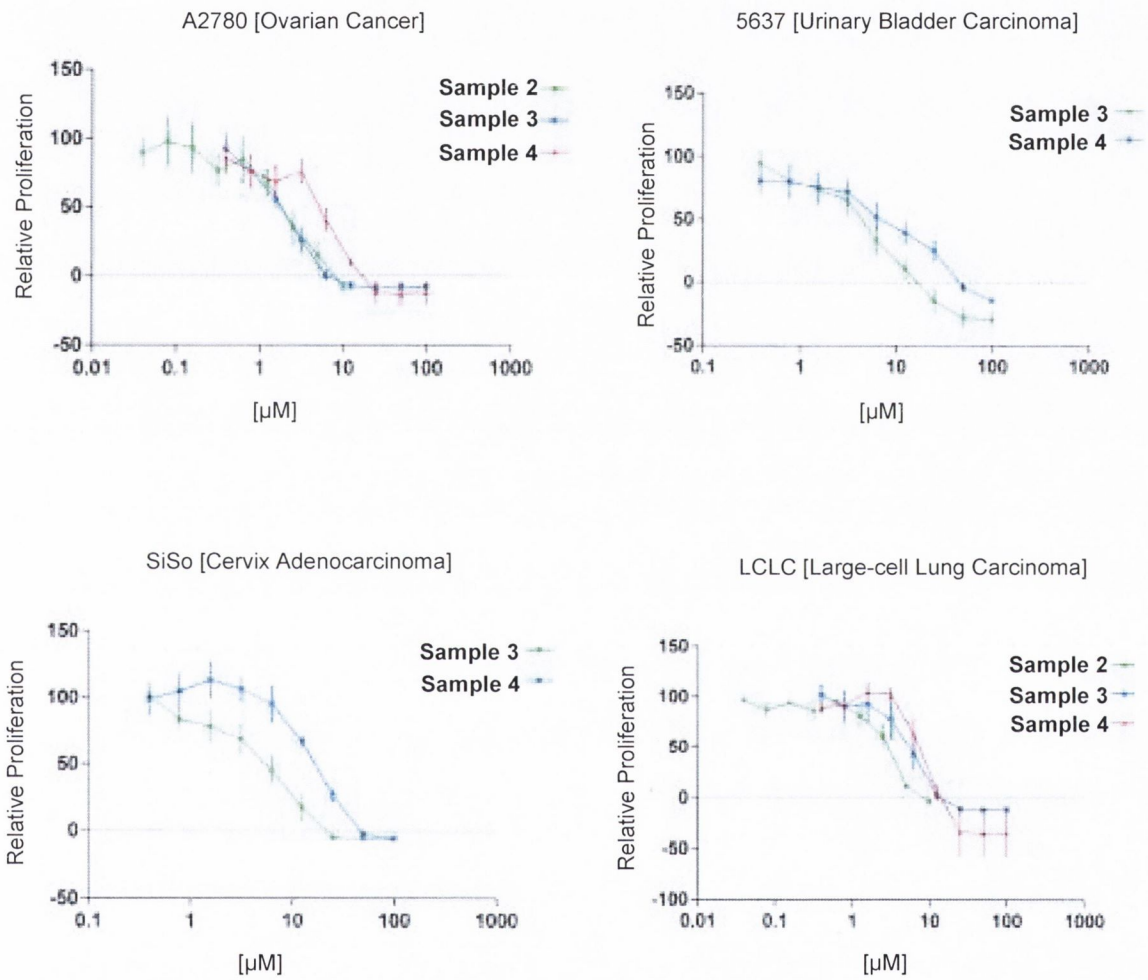

Figure 2.11: Three independent experiments were run to calculate GI_{50} values from the dose response data curves, along with a comparison with two commercial drugs used in anti-cancer therapy. Sample 2 (**16**), Sample 3 (**17**) and Sample 4 (**18**).

Compound **18** was found to have the lowest activity against all tested cell lines compared with compounds **16** and **17**. This suggests that the introduction of a pyrazine ring (**18**) instead of a quinoxaline ring (**16** and **17**) results in a decreased activity (7.77 μM and 5.35 μM against LCLC and A2780, respectively) highlighting a clear structure activity relationship with respect to the tested compounds. In addition, compound **18** showed a moderate activity (9.16-15.61 μM) against 5637 and SISo cell lines.

Table 2.4: GI_{50} for pentathiepin compounds **15-18** along with those of commercial drugs; cisplatin and carboplatin determined for four different cancer cell lines.

Compound Codes	Sample Codes	GI_{50} (μM)			
		LCLC	**5637**	**A2780**	**SISo**
15	1				
16	2	2.46 ± 0.94		2.73 ± 1.60	
17	3	5.01 ± 3.45	4.69 ± 3.10	1.70 ± 0.49	4.44 ± 1.82
18	4	7.77 ± 2.41	9.16 ± 6.56	5.35 ± 1.88	15.61 ± 2.72
Carboplatin[42]		15.59 ± 5.67	4.34 ± 1.70		3.08 ± 1.16
Cisplatin[42]		0.90 ± 0.19	± 0.10	0.75 ± 0.18	0.24 ± 0.06

A comparison of the average GI_{50} values of the tested compounds with respect to the tested cancer cell lines shows that compounds **16** and **17** were significantly more active against cancer cell line LCLC than carboplatin. Furthermore, compound **17** has nearly similar activities towards 5637 and SISo cell lines as carboplatin. Compound **18** exhibits moderate activity against all tested cancer cell lines except LCLC, where it was found to be twice active as carboplatin. All tested pentathiepin compounds were found to be more selective and effective against LCLC, when compared to carboplatin. However, the tested novel pentathiepin compounds were in general less active than the bench mark platinum(II) anti-cancer agent, *i.e.* cisplatin. It can be concluded that compounds **16**, **17** and **18** are significantly active against different tested cell lines and their activities are

comparable to the commercial drug carboplatin and even more selective in the case of LCLC. However, compound **15** showed less activity towards all cell lines, possibly due to its poorer solubility.

Other important factors for the activity of cancer treatment drugs are a certain lipohilicity for crossing membranes without compromising water solubility too much and of course stability in a biological environment. The obtained data clearly indicate that a more lipophilic nature of the compound makes a significant contribution to giving compounds better anti-cancer activity *i.e.* facilitates penetrating membranes.

On the basis of these studies, it can be suggested that substitution pattern plays an important role for better solubility and the inhibition activity of a compound. Moreover, results of DNA binding studies of pentathiepins can be correlated with the evaluated anti-cancer activities. For example, the least anti-cancer active compound **15** showed also the lowest DNA binding constant value, again possibly due to poor solubility. On the other hand, higher binding constant values were observed for the better soluble compounds **16**, **17** and **18**, which is consistent with their significant activities against cancer cell lines and highlight the relationship between DNA binding constant values and anti-cancer studies. This correlation suggested that replacement of CH_3 groups with CF_3 or OCH_3 on the quinoxaline ring for better solubility may result in increased anti-cancer activities. In addition, apoptosis and cell-cycling studies of pentathiepin derivatives will be of great interest for mechanistic investigations and work in this direction is still in progress. The discovery of novel pentathiepins and their biological activities, however, was a very pleasant surprise.

2.6 Conclusions

In conclusion, the number of attempted methodologies was used to synthesise the pyrazine derived dithiolene metal complexes as model for naturally occurring molybdenum enzyme. The main purpose for the synthesis of alkynyl-substituted pyrazine (**3** and **12**) and quinoxaline (**4** and **9-11**) derived compounds was the formation

of their respective target molybdenum complexes. During the attempts to synthesise target model complexes, novel heterocyclic pentathiepino-pyrrolo[1,2-*a*]-derivatives (**15-18**) were isolated unexpectedly and characterised by X-ray structural analysis (in case of compound **15**). Furthermore, three different assays were conducted to investigate the DNA binding properties of pentathiepin derivatives (**15-18**). The data obtained confirmed that pentathiepins do not intercalate, but bind to the surface of the DNA as a minor groove binding agents. Comparison of the averages of GI_{50} values of the tested compounds against all cancer cell lines shows that compounds **16** and **17** were significantly more active to that of carboplatin against LCLC. Furthermore, compound **17** showed nearly similar activities towards 5637 and SISo cell lines. However, compound **18** exhibited low activity against all cancer cell lines except LCLC, where it was found to have 2 fold more active than that of carboplatin. All tested pentathiepin compounds were found to be more selective and effective when compared to carboplatin, against LCLC, however, in general less active towards all tested cell lines compared to cisplatin. By comparing the anti-cancer activity of tested compounds, it could be suggested that the nature of the compound *i.e.* substitution plays an important role in inhibiting activity. As discussed earlier, the main motive of this work was to develop molybdenum complexes as models for MoCo. Further different synthetic strategies to design and synthesise the model compound as an analogue of MoCo will be described in Chapter 3.

2.7 Experimental details

This section details the synthetic procedures and techniques which were used to characterise the pyrazine and quinoxaline derived alkynyl-substituted compounds and their respective pentathiepin derivatives.

2.7.1 Material and methods

All commercially available chemicals were used as supplied by Sigma Aldrich, Fisher Scientific and Acros Organics and were used without further purification. All reactions were performed under an atmosphere of nitrogen or argon, using standard Schlenk-line techniques. Solvents were either degassed or purged with argon prior to use. Melting point values were recorded on a Stuart scientific SMP3 melting point apparatus and are uncorrected. All infrared spectra were recorded (4000–650 cm^{-1}) on a Perkin-Elmer Fourier-Transform Infrared (FTIR) spectrophotometer. All ^{1}H-NMR spectra were recorded on a Bruker AV400 operating at 400.13 MHz as well as $^{13}C\{^{1}H\}$-NMR spectra recorded at 100.65 MHz. All samples were dissolved in deuterated solvents and chemical shift values are reported in parts per million (ppm). High Resolution Mass Spectrometry (HRMS) analyses were carried out on a Water-Micromass Q-ToF (quadrupole - Time of Flight) hybrid mass spectrometer equipped with an orthogonal electrospray source (z–spray). This was operated in an electrospray positive ion mode (ESI^{+}) or electrospray negative ion mode (ESI^{-}). Sodium formate was used for mass calibration checks and optimal parameter tuning was performed using flow injection of standard solutions. All ToF measurements were performed at high resolution settings (5000 FWHM at mass 1500). Data were always taken in continuum mode. X-ray crystallographic studies were performed (by Prof. Carola Schulzke) for suitable single crystals of **14** and **15** which were coated in Paratone N heavy oil then mounted on a glass fiber. The respective data were collected on a Rigaku Saturn-724 diffractometer (graphite-monochromated Mo Kα radiation, λ = 0.71073 Å) at 108(2) K. The structures were solved by direct methods (SHELXS-97) and refined against all data by full matrix least-squares methods on F^2 (SHELXL-97).[39] All non-hydrogen atoms were refined

with anisotropic displacement parameters. The hydrogen atoms (except if found and refined freely) were refined isotropically on calculated positions using a riding model with their U_{iso} values constrained to 1.5 U_{eq} of their pivotal atoms for terminal sp^3 carbon atoms and to 1.2 times for all other carbon atoms.

2.7.2 Synthesis of hydroxyl and diethoxy alkynyl-substituted quinoxaline and pyrazine-derived compounds

2.7.2.1 Synthesis of 3-(pyrazin-2-yl)prop-2-yn-1-ol (3)

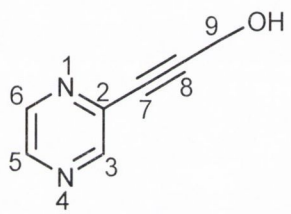

A solution of 2-chloropyrazine (5.00 ml, 56.0 mmol) and propargyl alcohol (3.50 ml, 60.0 mmol) in acetonitrile (60 ml) and triethylamine (30 ml) was degassed. Then palladium(II) acetate (0.11 g, 0.50 mmol), triphenylphosphine (0.78 g, 3.00 mmol) and copper(I) iodide (0.57 g, 3.00 mmol) were added. The reaction mixture was heated under reflux for 6 hrs. After evaporation of the organic solvents, the obtained solid residue was suspended in water (1 x 100 ml) and extracted with dichloromethane (3 x 50 ml). The combined organic extracts were washed with brine (50 ml), dried over $MgSO_4$ and then concentrated in vacuum. The purification of the concentrated mixture was achieved by column chromatography over silica gel, eluting with petroleum ether – diethyl ether (6:4) to give compound **3** as a brown solid.

Yield: 41%, 3.10 g. Molecular Formula: $C_7H_6N_2O$ (134.13 g/mol). M.P.: 112-113 °C. IR (KBr, ν_{max}/cm^{-1}): (OH) 3248, (C≡C) 2213, (C=N) 1514, (C-O) 1026. ^{1}H-NMR ($CDCl_3$) δ_H/ppm: 8.70 (s, 1H, Ar-H_3), 8.57 (br s, 1H, Ar-H_6), 8.53 (br s, 1H, Ar-H_5), 4.58 (br s, 2H, H_9), 2.19 (s, 1H, OH); $^{13}C\{^1H\}$-NMR ($CDCl_3$) δ_C/ppm: 147.2, 143.2, 142.8, 139.1, 91.4, 81.5, 50.8. HRMS (ESI): *m/z* Calculated for $C_7H_6N_2O$ $[M + H]^+$: 135.0550; Found: 135.0480.

2.7.2.2 Synthesis of 3-(quinoxalin-2-yl)prop-2-yn-1-ol (4)

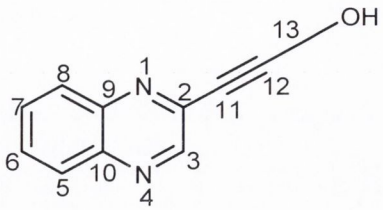

The experimental procedure used for the synthesis of this compound was the same as that employed to prepare compound **3** except 2-chloroquinoxaline (9.18 g, 56.0 mmol) was used instead of 2-chloropyrazine. Compound **4** was isolated as light brown solid.

Yield: 44%, 4.94 g. Molecular Formula: $C_{11}H_8N_2O$ (184.19 g/mol). M.P.: 140-141 °C. IR (KBr, ν_{max}/cm^{-1}): (OH) 3275, (C≡C) 2209, (C=N) 1544, (C-O) 1041. ^{1}H-NMR ($CDCl_3$) δ_H/ppm: 8.91 (s, 1H, Ar-H_3), 8.10 (m, 2H, Ar-$H_{8,5}$), 7.82 (m, 2H, Ar-$H_{7,6}$), 4.66 (br s, 2H, H_{13}), 2.28 (s, 1H, OH); ^{13}C{^{1}H}-NMR ($CDCl_3$) δ_C/ppm: 146.4, 141.5, 140.6, 138.3, 130.4, 130.3, 128.7, 128.7, 91.6, 82.5, 50.9. HRMS (ESI): *m/z* Calculated for $C_{11}H_8N_2O$ $[M + H]^+$: 185.0715; Found: 185.0735.

2.7.2.3 Synthesis of 7-methylquinoxalin-2(1H)-one (5)[5]

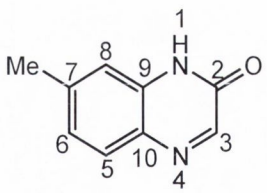

To a stirred solution of 4-methylphenylenediamine (5.00 g, 40.0 mmol) in absolute ethanol (70 ml), was added slowly a solution of ethyl glyoxylate in 50% toluene (12.0 ml, 60 mmol) at room temperature. The mixture was heated under reflux for 2 hrs then allowed to cool and again stirred for 1 hr at room temperature. The precipitated white solid was collected by filtration, washed with absolute ethanol (2 x 20 ml) and allowed to dry under vacuum.

Yield: 85%, 5.47 g. Molecular Formula: $C_9H_8N_2O$ (160.16 g/mol). M.P.: 280-281 °C. IR (KBr, ν_{max}/cm^{-1}): (N-H) 3006, (C=O) 1674, (C=N) 1542. ^{1}H-NMR (d_6-DMSO) δ_H/ppm: 12.35 (s, 1H, Ar-H_1), 8.09 (s, 1H, Ar-H_3) 7.60 (d, 1H, Ar-H_8, J = 7.9 Hz), 7.20-7.07 (m, 2H, $H_{5,6}$), 2.30 (s, 3H, H_{Me}); ^{13}C{^{1}H}-NMR (d_6-DMSO) δ_C/ppm: 155.0, 150.5, 141.0, 132.3, 130.3, 129.5, 128.5, 124.5, 20.88. HRMS (ESI): *m/z* Calculated for $C_9H_8N_2O$ $[M + H]^+$: 161.0714; Found: 161.0715.

2.7.2.4 Synthesis of 2-chloro-7-methyl-quinoxaline (6)[5]

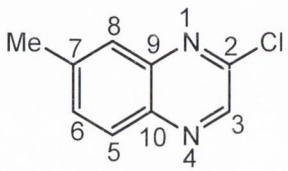

7-Methylquinoxalin-2(1*H*)-one (**5**) (4.80 g, 30.0 mmol) was heated under reflux in $POCl_3$ (22.4 ml, 240 mmol) on an oil bath for 6 hrs in inert gas atmosphere. After cooling to room temperature, the solvent was evaporated *in vacuo* giving a black oil. Cold water (15 ml) was added slowly to the black oil. Then the mixture was neutralised with solid $NaHCO_3$. The aqueous layer was extracted with ethyl acetate (3 x 20 ml). The combined organic extracts were washed with brine (50 ml), dried over $MgSO_4$ and the solvent evaporated. The obtained residue was washed with diethyl ether (2 x 20 ml) to give a brown solid.

Yield: 75%, 4.11 g. Molecular Formula: $C_9H_7ClN_2$ (178.62 g/mol). M.P.: 78-79 °C. IR (KBr, ν_{max}/cm^{-1}): (C=N) 1545, (C-Cl) 701. ^{1}H-NMR ($CDCl_3$) δ_H/ppm: 8.72 (s, 1H, Ar-H_3) 8.01-7.60 (m, 3H, Ar-$H_{8,5,6}$), 2.60 (s, 3H, H_{Me}); ^{13}C{^{1}H}-NMR ($CDCl_3$) δ_C/ppm: 144.3, 143.4, 141.6, 140.5, 139.9, 132.0, 128.3, 126.9, 21.0. HRMS (ESI): *m/z* Calculated for $C_9H_7ClN_2$ $[M + H]^+$: 179.0376; Found: 179.0379.

2.7.2.5 Synthesis of 6,7-dimethylquinoxalin-2(1H)-one (7)[5]

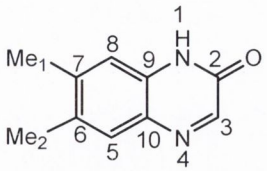

The experimental procedure used for the synthesis of this compound was the same as that employed to prepare compound **5** except 4,5-dimethylphenylenediamine (5.44 g, 40.0 mmol) was used instead of 4-methylphenylenediamine. A white solid was isolated.

Yield: 73%, 5.03 g. Molecular Formula: $C_{10}H_{10}N_2O$ (174.13 g/mol). M.P.: 311-312 °C. IR (KBr, ν_{max}/cm^{-1}): (N-H) 3008, (C=O) 1674, (C=N) 1542. ^{1}H-NMR (d_6-DMSO) δ_H/ppm: 12.30 (s, 1H, Ar-H_1), 8.06 (s, 1H, Ar-H_3) 7.55 (s, 1H, Ar-H_8), 7.06 (s, 1H, H_5), 2.30 (s, 3H, H_{Me1}), 2.28 (s, 3H, H_{Me2}); ^{13}C{^{1}H}-NMR (d_6-DMSO) δ_C/ppm: 155.9, 150.2, 140.2, 131.9, 130.5, 129.5, 128.5, 115.5, 19.7, 18.8. HRMS (ESI): *m/z* Calculated for $C_{10}H_{10}N_2O$ $[M + H]^+$: 175.0865; Found: 175.0866.

2.7.2.6 Synthesis of 2-chloro-6,7-dimethyl-quinoxaline (8)[5]

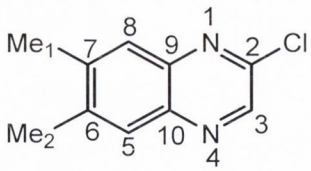

The experimental procedure used for the synthesis of this compound was the same as that employed to prepare compound **6** except 6,7-dimethylquinoxalin-2(1*H*)-one (6.00 g, 34.5 mmol) was used instead of 7-methylquinoxalin-2(1*H*)-one. An off-white solid was isolated.

Yield: 81%, 5.25 g. Molecular Formula: $C_{10}H_9ClN_2$ (192.65 g/mol). M.P.: 98-99 °C. IR (KBr, ν_{max}/cm^{-1}): (C=N) 1534, (C-Cl) 725. ^{1}H-NMR ($CDCl_3$) δ_H/ppm: 8.69 (s, 1H, Ar-H_3) 7.87 (s, 1H, Ar-H_8), 7.79 (s, 1H, Ar-H_5) 2.78 (s, 6H, $H_{Me1,Me2}$); ^{13}C{^{1}H}-NMR ($CDCl_3$) δ_C/ppm: 146.4, 143.7, 142.0, 140.9, 140.8, 139.8, 128.2, 127.5, 20.4, 20.1.

HRMS (ESI): *m/z* Calculated for $C_{10}H_9ClN_2$ $[M + H]^+$: 193.0527; Found: 193.0529.

2.7.2.7 Synthesis of 2-(3,3-diethoxyprop-1-ynyl)quinoxaline (9)

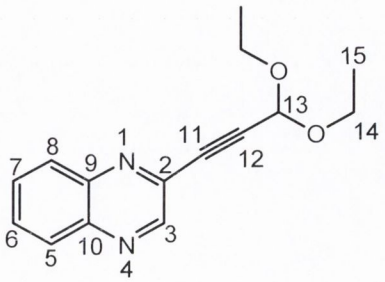

A solution of 2-chloroquinoxaline (5.00 g, 30.3 mmol) and 3,3-diethoxypropyne (5.00 ml, 35.0 mmol) in acetonitrile (60 ml) and triethylamine (30 ml) was degassed under low pressure Then were added palladium(II) acetate (0.11 g, 0.50 mmol), triphenylphosphine (0.78 g, 3.00 mmol) and copper(I) iodide (0.57 g, 3.00 mmol). The reaction mixture was heated under reflux for 6 hrs. After evaporation of organic solvents, the obtained solid residue was suspended with water (100 ml) and extracted with dichloromethane (3 x 50 ml). The combined organic extracts were washed with brine (50 ml), dried over $MgSO_4$ and then concentrated in vacuum. The purification of the concentrated mixture was achieved by column chromatography over silica gel, eluting with petroleum ether – diethyl ether (6:4) to give compound 9 as a brown oil.

Yield: 65%, 4.90 ml. Molecular Formula: $C_{15}H_{16}N_2O_2$ (256.29 g/mol). IR (KBr, ν_{max}/cm^{-1}): (C≡C) 2192, (C=N) 1542, (C-O) 1059. ^{1}H-NMR ($CDCl_3$) δ_H/ppm: 8.78 (s, 1H, Ar-H_3) 7.93 (d, 2H, Ar-$H_{8,5}$ J = 7.5 Hz), 7.63 (m, 2H, Ar-$H_{7,6}$ J = 7.5 Hz) 5.47 (s, 1H, H_{13}), 3.78-3.55 (m, 4H, H_{14}) 1.17 (t, 6H, H_{15}, J = 7.0 Hz); ^{13}C{^{1}H}-NMR ($CDCl_3$) δ_C/ppm: 148.6, 145.7, 143.5, 143.1, 140.2, 138.4, 129.4, 128.2, 93.1, 87.8, 83.2, 60.8, 14.6. HRMS (ESI): *m/z* Calculated for $C_{15}H_{16}N_2O_2$ $[M + H]^+$: 257.1290; Found: 257.1285.

2.7.2.8 Synthesis of 2-(3,3-diethoxyprop-1-ynyl)-7-methylquinoxaline (10)

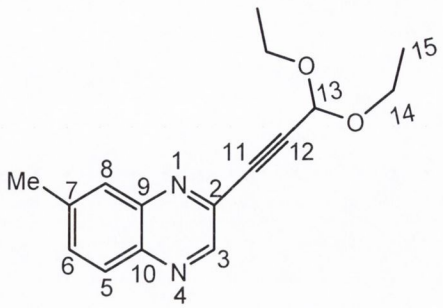

The experimental procedure used for the synthesis of this compound was the same as that employed to prepare compound **9** except 2-chloro-7-methylquinoxaline (**4**) (5.45 g, 30.3 mmol) was used instead of 2-chloroquinoxaline. Dark brown oil was isolated.

Yield: 59%, 4.85 ml. Molecular Formula: $C_{16}H_{18}N_2O_2$ (270.31 g/mol). IR (KBr, ν_{max}/cm^{-1}): (C≡C) 2180, (C=N) 1534, (Ar-CH_3) 1336, (C-O) 1049. ^{1}H-NMR ($CDCl_3$) δ_H/ppm: 8.61 (s, 1H, Ar-H_3) 7.71-7.68 (m, 1H, Ar-H_5), 7.56 (s, 1H, Ar-H_8), 7.33 (d, 1H, Ar-H_6, J = 7.4 Hz), 5.40 (s, 1H, H_{13}), 3.72-3.49 (m, 4H, H_{14}) 2.33 (s, 3H, H_{Me}), 1.10 (t, 6H, H_{15}, J = 7.0 Hz); ^{13}C{^{1}H}-NMR ($CDCl_3$) δ_C/ppm: 145.8, 141.4, 139.8, 138.9, 137.5, 132.3, 128.1, 127.3, 91.1, 87.4, 81.9, 60.7, 21.2, 14.4. HRMS (ESI): *m/z* Calculated for $C_{16}H_{18}N_2O_2$ $[M + Na]^+$: 293.1266; Found: 293.1254.

2.7.2.9 Synthesis of 2-(3,3-diethoxyprop-1-ynyl)-6,7-methylquinoxaline (11)

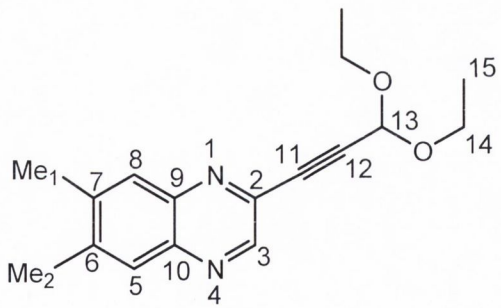

The experimental procedure used for the synthesis of this compound was the same as that employed to prepare compound **9** except 2-chloro-6,7-dimethylquinoxaline (**6**) (5.81 g, 30.3 mmol) was used instead of 2-chloroquinoxaline. A brown solid was isolated.

Yield: 71%, 6.13 g. Molecular Formula: $C_{17}H_{20}N_2O_2$ (284.35 g/mol). M.P.: 50-51°C. IR (KBr, ν_{max}/cm^{-1}): (C≡C) 2172, (C=N) 1531, (Ar-CH_3) 1360, (C-O) 1052. ^{1}H-NMR ($CDCl_3$) δ_H/ppm: 8.69 (s, 1H, Ar-H_3) 7.63 (s, 2H, Ar-$H_{8,5}$), 5.49 (s, 1H, H_{13}), 3.79-3.60 (m, 4H, H_{14}) 2.33 (s, 6H, $H_{Me1,Me2}$), 1.20 (t, 6H, H_{15}, J = 7.2 Hz); ^{13}C{^{1}H}-NMR ($CDCl_3$) δ_C/ppm: 145.7, 141.0, 140.7, 140.1, 139.6, 136.7, 127.6, 127.6, 91.0, 87.0, 82.1, 60.7, 19.8, 19.7, 14.5. HRMS (ESI): *m/z* Calculated for $C_{17}H_{20}N_2O_2$ $[M + Na]^+$: 307.1422; Found: 307.1423.

2.7.2.10 Synthesis of 2-(3,3-diethoxyprop-1-ynyl)pyrazine (12)

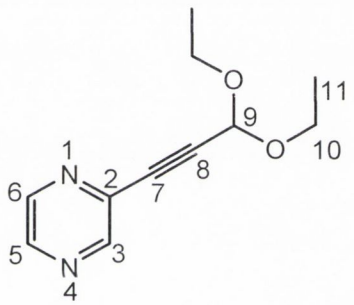

The experimental procedure used for the synthesis of this compound was the same as that employed to prepare compound **9** except 2-chloropyrazine (2.40 ml, 30.3 mmol) was used instead of 2-chloroquinoxaline. Yellowish brown oil was isolated.

Yield: 70%, 3.45 ml. Molecular Formula: $C_{11}H_{14}N_2O_2$ (206.24 g/mol). IR (KBr, ν_{max}/cm^{-1}): (C≡C) 2198, (C=N) 1555, (C-O) 1010. ^{1}H-NMR ($CDCl_3$) δ_H/ppm: 8.66 (s, 1H, Ar-H_3) 8.52 (br s, 1H, Ar-H_6), 8.47 (br s, 1H, Ar-H_5), 5.48 (s, 1H, H_9), 3.82-3.60 (m, 4H, H_{10}), 1.22 (t, 6H, H_{11}, J = 7.0 Hz); ^{13}C{^{1}H}-NMR ($CDCl_3$) δ_C/ppm: 150.7, 148.0, 144.6, 144.4, 91.8, 83.0, 76.4, 55.9, 14.1. HRMS (ESI): *m/z* Calculated for $C_{11}H_{14}N_2O_2$ $[M + H]^+$: 207.1134; Found: 207.1136.

2.7.3 Synthesis of pyrazine derived dithiolene-2-thione ligand

2.7.3.1 Synthesis of 4-phenyl-[1,3]dithiolane-2-thione (13)[3]

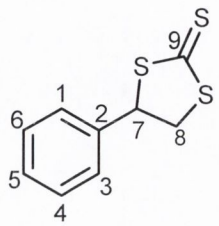

Styrene oxide (7.60 ml, 66.0 mmol) and potassium hydroxide (8.80 g, 220 mmol) were dissolved in methanol and stirred until the colour changed to orange. Then carbon disulfide (12.8 g, 168.4 mmol) was added drop wise to the orange solution and stirred for another 24 hrs at room temperature. The orange solid that precipitated was collected by filtration, washed with absolute ethanol (2 x 50 ml) and allowed to dry under vacuum.

Yield: 77%, 13.9 g. Molecular Formula: $C_9H_8S_3$ (212.35 g/mol). M.P.: 87-88 °C. IR (KBr, ν_{max}/cm^{-1}): (C=S) 889 ^{1}H-NMR ($CDCl_3$) δ_C/ppm: 7.54 (d, 1H, Ar-$H_{1,3}$, J = 7.8 Hz), 7.47-7.41 (m, 3H, Ar-$H_{4,5,6}$), 5.67 (dd, 1H, H_7, J = 5.8 Hz), 4.20-4.07 (m, 2H, H_8); $^{13}C\{^1H\}$-NMR ($CDCl_3$) δ_C/ppm: 226.9, 135.3, 129.3, 129.3, 129.2, 129.0, 127.5, 64.5, 49.5. HRMS (ESI): *m/z* Calculated for $C_9H_8S_3$ $[M + H]^+$: 212.9866; Found: 212.9873.

2.7.3.2 Synthesis of 4-pyrazin-2-yl-[1,3]dithiole-2-thione (14)

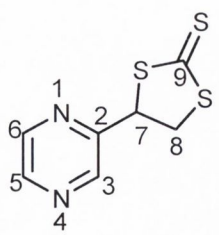

$BF_3{\cdot}Et_2O$ (2.30 ml, 48%) was added slowly to a stirred solution of 3-phenyldithiolane-2-thione (**13**) (0.96 g, 4.53 mmol) in tetrahydrofuran (5 ml) at 40 °C. The mixture was stirred for 10 min and then added dropwise to a solution of pyrazine derived alkyne-alcohol (**3**) (0.20 g, 1.50 mmol) in tetrahydrofuran (3 ml) *via* syringe and then heated for

30 mins. After cooling to room temperature, the reaction mixture was poured into water (50 ml) and made basic by the addition of solid $NaHCO_3$. Then the mixture was then extracted with dichloromethane (3 × 50 ml). The combined organic extracts were washed with brine (30 ml), dried and then concentrated *in vacuo*. The purification of the concentrated mixture was achieved by column chromatography over silica gel, eluting with dichloromethane – ethyl acetate (9:1) to give compound 14 as a yellow solid. The product was crystallised in dichloromethane to give yellow shiny crystalline needles of **14** which was suitable for X-ray diffraction (Apendices 6.1 and 6.3).

Yield: 37%, 0.11 g. Molecular Formula: $C_7H_6N_2S_3$ (214.33 g/mol). M.P.: 135-136 °C. IR (KBr, ν_{max}/cm^{-1}): (C-S) 895, (C=N) 1544. ^{1}H-NMR (d_6-DMSO) δ_H/ppm: 8.73 (s, 1H, Ar-H_3), 8.63 (d, 2H, Ar-$H_{5,6}$ J = 7.0 Hz), 6.88 (br s, 1H, H_7, J = 4.7 Hz), 5.41-5.28 (m, 2H, H_8); $^{13}C\{^1H\}$-NMR ($CDCl_3$) δ_C/ppm: 227.1, 144.8, 138.8, 138.7, 137.1, 64.8, 49.8. HRMS (ESI): *m/z* Calculated for $C_7H_6N_2S_3$ [M - H]: 212.9693; Found: 212.9973.

2.7.4 Attempted synthesis of pyrazine and quinoxaline derived molybdenum complexes (3a and 4a)

Method A

$(Et_4N)_2[MoO(S_4)_2]$ (0.31 g, 0.50 mmol) was dissolved in dry dimethylformamide (5 ml) by warming in an oil bath at 50 °C for 10 mins. Then 3-(pyrazin-2-yl)prop-2-yn-1-ol (**3**) (0.13 g, 1.00 mmol) or 3-(quinoxalin-2-yl)prop-2-yn-1-ol (**4**) (0.18 g, 1.00 mmol) was added to the reaction mixture and heated for another 40 mins. After cooling the reaction mixture to the room temperature, iso-propanol (50 ml) was added which resulted in the formation of red crystals that were collected by filtration and dried under vacuum.

Method B

$(Et_4N)_2[MoO(S_4)_2]$ (0.32 g, 0.50 mmol) was dissolved in dry acetonitrile (40 ml) by warming in an oil bath at 50 °C for 10 mins. Then 3-(pyrazin-2-yl)prop-2-yn-1-ol (**3**) (0.14 g, 1.00 mmol) or 3-(quinoxalin-2-yl)prop-2-yn-1-ol (**4**) (0.18 g, 1.00 mmol) was added to the reaction mixture and heated another 3-4 hrs. The reaction mixture was left for 3-4 days at 5 °C allowing crystallisation. The resulting crystals of both methods (A and B) were analysed by X-ray crystallography. The obtained data corresponded to the molybdenum precursor.

2.7.5 Synthesis of pentathiepino-pyrrolo[1,2-a]-pyrazine derivatives (15-18)

2.7.5.1 Synthesis of 10-ethoxy-pentathiepino-pyrrolo[1,2-a]-quinoxaline (15)[16]

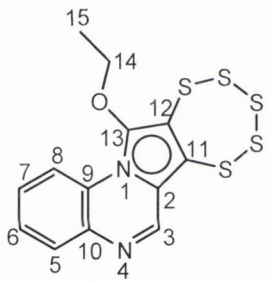

Method A

$(Et_4N)_2[MoO(S_4)_2]$ (0.25 g, 0.40 mmol) and elemental sulfur (0.20 g, 0.80 mmol) were added to dimethylformamide (5 ml) and dissolved by heating (40 °C) in an oil bath for 20 mins. Diethoxyprop-1-ynyl)quinoxaline (**9**) (0.20 ml, 0.80 mmol) was added to the reaction mixture and stirred for 3 hrs. After filtering to remove excess sulfur, the product was precipitated out by the addition of isopropanol which resulted in the formation of a brick red powder. The obtained solid residue was filtered and washed with diethyl ether (2 x 20 ml). The product was crystallised in acetonitrile to give red crystals of **15** which was suitable for X-ray diffraction (Apendices 6.2 and 6.4).

Method B

$(Et_4N)_2[MoO(S_4)_2]$ (0.25 g, 0.40 mmol) and elemental sulfur (0.20 g, 0.80 mmol) were added to acetonitrile (40 ml) and dissolved by heating (40 °C) in an oil bath for 20 mins.

Diethoxyprop-1-ynyl)quinoxaline (**9**) (0.20 ml, 0.80 mmol) was added to the reaction mixture and stirred for 5 hrs. After filtering to remove excess sulfur, the solvent was removed under reduced pressure and the residue was purified by column chromatography. Residual sulfur was removed by elution with dichloromethane and followed by subsequent elution with methanol – hexane (9:1) to give compound **15** as a red solid.

Yield A (relative to **9**): 37%, 0.11 g. Yield B (relative to **9**): 68%, 0.20 g. Molecular Formula: $C_{13}H_{10}N_2OS_5$ (370.55 g/mol). M.P.: 205-206 °C. IR (KBr, ν_{max}/cm^{-1}): (C=N) 1521, (C-O) 1012, (C-S) 752. ^{1}H-NMR ($CDCl_3$) δ_H/ppm: 8.88 (br s, 1H, Ar-H_3), 8.56 (d, 1H, Ar-H_8, J = 7.1 Hz), 7.94 (d, 1H, Ar-H_5, J = 7.9 Hz), 7.52-7.51 (m, 2H, Ar-$H_{7,6}$), 4.60-4.62 (m, 2H, H_{14}), 1.60 (t, 3H, H_{15}, J = 8.1 Hz); ^{13}C{^{1}H}-NMR ($CDCl_3$) δ_C/ppm: 146.3, 144.0, 138.6, 136.3, 133.9, 129.6, 127.8, 126.1, 118.5, 116.2, 114.2, 51.6, 15.1. HRMS (ESI): *m/z* Calculated for $C_{13}H_{10}N_2OS_5$ $[M]^+$: 370.9475; Found: 370.9526.

2.7.5.2 Synthesis of 7-methyl-10-ethoxy-pentathiepino-pyrrolo[1,2-a]-quinoxaline (16)[16]

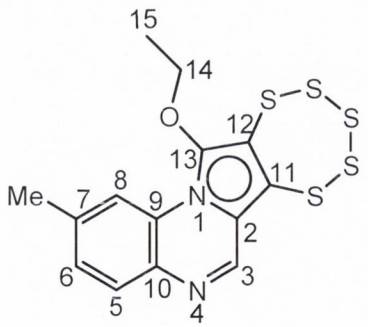

The experimental procedures used for the synthesis of this compound were the same as those employed to prepare compound **15** except 2-(3,3-diethoxyprop-1-ynyl)-7-methylquinoxaline (**10**) (0.21 ml, 0.80 mmol) was used instead of 2-(3,3-diethoxyprop-1-ynyl)quinoxaline (**9**). A red solid was isolated.

Yield A (relative to **10**): 33%, 0.10 g. Yield B (relative to **10**): 67%, 0.20 g. Molecular Formula: $C_{14}H_{12}N_2OS_5$ (384.58 g/mol). M.P.: 245-247 °C. IR (KBr, ν_{max}/cm^{-1}): (C=N)

1548, (C-O) 1017, (C-S) 783. ^{1}H-NMR (d_6-DMSO) δ_H/ppm: 8.87 (s, 1H, Ar-H_3), 8.44 (d, 1H, Ar-H_8, J = 7.6 Hz) 7.80 (d, 1H, Ar-H_5, J = 7.9 Hz), 7.47 (d, 1H, Ar-H_6, J = 7.8 Hz) 4.62-4.56 (m, 2H, H_{14}), 2.46 (s, 3H, H_{Me}, J = 7.3 Hz), 1.50 (t, 3H, H_{15} J = 7.1 Hz); ^{13}C{^{1}H}-NMR (d_6-DMSO) δ_C/ppm: 144.1, 143.1, 138.8, 136.2, 134.3, 129.8, 129.4, 125.9, 117.3, 116.4, 114.3, 51.4, 20.5, 15.4. HRMS (ESI): *m/z* Calculated for $C_{14}H_{12}N_2OS_5$ $[M]^+$: 384.9631; Found: 384.9632.

2.7.5.3 Synthesis of 6,7-dimethyl-10-ethoxy-pentathiepino-pyrrolo[1,2-a]-quinoxaline (17)[16]

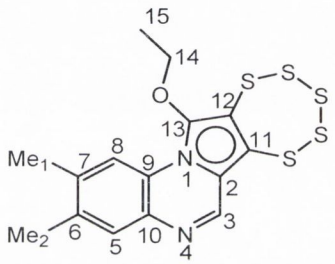

The experimental procedures used for the synthesis of this compound were the same as those employed to prepare compound **18** except 2-(3,3-diethoxyprop-1-ynyl)-6,7-dimethylquinoxaline (**11**) (0.22 ml, 0.80 mmol) was used instead of 2-(3,3-diethoxyprop-1-ynyl)quinoxaline (**9**). A reddish brown solid was isolated.

Yield A (relative to **11**): 32%, 0.10 g. Yield B (relative to **11**): 63%, 0.20 g. Molecular Formula: $C_{15}H_{14}N_2OS_5$ (398.60 g/mol). M.P.: 266-267 °C. IR (KBr, ν_{max}/cm^{-1}): (C=N) 1537, (Ar-CH_3) 1329, (C-O) 1016, (C-S) 742. ^{1}H-NMR (d_6-DMSO) δ_H/ppm: 8.84 (s, 1H, Ar-H_3), 8.39 (s, 1H, Ar-H_8) 7.71 (s, 1H, Ar-H_5), 4.67-4.59 (m, 2H, H_{14}), 2.46 (s, 3H, H_{Me1}), 2.41 (s, 3H, H_{Me2}), 1.34 (t, 3H, H_{15} J = 7.1 Hz); ^{13}C{^{1}H}-NMR (d_6-DMSO) δ_C/ppm: 145.7, 143.9, 137.7, 135.2, 134.3, 129.7, 124.2, 122.0, 117.8, 116.6, 114.5, 52.5, 20.5, 19.4, 15.0. HRMS (ESI): *m/z* Calculated for $C_{15}H_{15}N_2OS_5$ $[M]^+$: 398.9788; Found: 398.9786.

2.7.5.4 Synthesis of 10-ethoxy-pentathiepino-pyrrolo[1,2-a]-pyrazine (18)[16]

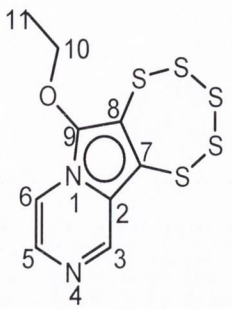

The experimental procedures used for the synthesis of this compound were the same as those employed to prepare compound **18** except 2-(3,3-diethoxyprop-1-ynyl)pyrazine (**12**) (0.16 ml, 0.80 mmol) was used instead of 2-(3,3-diethoxyprop-1-ynyl)quinoxaline (**9**). A red powder was isolated.

Yield A (relative to **12**): 27%, 0.07 g. Yield B (relative to **12**): 57%, 0.14 g. Molecular Formula: $C_9H_9N_2OS_5$ (321.50 g/mol). M.P.: 150-151 °C. IR (KBr, ν_{max}/cm^{-1}): (C=N) 1538, (C-O) 997, (C-S) 784. ^{1}H-NMR ($CDCl_3$) δ_H/ppm: 8.39 (s, 1H, Ar-H_3) 7.56 (d, 1H, Ar-H_5, J = 7.0 Hz), 7.00 (d, 1H, Ar-H_6, J = 6.0 Hz), 4.91-4.87 (m, 2H, H_{10}), 1.42 (t, 3H, H_{11}, J = 6.9 Hz); ^{13}C{^{1}H}-NMR ($CDCl_3$) δ_C/ppm: 143.2, 137.4, 135.0, 129.8, 124.4, 122.0, 116.2, 52.2, 15.0 HRMS (ESI): *m/z* Calculated for $C_9H_9N_2OS_5$ $[M]^+$: 320.9318; Found: 320.9310.

2.8 Biological testing details

This section details the assay used for DNA binding study experiments as well as anti-cancer studies on novel pentathiepino-pyrrolo[1,2-*a*]-compounds (**15-18**). DNA binding studies for the pentathiepin derivatives were carried out by Dr. Kellett's group, School of Chemical Sciences, Dublin City University, Dublin 9, Ireland. The anti-cancer screening for novel pentathiepin derivatives was investigated against number of cancer cell lines by Prof. Bednarski's group, at Institute of Pharmaceutical Biology, Ernst-Moritz-Arndt-University Greifswald, D-17489 Greifswald, Germany.

2.8.1 DNA binding experiments[32]

(i) Competitive ethidium displacement: A working solution of 20.0 μM UltraPure calf thymus DNA (CT-DNA, Invitrogen 15633-019, ε_{260} = 12,824 M $(bp)^{-1}$ cm^{-1}) along with 25.2 μM ethidium bromide (EtBr) in HEPES buffer (80 mM, pH = 7.2) and NaCl (40 mM) was prepared. Stock solutions of compounds, and groove binding drugs were prepared at ~4.0 mM in DMF and diluted further with ultra-pure water. 50 μL of DNA-Et working solution were placed each in a well of a 96 well microplate with the exception of the blanks which contained 100 μLHEPES buffer. Serial aliquots of the tested compound were added to the working solutions and the volume was adjusted to 100 μL in each well such that the final concentration of CT-DNA and EtBr were 10.0 μM and 12.6 μM, respectively. The plate was allowed to incubate at room temperature for 1 hr before being analysed using a Bio-Tek synergy HT multi-mode microplate reader with excitation and emission wavelengths being set to 530 and 590 nm, respectively. Concentrations of the tested compounds were optimized such that fluorescence was 30-40% of the initial control (i.e. 50 μL working solution + 50 μL HEPES buffer) at their highest reading. Each drug concentration was measured in triplicate and the apparent binding constants were calculated using $K_{app} = K_e \times 12.6/C_{50}$ where K_e[40,41] = 9.5×10^6 $M(bp)^{-1}$.

(ii) DNA–ethidium fluorescence quenching:[32] A working solution of 50.0 μM UltraPure calf thymus DNA (CT-DNA, Invitrogen 15633-019, ε_{260} = 12,824 M $(bp)^{-1}$ cm^{-1}) along with either 10.0 μM ethidium bromide (EtBr) or Hoechst 33258 (Sigma) in HEPES buffer (80 mM, pH = 7.2) and NaCl (40 mM) was prepared. Stock solutions of tested compounds and groove binding drugs were prepared at ~4.0 mM in DMSO and diluted further with ultra-pure water. 50 μL of DNA-Et or DNA-Hoechst working solution were placed each in a well of a 96 well microplate with the exception of the blanks which contained 100 μLHEPES buffer and 5 μM of either Hoechst or EtBr. Serial aliquots of the tested compound were added to the working solutions and the volume was adjusted to 100 μL in each well such that the final concentration of CT-DNA and EtBr/Hoechst were 25.0 μM and 5 μM, respectively. The plate was allowed to incubate at room temperature for 5 min before being analysed using a Bio-Tek synergy HT multi-mode microplate reader with excitation and emission wavelengths being set to 530 and 590 nm for Et detection or 360 nm and 460 nm for Hoechst 33258 detection. Concentrations of the tested compounds were optimised such that fluorescence was 30-40% of the initial control at their highest reading. Each drug concentration was measured in triplicate. From a plot of fluorescence versus added drug concentration, the Q value is given by the concentration required to effect 50% removal of the initial fluorescence of bound dye.

(iii) Viscosity experiments:[32] 15 mL dsDNA (Deoxyribonucleic acid sodium salt from Salmon Testes, Sigma-Aldrich, D1626- 1G) solution was prepared at 1 x 10^{-3} M in 80 mM HEPES buffer for each working sample. Stock solutions prepared in DMSO were added according to gradually increasing [drug]/[DNA] (r) ratios of 0.02, 0.04, 0.06, 0.08, 0.10, 0.12, 0.14, 0.16, 0.18 and 0.2. Viscosity values, η, (unit: cP) were directly obtained by running a 0# spindle in working samples at 60 rpm *via* a DV-II-Programmable Digital Viscometer equipped with an Enhanced Brookfield UL Adapter at room temperature. Data were presented as η/η_o values versus [compound]/[DNA] ratio, in which η_o and η refers to viscosity of each DNA working sample in the absence and presence of tested compound.

2.8.2 Anti-cancer Assay[42]

Protocol: Anti-cancer activities of the pentathiepins compounds were studied against a panel of four human cancer cell lines and are as follow; ovarian cancer (A2780), bladder carcinoma (5637), cervix carcinoma (SISo) and lungcell carcinoma (LCLC) (which were obtained from the German Collection of Microorganisms and Cell Cultures (DSMZ)). A well established microtiter assay based on cell staining with crystal violet, was used to measure the antiproliferative effects of the novel pentathiepino-pyrrolo[1,2-*a*]-compounds **15-18**. Testing was done with all cell lines growing in 96-well microtiter plates. Cells were plated out 24 hr prior to testing at a density of 1000 cells/well in 100 µl medium, except for LCLC cell line, which was plated out at 500 cells/well in 100 µl medium. Cells were then exposed to five serial dilutions of substances, added to the medium from 1000-fold concentrated stock solutions in DMF. The final DMF concentration in all wells was 0.1%. The untreated plate for each cell line was used as control. The assay measures the inhibition of cell growth caused by a 96 h continuous exposure to the test compounds. In primary screenings, tested samples that inhibited cell growth at 20 µM by 50% or more compared to untreated controls in at least one cell line were considered active. In secondary screenings, only two compounds were selected to be tested at low concentration (5 µM). All active compounds were tested to determine GI_{50} (the concentration required to inhibit cell growth by 50% compared to the untreated control over a 96 h treatment period) values at 5 serially diluted concentrations. The corrected T/C values (T/C_{corr}) for each concentration were calculated with the following equation:

$$T/C_{corr}\ (\%) = (OD_T - OD_{CO}) / (OD_C - OD_{CO})\ X\ 100$$

where T is the optical density at λ = 570 nm (OD_{570}) of the treated cells after a 96 h treatment time, C is the OD_{570} of the untreated cells after 96 h of growth without test compound, C0 is the OD_{570} of the cells at the time of treatment (i.e. 96 h before T and C). Linear regression analysis of the log concentration versus the T/C_{corr} plots was used

to estimate the concentration of test compounds that caused a T/C_{corr} = 50% (GI_{50}). At least three independent experiments were done to determine the GI_{50} values.

References

[1] K. Sonogashira, Y. Tohda, N. Hagihara, *Tetrahedron Lett.*, **1975**, 16, 4467.

[2] M. Armengol, J. A. Joule, *J. Chem. Soc., Perkin Trans.*, **2001**, 1, 978.

[3] C. C. J. Culvenor, W. Davies, K. H. Pausacker, *J. Chem. Soc.*, **1946**, 1050.

[4] M. A. Ansari, J. Chandrasekaran, S. Sarkar, *Inorginica chimica acta.*, **1987**, 133, 133.

[5] F. Alphonse, R. Karim, C. Cano-Soumillac, M. Hebray, D. Collison, C. D. Garner, J. A. Joule, *Tetrahedron*, **2005**, 614, 11010.

[6] C. Shi, C. C. Aldrich, *Org. Lett.*, **2010**, 12, 2286.

[7] L. Yin, J. Liebscher, *Chem. Rev.*, **2006**, 107, 133.

[8] R. Chinchilla, C. Najera, *Chem. Soc. Rev.*, **2011**, 40, 5084.

[9] B. Bradshaw, D. Collison, C. D. Garner, J. A. Joule, *J. Org. Biomol. Chem.*, **2003**, 1, 129.

[10] B. Bradshaw, A. Dinsmore, D. Collison, C. D. Garner, J. A. Joule, *J. Chem. Soc., Perkin Trans. 1.*, **2001**, 3239.

[11] B. Bradshaw, A. Dinsmore, D. Collison, C. D. Garner, J. A. Joule, *J. Chem. Soc., Perkin Trans. 1.*, **2001**, 3232.

[12] P. Chandrasekaran, K. Arumugam, U. Jayarathne, L. M. Perez, J. T. Mague, P. J. Donahue, *Inorg. Chem.*, **2009**, 48, 2103.

[13] P. P. Samuel, Molybdenum and tungsten compounds with dithiolene ligands inspired by molybdopterin as models for the molybdenum and tungsten cofactors, Universität zu Göttingen, PhD thesis, August, **2011**.

[14] D. Coucouvanis, A. Hadjikriacou, S. Koo, M. Draganjac, A. Salifoglou, *Inorg Chem.*, **1991**, 30, 754.

[15] J. P. Donahue, C. R. Goldsmithm, U. Nadiminti, R. H. Holm, *J. Am. Chem. Soc.*, **1998**, 120, 12869.

[16] M. Zubair, A. C. Ghosh, C. Schulzke, *Chem. Commun.*, **2013**, 49, 4343.

[17] S. A. Amelichev, S. L. Konstantinova, K. A. Lyssenko, C. W. Rees, *J. Org. Biomol. Chem.*, **2005**, 3, 3496.

[18] B. L. Chenard, R. L. Harlow, A. L. Johnson, *J. Am. Chem. Soc.*, **1985**, 107, 3871.

[19] A. Alam, M. Kon-no, S. Ogawa, R. Sato, *Tetrahedron*, **2007**, 63, 927.

[20] F. Compagnone, R. S. John, *Tetrahedron*, **1994**, 50, 12785.

[21] L. S. Konstantinova, O. A. Rakitin, *Chem. Rev.*, **2004,** 104, 2617.

[22] F. Compagnone, R. S. John, *Tetrahedron*, **1994**, 50, 12785.

[23] T. Chatterji, K. S. Gates, *Bioorg. Med. Chem. Lett.*, **1998**, 8, 535.

[24] J. A. Whiteford, C. V. Lu, P. J. Stang, *J. Am. Chem. Soc.*, **1997**, 119, 2524.

[25] P. J. Stang, B. Olenyuk, *Angew. Chem. Int. Ed. Engl.*, **1996**, 35, 732.

[26] http://roldarin.blogspot.ie/2011/06/estructura-del-adn.html

[27] M. Fujita, O. Sasaki, T. Mitsuhashi, T. Fujita, J. Yazaki, K. Yarnaguhi, K. Ogura, *Chem. Commun.*, **1996**, 1535.

[28] Z. Han, J. Jiang, J. Lu, D. Li, S. Cheng, J. Dou, *Dalton Trans.*, **2013**, 42, 1862.

[29] A. Prisecaru, M. Devereux, N. Barron, M. McCann, J. Colleran, A. Casey, V. McKeee, A. Kellett, *Chem. Commun.*, **2012**, 48, 6906.

[30] A. Kellett, O. Howeb, M. O'Connor, M. McCann, S. McClean, A. F. Kia, A. Casey, M. Devereux, *Free Radical Biol. Med.*, **2012**, 53, 564.

[31] A. Prisecaru, V. McKee, O. Howeb, G. Rochford, M. McCann, J. Colleran, M. Pour, N. Barron, N. Gathergood, A. Kellett, *J. Med. Chem.*, **2013**, 56, 8599.

[32] M. McCann, J. McGinley, K. Ni, M. O'Connor, K. Kavanagh, V. McKee, J. Colleran, M. Devereux, N. Gathergood, N. Barron, A. Prisecarue, A. Kellett, *Chem. Commun.*, **2013**, 49, 2341.

[33] World Health Organization. **2006**- Fact sheet, 297.

[34] C. Desantis, R. Siegel, A. Jemal, *American Cancer Society; Breast Cancer Fact & Figures.*, **2013-2014**.

[35] http://www.nlm.nih.gov/medlineplus/ency/imagepages/18015.htm

[36] Cancer Facts and Figures, *American Cancer Society.*, **2006**, GA, U.S.A.

[37] E. Pomarnacka, A. Kornicka, A. Kuchnio, M. Heinrichs, R. Grunert, M. Gdaniec, P. J. Bednarski, *Arch. Pharm. Chem. Life Sci.*, **2011**, 344, 431.

[38] D. A. William, *The Design and Development of Anticancer Drugs*; Chemical Processes in New Zealand, **2002**, Vol. 2.

[39] G. M. Sheldrick, *Crystallogr. Sect. A.*, **2008**, 64. 112.

[40] B. C. Baguley, W. A. Denny, G. J. Atwell, B. F. *Cain, J. Med. Chem.*, **1981**, 24, 170

[41] Bruce C. Baguley and E. Falkenhaug, *Nucleic Acids Research*, **1978**, 5, 161.

[42] K. Bracht, Boubakari, R. Grunert, P. J. Bednarski, *Anti-Cancer Drugs*, **2006**, 17, 41.

Chapter 3

Synthesis and spectroelectrochemical characterisation of pyrazine-substituted dithiolene complexes

3.1 Overview

This chapter summarises the synthetic strategies to develop pyrazine-substituted dithiolene ligands and their respective molybdenum and tungsten complexes as chemical analogues of the molybdenum cofactor (MoCo). This chapter comprise in two parts. The first part describes the successful synthesis of a model dithiolene-2-one ligand which is attached to the *N*-heteroatomic pyrazine ring. This pyrazine-substituted dithiolene-2-one ligand (**22**) was then used to bind with two different metal precursors *i.e.* $K_3Na[MoO_2(CN)_4].6H_2O$[1] and $K_3Na[WO_2(CN)_4].6H_2O$,[2] to generate the corresponding $[Ph_4P]_2[MoO(pzdt)_2]$ (**23**) and $[Ph_4P]_2[WO(pzdt)_2]$ (**24**) complexes. The second part describes the synthetic strategies to develop closed (**28**) and open alcohol form (**32**) ligands as chemical analogues of the MPT ligand in MoCo. Finally, the reaction of molybdenum oxo *bis*-tetrasulfides with electron deficient alkyne (**31**) resulted in the generation of target open alcohol form molybdenum complex (**33**).

3.2 Synthesis and characterisation of the pyrazine-substituted dithiolene-2-one ligand (22)

As described in Chapter 2, two different attempts were made to synthesise the pyrazine or quinoxaline-substituted dithiolene complexes (**3a** and **4a**) but remained unsuccessful, even though unexpectedly interesting pentathiepin compounds were isolated. The failure to develop this specific synthetic analogue of MoCo motivated us to search for other simple synthetic procedures. For instance, the use of different synthetic routes may allow designing and synthesising *N*-heterocyclic based dithiolene-2-one ligands and their respective molybdenum and tungsten complexes. Garner's group reported synthetic methods to construct asymmetrically substituted dithiolene-2-one ligands and their respective molybdenum and tungsten complexes.[3,4,5] Following this methodology, the selected pyrazine ring was asymmetrically attached to the dithiolene-2-one moiety to obtain a novel pyrazine-substituted dithiolene-2-one ligand (**22**). This ligand was further used to form the desired molybdenum (**23**) and tungsten (**24**) complexes. These unusual complexes not only show similar coordination environment but also include the pyrazine feature

of enzymatic MPT and therefore serve as a quite accurate model to this naturally occurring ligand system.

The synthesis of ligand **22** was achieved in three steps as shown in Scheme 3.1. The first step involves the bromination of acetyl pyrazine (**19**) with 2-pyrrolidone hydrotribromide (PHT) in the presence of tetrahydrofuran (THF). The reaction mixture was stirred overnight at room temperature. After work up, bromoacetyl pyrazine (**20**) was immediately used *in situ* for the next step due to its low stability.

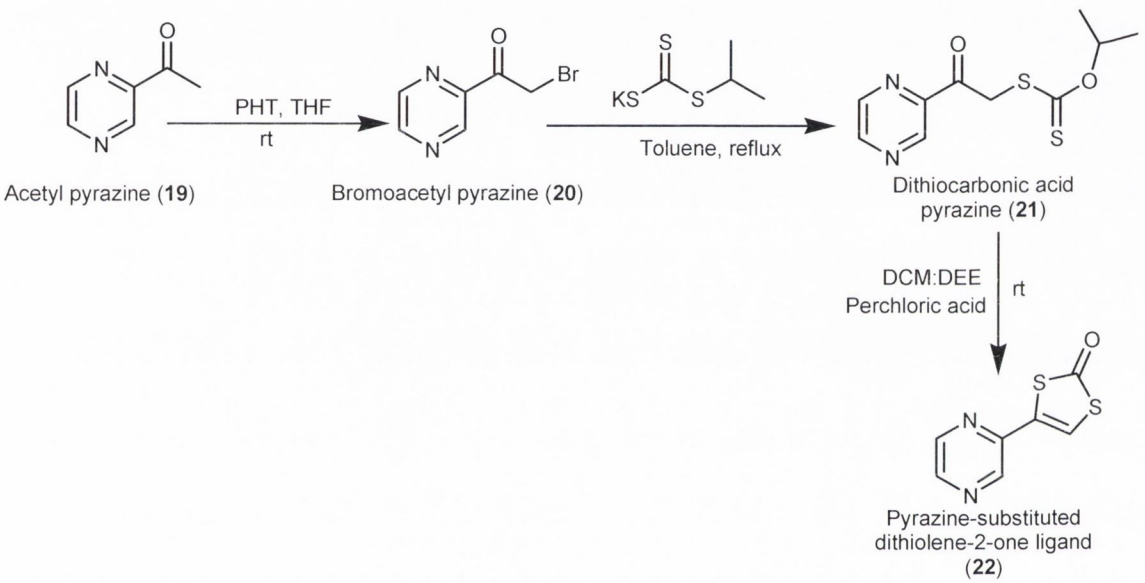

Scheme 3.1: General synthetic route for the preparation of pyrazine-substituted dithiolene-2-one ligand (**22**).

The bromination of acetyl group with PHT in the presence of tetrahydrofuran proceeds with the formation of pyrrolidonehydrobromide [(pyrrolidone)$_2$.HBr].[6] The pyrrolidonehydrobromide is an acid and undergoes an acid-catalysed enolisation of the carbonyl moiety and consequently produces a nucleophilic carbon centre which attacks the Br_2 and results in the formation of brominated product **20**. The possible mechanism for this bromination step is shown in Scheme 3.2.

In the next step, the bromine atom of compound **20** was replaced by the potassium salt of *O*-isopropyl carbonodithioate to yield dithiocarbonic acid pyrazine (**21**). Similar replacement reaction for other brominated compounds have been previously

reported by Madhu *et al.*[7] The only byproduct of this reaction is KBr which can be easily removed through filtration.

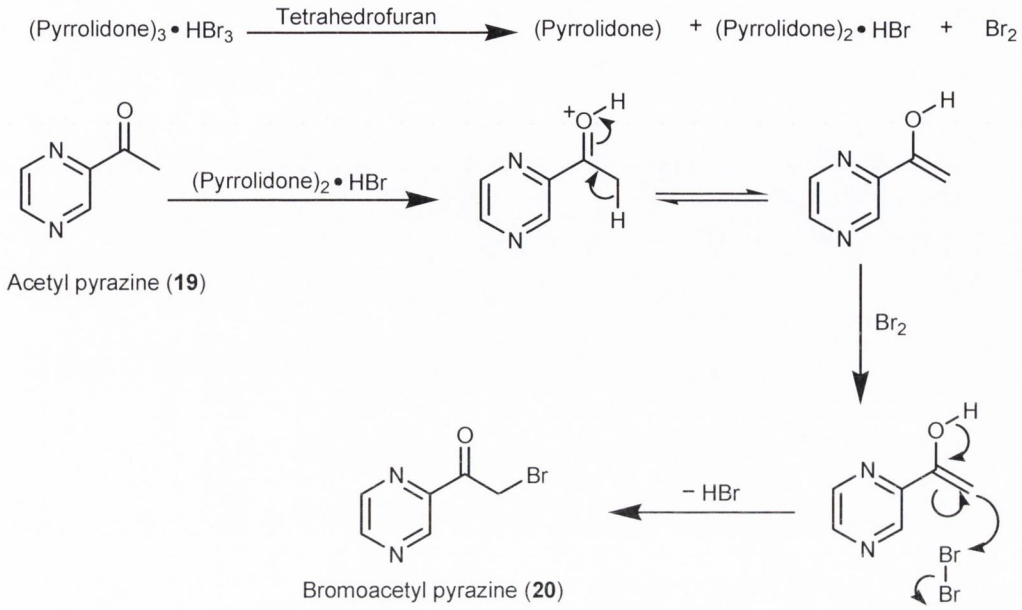

Scheme 3.2: Possible mechanism for the synthesis of bromoacetyl pyrazine **20**.

Compound **21** was characterised by IR spectroscopy. A characteristic band appeared at 1735 cm^{-1} corresponding to the carbonyl stretch υ(C=O) of dithiocarbonic moiety of **21**. The ^{1}H-NMR spectrum of **21** showed characteristic signals at 4.79 and 5.71 ppm corresponding to the methylene (CH_2) and methine (CH) groups of the dithiocarbonic moiety. In addition, the methyl (CH_3) group of the isopropyl functionality was found to be present at 1.38 ppm while all aromatic protons appeared in between 8.91-8.52 ppm. Finally, the obtained molecular mass value (257.0335 u) of **21** through ESI-HRMS was in good agreement with the calculated value (257.0418 u) based on the calculated molecular formula of this compound.

The final step for the synthesis of ligand **22** was the cyclisation of **21** in acidic medium. This ring closure step was very difficult to optimise as the amount of acid used was crucial and eventually the optimised reaction conditions after several repeated experiments are reported in the experimental procedure (see Section 3.8.2). The possible general reaction mechanism of the ring closure is shown in Scheme 3.3. The ring closure step starts with the attack of an acid proton on the thioketone

resulting in the elimination of the propylene molecule. This step is catalytic in nature as the used H^+ ion is released during the elimination of the prop-1-ene. Afterwards, the SH of the resulting intermediate state protonates the carbonyl group (C=O) adjacent to the pyrazine ring, generating a positively charged carbonyl carbon and negatively charged terminal sulfur atom. As a result, sulfur attempts a nucleophilic attack on the positively charged carbon atom to close the ring, followed by the elimination of water which results in the isolation of cyclised ligand **22**.

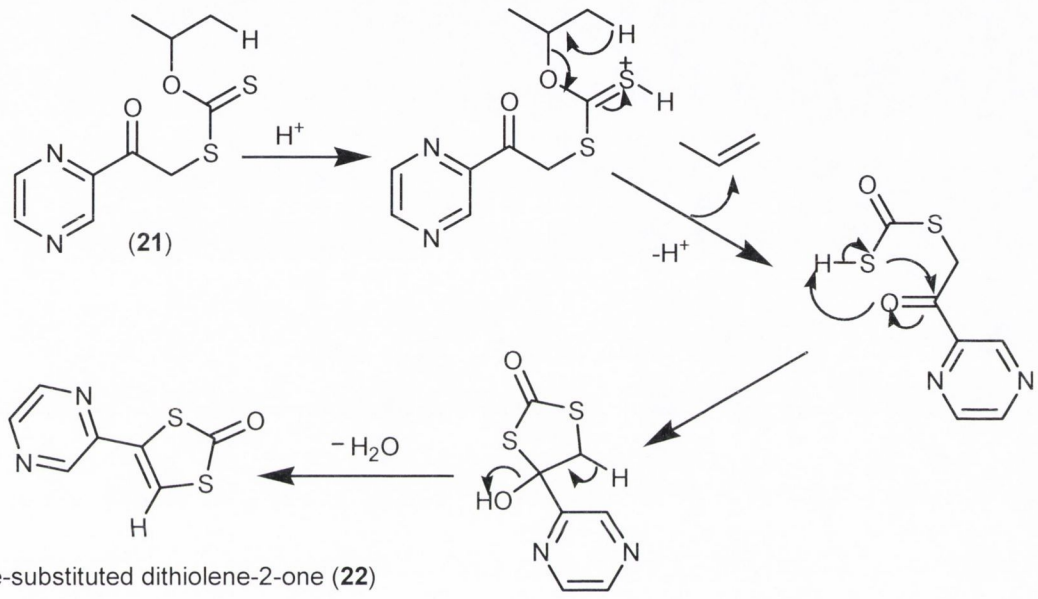

Scheme 3.3: Proposed reaction mechanism of the cyclisation of **21** to synthesise novel ligand **22**.

The IR spectrum of ligand **22** exhibited a characteristic band at 1759 cm^{-1} which is attributed to the stretching vibration of the carbonyl group ν(C=O), supporting the formation of the dithiolene-2-one functionality and is in the range of reported values for other substituted dithiolene-2-one ligands.[5,8,9] The ^{1}H-NMR spectrum of **22** showed a characteristic sharp singlet at 7.54 ppm which was assigned to the methine proton (CH) of the dithiolene moiety. This finding is consistent with other dithiolene derived ligands where this proton (CH) has been found in the range of 7.75-6.82 ppm.[10,11] Moreover, the aromatic protons appeared in the range of 8.85-8.51 ppm. The $^{13}C\{^1H\}$-NMR spectrum of **22** further supported the formation of the dithiolene-2-one moiety by the appearance of the most downfield signal at 191.1 ppm corresponding to the carbonyl group (C=O). Furthermore, signals appearing in

between 145.9-117.2 ppm were assigned to the aromatic carbons. Finally, the found molecular mass value (196.9860 u) of **22** through ESI-HRMS was consistent with the calculated value (196.9843 u) based on molecular formula.

X-ray structural analysis of a suitable single crystal confirmed the presence of dithiolene-2-one moiety in ligand **22**. The crystals were grown in a solution of acetonitrile at room temperature by slow evaporation. The structure was solved in the orthorhombic space group *$Pna_2(1)$*. The atomic numbering scheme of ligand **22** and its unit cell is shown in Figure 3.1 **A** and **B**, respectively. A summary of the crystallographic data collection and structural refinement parameters along with selected bond lengths and angles for ligand **22** are listed in Appendices 6.5 and 6.7, respectively.

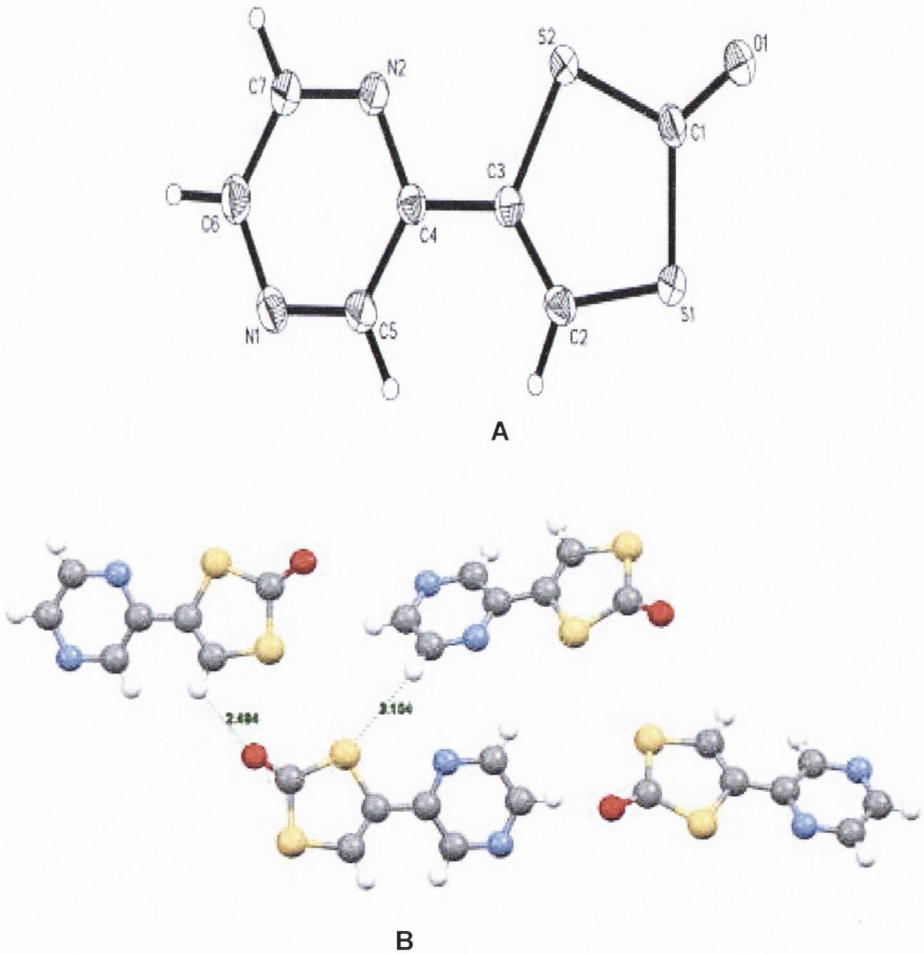

Figure 3.1: X-ray crystal structure of pyrazine-substituted dithiolene-2-one ligand (**22**); **A**) the atomic numbering scheme, **B**) the unit cell diagram.

The pyrazine and dithiolene rings are linked by the C(3)-C(4) bond with a distance of 1.459(4) Å. The dithiolene-2-one ring is not in the same plane as the pyrazine ring and bent in a dihedral angle of 11.21(3) Å. The distance between the C(2)-C(3) bond is 1.351(4) Å, confirming the presence of the double bond in the dithiolene moiety. The bonds, which the sulfur atoms form with the doubly bonded carbon atoms are 1.720(3) Å for C(2)-S(1) and 1.748(3) Å for C(3)-S(2), respectively. The bond angles around the sulfur atoms are 96.18(14)° for C(2)-S(1)-C(1) and 95.64(14)° for C(3)-S(2)-C(1). These findings are consistent with reported values for other dithiolene-2-one ligands.[12,13] The packing of **22** in a 1-D chain is facilitated by strong hydrogen bonds with a distance of 3.104(4) Å for S(2) and H(7) as well as 2.494(3) Å for O(1) and H(2), respectively. The angles measured for these hydrogen bonds C(3)-H(7)-S(2) and C(6)-H(2)-N(1) are 110.6(3)° and 115.5(7)°, respectively. After the synthesis and full characterisation of ligand **22**, its corresponding molybdenum and tungsten complexes were synthesised as described below.

3.3 Synthesis and characterisation of molybdenum (23) and tungsten (24) complexes derived from ligand 22

The synthesised ligand **22** was used to form complexes with two different metal salts *i.e.* $K_3Na[MoO_2(CN)_4].6H_2O1$ and $K_3Na[WO_2(CN)_4].6H_2O]2$ in a 2:1 ligand to metal ratio using a reported procedure which describes the formation of complexes as a mixture of *cis* and *trans* isomers.[12,14] The suitable metal precursor and sodium hydroxide was dissolved in oxygen free ethanol and then this mixture was transferred to the solution of ligand **22** in oxygen free ethanol. The reaction mixture was heated for 3-4 hrs and this resulted in the formation of the respective molybdenum (**23**) and tungsten (**24**) complexes. Both complexes were isolated using $[PPh_4]^+$ as counterion and were found to be air sensitive. The reaction scheme for the synthesis of both complexes and their proposed structures as pairs of *cis* and *trans* isomers are shown in Scheme 3.4.

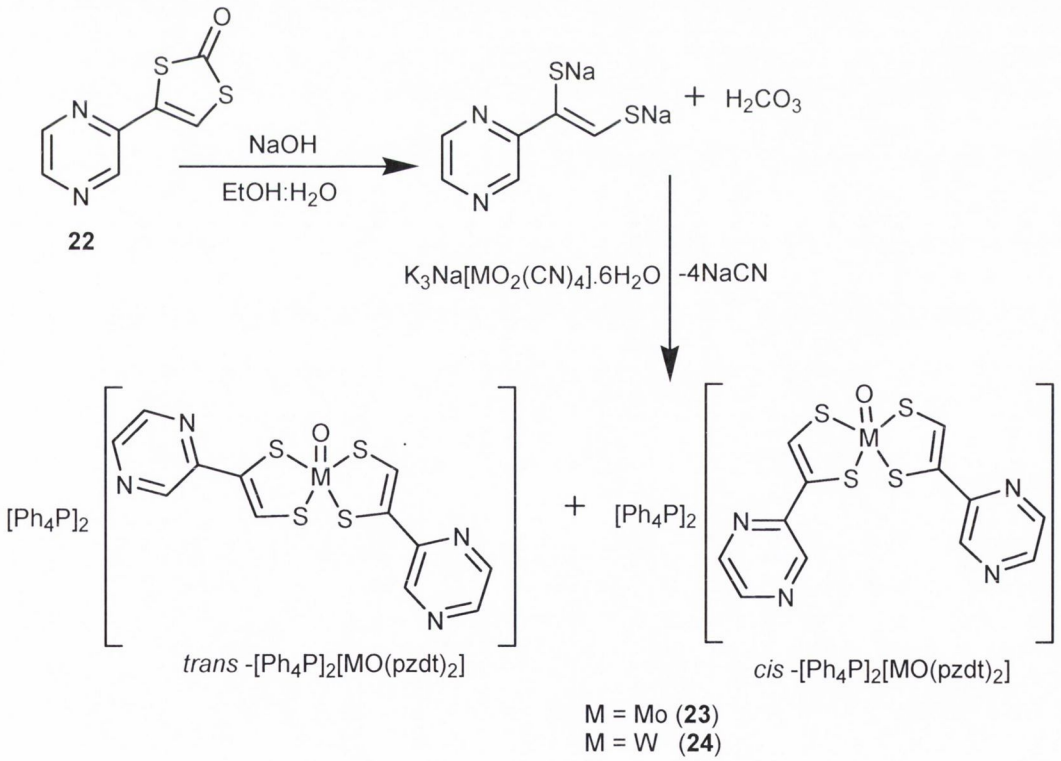

Scheme 3.4: Reaction scheme for the synthesis of pyrazine dithiolene derived molybdenum (**23**) and tungsten (**24**) complexes as a mixture of *cis* and *trans* isomers.

The reaction mechanism involves the cleavage of the sulfur carbonyl-carbon bonds of the dithiolene-2-one ring in the first step. This reaction is catalysed by the use of sodium hydroxide in ethanol which cleaves the S-C bonds to form an intermediate sodium salt of the substituted dithiolate. The byproduct in this step is formally carbonic acid. The four CN groups of the metal precursor are replaced by two *bis*-dithiolate ligands and the metal centre switches from the hexacoordinate to a pentacoordinate environment by releasing one of the oxo groups due to the presence of oxo groups *trans* to each other (trans effect). The formal oxidation state of the metal in both complexes is retained as M^{IV} state.

The IR spectra of the molybdenum (**23**) and tungsten (**24**) complexes exhibited the characteristic bands at 1491 and 1487 cm^{-1} corresponding to the υ(C=C) of dithiolene moiety, while the band for the υ(M=O) vibrations were seen at 917 and 919 cm^{-1}, respectively. These observed values for the υ(C=C) and υ(M=O) frequencies are in agreement with other published molybdenum and tungsten complexes.[12,13] A comparison of υ(M=O) values with the corresponding values of similar earlier reported complexes is illustrated in Table 3.1. Both complexes **23** and **24** showed slightly higher values for υ(M=O) frequencies compared to other reported complexes with weakened (M=O) character such as $[MoO(2\text{-}pedt)_2]^{2-}$,[3] $[WO(2\text{-}pedt)_2]^{2-}$,[13] $[MoO(cdt)_2]^{2-}$, and $[WO(cdt)_2]^{2-}$.[12] However, only strong electron withdrawing complexes $[MO(S_2C_2(CN)_2]^{2-}$ gave rise to high wave numbers (932-935 cm^{-1}).[15] The differences in υ(M=O) values of synthesised complexes with the earlier published ones can be explained when considering the electronegativity of the substituents attached to the dithiolene moiety. In contrast to the $[MO(2\text{-}pedt)_2]^{2-}$ and $[MO(cdt)_2]^{2-}$ complexes, the more electronegative pyrazine-substituted dithiolene ligand in $[MO(pzdt)_2]^{2-}$ complex makes sulfur to metal centre electron donation less efficient. Consequently, there is a more electronic contribution from oxygen to metal bonding and this results in an increase in υ(M=O) stretching frequencies. Similarly, a higher value for υ(M=O) frequency was observed for even more electronegative cyanide-substituted dithiolene complexes *i.e.* $[MO(S_2C_2(CN))_2]^{2-}$ when compared to the $[MO(pzdt)_2]^{2-}$ complexes.

Table 3.1: A comparison of characteristic υ(M=O) values for molybdenum (**23**) and tungsten (**24**) complexes with the corresponding values of the reported complexes.

Complex	υ(Mo=O) (cm^{-1})	Complex	υ(W=O) (cm^{-1})
$[MoO(pzdt)_2]^{2-}$	917	$[WO(pzdt)_2]^{2-}$	919
$[MoO(S_2C_2(CN))_2]^{2-}$	932[15]	$[WO(S_2C_2(CN))_2]^{2-}$	935[15]
$MoO(S_2C_2Me_2)_2]^{2-}$	889[16]	$[WO(S_2C_2Me_2)_2]^{2-}$	886[16]
$MoO(2\text{-}pedt)_2]^{2-}$	902[3]	$WO(2\text{-}pedt)_2]^{2-}$	905[14]
$[MoO(cdt)_2]^{2-}$	904.5[13]	$[WO(cdt)_2]^{2-}$	904.6[13]

The ^{1}H-NMR spectra for complexes **23** and **24** showed the most distinctive peaks associated with dithiolene protons in the region of 8.21-8.01 ppm. The chemical shifts of dithiolene protons are consistent with the values (8.50-7.13 ppm) of other dithiolene proton reported for molybdenum and tungsten complexes.[3,13] The ^{1}H-NMR spectra of both complexes indicated the presence of *cis* and *trans* isomers. The presence of these isomeric forms in both complexes is in agreement with those reported for other asymmetric dithiolene complexes.[3] This effect was especially pronounced for the environment of the ene fragment of the dithiolene which exhibited two distinct singlets, confirmed by running Heteronuclear Single Quantum Coherence (HSQC) experiment in a 1:3 ratio. However, precise assignments of the resonances to *cis* and *trans* isomers were not possible. All aromatic protons were found in the region of 9.23-8.15 ppm in both complexes. In addition, multiplets in the region of 7.96-7.74 ppm were attributed to the signals of aromatic protons of the counter cation $[PPh_4]^+$. The HRMS spectra finally confirmed the formation of these complexes in which the found molecular mass values were in perfect agreement with the calculated ones based on calculated molecular formulae. As an example, Figure 3.2 shows the characteristic molecular ion pattern (bottom) of molybdenum complex **23** which is well matched with the predicted isotopic distribution pattern (top). This experimentally found value (449.8631 u) was in agreement with the calculated value (449.8632 u) based on the proposed molecular formula of this complex.

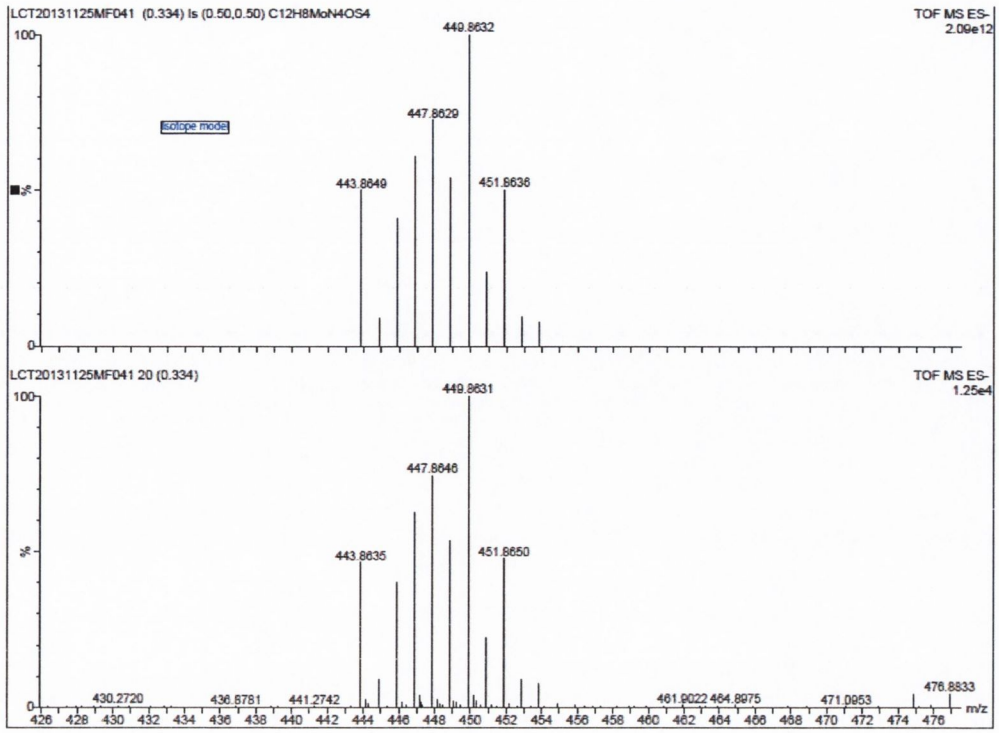

Figure 3.2: ESI-HRMS spectrum of complex **23** at the molecular ion region (bottom) and the calculated isotopic distribution pattern (top).

Further investigation such as X-ray structural analysis would be important to fully understand the exact geometry around the metal centre of these synthesised complexes and to compare these with the naturally occurring enzyme. A number of attempts were made by varying the cationic groups, such as $[PPh_4]^+$, $NEt_3(PhCH_2)]^+$ and K^+ to afford crystals. Unfortunately, crystals suitable for a X-ray structure analysis for both of the complexes (**23** and **24**) could not be isolated.

In summary, Sections 3.2 and 3.3 describe the successful synthesis and full characterisation of the novel pyrazine-substituted dithiolene-2-one ligand (**22**) and its respective molybdenum (**23**) and tungsten (**24**) complexes. The structure of ligand **22** was established by X-ray structural analysis. But unfortunately suitable crystals for its corresponding complexes could not be obtained possibly due to their presence as a mixture of *cis* and *trans* isomers. After the synthesis of these complexes, the next step was to explore their redox properties as discussed in the following Section 3.4.

3.4 Spectroelectrochemistry of molybdenum complex 23

The redox properties of synthesised complexes described above were investigated by cyclic voltammetry (CV), in combination with UV-Vis spectroelectrochemistry and electron paramagnetic resonance (EPR) spectroscopic techniques. These studies were carried out under supervision of Prof. Jon McMaster and Dr. Stephen E. Davies at the University of Nottingham, United Kingdom. Spectroelectrochemical data on molybdenum complex **23** is detailed in this section but unfortunately similar data for the tungsten complex **24** could not be generated due to its poor stability.

3.4.1 Cyclic voltammetry of complex 23

CV studies were performed by dissolving complex **23** in anhydrous DMF (5 ml) containing $[NBu^n_4][BF_4]$ (0.2 M) as the supporting electrolyte at 298 K, under a nitrogen atmosphere and the experimental procedure is described in Section 3.8.1. The obtained cyclic voltammogram for complex **23** is shown in Figure 3.3. The complex was found to be electroactive. Two oxidation processes (oxI and oxII) were observed with oxidation potential values at -303 and +439 mV, respectively; while one reduction potential value was found at -344 mV. The redox potential ($E_{1/2}$) value associated with the Mo^{V}-Mo^{IV} couple was calculated to be -323 mV.

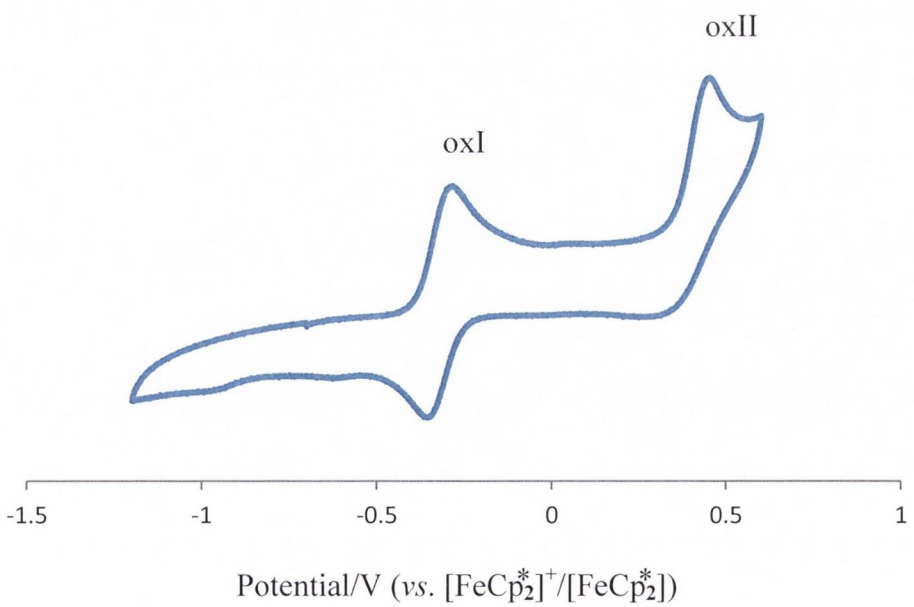

Figure 3.3: Cyclic voltammogram of complex **23** in DMF with $[NBu^n_4][BF_4]$ as the supporting electrolyte at 298K and scan rate 100 mVs^{-1}.

The electrochemical characteristic of the redox couple for complex **23** was also investigated. The separation of the peak potentials (ΔE) for the reversible redox couple was calculated to be 41 mV at a scan rate of 100 mVs^{-1}; this value was essentially the same as the corresponding ΔE value of the $[FeCp^*_2]^+/[FeCp^*_2]$ ($Cp^* = \eta^5$-C_5Me_5) couple used as an internal redox standard.

A study of the scan rate dependency of the peak currents (I_p^c and I_p^a) is shown in Figure 3.4 which illustrates that the peak currents changed linearly with the square root of the applied scan rate. The peak currents $-I_p^c/I_p^a$ ratio was equal to 1.0 in the scan range 20-300 mVs^{-1}, further confirming the fully reversible nature of the redox process (Mo^V-Mo^{IV}) at a range of applied scan rates.

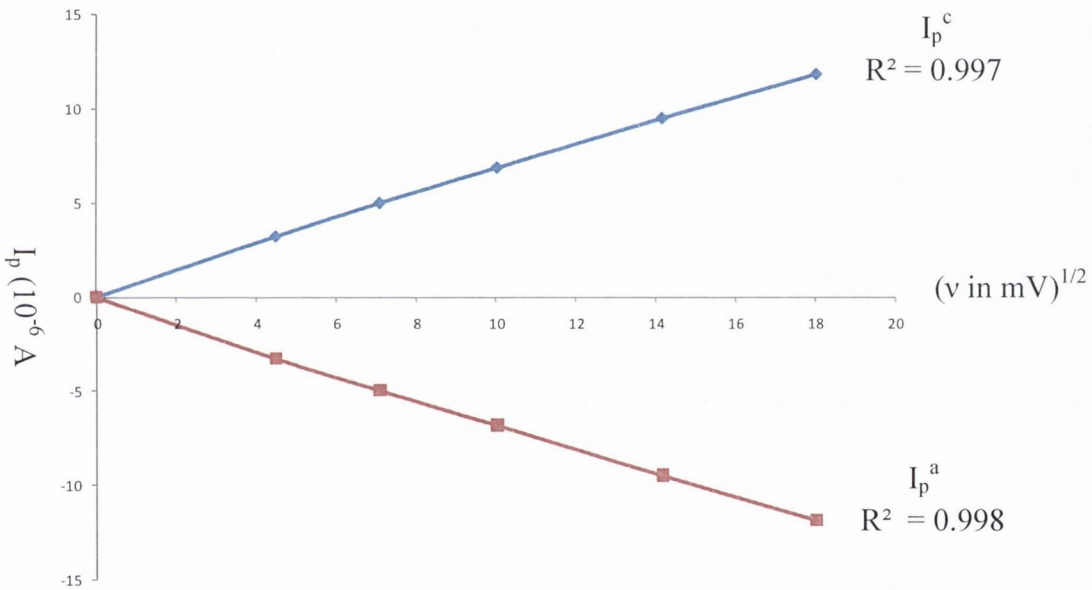

Figure 3.4: Plot of $-I_p^c/I_p^a$ *vs.* (scan rate)$^{1/2}$ for the fully reversible redox couple (Mo^V-Mo^{IV}) of complex **23**.

Literature reports have shown that the redox potential values for electron withdrawing substituted dithiolene based molybdenum complexes are more positive than those of electron donating substituted dithiolene complexes.[3,17,18,19] A comparison of the redox potential value of complex **23** with other substituted dithiolene molybdenum complexes is presented in Table 3.2. It reveals that the redox potential value of novel complex **23** is less negative ($E_{1/2}$ = -323 mV *vs.*

$[FeCp^*_2]^+/[FeCp^*_2]$) compared to the redox potential values ($E_{1/2}$ = -480 to -348 mV *vs.* $[FeCp^*_2]^+/[FeCp^*_2]$) determined for other reported dithiolene molybdenum complexes.[3] This positive value suggests more electron withdrawing character of the pyrazine ring attached to the dithiolene in this complex compared to other electrochemically characterised molybdenum complexes as illustrated in Table 3.2. Most importantly, this ligand also includes the pyrazine features of MPT, therefore, it is possible that electron withdrawing substituted dithiolene (*i.e.* MPT) plays an important role within the naturally occurring ligand system.

Table: 3.2: A comparison of the characteristic data of the redox potential for complex **23** with other reported values.

Complex	$E_{1/2}$ (mV) vs. $[FeCp^*_2]^+/[FeCp^*_2]$ (Mo^V-Mo^{IV})	Solvent
$[MoO(pzdt)_2]^{2-}$	-323	DMF
$[MoO(sdt)_2]^{2-}$	-480[3]	DMF
$MoO(2\text{-}pedt)_2]^{2-}$	-422[3]	DMF
$MoO(4\text{-}pedt)_2]^{2-}$	-348[3]	DMF

Complex **23** also exhibited another oxidation process (oxII, Figure 3.3) which appeared at a more positive potential (439 mV *vs.* $[FeCp^*_2]^+/[FeCp^*_2]$) and could be attributed to the $[MoO(pzdt)_2]^0$-$[MoO(pzdt)_2]^-$ couple. The irreversibility of this (Mo^{VI}-Mo^V) couple was not surprising as similar observations for oxidation of Mo^V centre to the Mo^{VI} has already been previously observed.[20,21] One possible reason is the formation of dimers or oligomers which may responsible for the generation of neutral Mo^{VI} complex.

3.4.2 UV-Vis spectroelectrochemical studies of complex 23

The objective of UV-Vis spectroelectrochemical studies on synthesised molybdenum complex was to characterise the absorption bands associated with the reduced $[MoO(pzdt)_2]^{2-}$ and oxidised $[MoO(pzdt)_2]^-$ forms of this complex. These studies were performed by dissolving the $[MoO(pzdt)_2]^{2-}$ in anhydrous DMF (5 ml) containing $[NBu^n_4][BF_4]$ (0.2 M) as the supporting electrolyte at 298 K, under

nitrogen atmosphere and the experimental procedure is described in Section 3.8.1. The obtained UV-Vis spectrum for complex $[MoO(pzdt)_2]^{2-}$ is shown in Figure 3.5. It clearly shows the characteristic absorption bands at 437, 355 and 309 nm which are in agreement with the typical UV-Vis spectral profiles reported for other *bis*-dithiolene oxo molybdenum complexes in literature.[3] The absorption band in the visible region (437 nm) has been attributed to the dithiolene ligand to metal (S ⟶ M) charge transfer transitions of dithiolene metallocycle, by comparison to the prior spectral assignments for $[MoO(bdt)_2]^{2-}$ and $[MoS(bdt)_2]^{2-}$ complexes.[22] However, the absorption bands in the UV region at 355 and 309 nm were assigned to the n ⟶ π^* and π ⟶ π^* transitions, respectively

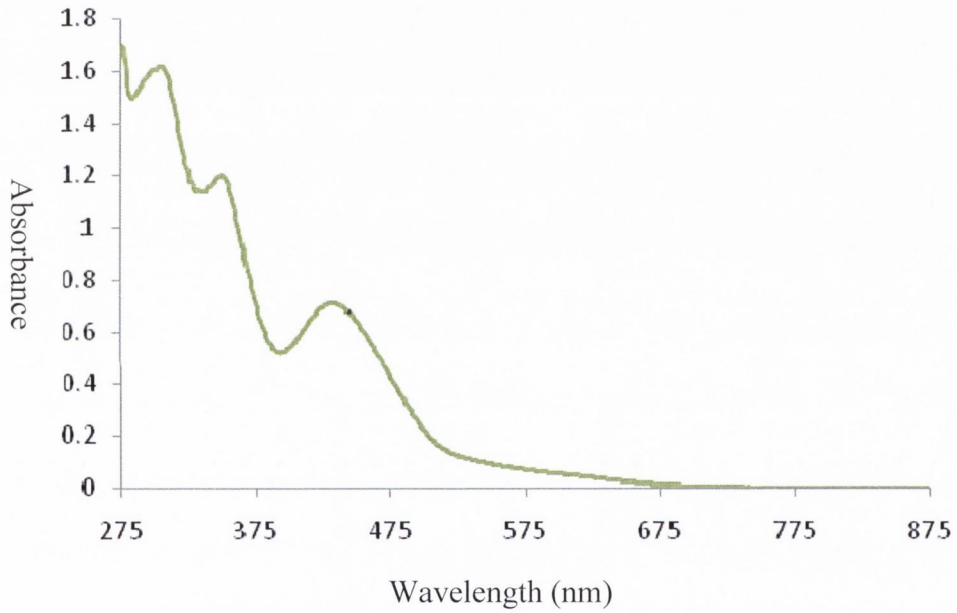

Figure 3.5: The UV-Vis spectrum of $[MoO(pzdt)_2]^{2-}$ at 273 K in DMF, containing the $[NBu^n_4][BF_4]$ (0.2 M) as the supporting electrolyte. (before applying any potential).

The oxidation process of $[MoO(pzdt)_2]^{2-}$ to $[MoO(pzdt)_2]^-$ was studied by UV-Vis spectroelectrochemistry. An initial potential of -600 mV was applied to the solution of $[MoO(pzdt)_2]^{2-}$ and the UV-Vis spectra were recorded in specific intervals of time (1 min) until no change in spectrum was observed. A stack of these UV-Vis spectra is shown in Figure 3.6. The first spectrum **1** corresponds to the $[MoO(pzdt)_2]^{2-}$ while the spectra from **2-9** represent its successive oxidation over the time. The final

spectrum **10** is that of the fully oxidised form *i.e.* $[MoO(pzdt)_2]^-$ complex. During this oxidation process, it was also noted that the colour of the solution of oxidised $[MoO(pzdt)_2]^-$ changed from orange to reddish brown. Figure 3.6 clearly shows that upon successive application of potential on molybdenum complex marked changes in the UV-Vis spectroscopic profile occurred. The intensity of the absorption maximum at 437 nm gradually decreased with the formation of a new absorption band at 826 nm due to the involvement of characteristic d ⟶ d transitions, with respect to prior assignments in literature reports.[3,23] Three distinct isobestic points at 596, 406 and 367 nm were observed which indicate that the oxidation of Mo^{IV} to Mo^{V} progresses smoothly, with possibly no intermediate structural change. Similar observations have been previously made for the oxidation of other $[MoO(dithiolene)_2]^{2-}$ to $[MoO(dithiolene)_2]^-$ complexes.[3]

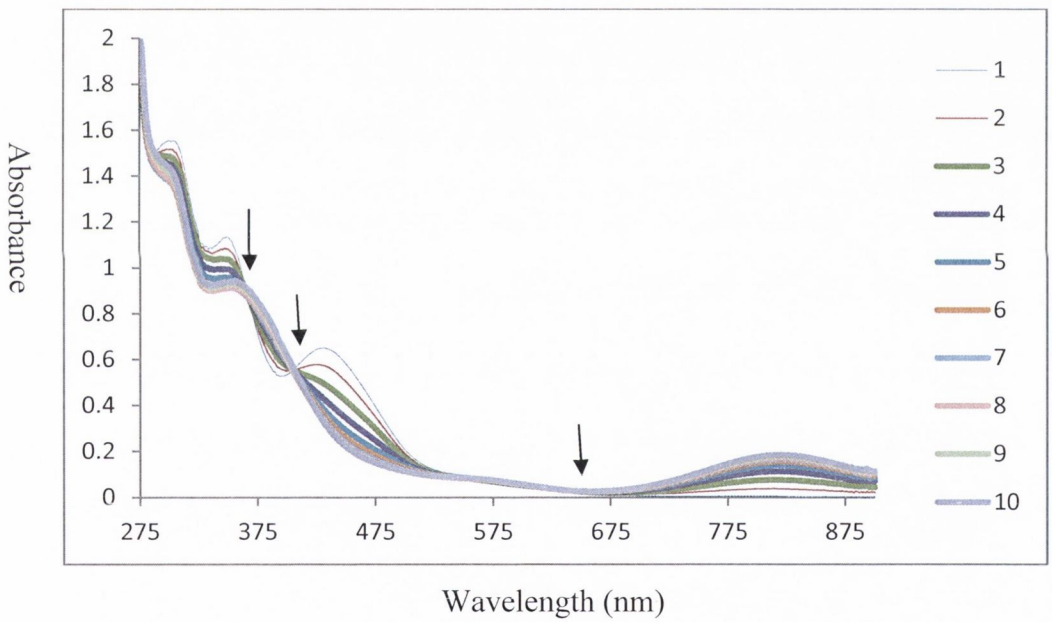

Figure 3.6: UV-Vis spectra observed for the oxidation of $[MoO(pzdt)_2]^{2-}$ to $[MoO(pzdt)_2]^-$ in DMF at 273 K with, containing $[NBu^n_4][BF_4]$ (0.2 M) as the supporting electrolyte in 9 mins. Isobestic points are indicated by arrows.

Afterwards, *in situ* reduction of $[MoO(pzdt)_2]^-$ to $[MoO(pzdt)_2]^{2-}$ was carried out and the results are shown in Figure 3.7. The initial potential 0.0 V was applied to the fully oxidised Mo^{V} complex solution and its UV-Vis spectra were recorded in specific intervals of time (1 min) until no change was observed. Spectrum **10** in

Figure 3.7 represents the fully oxidised form Mo^{V} while spectra **11-18** represent the successive reduction of the complex over time. Spectrum **19** shows the disappearance of the lowest energy band at 826 nm with regeneration of a similar spectral profile (Figure 3.5) as was observed for parent molybdenum complex **23**. The appearance of three isobestic points at 655, 415 and 362 nm indicates that the reduction of Mo^{V} to Mo^{IV} also progresses smoothly, again consistent with no significant structural change. Overall, the absorption spectra characteristics noted for oxidised $[MoO(pzdt)_2]^-$ and reduced $[MoO(pzdt)_2]^{2-}$ states are consistent with the published results for other $MoOS_4$ chromophores in both Mo^{IV} and Mo^{V} states in literature.[3,22]

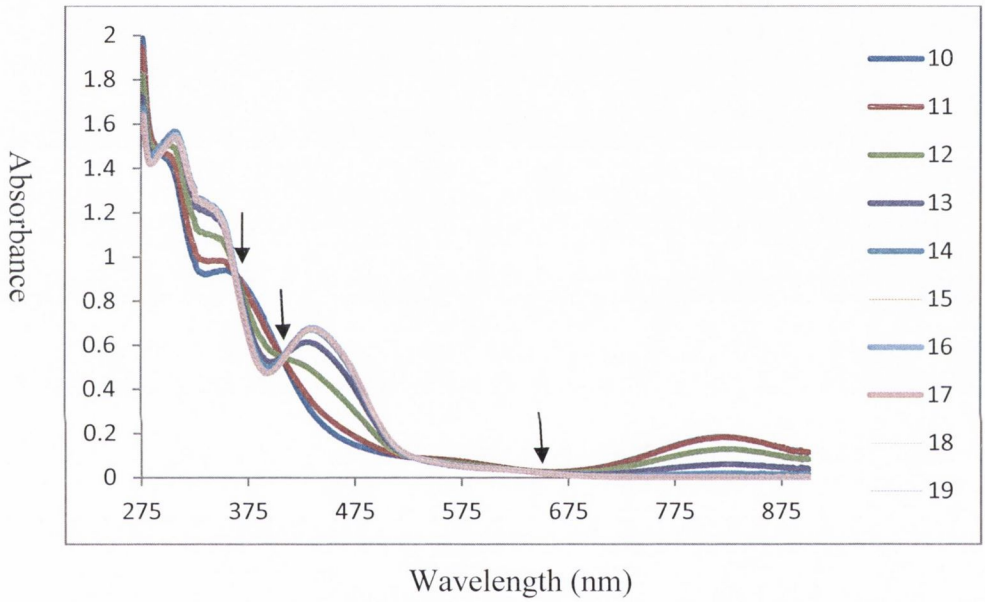

Figure 3.7: UV-Vis spectra observed for *in situ* reduction of $[MoO(pzdt)_2]^-$ to $[MoO(pzdt)_2]^{2-}$ in DMF at 273 K, containing $[NBu^n_4][BF_4]$ (0.2 M) as the supporting electrolyte in 9 mins. Isobestic points are indicated by downward arrows.

The low energy absorption bands for DMSO reductase in reduced (Mo^{IV})[24] and oxidised (Mo^{V})[25] forms have been reported 640 and 720 nm, respectively. However, the lowest energy band in the UV-Vis spectrum of molybdenum complex **23** was found at 826 nm. The lack of correlation in the UV-Vis data reported for reduced and oxidised forms of complex **23** and those published for DMSO reductase, however, illustrate the presence of different ligand field and charge transfer energies as a possible consequence between the two different systems.

3.4.3 Electron paramagnetic resonance spectrum of complex 23

EPR spectroscopy provides useful information on the electronic and geometric structure of transition metal ions by characterising the interaction of the metal centre spin with the applied magnetic field. The EPR investigation of complex **23** was operated at a fixed frequency of 9.5 GHz (X band), with a field strength of 3,400 gauss. The oxidation of complex **23** in anhydrous DMF (5 ml) was achieved by bulk electrolysis at a controlled potential (-0.75 V), containing the $[NBu^n_4][BF_4]$ (0.2 M) as the supporting electrolyte. The experimental procedure is described in Section 3.8.1. Upon electrolysis, it was noted that the colour of the solution of the molybdenum complex changed from orange to reddish brown due to change in the oxidation state from Mo^{IV} to Mo^{V}, in agreement with the UV-Vis spectral data observed for this process. The X-band EPR spectrum for the molybdenum complex was recorded in both fluid and frozen states at 298 and 77 K, respectively. A comparison of the fluid solution experimental (black line) and the simulated (red line) EPR spectra for $[MoO(pzdt)_2]^-$ is shown in Figure 3.8. The room temperature EPR spectrum exhibited six satellites for $^{95,97}Mo$ (I = 5/2) which superimposed upon the single line for the $^{92,94,96,98}Mo$ (I = 0) signal.

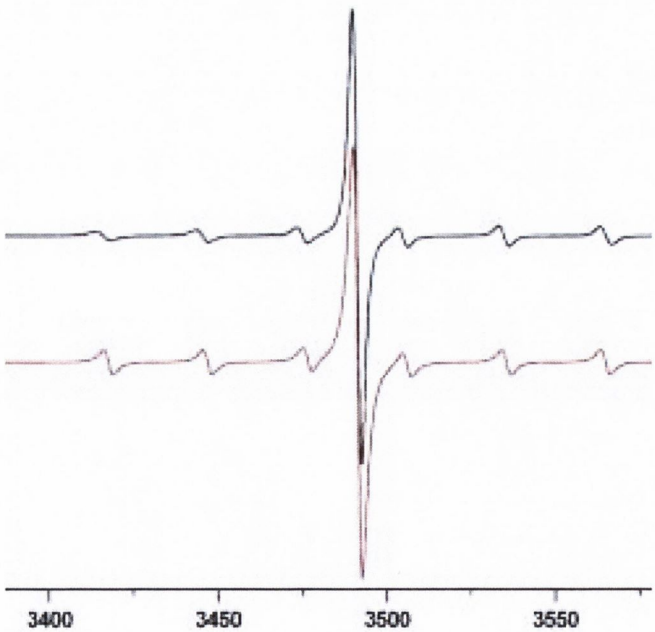

Figure 3.8: a) The experimental EPR spectrum (black line) of $[Mo^{V}O(pzdt)_2]^-$ in DMF at 298 K and b) simulated spectrum (red line) with linewidth (W_{iso} = 2.7 G).

The values of g_{iso} (1.994) and A_{iso} (27.5 x 10^{-4} cm^{-1}) are consistent with the parameters for $[MoO(4\text{-}pedt)_2]^-$ (1.995 and 27.0 x 10^{-4} cm^{-1})[3] and $[MoO(SCH_2CH_2S)_2]^-$ (1.999 and 30.3 x 10^{-4} cm^{-1})[20] and confirm the predominant metal based character for an unpaired electron.[26] The frozen solution experimental EPR spectrum (black line) for $[MoO(pzdt)_2]^-$ was also recorded at 77 K and is displayed with its simulated spectrum (red line) in Figure 3.9. In frozen solution, the g values were found to be in a rhombic pattern and are in agreement with other reported molybdenum complexes in literature.[3,20,27] EPR spectral simulation gave a rhombic g values with g_{xx} = 2.022, g_{yy} = 1.987, g_{zz} = 1.977, which is consistent with previously reported values for $[MoO(2\text{-}pedt)_2]^-$, $[MoO(4\text{-}pedt)_2]^-$ and $[MoO(S_2C_2(CN))_2]^{2-}$ complexes.[3,15]

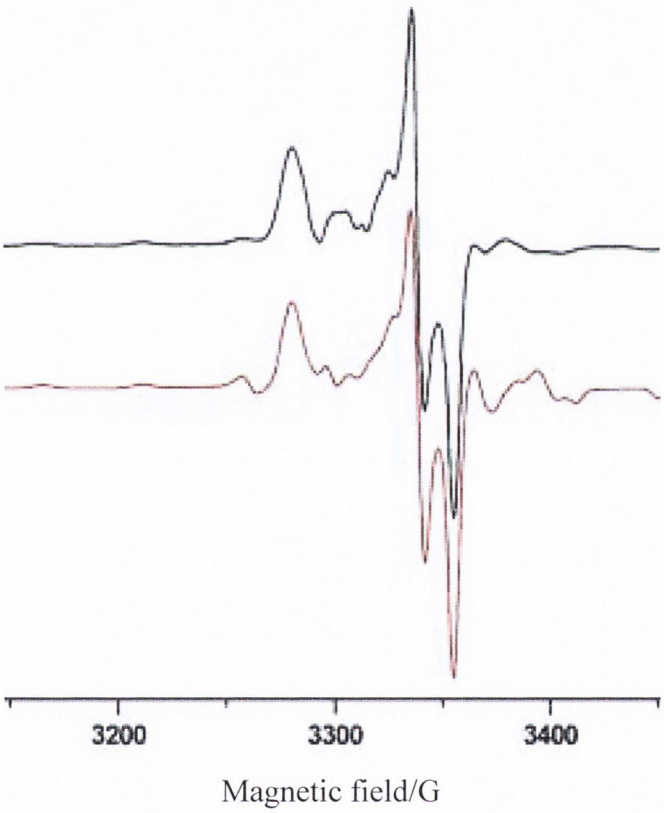

Figure 3.9: a) The frozen solution X-band EPR spectrum of $[Mo^VO(pzdt)_2]^-$ in DMF at 77 K (black line) and b) the simulated spectrum (red line).

By the measurement of anisotropic and subsequent simulated spectra, rhombic metal hyperfine interactions could be determined; A_{xx} = 43.5 x 10^{-4} cm^{-1}, A_{yy} = 17.0 x 10^{-4} cm^{-1}, A_{zz} = 35.0 x 10^{-4} cm^{-1}. The average anisotropic parameters from frozen solution (g_{ave} = 1.995) and A_{ave} = 31.8 10^{-4} cm^{-1}) were found to be in reasonable agreement

with the measured fluid solution isotropic g_{iso} and A_{iso} values, indicating that no major change in the structure of the $[MoO(pzdt)_2]^-$ was observed between fluid and frozen phases. Additionally, these values are within a range observed in other reported Mo^V *bis*-dithiolene complexes.[3,21,26] It was also noted that the hyperfine coupling at high field for the frozen solution (y and x) were ambiguous since the A_{ave} value from the frozen solution data (A_{ave} = (43.5 + 17.0 + 35.0)/3 = 31.8 x 10^{-4} cm^{-1}) was a bit higher when compared to the A_{iso} (27.5 x 10^{-4} cm^{-1}) value obtained for the fluid solution. This difference in values suggest that single crystal studies, however, required for detailed structural investigations. The direct measurement of sulfur hyperfine (which gives some indication of the electron density at sulfur) is not possible due to the low natural abundance of ^{33}S (I = 3/2, 0.78%). In order to estimate the non-innocence character of dithiolene in a complex, however, the use of detailed theoretical studies is required. Overall, the obtained fluid and frozen spectral profiles for $[MoO(pzdt)_2]^-$ are in good agreement with other reported dithiolene molybdenum complexes,[3] which have been observed to have square-based pyramidal geometry around the metal centre, suggesting to be similar in our case.

In conclusion, complex **23** bears four sulfur atoms that are coordinated to the oxo molybdenum centre, and serves as a synthetic structural analogue of the DMSO reductase family. The electrochemical properties in combination with UV-Vis as well as EPR parameters have been investigated for synthesised molybdenum complex **23** and compared with the literature. A fully reversible, one electron, redox couple for Mo^V-Mo^{IV} has been established by CV. The value of redox potential for this Mo^V-Mo^{IV} couple was calculated to be -323 mV (*vs.* $[FeCp^*_2]^+/[FeCp^*_2]$). The results of the UV-Vis spectroelectrochemical studies clearly indicate that there is no significant structural change involved for the complex during oxidation and reduction processes. Moreover, EPR spectroscopic data for the Mo^V state of complex **23** is consistent with the presence of unpaired electron which is coupled to the Mo (5/2) nucleus *i.e.* it is not significantly delocalised to the dithiolene ligands.

3.5 Synthesis of closed and open alcohol form MPT analogues of DMSO reductase

The work carried out in Sections 3.2 and 3.3 describes the successful synthesis of the pyrazine-substituted dithiolene-2-one ligand **22** and its respective molybdenum (**23**) and tungsten (**24**) complexes as structural models for DMSO reductase. Unfortunately, these models cannot provide any information regarding the interconversion of the closed (pyran) and open (alcohol) forms as observed for enzymatic structural states. Figure 3.10 illustrates the proposed interconversion of closed form **A** and open alcohol form **B** of the DMSO reductase. The structures of both of these forms have been confirmed by X-ray crystallographic studies.[28] It has also been noted that the pterin moiety in both forms **A** and **B** plays a key role due to its occurrence in different oxidation states.

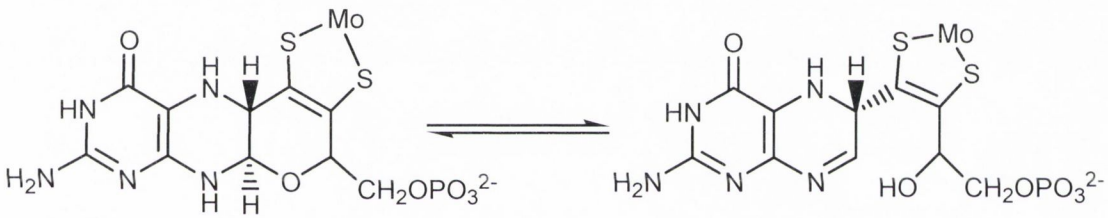

Closed form (**A**) Open alcohol form (**B**)

Figure 3.10: The interconversion of closed form (**A**) and open alcohol form (**B**) of the DMSO reductase.[27]

To synthesise structural models of DMSO reductase in forms **A** and **B**, there is a need to design an oxo molybdenum centre, which is not only coordinated to a *bis*-dithiolene ligand set but which also includes a pyrazine ring and the alcohol side chain features of enzymatic MPT. Such type of structural models will possibly help elucidating key structural, spectroscopic and reactivity properties of the enzymatic molybdenum centre of DMSO reductase. This section describes the efforts that were used for the synthesis of both targets; the closed and the open alcohol form structural models. Firstly, it was planned to synthesise a closed form ligand and the synthetic methodology used is discussed below.

The strategy as shown in Scheme 3.5, illustrates the attempted multi-step synthesis to construct the closed form ligand (**28**). Firstly, the synthesis of propynyl quinoxaline (**25**) was achieved by the reaction of 2-hydroxy quinoxaline with 3-bromo-1-propyne. Then the hydrogen of the terminal alkyne moiety in **25** was replaced by a bromo substituent to yield bromo-propynyl quinoxaline (**26**). Then the most important step would have been the ring closure of the 3-bromo-propynyl chain in **26** with its quinoxaline ring to form fused quinoxaline-pyran-4-one (**27**). A literature report has previously described a method to cyclise 3-bromo propynyl benzene to generate a pyran-4-one moiety.[29] Similar methodology was attempted to form compound **27** which is discussed in detail below. The main intention behind the synthesis of compound **27** was its utilisation to construct a dithiolene-2-one moiety on its pyran-4-one ring to produce the closed form ligand (**28**) using an already established protocol by our group.[12,16]

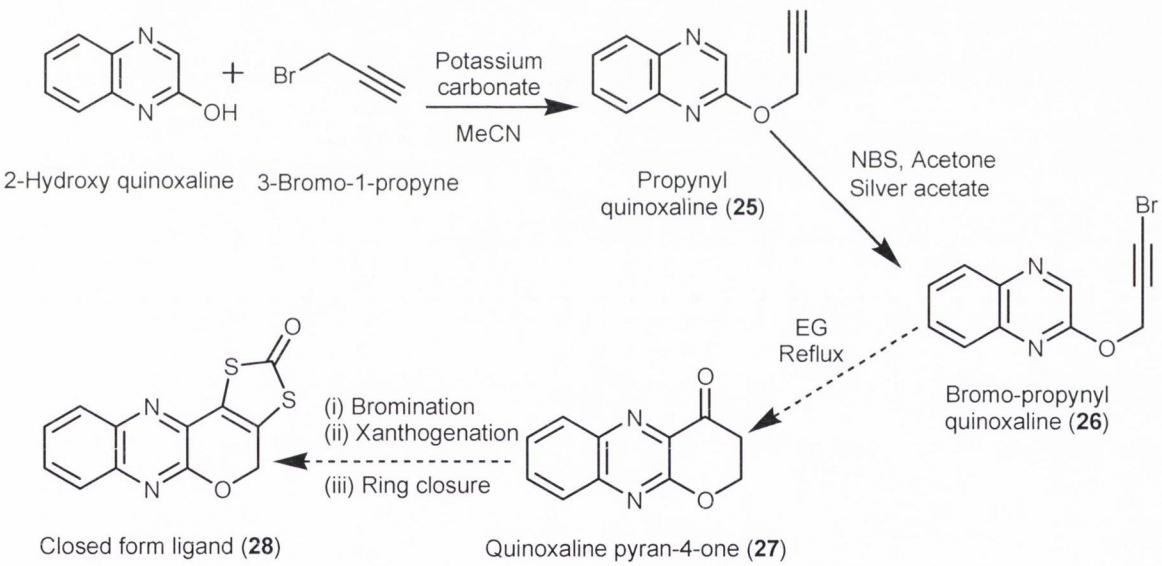

Scheme 3.5: Proposed multi-step synthetic route for the preparation of closed form ligand (**28**) as model for the MPT ligand in MoCo, starting from 2-hydroxy quinoxaline (**29**).

The alkylation of 2-hydroxy quinoxaline with 3-bromo-1-propyne was achieved in the presence of potassium carbonate. The reaction mixture was refluxed for 48 hrs in acetonitrile under nitrogen atmosphere and after work up an off-white crystalline product being propynyl quinoxaline (**25**) was obtained. The melting point temperature of **25** was found to be 174-175 °C. IR spectral studies showed two

characteristic absorption bands at 2121 and 1656 cm^{-1} corresponding to the alkyne moiety υ(C≡C) and υ(C=N) of the quinoxaline ring, respectively. The ^{1}H-NMR spectrum suggested the formation of desired product **25**. Two characteristic peaks at 5.07 and 3.35 ppm were observed corresponding to the methylene (CH_2) and methine (CH) protons of the propynyl chain. Aromatic protons appeared in between 8.29-7.44 ppm. The obtained spectral data are consistent with those earlier reported for the synthesis of other propynyl benzene derivatives.[28] The $^{13}C\{^{1}H\}$-NMR spectrum exhibited its most upfield peak at 31.1 ppm corresponding to the methylene carbon (CH_2), while the characteristic alkyne carbons (C≡C) were observed at 78.0 and 75.2 ppm. Aromatic carbons appeared in between 153.9-114.2 ppm. The formation of compound **25** was also confirmed by ESI-HRMS where the calculated mass value (185.0715 u) was in excellent agreement with the experimentally determined mass value (185.0716 u).

In the second step, the terminal alkyne hydrogen of compound **25** was replaced by bromine by employing a literature procedure.[30] The synthetic methodology involved the reaction of **25** with *N*-bromosuccinimide (NBS) in the presence of catalytic amount of silver acetate in acetone. The reaction mixture was heated under reflux for 4 hrs to give a light yellowish powder of bromo-propynyl quinoxaline (**26**).

The melting point temperature of **26** was found to be 109-110 °C. The IR spectrum of **26** showed a characteristic band at 645 cm^{-1} attributed to the υ(C-Br) vibrations. In addition, the distinct alkyne υ(C≡C) band appeared at 2251 cm^{-1}; this is shifted to lower wavenumbers (130 cm^{-1}) as compared to **25** due to the electron withdrawing nature of the attached bromine atom. The disappearance of the peak at 3.35 ppm in the ^{1}H-NMR spectrum of **26** supported the substitution of the terminal alkyne hydrogen with a bromine. In addition, as expected a slight downfield shift of 0.07 ppm in the methylene protons (CH_2) of the propynyl chain was also observed. All aromatic protons appeared around 8.29-7.45 ppm. Finally, ESI-HRMS confirmed the formation of compound **26** as the obtained molecular mass value (219.0322 u) was in good agreement with the calculated molecular mass value (219.0325 u).

After the successful synthesis of **26**, the next step was the cyclisation of the propynyl chain with the quinoxaline ring to construct a fused quinoxaline pyran-4-one (**27**).

Literature reports have shown that ring closure of a propynyl chain with methoxy benzene is successfully achieved in refluxing ethylene glycol.[28] Similar methodology was attempted for the cyclisation of **26** to desired compound **27**. Compound **26** was heated under reflux in ethylene glycol for 4 hrs under nitrogen atmosphere. After work up, the obtained red precipitates were crystallised by slow evaporation of DCM – hexane (1:1) to afford red crystals.

Surprisingly, X-ray structural analysis of the red crystals revealed the formation of a novel propyne quinoxalinone (**29**) instead of the desired cyclised compound **27**. The atomic numbering scheme and the unit cell diagram is shown in Figure 3.11 **A** and **B**, respectively. The structure was solved in the monoclinic space group $P2_1/c$ and contains four molecules in the unit cell and one independent molecule in the asymmetric unit. A summary of the crystallographic data collection and structural refinement parameters along with selected bond lengths and angles is listed in Appendices 6.6 and 6.8, respectively.

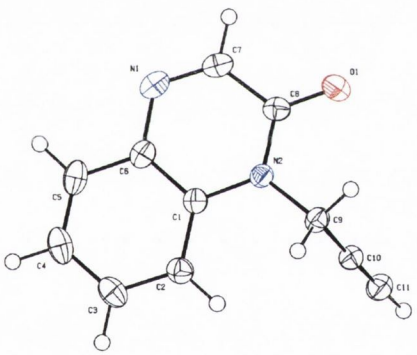

A

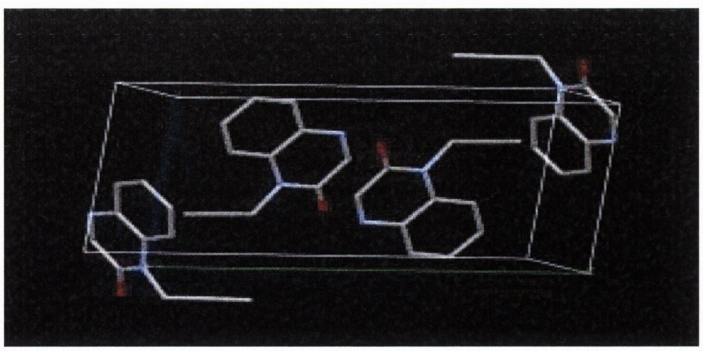

B

Figure 3.11: The X-ray crystal structure of propyne quinoxalinone (**29**); **A**) the atomic numbering scheme, **B**) the unit cell diagram.

The X-ray structure showed the attachment of the propyne group to the N(2) atom of the quinoxalinone ring. The bond length between C(8)-O(1) carbonyl group is 1.232(14) Å and consistent with other reported bond distances of carbonyl group of quinoxaline-2,3-dione.[31] The propyne was found to be twisted out of the quinoxalinone ring plane by an angle of 112.5(6)° and the bond distance of N(2) of quinoxaline and C(9) of propyne is 1.470(13) Å. The bond distance of 1.183(16) Å between C(10)-C(11) confirmed the presence of the alkyne moiety in the propyne chain. It was observed that the crystal structure of compound **29** was stabilised by the formation of a strong intermolecular hydrogen bond between the carbonyl O(1) and the hydrogen of the propyne chain H(11) with a distance of 2.177(7) Å and an angle C(8)-O(1)-H(11) of 119.4(6)°. In addition, relatively weak hydrogen bonding was also observed between O(1) and a hydrogen of benzene ring H(4) with a distance of 2.635(6) Å and an angle of C(4)-O(1)-H(4) of 135.7(4)°.

The melting point temperature of compound **29** was found in the range of 261-262 °C. The IR spectrum of **29** showed two absorption bands at 2142 and 1673 cm^{-1}, which were assigned to the frequencies of the carbonyl group υ(C=O) of the quinoxalinone and the alkyne moiety υ(C≡C) of the propyne chain, respectively. The ^{1}H-NMR spectrum of **29** exhibited the characteristic methylene (CH_2) and methine (CH) protons of the propyne chain at 5.01 and 3.64 ppm, respectively. The peaks of all aromatic protons were observed in the range of 8.19-7.22 ppm. Furthermore, the appearance of the most downfield peak at 155.3 ppm in the $^{13}C\{^{1}H\}$-NMR spectrum corresponded to the formation of the carbonyl group (C=O) on the quinoxalinone ring. Moreover, the formation of compound **29** was confirmed by running ESI-HRMS as the found molecular mass value (185.0815 u) was in good agreement with the calculated (185.0715 u) one.

In hindsight, the formation of compound **29** under the applied reaction conditions is not too surprising. A proposed mechanism for the formation of propyne quinoxalinone (**29**) is shown in Scheme 3.6. It is suggested that the bromine of **26** reacts with the ethylene glycol to form compound **A**, with the elimination hydrogen bromide as a side product. Afterwards, compound **A** is stabilised by the re-location of propyne from oxygen to the nitrogen atom to yield compound **C**. A possible mechanism for the rearrangement of propyne from oxygen to the nitrogen atom in

compound **C** can be envisioned by the aid of the Claisen re-arrangement (as illustrated in Scheme 3.6). Afterwards, it has been postulated that lone pair of oxygen in compound **C** attacks on hydronium ion to form compound D which finally resulted in the formation of propyne quinoxaline (**29**), with the regeneration of ethylene glycol.

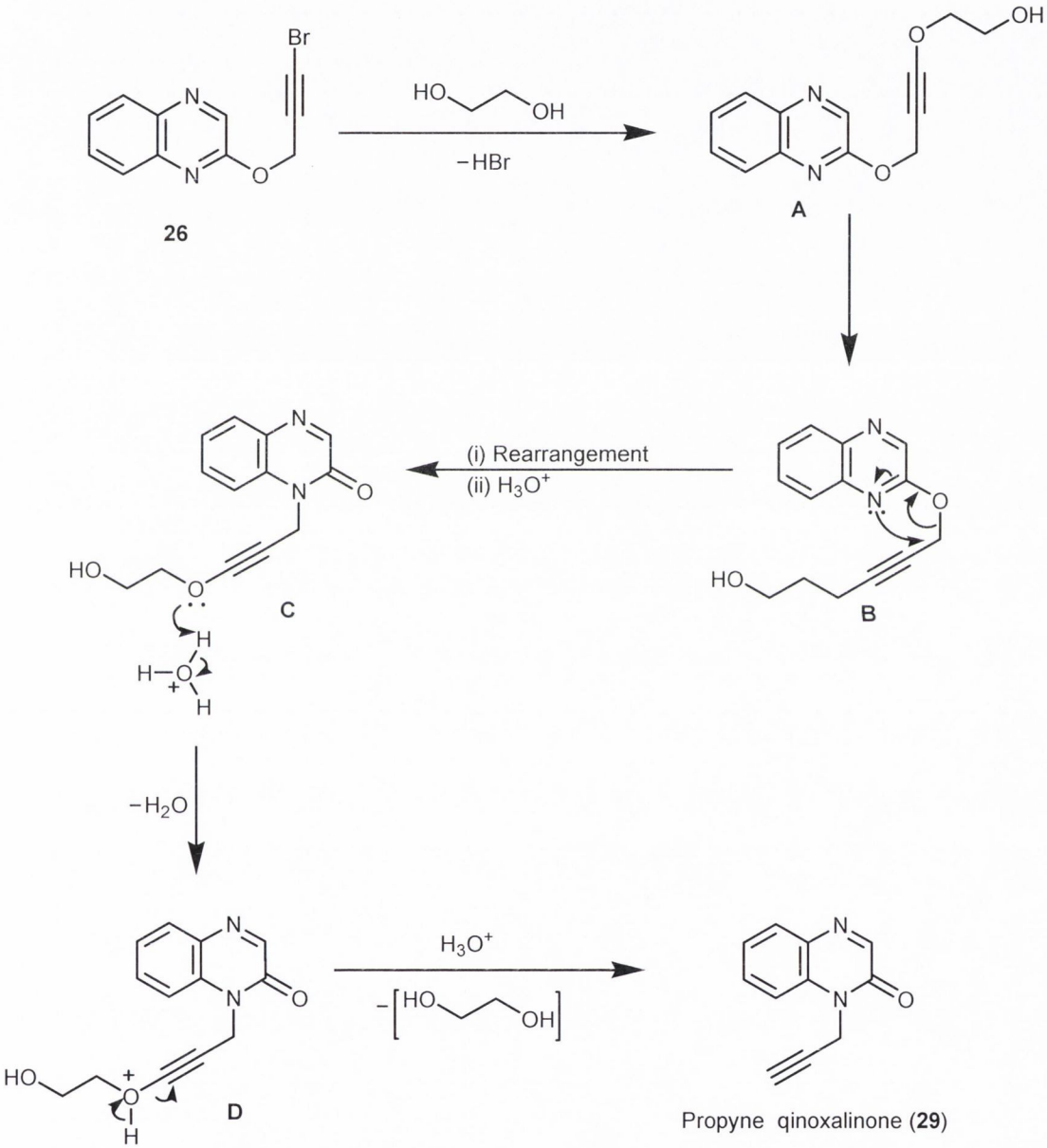

Scheme 3.6: Proposed reaction mechanism for the formation of propyne quinoxalinone (**29**).

A number of attempts were made to obtain the desired compound **27** by varying the reaction conditions such as reaction times and different temperature ranges. But unfortunately, after work up, the obtained red crystals were characterised as compound **29** in all cases. The failure of this methodology in our case is possibly due to the preferable re-arrangement of propyne from oxygen to nitrogen atom as described in the suggested mechanism. To avoid this undesired re-arrangement, one possible route is to to protect the nitrogen of the quinoxalinone ring which may result in desired compound **27**. Unfortunately, this compound could not be employed for further reaction to form a closed form ligand, however, a novel compound **29** has been isolated and fully characterised.

Attention was then turned to the desired open alcohol form ligand which, once made, could possibly be cyclised to generate the closed form analogue. Two synthetic methodologies have been adopted as discussed below. In the first strategy, as illustrated in Figure 3.12, a simple ligand with alcohol side chain **30** was targeted to be synthesised from the already available pyrazine-substituted dithiolene ligand (**22**, Section 3.2)

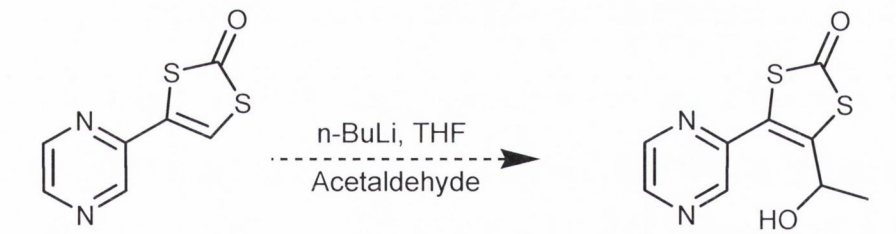

Pyrazine-substituted dithiolene-2-one (**22**)

Pyrazine hydroxy-dithiolene-2-one (**30**)

Figure 3.12: Attempted route to synthesise ligand (**30**) from pyrazine-substituted dithiolene-2-one ligand (**22**).

A reported procedure has been adopted to attach the alcohol side chain on to the dithiolene moiety of ligand **22**. Following this, ligand **22** was treated with *n*-BuLi in THF at -78 °C for 30 mins followed by dropwise addition of acetaldehyde. The reaction mixture was left to stir for 1 hr and allowed to warm to room temperature. The colour of the reaction mixture changed from light brown to orange but TLC still demonstrated the presence of starting material. Our assumption that a longer reaction

time would help to drive the reaction forward proved to be wrong. The reactions were repeated using the same reaction conditions and up to 12 hr stirring. The ^{1}H NMR analysis of the obtained solids, after the work up of these reactions, showed the characteristic peak of the dithiolene proton at 7.52 ppm corresponding to starting material **22**, suggesting the failure of the intended reaction to form ligand **30**.

After the failure of the first strategy, another possible route (shown in Scheme 3.7) was employed for the synthesis of an open alcohol ligand *i.e.* chloropyrazine hydroxy-dithiolene-2-one (**32**). Literature reports have shown that the direct synthesis of the dithiolene-2-one moiety is possible by the reaction of electron deficient alkynes with *bis*-alkyl xanthogen disulfides in the presence of radical initiator.[32,33,34] Following this approach, a chloropyrazine hydroxy-alkyne (**31**) was synthesised, to react with *bis*-alkyl xanthogen disulfides. It was thought that the introduction of the electron withdrawing chloro group on pyrazine, would make the alkyne moiety in **26** more electron deficient in nature and consequently would favour the formation of the dithiolene moiety *via* the cycloaddition reaction as discussed below.

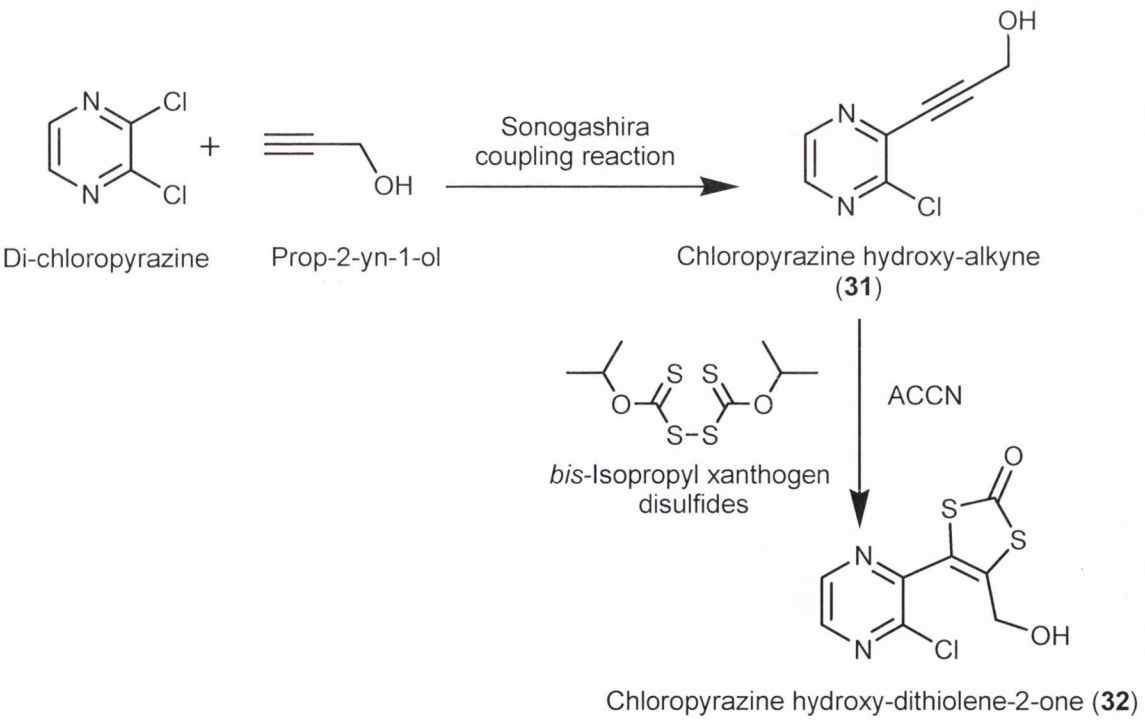

Scheme 3.7: Synthetic route for the preparation of open alcohol ligand **32** from the chloropyrazine-hydroxy alkyne (**31**).

The synthesis of **31** was achieved by the reaction of di-chloropyrazine with prop-2-yn-1-ol using the Sonogashira coupling reaction. The reaction procedure involved 6 hrs reflux under argon. After cooling the reaction mixture to room temperature, the crude product was obtained as dark brown powder. The purification of the compound was achieved by silica column chromatography to afford air stable **31**.

The melting point temperature of **31** was found in the range of 96-97 °C. The IR spectrum of **31** showed two prominent absorption bands at 3223 and 2231 cm^{-1} which were ascribed to the vibrations of υ(OH) and υ(C≡C) of the propynyl chain, respectively. The appearance of characteristic singlets at 4.63 and 1.91 ppm in the ^{1}H-NMR spectrum of **31** correspond to the methylene (CH_2) and hydroxyl (OH) groups of the propynyl chain, respectively. The signals for aromatic protons were seen in between 8.50-8.34 ppm. The $^{13}C\{^{1}H\}$-NMR spectrum of **31** exhibits distinct alkyne carbon signals at 95.6 and 80.1 ppm. Aromatic carbons appeared in the range of 150.2-138.3 ppm while the carbon for methylene (CH_2) was observed at 50.8 ppm. Finally, the obtained molecular mass value (169.0246 u) of compound **31** was in agreement with the calculated molecular mass value (169.0883 u) based on the molecular formula of this compound.

After successful synthesis of **31**, it was reacted with *bis*-isopropyl xanthogen disulfides in the presence of the radical initiator ACCN (1,1'-azo *bis*(cyclohexane-carbonitrile)) as shown in Scheme 3.7. The reaction mixture was heated under reflux for 12 hrs and a change in colour was observed from brown to orange. After work up, the crude product was purified by passing through a short column of silica to obtain yellow solid, which was characterised as the open alcohol ligand (**32**).

A possible mechanism for this reaction is shown in Scheme 3.8. It was suggested that the S-S bond of *bis*-isopropyl xanthogen disulfides cleaves homolytically to form the thiyl radical in the presence of ACCN.[32,33] Afterwards, this radical adds to the alkyne moiety of **31** to form a vinyl radical which cyclises to yield dithiolene-2-one moiety of ligand **32**, accompanied by the loss of an isopropyl radical.

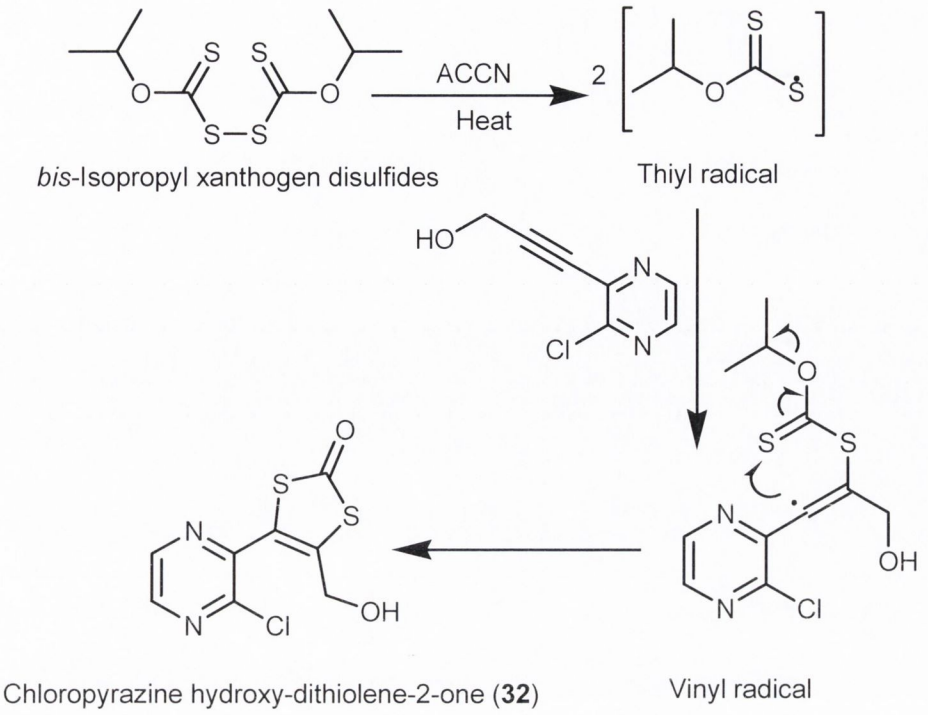

Scheme 3.8: Mechanistic steps for the construction of the dithiolene-2-one moiety in open alcohol ligand **32**.

The melting point temperature of **32** was observed in between 156-157 °C. A characteristic band at 1743 cm^{-1} was noticeable in the IR spectrum of **32** which was attributed to the stretching vibration of the carbonyl group υ(C=O) of the dithiolene-2-one moiety and comparable with reported values in literature.[8,10,12] The absorption band for the hydroxyl group (OH) observed at 3248 cm^{-1}.The ^{1}H-NMR spectrum of **32** showed two signals at 4.67 and 2.03 ppm corresponding to the (CH_2) and (OH) protons of the alcohol side chain. The aromatic peaks were present in the region of 8.52-8.34 ppm. The $^{13}C\{^{1}H\}$-NMR spectrum further suggested the formation of the desired dithiolene-2-one moiety as the most downfield signal at 193.5 ppm could be attributed to the carbonyl group of this moiety. Aromatic carbons appeared in the range of 164.2-138.3 ppm while the methylene carbon (CH_2) was found at 51.2 ppm. Moreover, the obtained molecular mass value (260.9560 u) of compound **32** was in agreement with the calculated molecular mass value (260.9559 u). After synthesis of ligand **32**, the next step was its use to form the respective molybdenum complex as discussed in Section 3.6.

3.6 Synthesis of open alcohol form molybdenum complex (33)

The synthesised open alcohol form ligand **32** is very promising in terms being one of the closest structural models of the open alcohol form of MPT in MoCo. Naturally, it was used to construct an open alcohol form molybdenum complex (**33**) as illustrated in Scheme 3.9 (Method **A**). The synthesis of this complex was attempted using a reported methodology, which describes the formation of the complex possibly as a mixture of *cis* and *trans* isomers.[16]

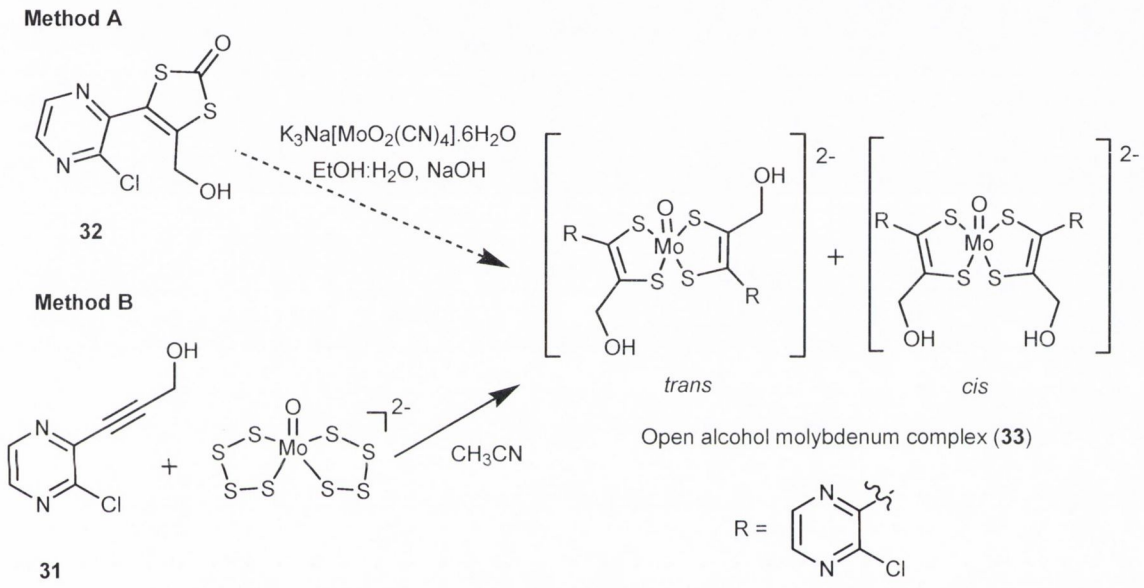

Scheme 3.9: Synthesis of the open alcohol form molybdenum complex (**33**) as *cis* and *trans* isomers; Method **A**) from chloropyrazine hydroxy-dithiolene-2-one (**32**) and Method **B**) from chloropyrazine hydroxy-alkyne (**31**).

An attempt was made to react compound **32** with the suitable metal precursor *i.e.* $K_3Na[MoO_2(CN)_4].6H_2O$[1] in a 1:2 metal to ligand ratio. The metal precursor and sodium hydroxide were dissolved in oxygen free ethanol and then this mixture was transferred to the solution of ligand **32** in oxygen free ethanol. The reaction mixture was heated for 4 hrs and the colour of the solution changed from brown to orange. After work up, the slow addition of $[PPh_4]Cl$ or $[Et_4N]Br$ as counterions produced a black solid. However, even after several attempts of the optimising this reaction, a sticky blackish mass was always obtained which could not be characterised as desired complex (**33**) using ^{1}H-NMR and HRMS analysis. One possible explanation

for the failure of this complexation reaction would be the presence of the base that not only favours the ring opening of the dithiolene moiety but might also deprotonate the alcohol moiety generating a very unstable intermediate which quickly decomposed to a black mass. After the failure of this strategy, another direct method, as illustrated in Scheme 3.9 **B**, was designed to synthesise the target molybdenum complex (**33**).

This strategy required the use of an electron deficient alkyne, for which ligand **31** was selected as a pivotal compound that would allow the cycloaddition reaction with the tetrasulfido (S_4^{2-}) ligands of the metal precursor to generate desired open alcohol molybdenum complex (**33**) (Scheme 3.9 **B**). Similar transformations have previously been documented by the reaction of other electron deficient alkynes with molybdenum oxo *bis*-tetrasulfides in the literature.[35,36] Compound **31** was treated with molybdenum oxo *bis*-tetrasulfides using a 2:1 ligand to metal ratio, according to the procedure described in literature.[34] The reaction mixture was heated under reflux for 8 hrs in dry acetonitrile. A change in colour of the reaction mixture from red to dark brown was observed. After work up, the crude product was recrystallised with methanol and diethyl ether to yield complex **33** as a brown solid.

The complex **33** was found to be decomposed in between 160-162 °C. The IR spectrum of **33** showed two characteristic absorption bands at 1577 and 869 cm^{-1} corresponding to the υ(C=C) of dithiolene ring and υ(Mo=O) frequencies, respectively. These values are comparable with those reported for the reduced Mo^{IV} form of DMSO reductase from *Rhodobacter sphaeroides*.[23] A strong broad band at 3423 cm^{-1} was also observed and assigned to the hydroxyl group υ(OH) of the alcohol side chain. The ^{1}H-NMR spectrum of **33** showed two peaks at 1.71 and 4.65 ppm corresponding to the hydroxyl group (OH) and methylene (CH_2) protons of the alcohol side chain. The aromatic signals appeared in between 8.46-8.31 ppm. Finally, the obtained ESI-HRMS spectrum confirmed the formation of complex **33** as the experimentally found value (610.7918 u) was in excellent agreement with the calculated value (610.8394 u) based on the proposed molecular formula of this complex. As shown in Figure 3.12, the observed characteristic molecular ion pattern (bottom) of complex **33** is well matched with the predicted isotopic distribution pattern (top).

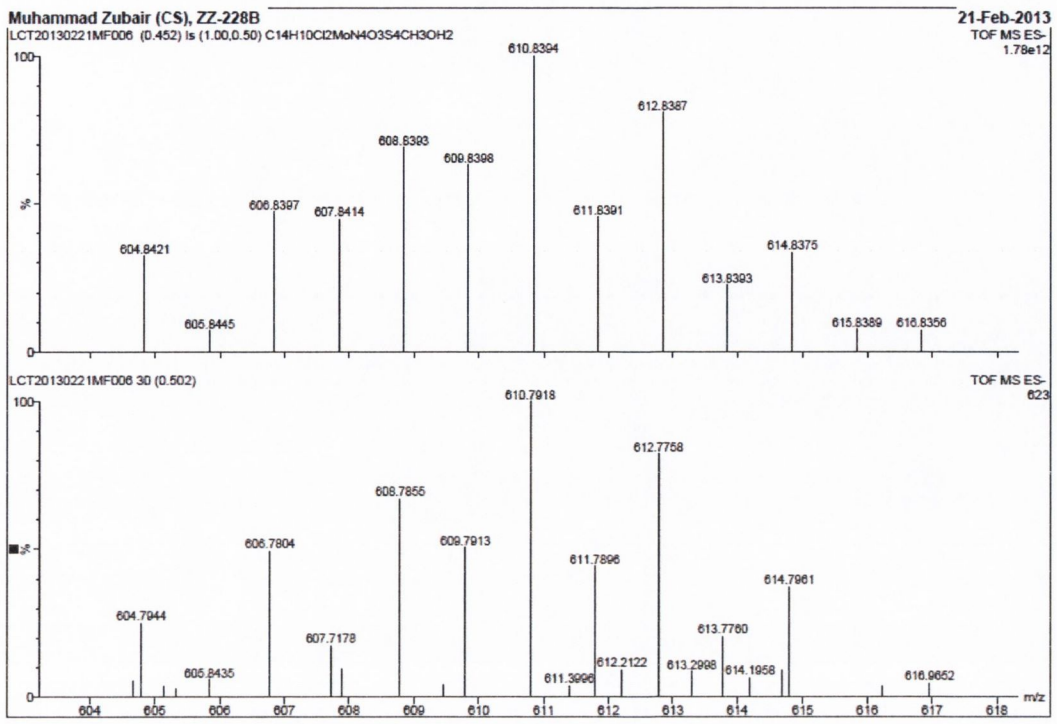

Figure 3.12: ESI-HRMS mass spectrum of complex **33** at the molecular ion region (bottom) and the calculated isotopic distribution pattern (top).

In the obtained ESI-HRMS spectrum of **33** another prominent molecular ion peak with the molecular mass of 436.7560 u was also noted which could be attributed to an inorganic impurity possibly related to the molybdenum precursor. A number of efforts were made to isolate the pure complex but remained unsuccessful. This suggests a similar solubility of the impurity present in the mixture which made isolation of the pure complex impossible to achieve. Other purification techniques such as column chromatography could not be used in this case because of the air sensitive nature of the molybdenum complex. Despite the purity issue, the successful synthesis of the desired open alcohol form molybdenum complex (**33**) is exciting achievement as it represents the closest structural model of the active site of DMSO reductase with an open form MPT available to date.

3.7 Conclusions

This research work was originally focussed on designing synthetic analogues of DMSO reductase. The use of dithiolene-2-ones as precursors had been the main idea for the synthesis of novel ligands because of the presence of the dithiolene moiety in large number of molybdenum enzymes and its key involvement in the catalytic activities. Towards this goal, a novel ligand, pyrazine-substituted dithiolene-2-one (**22**), was developed and used to synthesise its corresponding molybdenum (**23**) and tungsten (**24**) complexes. The structures of the ligand and its respective complexes were established by spectroscopic techniques (IR, ^{1}H and $^{13}C\{^{1}H\}$-NMR along with HRMS). The most promising results of the present research were acquired from the X-ray crystals of **22** which confirmed the formation of the dithiolene-2-one moiety in the novel ligand's precursor. To exactly compare the geometry around the metal centre of the novel complexes (**23** and **24**) with naturally occurring enzymes, X-ray crystals were needed. But unfortunately, all attempts to obtain crystals suitable for X-ray analysis remained unsuccessful. However, the obtained data from IR, ^{1}H and NMR along with HRMS studies suggested the formation of complex **23** and **24** which bear four sulfur atoms that are coordinated to the oxo molybdenum/tungsten centre, and serve as a synthetic structural analogue of the DMSO reductase family. The spectroelectrochemical properties of molybdenum complex **23** were studied in detail and compared to those of previously reported other molybdenum dithiolene complexes. It was established that complex **23** is electroactive, showing a one electron, reversible reduction couple (Mo^{V}-Mo^{IV}) at negative redox potential of -323 mV. This less negative value suggests more electron withdrawing character of the pyrazine ring attached to the dithiolene in this complex compared to other electrochemically characterised molybdenum complexes (illustrated in Table 3.2). Most importantly, this ligand also includes the pyrazine features of MPT, therefore, it is possible that electron withdrawing substituted dithiolene (*i.e.* MPT) plays an important role within the naturally occurring ligand system. Furthermore, It was confirmed by UV-Vis spectroelectrochemical studies that there are no structural changes of the complex associated with oxidation and reduction processes and the obtained spectra were consistent with the $MoOS_4$ chromphore in these states. However, the UV-Vis data reported for reduced and oxidised forms of complex **23**

and those published for DMSO reductase were not correlated well. This difference in spectral data highlights the presence of different ligand field and charge transfer energies as a possible effect between the two different ligand systems. Moreover, an unpaired electron coupled to the molybdenum nucleus Mo^{V} was also confirmed by EPR spectroscopic data. *i.e.* it is not significantly delocalised to the dithiolene ligands. This means that the typical non-innocence of dithiolene ligands is negligible for this system.

The second part of this chapter describes the different strategies utilised for the synthesis of closed and open alcohol form ligands and their respective molybdenum complexes. In order to synthesise the closed form ligand, a completely new approach was used to prepare target closed form ligand **28** using 2-hydroxy quinoxaline as starting material. Unfortunately, the desired ligand could not be acquired using this methodology but a novel and interesting compound **29** was isolated and fully characterised.

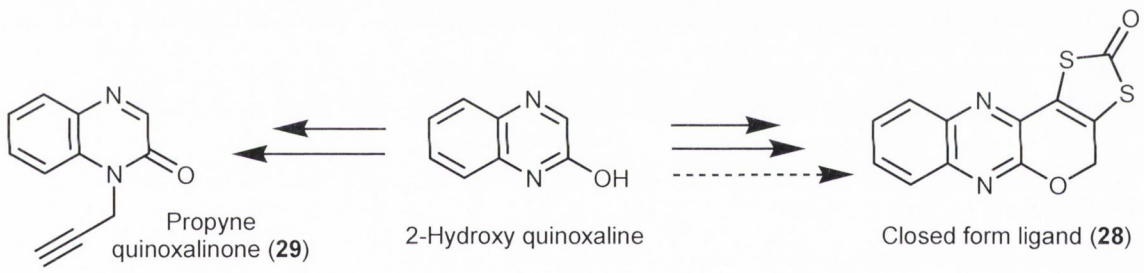

Scheme 3.10: Attempted route for the synthesis of closed form ligand.

Then the attention turned for the synthesis of target open alcohol form ligand and two different strategies were adopted. Firstly, the attachment of the alcohol side chain to the dithiolene ring was attempted using ligand **22** to generate an open alcohol ligand **30**, but was unsuccessful. A second strategy was investigated being the coupling of the electron deficient akyne **31** with *bis*-alkyl xanthogen disulfides as shown in Scheme 3.11. This resulted in the successful synthesis of the target open alcohol ligand **32** but the efforts to synthesise its respective molybdenum complex did not succeed. However, the synthesis of the open alcohol ligand **32** is in fact already a great achievement as it is one of the closest model for the open form MPT ligand in molybdenum enzymes. Finally, a direct approach was applied which resulted in the successful synthesis of the target open alcohol molybdenum complex

(**33**) from the reaction of the electron deficient alkyne **31** with molybdenum oxo *bis*-tetrasulfides (Scheme 3.11).

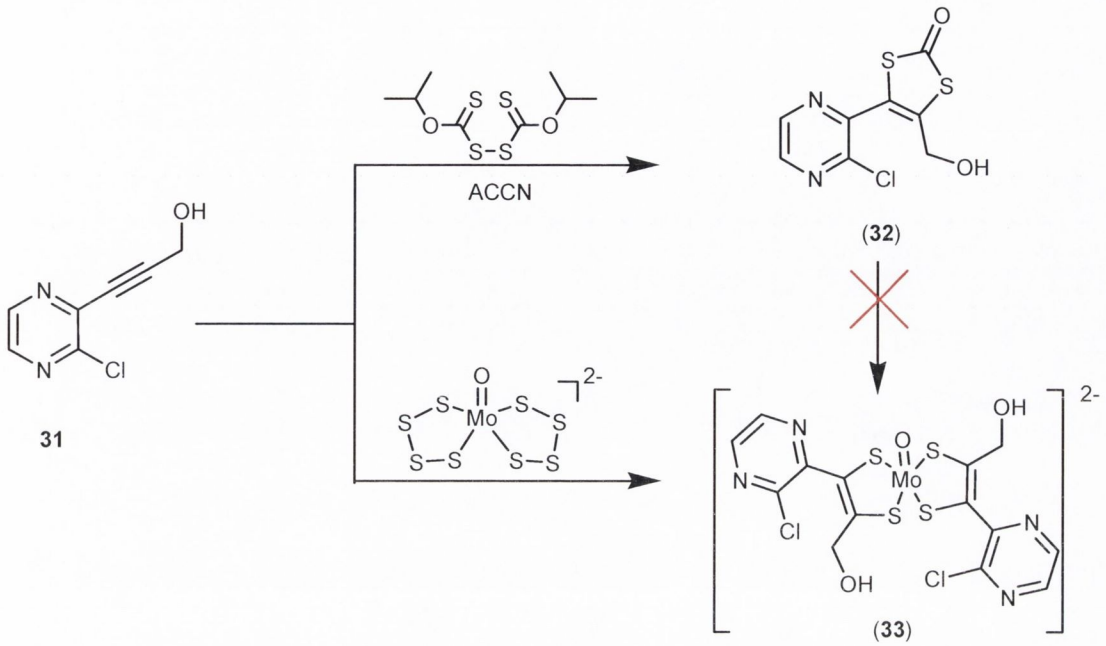

Scheme 3.11: Synthesis of open alcohol form ligand (**32**) and molybdenum complex (**33**) (here only trans isomer is shown).

Formation of complex **33** was confirmed by spectroscopic data. However, ESI-HRMS data indicated the presence of not only the complex **33** but also an inorganic impurity possibly related to the used molybdenum precursor which was impossible to separate. Even with this purity issue, this reported novel molybdenum complex **33** has considerable promise as a more accurate structural synthetic model of DMSO reductase with MPT in the open alcohol form.

3.8 Experimental section

This section details the experimental specifics of the pyrazine-substituted dithiolene-2-one ligand and its corresponding complexes as well as synthetic procedures to generate the open and closed form analogues of the active site of the molybdenum enzymes.

3.8.1 Physical methods

All commercially available chemicals were used as supplied by Sigma Aldrich, Fischer Scientific and Acros Organics and were used without further purification. Other precursors such as potassium-*O*-isopropyl carbonodithioate,[37] molybdenum oxo *bis*-tetrasulfides,[34] $K_3Na[MoO_2(CN)_4].6H_2O$[1] and $K_3Na[WO_2(CN)_4].6H_2O$,[2] were synthesised according to the reported procedures. All reactions were performed under an atmosphere of nitrogen or argon, using standard Schlenk-line techniques. Solvents were either degassed or purged with argon prior to use. Melting point values were recorded on a Stuart scientific SMP3 melting point apparatus and are uncorrected. All infrared spectra were recorded (4000–650 cm^{-1}) on a Perkin-Elmer Fourier-Transform Infrared (FTIR) spectrophotometer. All ^{1}H-NMR spectra were recorded on a Bruker AV400 operating at 400.13 MHz as well as $^{13}C\{^1H\}$-NMR spectra recorded at 100.65 MHz. All samples were dissolved in deuterated solvents and chemical shift values are reported in parts per million (ppm). High Resolution Mass Spectrometry (HRMS) analyses were carried out on a Water-Micromass Q-ToF (quadrupole - Time of Flight) hybrid mass spectrometer equipped with an orthogonal electrospray source (z–spray). This was operated in an electrospray positive ion mode (ESI^+) or electrospray negative ion mode (ESI^-). Sodium formate was used for mass calibration checks and optimal parameter tuning was performed using flow injection of standard solutions. All ToF measurements were performed at high resolution settings (5000 FWHM at mass 1500). Data were always taken in continuum mode. X-ray crystallographic studies were performed for suitable single crystals of **22** and **29**, which were coated in Paratone N heavy oil then mounted on a glass fiber. The respective data were collected on a Rigaku Saturn-724 diffractometer (graphite-monochromated Mo Kα radiation, λ = 0.71073 Å) at 108(2) K. The

structures were solved by direct methods (SHELXS-97) and refined against all data by full matrix least-squares methods on F^2 (SHELXL-97).[38] All non-hydrogen atoms were refined with anisotropic displacement parameters. The hydrogen atoms (except if found and refined freely) were refined isotropically on calculated positions using a riding model with their U_{iso} values constrained to 1.5 U_{eq} of their pivotal atoms for terminal sp^3 carbon atoms and to 1.2 times for all other carbon atoms.

Electrochemical measurements were carried out by collaboration with Prof. Jonathan McMaster and Dr. Stephen Davies at Department of Chemistry, University of Nottingham, United Kingdom (COST funding, CM1003, biological oxidations and reductions). Cyclic voltammetric studies were performed using an EG & G PAR Model 362 Scanning Potentiostat with a Lloyds Instruments PL3 X-Y recorder. Either a glassy carbon or Pt wire working electrode, a Pt wire secondary electrode, and saturated calomel electrode (SCE) as a reference electrode with supporting electrolyte $[NBu^n_4][PF_6]$,[39] were used in the cell. All voltammograms were recorded for complex **23** in DMF solution (1 mmol), containing a supporting electroyte 0.2 M $[NBu^n_4][PF_6]$ under nitrogen atmosphere. The $[FeCp^*_2]^+/[FeCp^*_2]$ (Cp = η^5-C_5Me_5) couple was used as an internal redox standard with ΔE = 41 mV under these conditions.[40] This redox process was referenced and calibrated with $[FeCp_2]^+/[FeCp_2]$ (Cp = η^5-C_5H_5) with a separation of 476 mV between these couples in DMF. Optically transparent thin-layer electrode (OTTLE) measurements were executed using a Varian Cary 1 spectrophotometer in conjunction with a Sycopel Scientific Ltd. DD10M potentiostat.[39] The initial voltages were chosen to be *ca.* 200 mV more negative than the $E_{1/2}$ value for the respective Mo^V–Mo^{IV} couple and the final voltages *ca.* 200 mV more positive, or until the spectrum no longer changed with increasingly positive potential. The applied potential was increased in 20 mV increments from the initial voltage. The reversibility of the system was confirmed by applying the initial potential after oxidation had been completed and reproducing the initial spectrum.

Bulk electrolysis experiment was carried out using a two compartment cell at controlled potential. A Pt/Rh gauze basket working electrode was separated from a wound Pt/Rh gauze secondary electrode by a glass frit. A SCE was bridged to the test solution through a vycor frit that was orientated at the centre of the working

electrode. The working electrode compartment was fitted with a magnetic stirring bar and the test solution was stirred rapidly during electrolysis. An ice-water bath was used to maintain a temperature of 0 °C. Each solution contained $[NBu^n_4][BF_4]$ (0.2 M) as the supporting electrolyte and the complex **23** (10^{-3} M). All solutions were prepared using Schlenk line technique.

3.8.2 Synthesis of the pyrazine-substituted dithiolene-2-one ligand and its respective complexes

3.8.2.1 Synthesis of 2-bromo-1-(pyrazin-2-yl)ethanone (20)

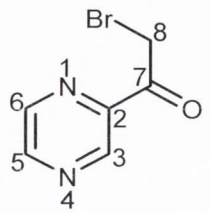

A solution of 2-pyrrolidinone hydrotribromide (21.8, 44.0 mmol) in tetrahydrofuran (80 ml) was added dropwise to the solution of acetyl pyrazine (**19**) (4.88 g, 40.0 mmol) in tetrahydrofuran (20 ml) over the period of 10 mins. The reaction mixture was stirred for 48 hrs at room temperature which resulted in discolouration of the solution. Then the reaction mixture was cooled in an ice-bath and cold water (30 ml) was added into the mixture until the formed precipitates re-dissolved again. The aqueous layer was extracted with toluene (3 x 20 ml). The combined organic extracts were washed with brine (50 ml), dried over $MgSO_4$ and evaporated. The obtained compound **20** was very unstable once isolated and consequently immediately used *in situ* for the next step (using toluene as a solvent) without any further characterisation.

3.8.2.2 Synthesis of O-isopropyl-S-2-oxo-2-(pyrazin-2-yl)ethyl carbonodithioate (21)

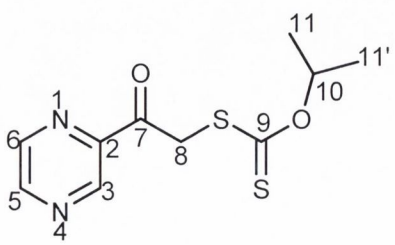

To a solution of compound **20** (7.00 g, 35.0 mmol) in toluene (60 ml) was added potassium *O*-isopropyl carbonodithioate (7.40 g, 43.0 mmol) in small portions over the period of 30 mins. The mixture was heated under reflux for 3 hrs and the precipitated KBr was filtered off. The remaining solvent was evaporated from the reaction mixture and then the obtained solid residue was treated with hydrochloric acid (2.5 M) and left stirring for another 30 mins. Then the aqueous layer was extracted with diethyl ether (3 x 20 ml). The combined organic extracts were washed with brine (50 ml), dried over $MgSO_4$ and the solvent was evaporated. The obtained residue was washed with diethyl ether (2 x 10 ml) and dried to yield a yellowish brown solid.

Yield: 79%, 7.10 g. Molecular Formula: $C_{10}H_{12}N_2O_2S_2$ (256.34 g/mol). M.P.: 98-99 °C. IR (KBr, ν_{max}/cm^{-1}): (C=N) 1543, (C=O) 1735, (C=S) 1188, (C-O) 1045. ^{1}H-NMR ($CDCl_3$) δ_H/ppm: 8.91 (s, 1H, Ar-H_3), 8.78 (d, 1H, Ar-H_6, J = 7.8 Hz), 8.52 (d, 1H, Ar-H_5, J = 7.1 Hz), 5.71 (sept, 1H, H_{10}, J = 6.3 Hz), 4.79 (s, 2H, H_8), 1.38 (d, 6H, $H_{11,11'}$, J = 6.0 Hz); ^{13}C{^{1}H}-NMR ($CDCl_3$) δ_C/ppm: 215.3, 188.1, 154.8, 144.1, 143.2, 141.3, 66.3, 40.1, 23.8. HRMS (EI): *m/z* Calculated for $C_{10}H_{12}N_2O_2S_2$ [M + H]$^+$: 257.0418; Found: 257.0335.

3.8.2.3 Synthesis of 4-pyrazin-2-yl-[1,3]dithiolene-2-one (22)

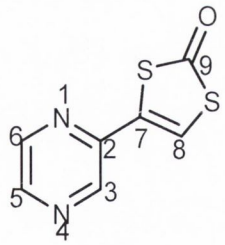

A solution of compound **21** (6.88 g, 27.3 mmol) in a mixture of diethyl ether (15 ml) and dichloromethane (15 ml) was added slowly to a perchloric acid (70 ml) solution in an ice-bath. The solution turned to black and was allowed to warm to room temperature. After 24 hrs stirring, the product was precipitated out by pouring into ice-cold water. The brown solid was collected by filtration using a buchner funnel and was washed with distilled water (3 x 20 ml). The obtained solid was dried in air for 2 hrs and then in the oven at 70 °C overnight. The product was crystallised in acetonitrile to give brown shiny needles of **22** which were suitable for X-ray

diffraction (Appendices 6.5 and 6.7)

Yield: 47%, 2.53 g. Molecular Formula: $C_7H_4N_2OS_2$ (196.24 g/mol). M.P.: 140-141 °C. IR (KBr, ν_{max}/cm^{-1}): (C=O) 1759, (C=N) 1544, (C=C) 1483. ^{1}H-NMR (d_3-$CDCl_3$) δ_H/ppm: 8.85 (s, 1H, Ar-H_3), 8.57 (d, 1H, Ar-H_6, J = 7.3 Hz), 8.51 (d, 1H, Ar-H_5, J = 7.0 Hz), 7.54 (s, 1H, H_8); ^{13}C{^{1}H}-NMR ($CDCl_3$) δ_C/ppm: 191.1, 145.9, 143.6, 143.2, 140.1, 132.4, 117.2. HRMS (ESI): *m/z* Calculated for $C_7H_4N_2OS_2$ [M + H]$^+$: 196.9843; Found: 196.9860.

3.8.2.4 Synthesis of the 4-pyrazin-2-yl-[1,3]dithiolene-2-one-derived molybdenum complex (23)

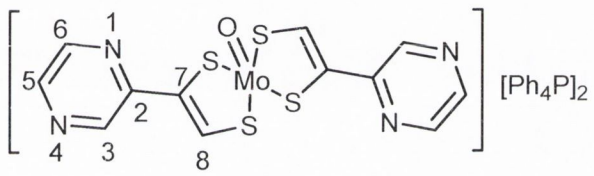

$K_3Na[MoO_2(CN)_4]\cdot 6H_2O$ (0.37 g, 0.77 mmol) was dissolved in oxygen free ethanol and stirred for 40 mins with sodium hydroxide (0.60 g, 15.00 mmol). To this solution, compound **22** (0.30 g, 1.55 mmol) in 20 ml of oxygen free ethanol was added under nitrogen atmosphere. The reaction mixture was left stirring for 3 hrs at 45 °C. The colour of the reaction mixture changed from brown to dark red. After cooling to room temperature, the evaporation of the solvent afforded a red solid. The obtained product was dissolved again in oxygen free water (20 ml) and a solution of $[PPh_4]Cl$ (0.61 g, 1.60 mmol) in oxygen free water (5 ml) was added dropwise under stirring. The precipitated orange solid was filtered, washed with water (2 x 10 ml) and dried *in vacuo*.

Yield: 24%, 0.22 g. Molecular Formula: $C_{60}H_{48}MoN4OP_2S_4$ (1127.19 g/mol). M.P.: 316-317 °C. IR (KBr, ν_{max}/cm^{-1}): (C=N) 1548, (C=C) 1491, (Mo=O) 917. ^{1}H-NMR (d_6-DMSO) δ_H/ppm: 9.23, 9.21 (2 x s, 2 x 1H, Ar-H_3), 8.33 (br, 2H, Ar-H_5), 8.18-8.15 (m, 2H, Ar-H_6), 8.03, 8.01 (2 x s, 2 x 1H, Ar-H_8), 7.96-7.74 (m, 40H, PPh_4). HRMS (ESI): *m/z* Calculated for $C_{12}H_8MoN_4OS_4$ [M - H]: 449.8632; Found: 449.8631.

3.8.2.5 Synthesis of 4-pyrazin-2-yl-[1,3]dithiolene-2-one-derived tungsten complex (24)

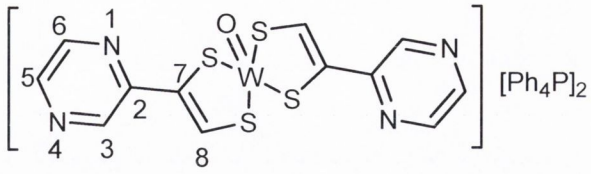

The experimental procedures used for the synthesis of this compound were the same as those employed to prepare complex **23** except $K_3Na[WO_2(CN)_4]\cdot 6H_2O$ (0.48 g, 0.77 mmol) was used instead of $K_3Na[MoO_2(CN)_4]\cdot 6H_2O$. The precipitated red solid was filtered, washed with chloroform (2 x 10 ml) and dried.

Yield: 17%, 0.16 g. Molecular Formula: $C_{60}H_{48}WN_4OP_2S_4$ (1215.09 g/mol). M.P.: 175 °C (decomposed) °C. IR (KBr, ν_{max}/cm^{-1}): (C=N) 1549, (C=C) 1487, (W=O) 919. ^{1}H-NMR (d_6-DMSO) δ_H/ppm: 9.14, 9.07 (2 x s, 2 x 1H, Ar-H_3), 8.56-8.47 (m, 4H, Ar-$H_{5,6}$), 8.21, 8.16 (2 x s, 2 x 1H, Ar-H_8), 7.96-7.74 (m, 40H, PPh_4). HRMS (ESI): *m/z* Calculated for $C_{12}H_7WN_4OS_4.CH_3OH$ [M - H]: 566.9264; Found: 566.9274.

3.8.3 Synthesis of open alcohol and closed form synthetic analogues of MoCo

3.8.3.1 Synthesis of 2-prop-12-ynyloxy-quinoxaline (25)

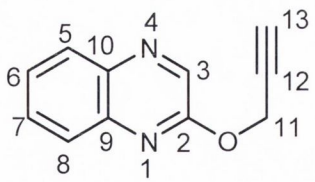

2-Hydroxy quinoxaline (4.70 g, 32.3 mmol), propargyl bromide (4.00 ml of 80% in toluene, 35.0 mmol), and potassium carbonate (8.00 g, 60.0 mmol) were dissolved in acetonitrile (60 ml) under nitrogen atmosphere. The resulting mixture was heated under reflux for 48 hrs. The solvent was evaporated under reduced pressure, and the residue taken into water and extracted with ethyl acetate. The organic layers were combined, dried, and evaporated under reduced pressure to give an off-white crystalline product.

Yield: 70%, 4.49 g. Molecular Formula: $C_{11}H_8N_2O$ (184.19 g/mol). M.P.: 174-175 °C IR (KBr, ν_{max}/cm^{-1}): (C≡C) 2121, (C=N) 1656. ^{1}H-NMR (d_6-DMSO) δ_H/ppm: 8.29 (s, 1H, H_3), 7.87 (d, 1H, Ar-H_5, J = 8.6 Hz), 7.72 (t, 1H, Ar-H_6, J = 7.8 Hz), 7.64 (d, 1H, Ar-H_8, J = 8.4 Hz), 7.44 (t, 1H, Ar-H_7, J = 7.5 Hz) 5.07 (s, 2H, H_{11}) 3.35 (s, 1H, H_{13}); ^{13}C{^{1}H}-NMR (d_6-DMSO) δ_C/ppm: 153.9, 149.8, 133.5, 131.6, 131.2, 130.6, 124.1, 114.2, 78.0, 75.2, 31.1. HRMS (ESI): *m/z* Calculated for $C_{11}H_9N_2O_2$ $[M+H]^+$: 185.0715; Found: 185.0716.

3.8.3.2 Synthesis of 2-(13-bromo-prop-12-ynyloxy)-quinoxaline (26)

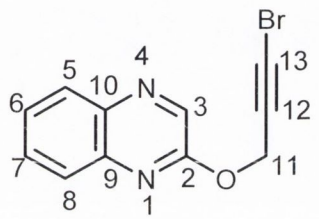

Compound **25** (3.68 g, 20.0 mmol) was dissolved in acetone (100 ml) under nitrogen atmosphere. *N*-bromosuccinimide (4.42 g, 25.0 mmol) and silver acetate (0.41 g, 2.50 mmol) were added pinch wise as a solid, and the reaction mixture was heated under reflux for 4 hrs. After cooling, the silver salts were removed by filtration and the filtrate evaporated under reduced pressure. The residue was dissolved in ethyl acetate, washed with water (2 x 20 ml) and saturated aqueous sodium bicarbonate (2 x 10 ml) sequentially. The combined organic solvents were dried, and then evaporated under reduced pressure to give a light yellowish powder.

Yield: 74%, 4.10 g. Molecular Formula: $C_{11}H_7ClN_2O$ (218.63 g/mol). M.P.: 109-110 °C IR (KBr, ν_{max}/cm^{-1}): (C≡C) 2251, (C-O) 1195, (C=N) 1658, (C-Cl) 645. ^{1}H-NMR (d_6-DMSO) δ_H/ppm: 8.29 (s, 1H, H_3), 7.88 (d, 1H, Ar-H_5, J = 8.0 Hz), 7.73 (t, 1H, Ar-H_6, J = 7.5 Hz), 7.65 (d, 1H, Ar-H_8, J = 8.6 Hz), 7.45 (t, 1H, Ar-H_7, J = 7.9 Hz) 5.14 (s, 2H, H_{11}); ^{13}C{^{1}H}-NMR (d_6-DMSO) δ_C/ppm: 155.0, 150.7, 133.7, 132.0, 131.7, 130.7, 124.7, 115.6, 78.3, 75.5, 31.7. HRMS (ESI): *m/z* Calculated for $C_{11}H_8ClN_2O$ $[M+H]^+$: 219.0325; Found: 219.0322.

3.8.3.3 Synthesis of 1-prop-12-ynyl-1H-quinoxalin-2-one (29)

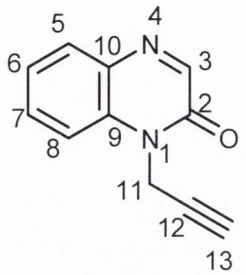

Compound **26** (2.00 g, 9.17 mmol) was heated under reflux in ethylene glycol (25 ml) for 4 hrs under nitrogen atmosphere. After cooling to room temperature, the reaction mixture was poured into water, and extracted with diethyl ether. The organic layers were combined, washed with sodium hydroxide (1N) and saturated ammonium carbonate sequentially. The reddish solid, that precipitated, was filtered and dried in an oven at 100 °C. The residues were dissolved in a mixture of DCM – hexane (1:1) and then passed through a short column of silica gel. Finally, the solvent was evaporated under reduced pressure to give a reddish crystalline solid. The product was crystallised in DCM to give red shiny needles of **29** which were suitable for X-ray diffraction (Appendices 6.6 and 6.8)

Yield: 44%, 0.71 g. Molecular Formula: $C_{11}H_8N_2O$ (184.19 g/mol). M.P.: 261-262 °C IR (KBr, ν_{max}/cm^{-1}): (C≡C) 2142, (C=O) 1673, (C=N) 1652. ^{1}H-NMR ($CDCl_3$) δ_H/ppm: 8.19 (s, 1H, H_3), 7.73 (d, 1H, Ar-H_5, J = 7.7 Hz), 7.57 (d, 1H, Ar-H_8, J = 8.5 Hz), 7.45 (t, 1H, Ar-H_6, J = 7.5 Hz), 7.22 (t, 1H, Ar-H_7, J = 7.4 Hz) 5.01 (s, 2H, H_{11}) 3.64 (s, 1H, H_{13}); ^{13}C{^{1}H}-NMR ($CDCl_3$) δ_C/ppm: 155.3, 149.6, 133.1, 132.4, 130.1, 129.6, 123.1, 115.3, 65.3, 64.4, 47.3. HRMS (ESI): *m/z* Calculated for $C_{11}H_8N_2O$ $[M+H]^+$: 185.0715; Found: 185.0815.

3.8.3.4 Attempted synthesis of 4-(10-hydroxy-ethyl)-5-pyrazin-dithiol-[7,8]ene-2-one (30)

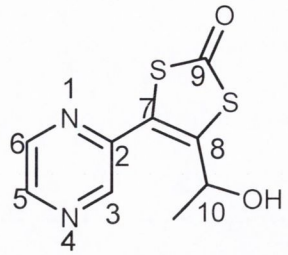

A solution of compound **22** (0.196 g, 1 mmol) was cooled to -78 °C in dry THF (40 ml) under nitrogen atmosphere. *n*-BuLi (1.57 M in hexane, 625 ml, 2.4 equivalent) was added dropwise with efficient stirring. After 45 mins, acetaldehyde (.05 ml, 1 mmol) was added and the reaction mixture stirred for 12 hrs at -78. The resulting solution was warmed to room temperature and quenched by addition of saturated aqueous NH_4Cl (1 x 30 ml). The layers were separated and the aqueous phase extracted with EtOAc (3 x 50 ml). The combined organic extracts were washed with brine (15 ml), dried and the solvent evaporated under vacuum giving a red solid, characterised as a starting compound **22**.

^{1}H-NMR (d_3-$CDCl_3$) δ_H/ppm: 8.86 (s, 1H, Ar-H_3), 8.57 (d, 1H, Ar-H_6, J = 7.3 Hz), 8.51 (d, 1H, Ar-H_5, J = 7.0 Hz), 7.55 (s, 1H, H_8). HRMS (ESI): m/z Calculated for $C_7H_4N_2OS_2$ $[M + H]^+$: 196.9843; Found: 196.9860.

3.8.3.5 Synthesis of 3-(3'-chloro-pyrazin-2-yl)-prop-8-yn-9-ol (31)

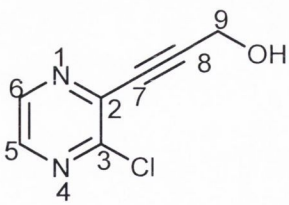

A solution of 2,3-di-chloropyrazine (4.48 g, 30.0 mmol) and propargyl alcohol (2.20 ml, 37.0 mmol) in acetonitrile (60 ml) and triethylamine (30 ml) was degassed under vacuum. Palladium(II) acetate (0.34 g, 1.50 mmol), triphenylphosphine (0.79 g, 3.00 mmol) and copper(I) iodide (0.57 g, 3.00 mmol) were then added to the reaction mixture. The reaction mixture was heated under reflux for 6 hrs. After evaporation of the organic solvents, the obtained solid residue was mixed with water (1 x 100 ml)

and extracted with dichloromethane (3 x 50 ml). The combined organic extracts were washed with brine (50 ml), dried over $MgSO_4$ and then concentrated in vacuum. The purification of the concentrated mixture was achieved by column chromatography over silica gel, eluting with dichloromethane – ethyl acetate (6:4) to give the product as a reddish brown solid.

Yield: 39%, 2.01 g. Molecular Formula: $C_7H_5ClN_2O$ (168.58 g/mol). M.P.: 96-97 °C. IR (KBr, ν_{max}/cm^{-1}): (OH) 3223, (C≡C) 2231, (C=N) 1514, (C-Cl) 588. ^{1}H-NMR ($CDCl_3$) δ_H/ppm: 8.50 (d, 1H, Ar-H_6, J = 7.4 Hz), 8.34 (s, 1H, Ar-H_5, J = 7.2 Hz), 4.63 (s, 2H, H_9), 1.91 (s, 1H, OH); $^{13}C\{^1H\}$-NMR ($CDCl_3$) δ_C/ppm: 150.2, 141.8, 141.7, 138.3, 95.6, 80.1, 50.8. HRMS (ESI): *m/z* Calculated for $C_7H_6ClN_2O$ $[M + H]^+$: 169.0883; Found: 169.0246.

3.8.3.6 Synthesis of 4-(3-chloro-pyrazin-2'-yl)-10-hydroxymethyl-dithiol-[7,8]ene-2-one (32)

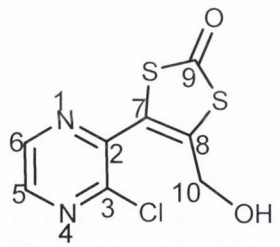

Compound **31** (0.17 g, 1.00 mmol), 1,1'-azo *bis*(cyclohexane carbonitrile) (1.25 g, 0.50 mmol) and *bis*-isopropyl xanthogen disulfides (**27**) (0.96 g, 4.00 mmol) were degassed under vacuum and then added to dry toluene (15 ml). The resulting mixture was heated under reflux for 12 hrs. After cooling to room temperature, the solvent was concentrated under vacuum. The purification of the concentrated mixture was achieved by column chromatography over silica gel, eluting with dichloromethane – methanol (9:1) to yield a reddish brown solid.

Yield: 22%, 0.22 g. Molecular Formula: $C_8H_5ClN_2O_2S_2$ (260.72 g/mol). M.P.: 156-157 °C. IR (KBr, ν_{max}/cm^{-1}): (OH) 3248, (C=O) 1743, (C=N) 1520, (C-Cl) 691. ^{1}H-NMR ($CDCl_3$) δ_H/ppm: 8.52 (d, 1H, Ar-H_6, J = 7.7 Hz), 8.34 (s, 1H, Ar-H_5, J = 7.3 Hz), 4.67 (s, 2H, H_{10}), 2.03 (s, 1H, OH); $^{13}C\{^1H\}$-NMR ($CDCl_3$) δ_C/ppm: 193.5 164.2, 141.9, 141.7, 138.3, 133.4, 124.7, 51.2. HRMS (ESI): *m/z* Calculated for

$C_8H_6ClN_2O_2S_2$ $[M + H]^+$: 260.9559; Found: 260.9560.

3.8.4 Synthesis of 4-(3-chloro-pyrazin-2'-yl)-9-hydroxymethyl-dithiol-[7,8]ene derived molybdenum complex (33)

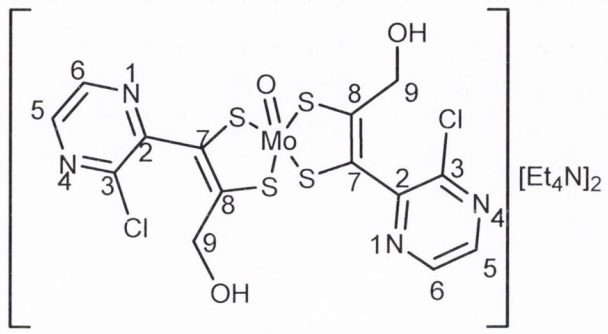

Method A: $K_3Na[MoO_2(CN)_4]\cdot 6H_2O$ (0.37 g, 0.77 mmol) was dissolved in oxygen free ethanol and stirred for 40 mins with sodium hydroxide (0.60 g, 15.00 mmol). To this solution, compound **32** (0.30 g, 1.55 mmol) in 20 ml of oxygen free ethanol was added under nitrogen atmosphere. The reaction mixture was left stirring for 3 hrs at 45 °C. The colour of the reaction mixture changed from brown to dark red. After cooling to room temperature, the evaporation of the solvent afforded a red solid. The obtained product was dissolved again in oxygen free water (20 ml) and a solution of $[PPh_4]Cl$ (0.61 g, 1.60 mmol) or $[Et_4N]Br$ (0.13 g, 1.6 mmol) in oxygen free water (5 ml) was added dropwise under stirring. The precipitated sticky black was filtered, washed with water (2 x 10 ml) and dried *in vacuo*. The black solid could not be characterised as molybdenum complex **33**.

Method B: Compound **31** (0.08 g, 0.50 mmol) and molybdenum oxo *bis*-tetrasulfides (0.15 g, 0.25 mmol) were degassed in a Schlenk flask under vacuum. Dry acetonitrile (10 ml) was added and this mixture was heated under reflux for 8 hrs. An immediate change in colour was noted from red to dark brown. After cooling to room temperature, the reaction mixture was filtered to remove any unreacted molybdenum precursor. The filtrate was evaporated under vacuum. The resulting solid was again dissolved in methanol (5 ml) and precipitated out by slow addition of diethyl ether to give a brown solid which was filtered off and dried under vacuum.

Method B: Yield: 32%, 0.09 g. Molecular Formula: $C_{30}H_{50}Cl_2MoN_6O_3S_4$ (837.86

g/mol). M.P. 160-162 °C (decomposed). IR (KBr, ν_{max}/cm^{-1}): (OH) 3423, (C=C) 1577, (Mo=O) 869, (C-Cl) 685. ^{1}H-NMR (d_6-DMSO) δ_H/ppm: 8.46 (d, 2H, Ar-H_6, J = 7.5 Hz), 8.31 (d, 2H, Ar-H_5, J = 7.1 Hz), 4.56 (s, 4H, H_9), 3.46 (q, 16H, $CH_3CH_2N^+$, J = 6.4 Hz), 1.71 (br s, 2H, OH), 1.39 (t, 24H, $CH_3CH_2N^+$, J = 6.9 Hz). HRMS (ESI): *m/z* Calculated for $C_{14}H_{11}Cl_2N_4O_3S_4.CH_3OH$ [M - H]: 610.8394; Found: 610.7918.

References

[1] J. P. Smith, W. Purcell, A. Roodt, J. G. Leipoldt, *Polyhedron*, **1993**, 12, 2271.

[2] A. Roodt, S. S. Basson, J. Leipoldt, *Polyhedron*, **1994**, 13, 599.

[3] E. S. Davies, R. L. Beddoes, D. Collison, A. Dinsmore, A. Docrat, J. A. Joule, C. R. Wilson, C. D. Garner, *J. Chem. Soc., Dalton Trans.*, **1997**, 3985.

[4] D. J. Rowe, C. D. Garner, J. A. Joule, *J. Chem. Soc., Perkin Trans. 1.*, **1985**, 1907.

[5] A. Dinsmore, J. H. Birks, C. D. Garner, J. A. Joule, *J. Chem. Soc., Perkin Trans. 1.*, **1997**, 801.

[6] D. V. C Awang, S. Wolfe, *Can. J. Chem.*, **1969**, 47, 706.

[7] V. Madhu, S. K. Das, *Inorg. Chem.*, **2008**, 47, 5055.

[8] P. Chandrasekaran, J. P. Donahue, *Org. Synth.* **2009**, 86, 333.

[9] B. Bradshaw, A. Dinsmore, D. Collison, C. D. Garner, J. A. Joule, *J. Chem. Soc., Perkin Trans. 1.*, **2001**, 3232.

[10] A. K. Bhattacharya, A. G. Hortmann, *J. Org. Chem.*, **1974**, 39, 95.

[11] F. Alphonse, R. Karim, C. Cano-Soumillac, M. Hebray, D. Collison, C. D. Garner, J. A. Joule, *Tetrahedron*, **2005**, 614, 11010.

[12] P. Chandrasekaran, K. Arumugam, U. Jayarathne, L. M. Perez, J. T. Mague, P. J. Donahue, *Inorg. Chem.*, **2009**, 48, 2103.

[13] A PhD thesis of Prinson P. Samuel, Molybdenum and tungsten compounds with dithiolene ligands inspired by molybdopterin as models for the molybdenum and tungsten cofactors, Georg-August-Universität Göttingen, **2011**.

[14] E. S. Davies, G. M. Aston, R. L. Beddoes, D. Collison, A. Dinsmore, A. Docrat, J. A. Joule, C. R. Wilson, C. D. Garner, *J. Chem. Soc., Dalton Trans.*, **1998**, 3647.

[15] J. P. Donahue, C. R. Goldsmith, U. Nadiminti, R. H. Holm, *J. Am. Chem. Soc.*, **1998**, 120, 12869.

[16] C. A. Goddard, R. H. Holm, *Inorg. Chem.*, **1999**, 38, 5389.

[17] C. Schulzke, *Dalton Trans.*, **2005**, 713.

[18] A. L. Whalley, A. J. Blake, D. Collison, E. S. Davies, H. J. Disley, M. Helliwell, F. E. Mabbs, J. McMaster, C. Wilson, C. D. Garner, *Dalton Trans.*, **2011**, 40, 10457.

[19] D. V. Fomitchev, B. S. Lim and R. H. Holm, *Inorg. Chem.*, **2001**, 40, 645.

[20] H. Sugimoto, S. Tatemoto, K. Suyama, H. Miyake, R. P. Mtei, S. Itoh, M. L. Kirk, *Inorg. Chem.*, **2010**, 49, 5368.

[21] S. R. Ellis, D. Collison, C. D. Garner, W. Clegg, *J. Chem. Soc., Chem. Commun.*, **1986**, 1483.

[22] H. Sugimoto, H. Tano, K. Soyama, T. Kobayashi, H. Miyake, S. Itoh, R. P .Mtei, M. L. Kirk, *Dalton Trans.*, **2011**, 40 ,1119.

[23] E. A. Allen, B. J. Brisdon, D. A. Edwards, G. W. A. Fowles, R. G. Williams, *J. Chem. Soc.*, **1963**, 4649.

[24] S. Gruber, L. Kilpatrick, N. R. Bastian, K. V. Rajagopalan, T. G. Spire, *J. Am. Chem. Soc.*, **1990**, 112, 8179.

[25] M. G. Finnegan, J. Hilton, K. V. Rajagopalan, M. K. Johnson, *Inorg. Chem.*, **1993**, 32, 2616.

[26] I. K. Dhawan, J. H. Enemark, *Inorg. Chem.*, **1996**, 35, 4873.

[27] B. Bennett, N. Benson, A. G. McEwan, R. C. Bray, *Eur. J. Biochem.*, **1994**, 225, 321.

[28] G. Bertero, R. A. Rothery, M. Palak, C. Hou, D. Lim, F. Blasco, J. H. Weiner, N. C. J. Strynadka, *Nat. Struct. Biol.*, **2003**, 10, 681.

[29] R. G. Schmidt, E. K. Bayburt, S. P. Latshaw, J. R. Koenig, J. F. Daanen, H. A. McDonald, B. R. Bianchi, C. Z. S. Joshi, P. Honore, K. C. Marsh, C. Lee, C. R. Faltynek, A. Gomtsyan, *Bioinorg. Med. Chem. Lett.*, **2011**, 21, 1338.

[30] L. S. Sheng, Y. L. Wu, *Tetrahedron Lett.*, **2002**, 43, 2427.

[31] F. Eya, A. Meva, D. Schaarschmidt, M. A. Abdulmalic, T. Ruffer, *Acta Crystallogr. Sect. E.*, **2012**, 68, 3460.

[32] Y. Gareau, A. Beauchemin, *Phosphorus, Sulfur and Silicon,* **1997**, 120, 393.

[33] Y. Gareau, *J. Chem. Soc., Chem. Commun.*, **1995**, 1429.

[34] B. Bradshaw, D. Collison, C. D. Garner, J. A. Joule, *Org. Biomol. Chem.*, **2003**, 1, 129.

[35] M. A. Ansari, J. Chandrasekaran, S. Sarkar, *Inorg. Chim. Acta.*, **1987**, 133, 133.

[36] G. Moula, M. Bose, B. K. Maitia, S. Sarkar, *Dalton Trans.*, **2012**, 41, 12926.

[37] L. Jamir, R. Yellah, B. K. Patel, *J. Sulfur Chem.*, **2009**, 30, 128.

[38] G. M. Sheldrick, *Acta Crystallogr. Sect. A.*, **2008**, 64. 112.

[39] C. J. Pickett, *J. Chem. Soc., Chem. Commun.*, **1985**, 323.

[40] R. R. Gagne, C. A. Koval, G. C. Lisensky, *Inorg. Chem.*, **1980**, 19, 2854.

Chapter 4

Synthesis and spectroelectrochemical characterisation of methoxyphenyl and pyrazine dithiolene CpCo complexes

4.1 Overview

This chapter describes the development of mixed ligand dithiolene complexes based on cyclopentadienyl cobalt (CpCo) centre. The air stable nature of the CpCo dithiolene complexes make them more interesting as to investigate the electronic interaction process between pyrazine and cobaltadithiolene moieties upon protonation. This could be achieved by comparison of redox properties of synthesised dithiolene CpCo complexes in the presence or absence of acid. The obtained data may provide useful information in relevance to the pyrazine features of the naturally occurring molybdenum enzymes where protons are an integral part of the regenerating oxidation or reduction processes. These types of studies were not possible with the already established molybdenum or tungsten based dithiolene complexes (described in Chapter 3) due to their unstable nature under acidic conditions. In the present work, two different type of ligands *i.e.* pyrazine dithiolene-2-one (**22**) (the synthesis of which is described in Section 3.2) and methoxyphenyl dithiolene-2-one (**36**) (the synthesis of which is discussed in Section 4.2) were reacted with $[CpCo(CO)I_2]$ (obtained from Prof. J. McMaster laboratory),[1] to generate their respective methoxyphenyl dithiolene CpCo [CpCo(OMe-phdt)], (**37**) and pyrazine dithiolene CpCo [CpCo(pzdt)], (**38**) complexes. The characterisation of the synthesised ligands and their respective complexes was carried out using M.P, IR, ^{1}H and $^{13}C\{^{1}H\}$-NMR spectroscopic techniques, along with X-ray crystallographic studies. In addition, the spectroelectrochemical properties of these complexes were investigated and discussed in detail in Section 4.4.

4.2 Synthesis of methoxyphenyl dithiolene-2-one ligand (36)

The synthesis of methoxyphenyl dithiolene-2-one ligand (**36**) was achieved in two steps using methoxyphenyl bromoacetyl (**34**) and is shown in Scheme 4.1. The first step is the replacement of the bromine in **34** with the potassium *O*-isopropyl carbonodithioate group to yield methoxyphenyl dithiocarbonic acid (**35**). The only by product of this reaction is KBr which can be readily removed through filtration. Compound **35** showed characteristic band which appeared at 1724 cm^{-1} corresponding to the carbonyl stretch υ(C=O) of the dithiocarbonic moiety. The ^{1}H-

NMR spectrum of **35** showed two signals at 4.78 and 5.56 ppm corresponding to the methylene (CH_2) and methine (CH) of the dithiocarbonic moiety. Moreover, the methyl (CH_3) groups of the isopropyl functionality were found to be present at 1.24 ppm while the aromatic protons appeared in the range of 7.65-7.26 ppm. In addition, the presence of methoxy group (OCH_3) in **35** was confirmed by the appearance of signal at 3.83 ppm. The $^{13}C\{^1H\}$-NMR spectrum of **35** showed two characteristic downfield resonances at 212.2 and 192.8 ppm which were assigned to the thioketone group (C=S) and the carbonyl group (C=O) of the carbonodithioate moiety, respectively. Aromatic carbons appeared in between 159.5-112.8 ppm. Finally, the obtained molecular mass value (285.0613 u) of **35** through HRMS was in good agreement with the calculated value (285.0619 u) based on the molecular formula of this compound.

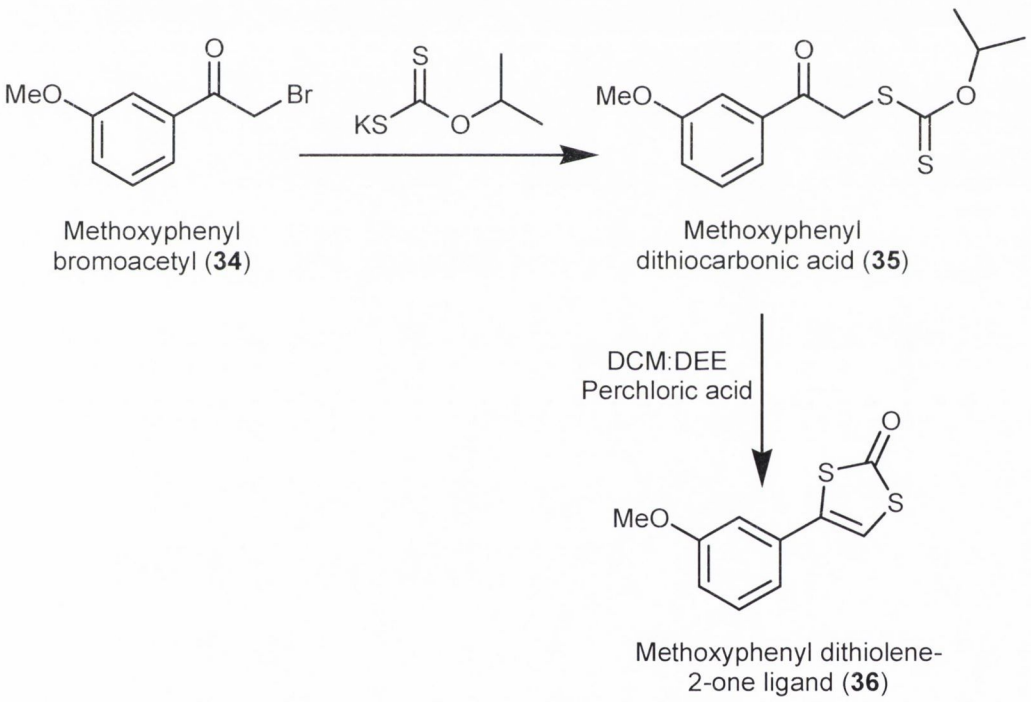

Scheme 4.1: Synthetic route for methoxyphenyl dithiolene-2-one ligand (**36**).

The second step was the cyclisation of **35** which was achieved successfully under acidic conditions to yield compound **36** as illustrated in Scheme 4.1. The IR spectrum of **36** exhibited a characteristic band at 1745 cm^{-1} and attributed to the stretching vibration of the carbonyl ν(C=O) group, which is consistent with the reported values for formation of the protected dithiolene-2-one functionality.[2,3] The ^1H-NMR spectrum of **36** showed a characteristic sharp singlet at 7.08 ppm which assigned to the dithiolene proton while the aromatic protons appeared in the range of

7.68-6.99 ppm. The $^{13}C\{^1H\}$-NMR spectrum showed the most downfield signal at 171.2 ppm corresponding to the carbonyl group (C=O) of the dithiolene-2-one moiety. The signals appeared in between 159.7-114.6 ppm assigned to the aromatic carbons in this compound. The ^1H and $^{13}C\{^1H\}$ NMR spectra also showed the absence of resonances associated with the isopropyl group. Moreover, the found molecular mass value (223.9971. u) of **36** through HRMS was in excellent agreement with the calculated value (223.9966 u) based on the molecular formula of this compound.

4.3 Synthesis and characterisation of methoxyphenyl (37) and pyrazine (38) dithiolene CpCo complexes

The ligands **22** and **36** were used to form their respective complexes using cobalt precursor *i.e.* $[CpCo(CO)I_2]$ in a 1:1 metal to ligand ratio using a reported procedure.[4] The appropriate ligand and sodium hydroxide was dissolved in oxygen free ethanol and stirred for 15 mins. Then the solution of $[CpCo(CO)I_2]$ in oxygen free ethanol was added dropwise and an immediate colour change was observed from brown to deep blue. The reaction mixture was left to stir overnight at room temperature under inert atmosphere. The reaction mechanism involves the cleavage of the sulfur carbonyl-carbon bonds of the dithiolene-2-one ring using sodium hydroxide to form an intermediate sodium salt of dithiolene. In the next step, salt metathesis occurs with the elimination of NaI and dissociation of the CO ligand to form the CpCo complexes **37** and **38**. The purification of the complex was achieved by column chromatography. The obtained solid was crystallised in appropriate solvent (described in Section 4.6.3) to give single crystals suitable for X-ray analysis in case of both complexes. The steps involved for the synthesis of these complexes and their structures are shown in Scheme 4.2.

The IR spectra of complexes **37** and **38** showed the stretching vibrations for υ(C=C) at 1457 and 1487 cm^{-1}, respectively. These assignments were made by analogy with other reported CpCo dithiolene complexes in literature. [5,6,7] In addition, the disappearance of the carbonyl stretch υ(C=O) of dithiolene-2-one in IR spectra of both complexes was also observed.

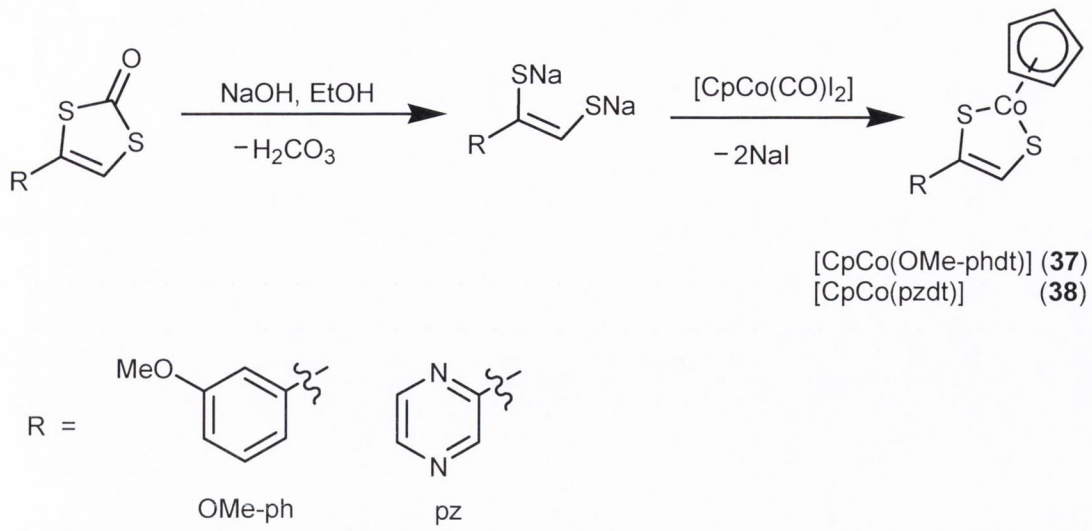

Scheme 4.2: Reaction scheme for the synthesis of CpCo dithiolene complexes **37** and **38**.

The ^{1}H-NMR spectra for complexes **37** and **38** showed the most downfield peaks at 9.03 and 9.54 ppm corresponding to the dithiolene proton. It has been suggested that such a downfield chemical shifts of dithiolene protons are typical of an aromatic proton[5,6,7] and consistent with those complexes having 1,3-dithiolate character.[4,8] The characteristic sharp singlet for Cp protons of complexes **37** and **38** was seen at 5.41 and 5.46 ppm, respectively. Moreover, all of the other protons for these complexes were found in the region of 8.76-6.91 ppm. Complex **37** showed an additional singlet at 3.87 ppm which confirmed the presence of methoxy group on to the phenyl ring. Moreover, HRMS spectra confirmed the formation of complexes **37** and **38** in which found molecular mass values were in excellent agreement with the calculated ones based on molecular formulae of these complexes (see details in Section 4.6.3).

X-ray structural analysis of suitable single crystal finally confirmed the coordination of dithiolate moiety to the Co centre in complexes **37** and **38**. The atomic numbering schemes for complexes **37** and **38** are shown in Figure 4.1 **A** and **B**, respectively. A summary of the crystallographic data collection and structural refinement parameters along with selected bond lengths and angles for both complexes **37** and **38** are listed in Appendices 6.9, 6.11 as well as 6.10, 6.12, respectively. Complex **37** was crystallised in the orthorhombic, space group *Pbca* with two crystallographically

independent molecules in the unit cell while the complex **38** was solved in monoclinic space group *P 21/n* with one independent molecule.

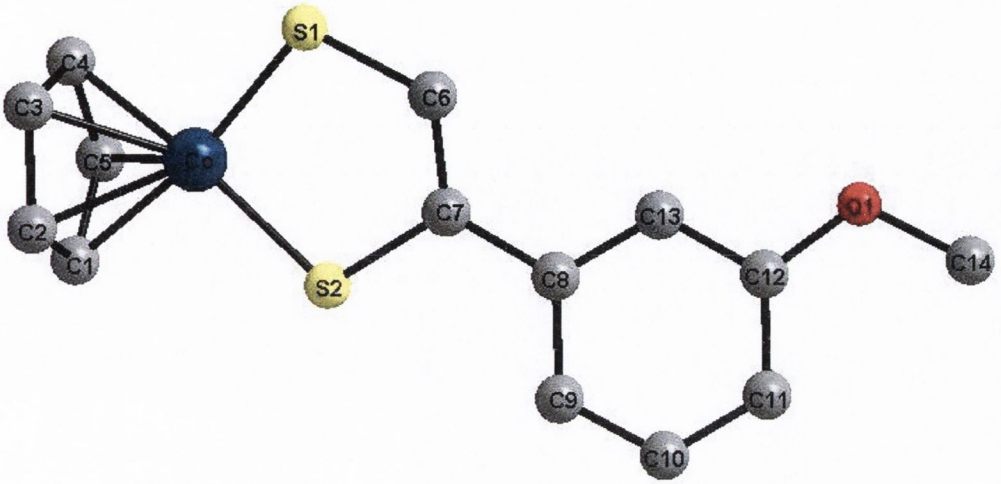

(**A**) Methoxyphenyl dithiolene CpCo complex (**37**) (H-atoms are omitted for clarity).

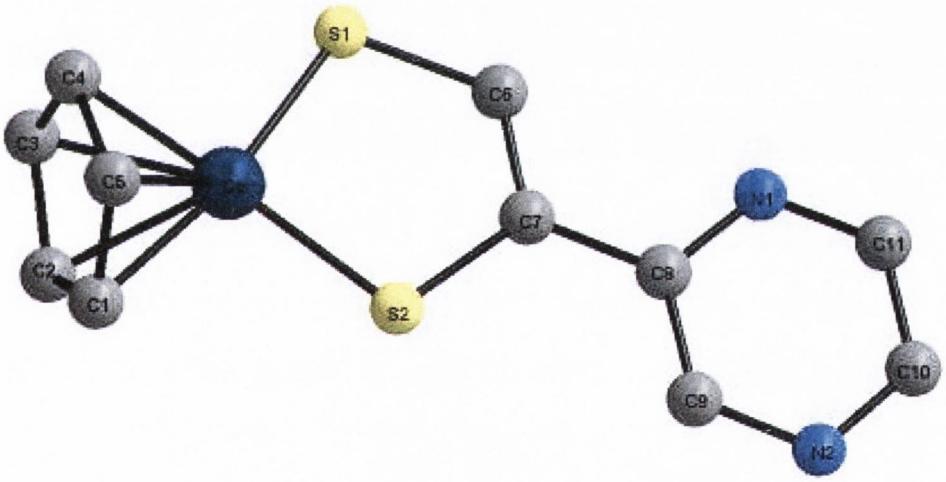

(**B**) Pyrazine dithiolene CpCo complex (**38**) (H-atoms are omitted for clarity).

Figure 4.1: X-ray crystal structures with atomic numbering schemes for complexes: **A**) [CpCo(OMe-phdt)] (**37**) and **B**) [CpCo(pzdt)] (**38**).

In the crystal structure of complexes **37** and **38**, the aromatic and cobaltadithiolene rings are linked by a single bond with a distance of 1.482(3) and 1.471(5) Å, respectively. The methoxyphenyl and cobaltadithiolene ring in complex **37** are not in the same plane and make a dihedral angle of 13.2(1)°, however, both rings are found to be almost planar in complex **38**. The dihedral angles between the

cobaltadithiolene moieties and Cp planes are almost at right angles (88.9-86.0°) in both complexes which is in agreement with the typical two legged piano-stool geometries, identical to those of previously published for Co^{III} as half sandwiched metal dithiolene complexes.[9,10,11] The average Co-S bond lengths (2.163(6) Å for **37** and 2.102(12) Å for **38**) are consistent with those previously reported [2.126(7)-2.146(3) Å] for other CpCo dithiolene complexes.[9,12,13] However, these values are shorter than those of the dimeric $[CpCo(bdt)]_2$ complex (Co-S = 2.21-2.48 Å).[14,15,16] In addition, the intra-ligand (S-C) bond lengths in complexes **37** and **38** are amounted to be 1.734(2) and 1.715(2), respectively. The observed (S-C) distances are typical of ligand binding in dithiolate mode, in agreement with those reported for having dithiolate coordination characteristics.[9,17,18]

The solid state packing diagrams for both complexes **37** and **38** are shown in Figure 4.2 **A** and **B**, respectively. Both complexes in a 1-D chain are stabilised by π-π stacking as well as hydrogen bonding interactions between two independent molecules. In crystal structure of complex **37**, two methylene (CH....π) T-shape interactions which are C(2)-H(2)....π[(C8)-(C9)-(C10)-(C11)-(C12)-(C13)] and C(14)-H(14)....π[(C8)-(C9)-(C10)-(C11)-(C12)-(C13)] and the distances of H(3) or H(14) to the centre of adjacent aromatic ring [(C8)-(C9)-(C10)-(C11)-(C12)-(C13)] are 2.743(2) and 2.848(2) Å, respectively. Similarly, complex **38** also exhibited the one methylene (CH....π) T-shape interaction for C(2)-H(2)....π[(C6)-(C7)-(S1)-(S2)-(Co)] with a distance of 3.063(5) Å. Moreover, three inter-molecular hydrogen bonding interactions are present in complex **37**: [C(13)-H(13)....S(1)], [C(4)-H(4)....S(1)] and [C(10)-H(10)....S(2)] with distances of 2.995, 2.833 and 2.833 Å along with angles of 162°, 159° and 168°, respectively. In addition, three inter-molecular hydrogen bonding interactions are also observed in complex **38**: [C(11)-H(11)....S(1)], [C(6)-H(6)....N(1)] and [C(5)-H(5)....N(1)] with distances and angles of 2.758, 2.690 and 2.430 Å as well as 156°, 148° and 162°, respectively. Thus, the solid state structures of both complexes are packed, stabilised and arranged through π-π stacking interactions and strong hydrogen bonding interactions.

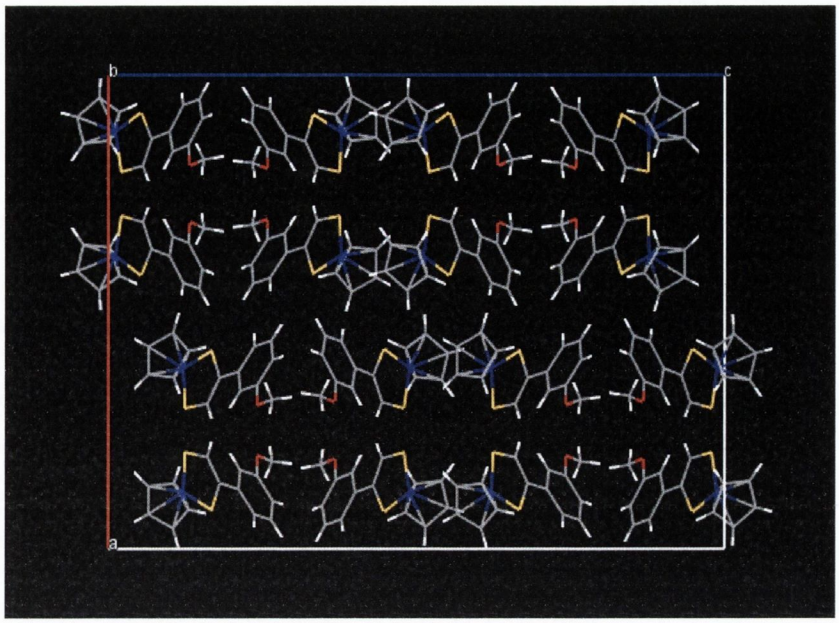

A

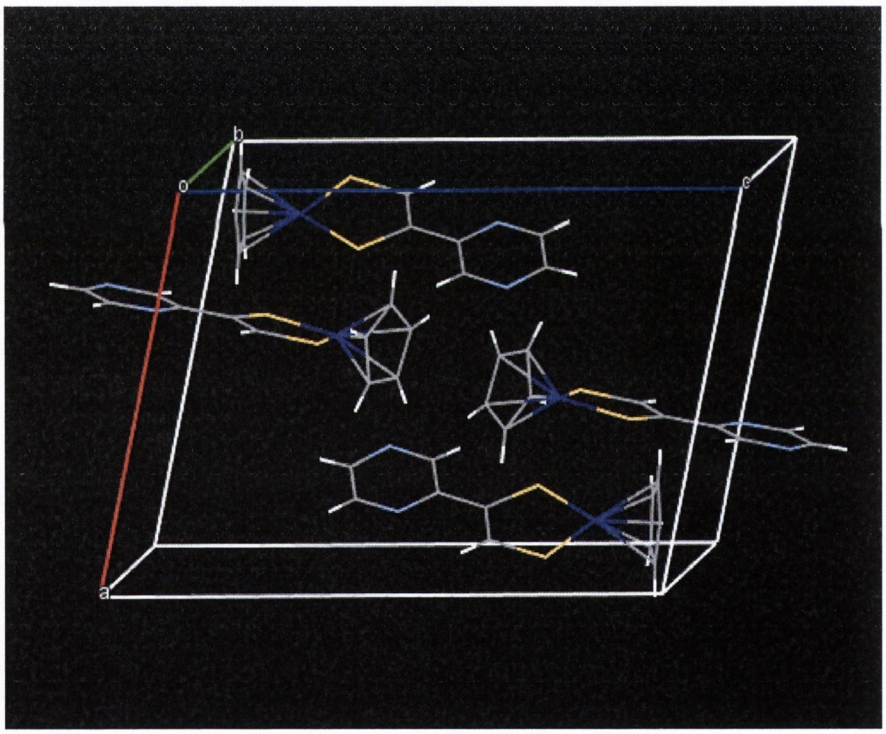

B

Figure 4.2: Crystal packing diagrams for complexes: **A**) [CpCo(OMe-phdt)] (**37**) and **B**) [CpCo(pzdt)] (**38**).

In summary, the work carried out in the Sections 4.2 and 4.3 details the synthesis and characterisation of methoxyphenyl dithiolene ligand (**36**) as well as CpCo dithiolene complexes **37** and **38**. X-ray structural analysis of novel complexes **37** and **38** reveals the coordination of dithiolene ligand to the Co centre and behaves as half sandwiched cobaltadithiolene complexes, showing typical two legged piano-stool geometries. After successful synthesis, these complexes were subjected to the investigation of their spectroelectrochemical properties and detailed in section 4.4.

4.4 Spectroelectrochemistry of complexes 37 and 38

The spectroelectrochemical properties of synthesised CpCo complexes **37** and **38** were investigated by cyclic voltammetry, in combination with UV-Vis spectroelectrochemistry and electron paramagnetic resonance (EPR) spectroscopic techniques. These studies were carried out in collaboration with supervision of Prof. Jon McMaster and Dr. Stephen E. Davies at University of Nottingham, United Kingdom.

4.4.1 Cyclic voltammetry of complexes 37 and 38

Electrochemical studies were performed by dissolving the complex under study in anhydrous DMF (5 ml) containing $[NBu^n_4][BF_4]$ (0.2 M) as the supporting electrolyte at 298 K, under a nitrogen atmosphere (the experimental procedure is described in Section 4.6.1). The obtained voltammograms for complexes [CpCo(OMe-phdt)] (**37**) and [CpCo(pzdt)] (**38**) are shown in Figures 4.3 and 4.4, respectively. Each voltammogram showed similar electroactive processes; a reduction process at negative potential and oxidation process at a positive potential. Both complexes displayed a fully reversible redox couple for Co^{III}-Co^{II}, as has been previously described for other [CpCo(dithiolene)] complexes.[8,19] The oxidation processes for complexes **37** and **38** were observed at -683 and -575 mV, which were accompanied with reduction processes at -720 and -619 mV, respectively. Furthermore, the redox potential ($E_{1/2}$) values associated with the Co^{III}-Co^{II} couple were calculated to be -701 mV and -595 mV for complexes **37** and **38**, respectively.

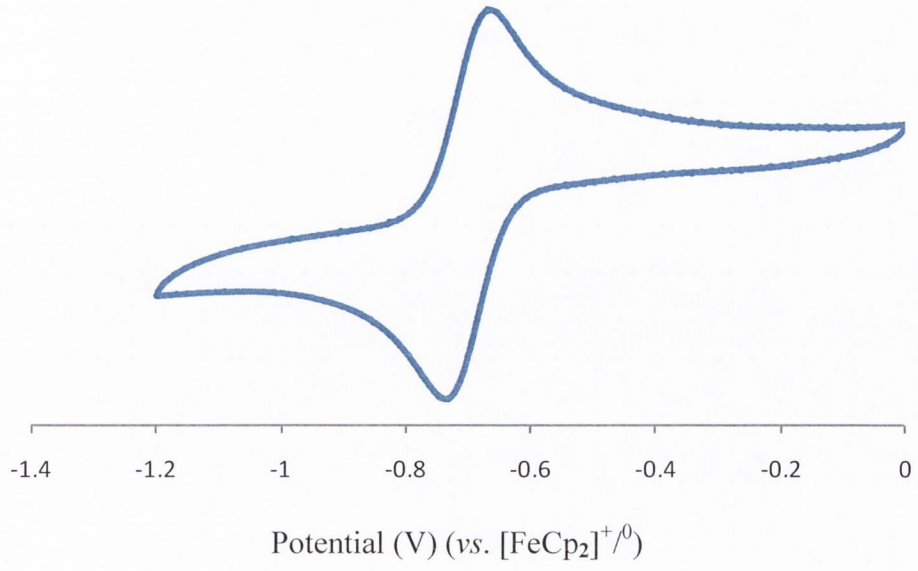

Figure 4.3: Cyclic voltammogram of complex **37** in DMF with $[NBu^n_4][BF_4]$ as the supporting electrolyte at 298 K and scan rate 100 mVs^{-1}.

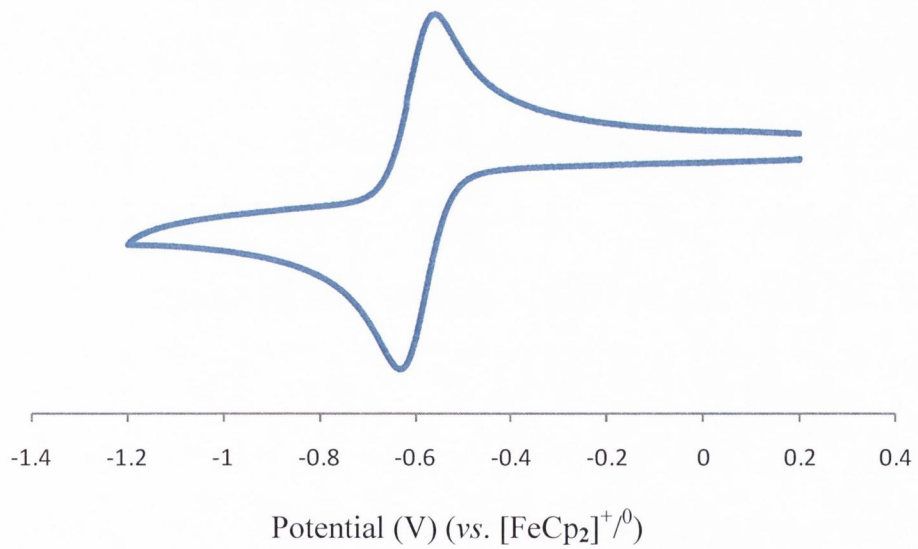

Figure 4.4: Cyclic voltammogram of complex **38** in DMF with $[NBu^n_4][BF_4]$ as the supporting electrolyte at 298 K and scan rate 100 mVs^{-1}.

Moreover, it has been reported that the nature of substituents attached at metalladithiolene ring have large effects on their redox properties and vary in a manner consistent with the nature of electron withdrawing or donating nature of the attached ligands.[4,19] Similarly, the redox behaviour for synthesised complexes revealed that the pyrazine-substituted complex **38** found to be at less negative potential value ($E_{1/2}$ = -597 mV) compared to the redox potential value for methoxyphenyl-substituted complex **37** ($E_{1/2}$ = -701 mV). This less negative potential value could be attributed to the electron withdrawing character of pyrazine functionality substituted to the cobaltadithiolene ring in complex **38**.

The single electron transfer process for complexes **37** and **38** was confirmed by bulk electrolysis (detailed in Section 4.6.1) where the calculated charge values were in agreement with the experimentally determined ones. As an example, a plot of charge *vs.* time for the one electron reduction process of **38** is presented in Figure 4.5. The calculated charge of a single electron process for 1 mM solution (7 ml DMF) of **38** was 0.72 C. The observed value for this process was 0.675 C (94%), confirming the one electron transfer process. This conclusion is consistent with the results of previously electrochemical studies of other CpCo dithiolene complexes,[8] *i.e*, the process is confirmed as a one electron transfer and assigned to the $[CpCo(dithiolene)]^{0/-1}$ couple.

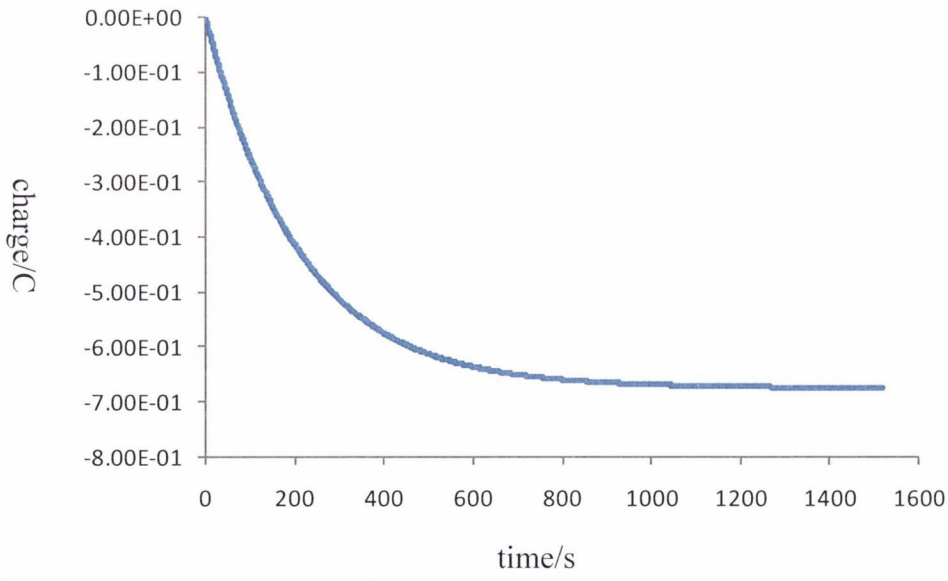

Figure 4.5: A plot of charge *vs.* time for the single electron transfer process by bulk electrolysis of complex **38**.

The electrochemical characteristics of the redox couple for both complexes were also investigated. The separation of the peak potentials (ΔE) for reversible redox couple for complexes **37** and **38** were calculated to be 37 and 44 mV, respectively at a scan rate of 100 mVs^{-1}; these values were essentially the same as corresponding ΔE value of the $[FeCp_2]^{+/0}$] (Cp = η^5-C_5H_5) couple used as an internal redox standard.

A study of the scan rate dependency of the peak currents (I_p^c and I_p^a) for reduction couple associated with both complexes showed that the peak currents varied linearly with the square root of the applied scan rate, confirming the fully reversible redox couple (Co^{III}-Co^{II}) at range of applied scan rates. As a typical example, Figure 4.6 illustrates this behaviour for complex **38**. The graph between peak currents ($-I_p^c/ I_p^a$) and square root of the scan rate illustrates that ratio of $-I_p^c/ I_p^a$ is equal to 1.0 for the redox process of complex **38**; this was essentially equal to the internal standard $[FeCp_2]^{+/0}$].

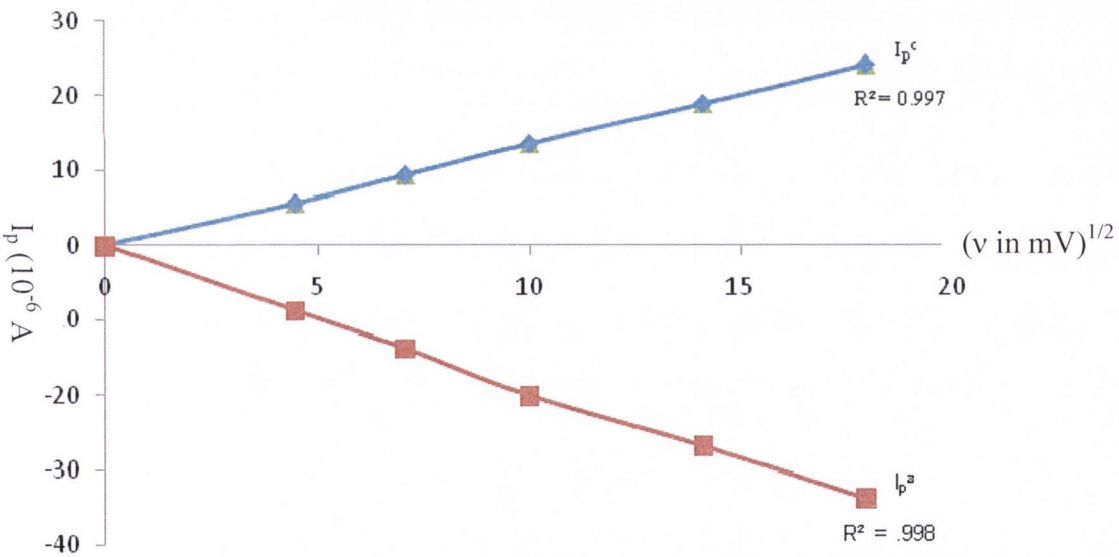

Figure 4.6: Plot of $-I_p^c/ I_p^a$ *vs.* (scan rate)$^{1/2}$ for a fully reversible redox couple (Co^{III}-Co^{II}) of complex **38**.

4.4.2 Cyclic voltammetry of pyrazine dithiolene CpCo complex (38) in the presence of acid

Literature reports have described that the addition of acid protonate the nitrogen

atom of heterocyclic ligand attached to metalladithiolene system.[4,8] This protonation effect may be communicated *via* unsaturated system from ligand to the metallacycle and causing a positive shift in the redox potential of the Co centre.[8,20] In order to investigate the protonation effect on pyrazine dithiolene CpCo complex (**38**), cyclic voltammograms were recorded in DMF at room temperature before and after addition of 1 and 5 equivalents of *p*-toluenesulfonic acid (TsOH) using $[NBu^n_4][BF_4]$ as a supporting electrolyte and are stacked in Figure 4.7.

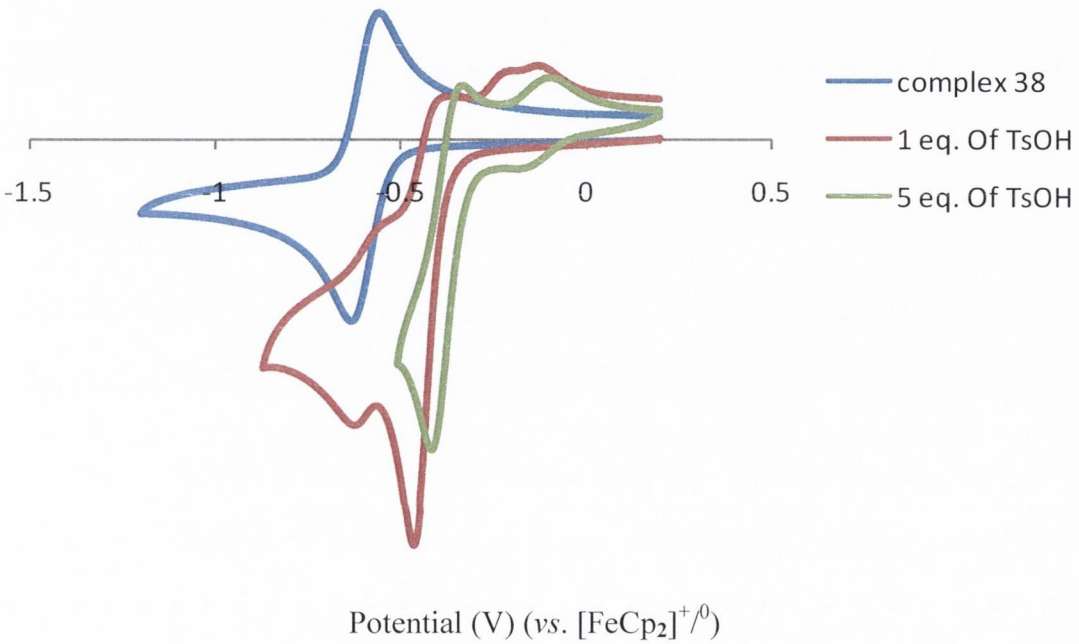

Figure 4.7: Cyclic voltammogram of complex **38** without addition of TsOH (blue line) after addition of 1 (red line) and then 5 equivalents (green line) in DMF at 298 K and scan rate 100 mVs^{-1}.

It can be clearly seen that the addition of 1 equivalent of acid results in; (i) the reduction process shifts to a positive potential from -619 mV to -465 mV and (ii) I_p^c are observed to be large in magnitude and I_p^a being small in comparison to the size of redox couple present in the absence of acid. Afterwards, the addition of 5 equivalents of acid fully protonates the complex **38** which results in a shift to a more positive value (hence the difference of shift of the redox potential by +213 mV). Similar results have been published for quinoxaline dithiolene metal complexes where protonation results in the shift of reduction couple to a more positive value

compared to parent complex.[8,19] Moreover, the observed positive shift in the complex **38** could be attributed to the effect of protonation of nitrogen of pyrazine and can be rationalised with the structure of this complex as shown in Figure 4.8. Two possible resonance forms **A** and **B** suggest that the protonation effect may be communicated from pyrazine to the cobaltadithiolene moiety and as a result withdraw electron density from the cobaltadithiolene ring.

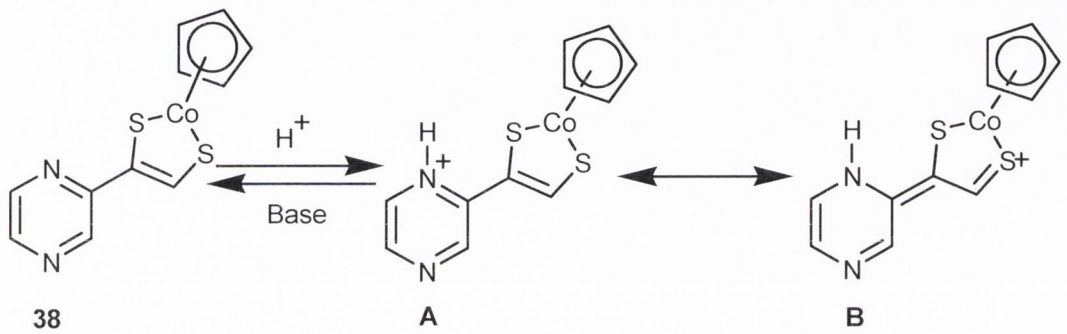

Figure 4.8: Resonance forms of complex **38** after protonation by addition of excess TsOH.

Moreover, the cyclic voltammogram of the neutralised solution (by addition of excess triethylamine showed a reverse shift (-213 mV) in redox couple. This result confirms the process is fully reversible, as addition of excess base again regenerates the similar CV profiles as observed for parent redox couple in the absence of acid.

4.4.3 UV-Vis spectroelectrochemical studies of complexes 37 and 38

The objective of UV-Vis spectroelectrochemical studies of complexes **37** and **38** was to investigate the characteristic absorption bands associated with reduced and oxidised states of these complexes. These studies were performed by dissolving the complex under study in anhydrous DMF (5 ml) containing $[NBu^n_4][BF_4]$ (0.2 M) as the supporting electrolyte at 273 K, under nitrogen atmosphere and the experimental procedure is described in Section 4.6.1. The obtained UV-Vis spectra for [CpCo(OMe-phdt)] and [CpCo(pzdt)] complexes are shown in Figures 4.9 and 4.10, respectively.

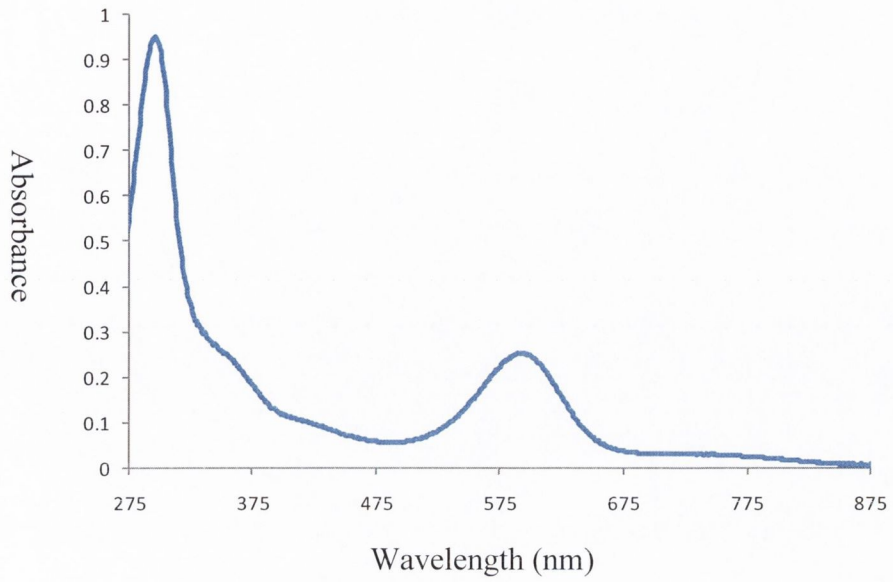

Figure 4.9: The UV-Vis spectrum of complex **37** at 273 K in DMF, containing the $[NBu^n_4][BF_4]$ (0.2 M) as the supporting electrolyte. (before applying any potential).

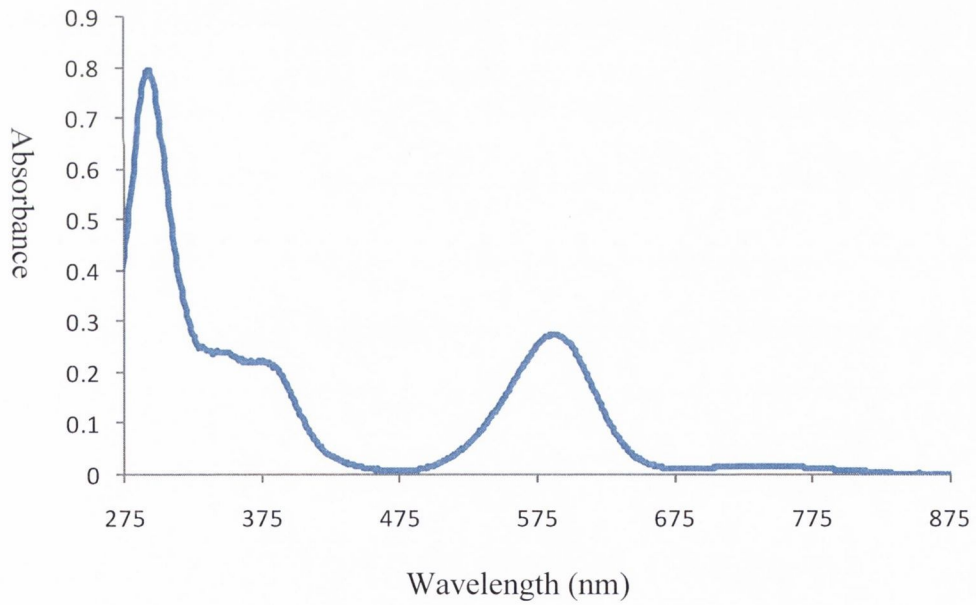

Figure 4.10: The UV-Vis spectrum of complex **38** at 273 K in DMF, containing the $[NBu^n_4][BF_4]$ (0.2 M) as the supporting electrolyte. (before applying any potential).

Each compound exhibited absorption bands in the regions of 590-577 and 295-289 nm. The absorption band observed in the visible region has been attributed to the ligand to metal (S ⟶ Co) charge transfer transitions, consistent with the similar

spectral assignments made by Nomura *et al.*[13,21] The other band observed in the UV region has been attributed to the $\pi \longrightarrow \pi^*$ transitions of aromatic rings in both complexes. Furthermore, the absorption band at 382 nm in spectrum of complex **38** was attributed to the $n \longrightarrow \pi^*$ transitions within the pyrazine ring system. The obtained UV-Vis spectra for both complexes are in agreement with the typical UV-Vis spectral profiles reported for other [CpCo(dithiolene)] complexes in literature.[13,19]

The reduction process for [CpCo(dithiolene)] to $[CpCo(dithiolene)]^-$ for complexes **37** and **38** were studied by UV-Vis spectroelectrochemical technique. The reduction of each compound resulted in the significant changes in the UV-Vis spectral profiles. As a typical example, a stack of all UV-Vis spectra for reduction of [CpCo(OMe-phdt)] to $[CpCo(OMe\text{-}phdt)]^-$ are shown in Figure 4.11.

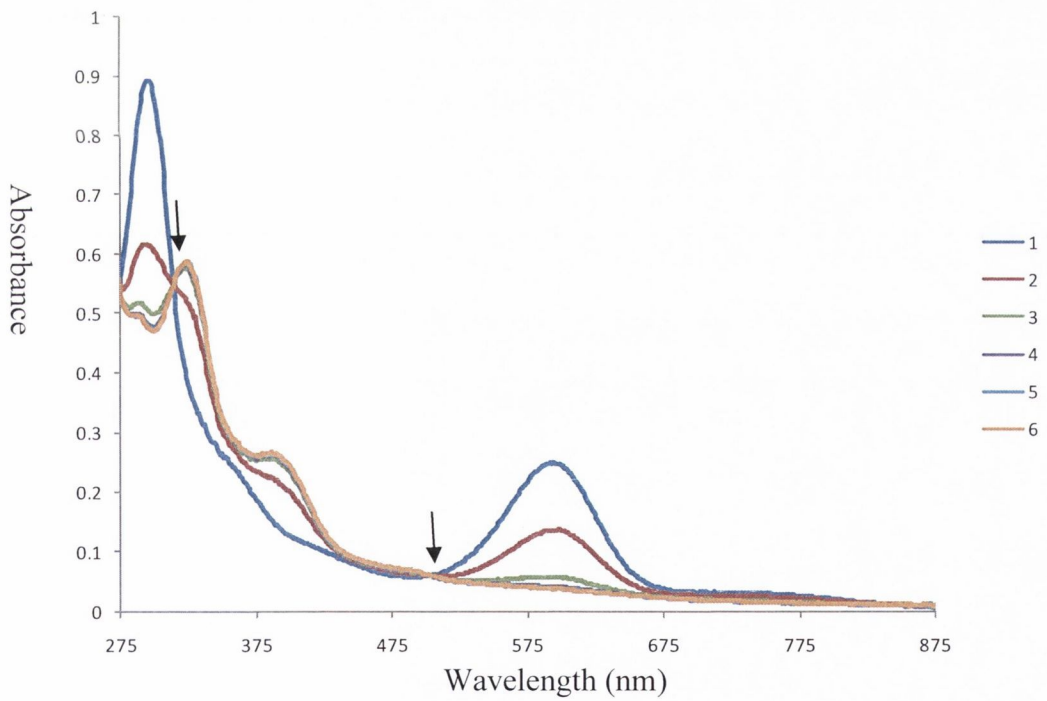

Figure 4.11: A stack of UV-Vis spectra observed for the reduction of [CpCo(OMe-phdt)] to $[CpCo(OMe\text{-}phdt)]^-$ in DMF at 273 K, containing $[NBu^n_4][BF_4]$ (0.2 M) as the supporting electrolyte in 5 mins. Isobestic points are indicated by arrows.

An initial potential of -1.1 V was applied to the solution of [CpCo(OMe-phdt)] and the UV-Vis spectra were recorded with the successive intervals of time until no change in spectrum was observed. The first spectrum **1** corresponds to the [CpCo(OMe-phdt)] complex while the spectra from **2-5** represent the successive reduction over 5 mins. The final spectrum **6** is being of fully reduced form of $[CpCo(OMe\text{-}phdt)]^-$ complex. During this reduction process, it was also noted that the colour of the solution of complex was changed from blue to brownish/green due to change in oxidation state. Figure 4.11 clearly shows that upon successive applications of potential on [CpCo(OMe-phdt)] exhibits marked changes in the UV-Vis spectroscopic profiles. The intensity of the absorption maximum at 590 nm gradually decreases with the formation of a new absorption band at 385 nm due to the involvement of the dithiolene to the Co^{II} charge transfer transitions. Two distinct isobestic points at 498 and 312 nm observed which indicate that the reduction of Co^{III}–Co^{II} progresses smoothly, with no intermediate structural change. Afterwards, *in situ* oxidation of $[CpCo(OMe\text{-}phdt)]^-$ to [CpCo(OMe-phdt)] was carried out and the results are shown in Figure 4.12.

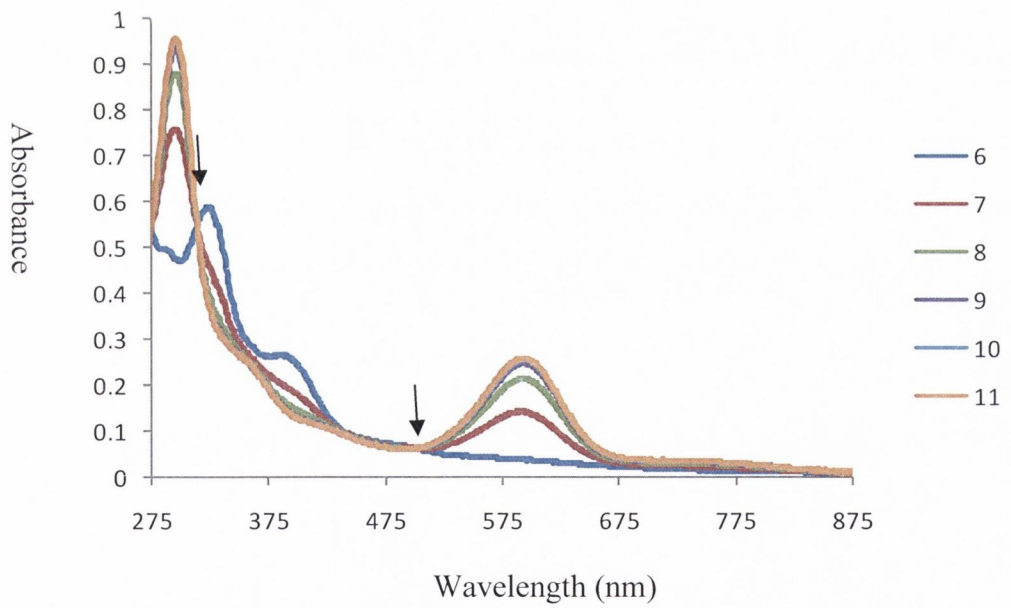

Figure 4.12: A stack of UV-Vis spectra observed for *in situ* oxidation of $[CpCo(OMe\text{-}phdt)]^-$ to [CpCo(OMe-phdt)] in DMF at 273 K, containing $[NBu^n_4][BF_4]$ (0.2 M) as the supporting electrolyte in 5 mins. Isobestic points are indicated by arrows.

The initial potential 1 V was applied to the fully reduced Co^{II} complex solution and UV-Vis spectra were recorded in 1 min intervals until no change in spectrum was observed. Spectrum **6** represents the fully reduced form Co^{II} state while spectra 7-10 represent the successive oxidation of complex over time. The final spectrum **11** is fully oxidised form of [CpCo(OMe-phdt)] complex. During this oxidation process, the appearance of two isobestic points at 489 and 318 nm indicate that the oxidation of Co^{II}–Co^{III} also progresses smoothly, again consistent with no significant structural change. Moreover, the spectrum **11** shows the disappearance of the band in visible region at 385 nm with regeneration of the similar spectral profiles as were seen in parent [CpCo(OMe-phdt)] complex, confirming the reversibility of the Co^{II}–Co^{III} couple. Similar spectroscopic changes upon the reduction and subsequent re-oxidation were observed for the [CpCo(pzdt)] complex and is illustrated in Table 4.1.

Table 4.1: UV-Vis characteristic spectral data for reduction and subsequent re-oxidation of complexes **37** and **38**.

Complex	λ_{max}/nm [Co] (ε/mol^{-1}dm^{3}cm^{-1})	λ_{max}/nm $[Co]^-$ (ε/mol^{-1}dm^{3}cm^{-1})	Isobestic points $[Co]^-$/[Co]
37	295 (17740), 590 (4840)	317 (11460), 385 (5320)	312, 498/ 314, 495
38	289 (15700), 374 (4480) 577 (5140)	319 (9160), 389 (4620), 437 (4020)	523, 383, 316/ 519, 376, 311

Each reduction process was found to be fully reversible and each series of spectra contained isobestic points. The characteristic absorptions of UV-Vis spectra associated with redox couple for complexes **37** and **38** are summarised in Table 4.1. Overall, the reversibility of reduced $[CpCo(dithiolene)]^-$ and oxidised [CpCo(dithiolene)] states of each complex is consistent with the published results for CoS_2 chromophore in other CpCo complexes.[8,12,19]

Keeping in mind the significance of dithiolene ring, it is also important to consider the roles of other components of MPT[22] *i.e.* pyrazine may provide the basic sites to handle the protons that are an integral part of redox process. The study of complex **38** in the presence of acid, resulted in a shift of the redox potential of the Co centre to a more positive value due to the protonation of the basic sites of *N*-heterocyclic moiety attached to dithiolene ring. The observed shift suggested the effect of protonation which communicated from pyrazine moiety of the ligand to the cobaltadithiolene moiety. With respect to this point it can be proposed that MPT could facilitate a route for electronic communication to, or from, the Mo/W centre during enzymatic catalytic reactions.

4.4.4 Electron paramagnetic resonance of complexes 37 and 38

The EPR experiment for complexes **37** and **38** are operated at a fixed frequency of 9.5 GHz (X band), with a field strength of 3,400 gauss. The reduction of both complexes in anhydrous DMF (5 ml) was achieved by bulk electrolysis at a controlled potential (-0.90 V), containing the $[NBu^n_4][BF_4]$ (0.2 M) as the supporting electrolyte. The experimental procedure is described in Section 4.6.1. Upon electrochemical reduction, there was marked changes in the colour of solution of $[CpCo(OMe\text{-}phdt)]^-$ and $[CpCo(pzdt)]^-$ from deep blue to brownish/green and brownish/orange, respectively due to change in the oxidation state from Co^{III} to Co^{II}. The EPR spectra for both reduced complexes were recorded in fluid and frozen states at 298 and 77 K, respectively.

The fluid solution EPR spectra of both complexes exhibited eight lines for $^{53,54}Co$ (I = 7/2) at room temperature. These spectra were found to be consistent with the presence of an unpaired electron coupled to Co nucleus, with no resolvable hyperfine coupling to sulfur, as similar spectral profiles have been previously reported for other [CpCo(dithiolene)] complexes.[19] The fluid solution EPR spectra for reduced $[CpCo(OMe\text{-}phdt)]^-$ and $[CpCo(pzdt)]^-$ complex are shown in Figure 4.13 and 4.14, respectively.

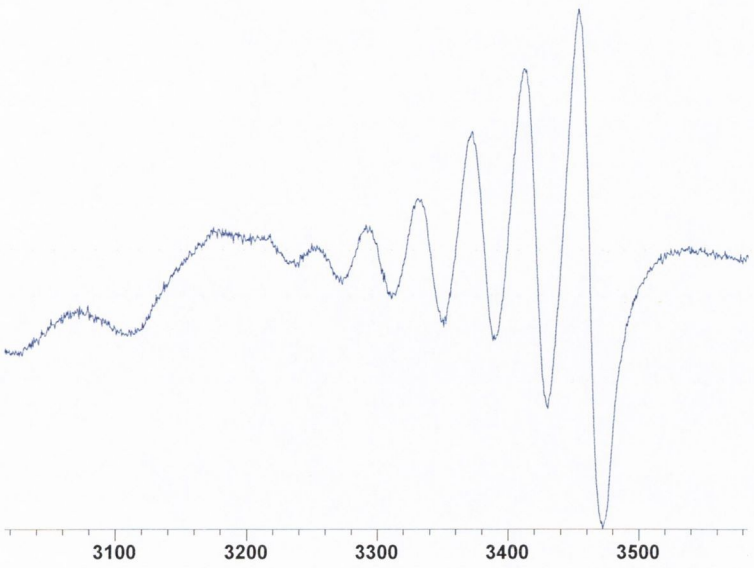

Figure 4.13: The fluid solution EPR spectrum of reduced $[CpCo(OMe\text{-}phdt)]^-$ in DMF at 298 K, containing $[NBu^n_4][BF_4]$ (0.2 M) as an internal standard.

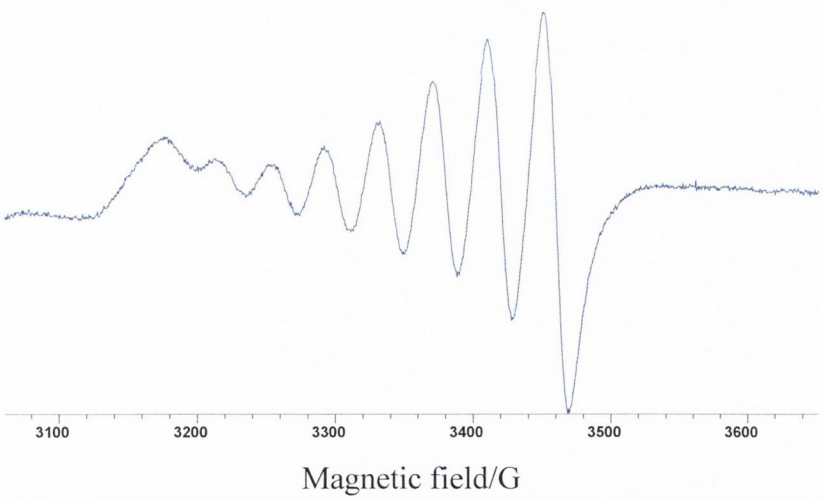

Figure 4.14: The fluid solution EPR spectrum of reduced $[CpCo(pzdt)]^-$ in DMF at 298 K, containing $[NBu^n_4][BF_4]$ (0.2 M) as an internal standard.

The frozen solution EPR spectra for reduced $[CpCo(OMe\text{-}phdt)]^-$ and $[CpCo(pzdt)]^-$ were also recorded at 77 K and are shown in Figures 4.15 and 4.16, respectively. The obtained spectra are found to be in a rhombic pattern; in agreement with other reported CpCo complexes in literature.[19] Overall, the obtained fluid and frozen

spectral profiles for both complexes are well matched with other reported CpCo(dithiolene) complexes.[19] However, reproduction of all the features in the experimental spectra of both complexes using assimilation are still under study.

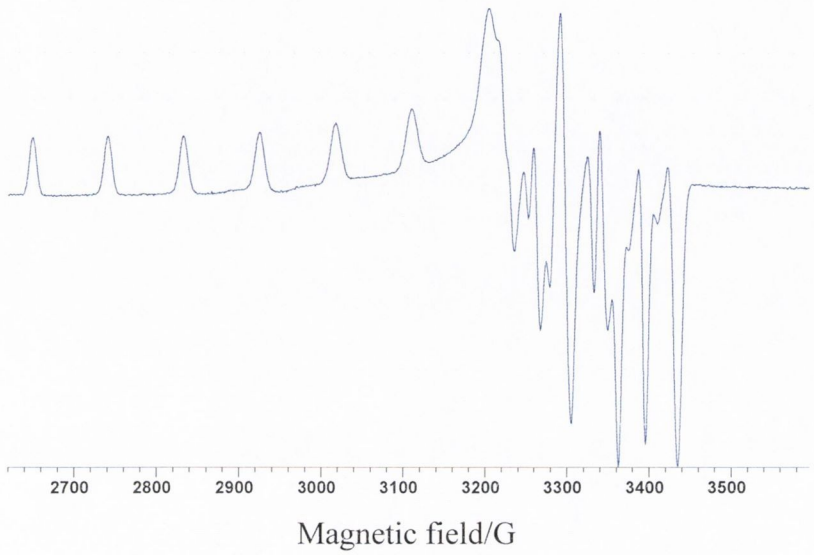

Figure 4.15: The frozen solution EPR spectrum of reduced $[CpCo(OMe\text{-}phdt)]^-$ in DMF at 77 K, containing $[NBu^n_4][BF_4]$ (0.2 M) as an internal standard.

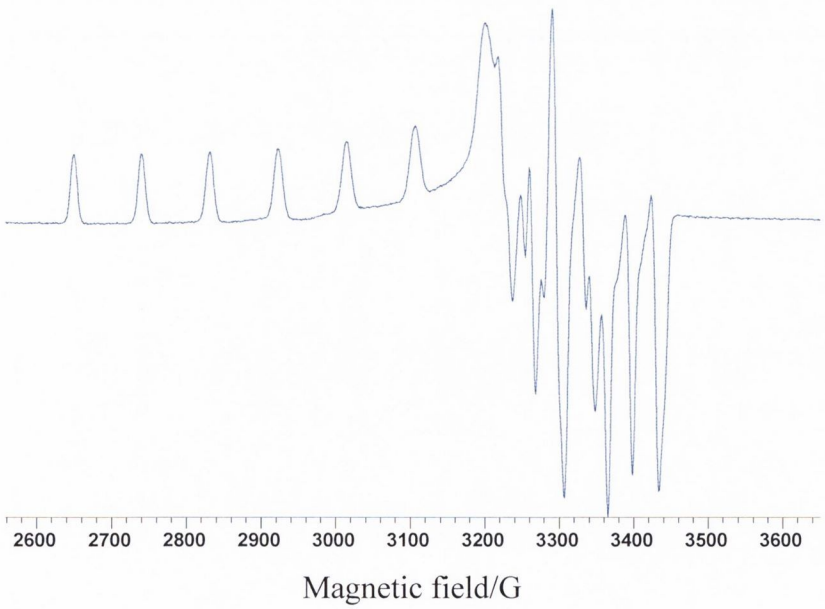

Figure 4.16: The frozen solution EPR spectrum of reduced $[CpCo(pzdt)]^-$ in DMF at 77 K, containing $[NBu^n_4][BF_4]$ (0.2 M) as an internal standard.

4.5 Conclusions

In the present work, synthesised ligands **22** and **36** were reacted with the [CpCo(CO)I_2] to isolate novel methoxyphenyl dithiolene CpCo **(37)** and pyrazine dithiolene CpCo (**38**) complexes, respectively. These complexes were fully characterised by spectroscopic techniques (IR, ^{1}H-NMR, HRMS) along with X-ray structure analysis. The ^{1}H-NMR and X-ray structural studies on complexes **37** and **38** confirm the coordination of dithiolate to Co centre, showing typical two legged piano-stool geometry. The electrochemical investigations show a rich redox chemistry for both complex **37** and **38**, confirming a fully reversible, one electron, redox couple for Co^{III}–Co^{II} complexes. Furthermore, the protonation of complex **38** results in a shift of the redox potential of the Co centre to a more positive value. The observed shift suggests the possible effect of protonation of the ligand to the metal centre, hence modulating the redox properties of MPT towards metal centre. The results of UV-Vis spectroelectrochemical studies clearly indicate that there is no structural changes involved in the complex solution during reduction and re-oxidation processes. This reversible nature suggests that both reduced complexes [(CpCo(dithiolene)]$^-$ were stable enough on the time scale of CV measurements. Moreover, EPR spectroscopic data for Co^{II} state of both complexes are in consistent with the presence of unpaired electron which is coupled to the Co (I = 7/2) nucleus. However, reproduction of all the features in the experimental spectra of both complexes requires the assimilation which is still under study.

4.6 Experimental

This chapter details the synthesis and characterisation of methoxyphenyl dithiolene-2-one ligand (**36**). In addition, synthesis and characterisation of CpCo complexes (**37** and **38**) which were derived from methoxyphenyl (**36**) and pyrazine (**22**) dithiolene-2-one ligands is also discussed.

4.6.1 Physical methods

All commercially available chemicals were used as supplied by Sigma Aldrich and were used without further purification. The metal precursor $[CpCo(CO)I_2]$ was synthesised according to the reported procedures.1 All reactions were performed under an atmosphere of nitrogen or argon, using standard Schlenk-line techniques. Solvents were either degassed or purged with argon prior to use. Melting point values were recorded on a Stuart scientific SMP3 melting point apparatus and are uncorrected. All infrared spectra were recorded (4000–650 cm^{-1}) on a Perkin-Elmer Fourier-Transform Infrared (FTIR) spectrophotometer. All ^{1}H-NMR spectra were recorded on a Bruker AV400 operating at 400.13 MHz. All samples were dissolved in deuterated solvents and chemical shift values are reported in parts per million (ppm). High Resolution Mass Spectrometry (HRMS) analyses were carried out on a Water-Micromass Q-ToF (quadrupole - Time of Flight) hybrid mass spectrometer equipped with an orthogonal electrospray source (z–spray). This was operated in an electrospray positive ion mode (ESI^+) or electrospray negative ion mode (ESI^-). Sodium formate was used for mass calibration checks and optimal parameter tuning was performed using flow injection of standard solutions. All ToF measurements for ligand **36** were performed at high resolution settings (5000 FWHM at mass 1500). The samples **37** and **38** were analysed using MALDI-Q-ToF Premier system *i.e.* matrix assisted laser desorption/ionisation - quadrupole - Time of Flight. Both samples were prepared using 2-[3-(4-*t*-butyl-phenyl)-2-methyl-2-propenylidene]malononitrile (DCTB) as a matrix. All ToF measurements were performed at high resolution settings (5000 FWHM at mass 1500). Data were always taken in continuum mode. X-ray crystallographic studies were performed for suitable single crystals of **37** and **38** which were coated in Paratone N heavy oil then mounted on a glass fibre. The respective data were collected on a Rigaku Saturn-724

diffractometer (graphite-monochromated Mo Kα radiation, λ = 0.71073 Å) at 108(2) K. The structures were solved by direct methods (SHELXS-97) and refined against all data by full matrix least-squares methods on F^2 (SHELXL-97).[23] All non-hydrogen atoms were refined with anisotropic displacement parameters. The hydrogen atoms (except if found and refined freely) were refined isotropically on calculated positions using a riding model with their U_{iso} values constrained to 1.5 U_{eq} of their pivotal atoms for terminal sp^3 carbon atoms and to 1.2 times for all other carbon atoms.

Electrochemical measurements were carried out by collaboration with Prof. Jonathan McMaster and Dr. Stephen E. Davies at Department of Chemistry, University of Nottingham, United Kingdom (COST funding, CM1003, biological oxidations and reductions). Cyclic voltammetric studies were performed using an EG & G PAR Model 362 Scanning Potentiostat with a Lloyds Instruments PL3 X-Y recorder. Either a glassy carbon or Pt wire working electrode, a Pt wire secondary electrode, a saturated calomel electrode (SCE) as reference electrode and the electrolyte $[NBu^n_4][PF_6]$[24] were used in the cell. All voltammograms were recorded for complexes **37** and **38** in DMF solution (1 mmol), containing a supporting electroyte 0.2 M $[NBu^n_4][PF_6]$ under nitrogen atmosphere. The $[FeCp_2]^+/[FeCp_2]$) (Cp = η^5-C_5H_5) couple was used as an internal redox standard under these conditions.[25] Optically transparent thin-layer electrode (OTTLE) measurements were obtained using a Varian Cary 1 spectrophotometer in conjunction with a Sycopel Scientific Ltd. DD10M potentiostat.[25] The initial voltages were chosen to be *ca.* 200 mV more negative than the $E_{1/2}$ value for the respective Co^{III}–Co^{II} couple and the final voltages *ca.* 200 mV more positive, or until the spectrum no longer changed with increasingly positive potential. The applied potential was increased in 20 mV increments from the initial voltage. The reversibility of the system was confirmed by applying the initial potential after reduction had been completed and reproducing the initial spectrum.

Bulk electrolysis experiment was carried out using a two compartment cell at controlled potential. A Pt/Rh gauze basket working electrode was separated from a wound Pt/Rh gauze secondary electrode by a glass frit. A SCE was bridged to the test solution through a vycor frit that was orientated at the centre of the working electrode. The working electrode compartment was fitted with a magnetic stirrer bar

and the test solution was stirred rapidly during electrolysis. An ice-water bath was used to maintain a temperature of 0 °C. Each solution contained $[NBu^n_4][BF_4]$ (0.2 M) as the supporting electrolyte and the compound (10^{-3} M). All solutions were prepared using Schlenk line technique.

4.6.2 Synthesis of methoxyphenyl dithiolene-2-one ligand (36)

4.6.2.1 Synthesis of O-isopropyl-S-2-oxo-2-(3-methoxy-phenyl-2-yl)ethyl carbonodithioate (35)

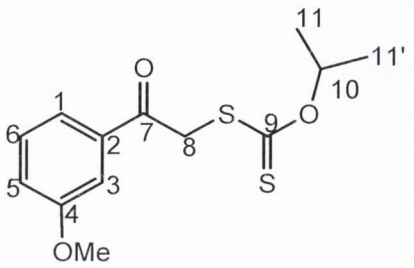

To a solution of 2-bromo-1-phenyl-ethanone (3.50 g, 23.3 mmol) in acetone (30 ml) was added potassium *O*-isopropyl carbonodithioate (3.70 g, 21.5 mmol) in small portions over period of 30 mins. The mixture was heated under reflux for 3 hrs and the precipitated KBr was filtered off. The remaining solvent was evaporated from the reaction mixture and then the obtained solid residue was treated with hydrochloric acid (2.5 M) and left stirring for another 30 mins. The aqueous layer was then extracted with diethyl ether (3 x 20 ml) and combined organic extracts washed with brine (50 ml), dried over $MgSO_4$ and the solvent evaporated. The obtained residue was washed with diethyl ether (2 x 20 ml) and dried to yield a yellowish brown solid.

Yield: 60%, 4.52 g. Molecular Formula: $C_{13}H_{16}O_3S_2$ (284.3 g/mol). M.P.: 108-109 °C. IR (KBr, ν_{max}/cm^{-1}): (C=O) 1724, (C=S) 1175, (C-O) 1043. ^{1}H-NMR (d_6-DMSO) δ_H/ppm: 7.65 (d, 1H, Ar-H_1, J = 7.6 Hz), 7.50 (d, 1H, Ar-H_6, J = 8.3 Hz), 7.47 (s, 1H, Ar-H_3), 7.26 (d, 1H, Ar-H_5, J = 7.5 Hz) 5.56 (sept, 1H, H_{10}, J = 6.2 Hz), 4.78 (s, 2H, H_8), 3.83. (s, 3H, OMe) 1.24 (d, 6H, $H_{11,11'}$, J = 6.5 Hz); ^{13}C{^{1}H}-NMR (d_6-DMSO) δ_C/ppm: 212.2, 192.8, 159.5, 136.8, 130.0, 120.9, 119.7, 112.8, 78.7, 55.2, 42.4, 20.8. HRMS (EI): *m/z* Calculated for $C_{13}H_{16}O_3S_2$ $[M + H]^+$: 285.0619; Found: 285.0613.

4.6.2.2 Synthesis of 4-(3-methoxy-phenyl)-1,3-dithiolene-2-one (36)

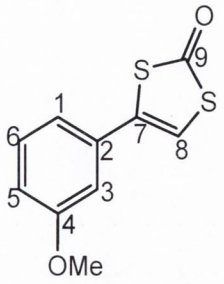

A solution of compound **35** (3.50 g, 18.0 mmol) in a mixture of diethyl ether (15 ml) and dichloromethane (15 ml) was added slowly to a 70% perchloric acid (70 ml) solution in an ice-bath. The solution turned to black and was allowed to warm to room temperature. After 24 hrs stirring, the product was precipitated out by pouring into ice-cold water. The reddish brown solid was collected by filtration using a buchner funnel and was washed with distilled water (3 x 20 ml). The obtained solid was dried in air for 2 hrs and then in the oven at 70 °C overnight.

Yield: 59%, 3.11 g. Molecular Formula: $C_{10}H_8O_2S_2$ (224.2 g/mol). M.P.: 161-162 °C. IR (KBr, ν_{max}/cm^{-1}): (C=O) 1745, (C=C) 1465. ^{1}H-NMR (d_6-DMSO) δ_H/ppm: 7.68 (s, 1H, Ar-H_3), 7.38 (t, 1H, Ar-H_6, J = 7.7 Hz), 7.10 (d, 1H, Ar-H_1, J = 8.0 Hz), 7.08 (s, 1H, H_8), 6.99 (d, 1H, Ar-H_5, J = 7.4 Hz), 3.81 (s, 3H, OMe); ^{13}C{^{1}H}-NMR (d_6-DMSO) δ_C/ppm: 171.2, 159.7, 133.2, 132.9, 130.4, 118.6, 115.1, 114.6, 111.4, 55.4. HRMS (ESI): *m/z* Calculated for $C_{10}H_8O_2S_2$ $[M + H]^+$: 223.9966; Found: 223.9971.

4.6.3 Synthesis of methoxyphenyl and pyrazine-substituted dithiolene CpCo complexes (37-38)

4.6.3.1 Synthesis of 4-(3-methoxy-phenyl)-1,3-dithiolene-2-one-derived CpCo complex (37)

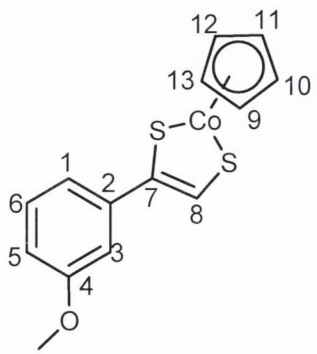

Compound **36** (0.21 g, 0.90 mmol) and sodium hydroxide (0.10 g, 2.50 mmol) were dissolved in dry ethanol (10 ml) to give a brown solution. A solution of [CpCo(CO)I_2] (0.40 g, 1.00 mmol, obtained from Prof. J. McMaster laboratory) in ethanol (5 ml), was added dropwise to the reaction mixture and an immediate colour change was observed from brown to deep blue. The resulting blue solution was stirred overnight at room temperature under inert atmosphere. The solvent was removed under vacuum to yield a blue-brown solid. The purification of the product was achieved by column chromatography over silica gel, eluting with dichloromethane – methanol (99:1) to give complex **37** as a blue solid. The product was crystallised in hexane (2 ml) to give blue rectangular crystals which were suitable for X-ray diffraction (Appendices 6.9 and 6.11)

.

Yield: 44%, 0.09 g. Molecular Formula: $C_{14}H_{13}CoOS_2$ (320.31 g/mol). M.P.: 276-277 °C. IR (KBr, ν_{max}/cm^{-1}): (C=C) 1457. ^{1}H-NMR (d_3-CD_3CN) δ_H/ppm: 9.03 (s, 1H, Ar-H_8), 7.39-7.32 (m, 2H, Ar-$H_{3,6}$) 6.98-6.91 (m, 2H, Ar-$H_{1,5}$), 5.41 (s, 5H, Cp) 3.87 (s, 3H, OMe). HRMS (MALDI-ToF): *m/z* Calculated for $C_{14}H_{13}CoOS_2$ [M]$^+$: 319.9740; Found: 319.9735.

4.6.3.2 Synthesis of 4-pyrazin-2-yl-1,3-dithiolene-2-one-derived CpCo complex (38)

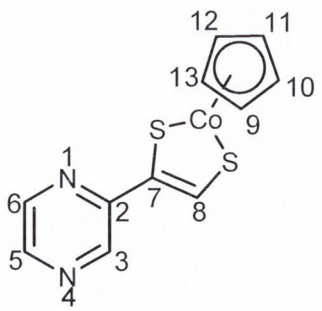

The experimental procedure used for the synthesis of this compound was the same as those employed to prepare complex **37** except 4-pyrazin-2-yl-1,3-dithiolene-2-one (**22**) (0.18 g, 0.90 mmol) was used instead of 4-(3-methoxy-phenyl)-1,3dithiolene-2-one (**36**). The obtained dark blue solid was washed with chloroform (2 x 10 ml) and dried. The product was crystallised in dichloromethane – hexane (5:2) to give blue shiny crystals which were suitable for X-ray diffraction (Appendices 6.10 and 6.12).

Yield: 33%, 0.08 g. Molecular Formula: $C_{11}H_9CoN_2S_2$ (292.26 g/mol). M.P.: 297-298 °C. IR (KBr, ν_{max}/cm^{-1}): (C=N) 1550, (C=C) 1487. ^{1}H-NMR (d_3-$CDCl_3$) δ_H/ppm: 9.54 (s, 1H, Ar-H_8), 9.34 (s, 1H, Ar-H_3), 8.52 (br s, 1H, Ar-H_5), 8.49 (br s, 1H, Ar-H_6) 5.46 (s, 5H, Cp); $^{13}C\{^1H\}$-NMR ($CDCl_3$) δ_C/ppm: C_2 – 165.45, C_8 – 160.18, C_7 – 151.71, C_3 – 143.96, C_5 – 142.28, C_6 – 141.33, C_2 – 79.73. HRMS (MALDI-ToF): *m/z* Calculated for $C_{11}H_{10}CoN_2S_2$ $[M + H]^+$: 292.9617; Found: 292.9624.

References

[1] R. B. King, *Inorg. Chem.*, **1966**, 5, 82.

[2] P. Chandrasekaran, J. P. Donahue, *Org. Synth.*, **2009**, 86, 333.

[3] B. Bradshaw, A. Dinsmore, D. Collison, C. D. Garner, J. A. Joule, *J. Chem. Soc., Perkin Trans. 1*, **2001**, 3232.

[4] A. L. Whalley, A. J. Blake, D. Collison, E. S. Davies, H. J. Disley, M. Helliwell, F. E. Mabbs, J. McMaster, C. Wilson, C. D. Garner, *Dalton Trans.*, **2011**, 40, 10457.

[5] G. Periyasamy, N. A. Burton, I. H. Hillier, M. A. Vincent, H. Disley, J. McMaster, C. D. Garner, *Faraday Discuss.*, **2007**, 135, 469.

[6] S. Boyde, C. D. Garner, J. A. Joule, D. J. Rowe, *J. Chem. Soc., Chem. Commun.*, **1987**, 800.

[7] A. Dinsmore, J. H. Birks, C. D. Garner, J. A. Joule, *J. Chem. Soc., Perkin Trans. 1.*, **1997**, 801.

[8] J. K. Hsu, C. J. Bonangelino, S. P. Kaiwar, C. M. Boggs, J. C. Fettinger, R. S. Pilato, *Inorg. Chem.*, **1996**, 35, 4743.

[9] M. Nomura, M, Kajitani, *J. Organomet. Chem.*, **2006**, 691, 2691.

[10] M. Nomura, M. Fourmigue, *Inorg. Chem.*, **2008**, 47, 4.

[11] H. W. Baird, B. M. White, *J. Am. Chem. Soc.*, **1966**, 88, 4744.

[12] C. Takayama, M. Kajitani, T. Sugiyama, A. Sugimori, *J. Organomet. Chem.*, **1998**, 563, 161.

[13] M. Nomura, E. Tsukano, C. Fujita-Takayama, T. Sugiyama, M. Kajitani, *J. Organomet. Chem.*, **2009**, 694, 3116.

[14] M. Nomura, T. Sasao, T. Hashimoto, T. Sugiyama, M. Kajitani, *Inorg. Chim. Acta.*, **2010**, 363, 3647.

[15] E. J. Miller, T. B. Brill, A. L. Rheingold, W. C. Fultz, *J. Am. Chem. Soc.*, **1983**, 105, 7580.

[16] G. N. Shrauzer, *Acc. Chem. Res.*, **1969**, 2, 72.

[17] P. Chaudhuri, C. N. Verani, E. Bill, E. Bothe, T. Weyhermüller, K. Wieghardt, *J. Am. Chem. Soc.*, **2001**, 123, 2213.

[18] E. I. Stiefel, K. D. Karlin, Progress in Inorganic Chemistry, Dithiolene Chemistry; Synthesis, Properties, and Applications, Wiley, John & Sons, **2004**, 52.

[19] A PhD thesis of Trajeet Singh, University of Nottingham, United Kingdom, **2006**.

[20] E. M. Armstrong, M. S. Austerberry, H. J. Birks, J. A. Joule, C. D. Garner, *Heterocycles*, **1993**, 35, 563.

[21] M. Nomura, M. Fourmigue, *J. Organomet. Chem.*, **2007**, 692, 2491.

[22] F. J. Hine, A. J. Taylor, C. D. Garner, *Coord. Chem. Rev.*, **2010**, 254, 1570.

[23] G. M. Sheldrick, *Acta. Crystallogr. Sect. A.*, **2008**, 64. 112.

[24] C. J. Pickett, *J. Chem. Soc., Chem. Commun.*, **1985**, 323.

[25] R. R. Gagne, C. A. Koval, G. C. Lisensky, *Inorg. Chem.*, **1980**, 19, 2854.

Chapter 5

Conclusions

5.1 Conclusions

Research in this project was originally focussed on the design and synthesis of dithiolene-2-one based ligands, which play a crucial role almost in all naturally occurring molybdenum enzymes being an integral component of MPT. These ligands were used to form their respective model complexes in which the dithiolene moiety coordinated to the metal centre in a similar fashion as was observed in the catalytically active site of MoCo. These molybdenum and tungsten cofactors catalyse a wide range of reactions and are present in a large number of living systems. Several of these enzymes have been structurally characterised and their spectroscopic data indicate that oxygen atom transfer reactions take place at the metal centre. More importantly, this catalytic activity relates to the change in oxidation state of Mo^{VI} to Mo^{IV} or vice versa. A number of synthetic models have been synthesised and characterised to mimic the chemistry of these catalytically active sites, but still remains as a challenge to bio-inorganic chemists. In order to investigate this catalytic activity, the main objective of this work was to synthesise the *N*-heterocyclic based dithiolene molybdenum and tungsten complexes as a structural analogue of molybdenum enzymes as well as investigation of their spectroelectrochemical properties.

Towards this goal, a number of methodologies was attempted which were used to synthesise the *N*-heterocyclic based dithiolene ligands and their respective metal complexes as models for naturally occurring molybdenum enzymes. Successful syntheses and characterisation of pyrazine (**3** and **12**) and quinoxaline (**4** and **9-11**) based ligands were achieved which were used as precursors for the target molybdenum complexes. During the attempts to synthesise target model complexes, the most promising results of the present research were acquired unexpectedly from the X-ray structural analysis, which confirmed the formation of novel tetracyclic pentathiepino-pyrrolo[1,2-*a*]-quinoxaline (**15**). The structures for all the synthesised pentathiepin derivatives (Scheme 5.1) were confirmed based on the obtained spectroscopic data. To the best of our knowledge, this is the first example of the synthesis of pentathiepin based compounds with the aid of a molybdenum complex in mild and comparably environmentally friendly conditions.

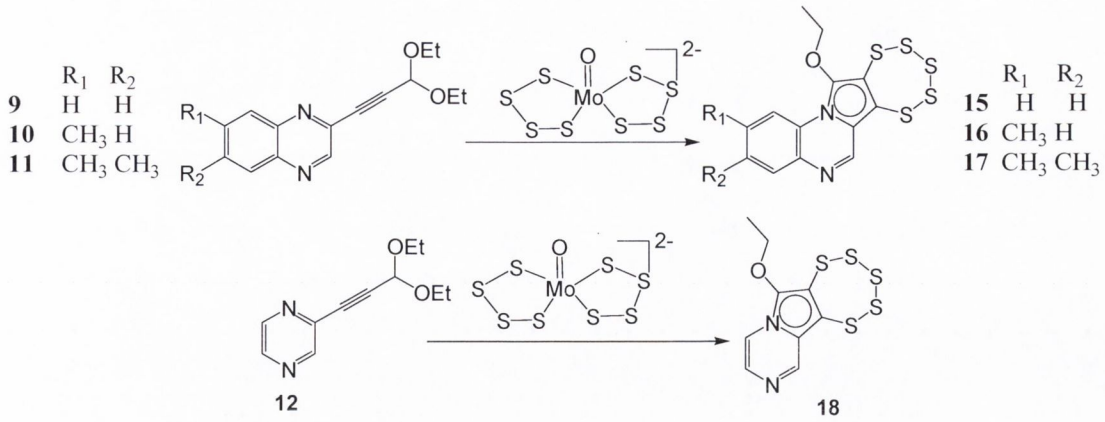

Scheme 5.1: Synthesis of series of novel pentathiepino-pyrrolo[1,2-*a*] derivatives (**15-18**).

Further on, a study has been made with regard to the synthesis and derivatisation of these novel pentathiepin compounds to evaluate the influence of different groups on the biological properties of these compounds. The DNA binding properties of pentathiepins have prompted us to broaden the range of study of these compounds. In the present research DNA binding properties of novel pentathiepin derivatives (**15-18)** have been studied in detail and have been compared to those of commercially available DNA binding agents. It is concluded that these novel pentathiepins (**15-18**) are excellent DNA binders as significantly high DNA binding constant values (1.98-2.29 x 10^6) were recorded compared to commercial drug pentamidine (1.09 x 10^6), however, lesser than netropsin (2.99 x 10^6). The data obtained also confirmed that these compounds do not intercalate, but bind to the surface of the DNA as minor groove binding agents. In addition, viscosity experiment on pentathiepin derivatives further confirmed them to be minor groove binders towards DNA.

The remarkable results of the DNA binding mode studies encouraged us to test these compounds for their potential activity against cancer cell lines. The obtained data confirmed that three of pentathiepin derivatives (**16-18**) exhibited promising activity against tested cancer cell lines. On examination of the activity data, it is concluded that the activity was strongly influenced by the type of substituent present on the quinoxaline ring. The comparison of the averages of GI_{50} values revealed that compounds **16** and **17** were significantly more active to that of carboplatin against

LCLC. Furthermore, compound **17** showed nearly similar activities as carboplatin towards 5637 and SISo cell lines. The most promising result was obtained against A2780, where the compound with a dimethyl substituent at the quinoxaline ring (**17**) showed greatest activity (1.70 μM) compared to the compound with only one methyl substituent at the same ring (**16**). However, the compound with pyrazine ring (**18**) was found to have low activity against all cancer cell lines compared with compounds having methyl (**16**) and dimethyl (**17**) substituent at the quinoxaline ring, highlighting a clear structure activity relationship. All tested pentathiepin compounds were found to be more selective and effective when compared to carboplatin, against LCLC, however, in general less active towards all tested cell lines compared to cisplatin. The by chance synthesis of novel pentathiepins and their significant biological activities, however, was a very pleasant discovery of the first part of this thesis.

Having completed the first part of the project, further studies were continued at designing the synthetic model of MoCo using dithiolene as scaffold. Towards this, a novel ligand, pyrazine-substituted dithiolene-2-one (**22**), was developed which was used to synthesise its corresponding molybdenum (**23**) and tungsten (**24**) complexes as shown in Scheme 5.2. The structure of the ligand and its respective complexes were established by spectroscopic techniques (IR, ^{1}H and $^{13}C\{^{1}H\}$-NMR along with HRMS). The structure of the ligand **22** was further studied by X-ray structural analysis which confirmed the presence of the protected dithiolene-2-one moiety. Furthermore, X-ray structural analysis for complexes (**23** and **24)** is important to fully understand the exact geometry around metal centre in comparison with the naturally occurring enzyme. A number of attempts were made by varying the cationic groups, such as $[PPh_4]^+$, $NEt_3(PhCH_2)]^+$, and K^+ to afford crystals. Unfortunately, crystals suitable for an X-ray structure analysis for the molybdenum and tungsten complexes could not be isolated.

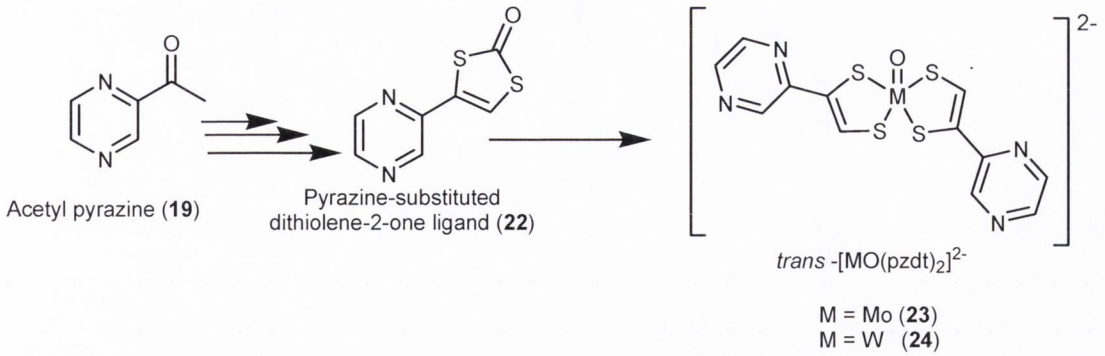

Scheme 5.2: Synthesis of pyrazine-substituted dithiolene-2-one ligand (**22**) and its respective molybdenum (**23**) and tungsten (**24**) complexes as a mixture of *cis* and *trans* isomers; here only the *trans* isomer is shown.

The spectroelectrochemical properties of molybdenum complex **23** were studied in detail and compared to those of previously reported other molybdenum dithiolene complexes. It was established that complex **23** is electroactive, showing a one electron, reversible reduction couple (Mo^{V}-Mo^{IV}) at negative redox potential of -323 mV. Moreover, it was confirmed by UV-Vis spectroelectrochemical studies that there are no structural changes of the complex associated with oxidation and reduction processes. In addition, both oxidised and reduced UV-Vis spectra were in agreement with the presence of a MoOS4 chromophore. The presence of an unpaired electron coupled to the molybdenum nucleus Mo^{V} was also confirmed by EPR spectroscopic data. *i.e.* it is not delocalised to the dithiolene ligands. This means that the typical non-innocence of dithiolene ligands is negligible for this system.

Further studies were aimed at exploring and exploiting closed and open alcohol form ligands and their respective molybdenum complexes. This part describes a completely new approach which was used to synthesise closed form ligand **28** using 2-hydroxy quinoxaline as a starting precursor (Scheme 5.3). Unfortunately, the desired ligand **28** could not be achieved using this methodology but a novel and interesting compound **29** was isolated analytically pure and characterised by X-ray structural analysis.

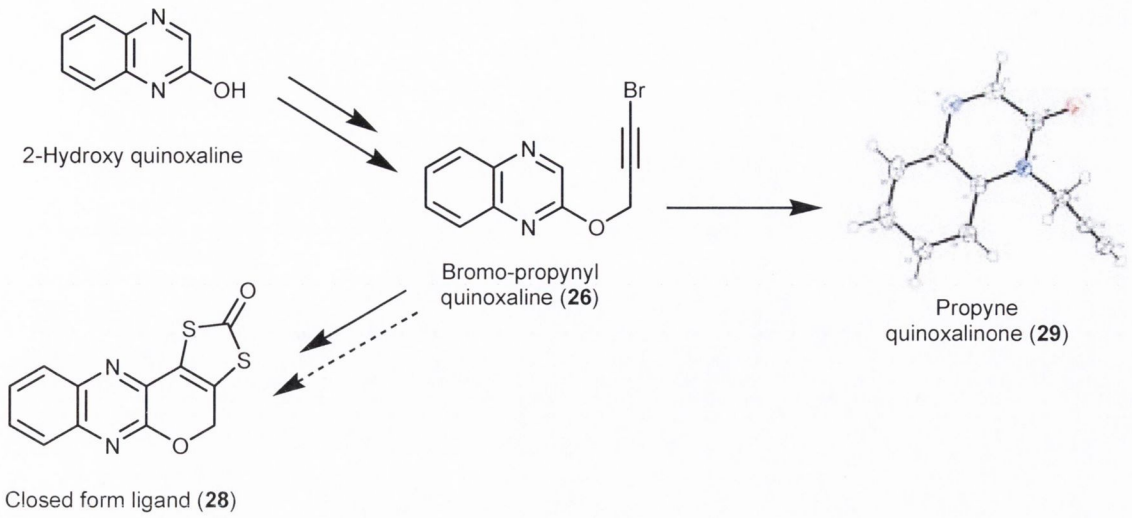

Scheme 5.3: Attempted route for the synthesis of closed form ligand **28**.

After failure of this methodology, attention was then diverted to synthesise the desired open alcohol form ligand. Figure 5.1 shows an attempt which involved the attachment of alcohol side chain to the pyrazine dithiolene ligand (**22**) by replacing its dithiolene proton but remained unsuccessful to obtain desired ligand **30.**

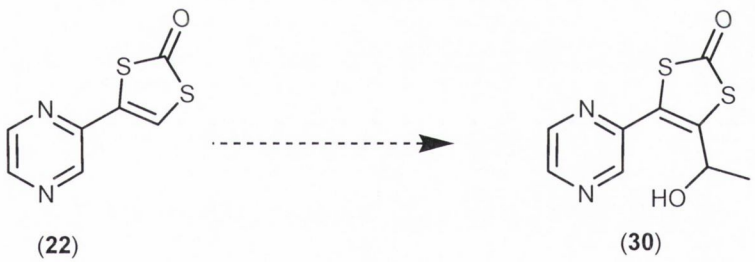

Figure 5.1: Attempted route to synthesise open alcohol form ligand **30**.

Follow on to the goal of open alcohol form ligand synthesis, another methodology was adopted and is illustrated in Scheme 5.4. This involved the reaction of electron deficient alkyne **31** with *bis*-alkyl xanthogen disulfide which successfully resulted in the formation of desired open alcohol form ligand (**32**) in the presence of radical initiator (ACCN). Our expectation that transformation of this open alcohol form ligand (**32**) into corresponding molybdenum complex turned out to be unsuccessful. However, the synthesis of the open alcohol ligand (**32**) is in fact a great achievement as it is one of the closest model for the open form MPT ligand in molybdenum enzymes.

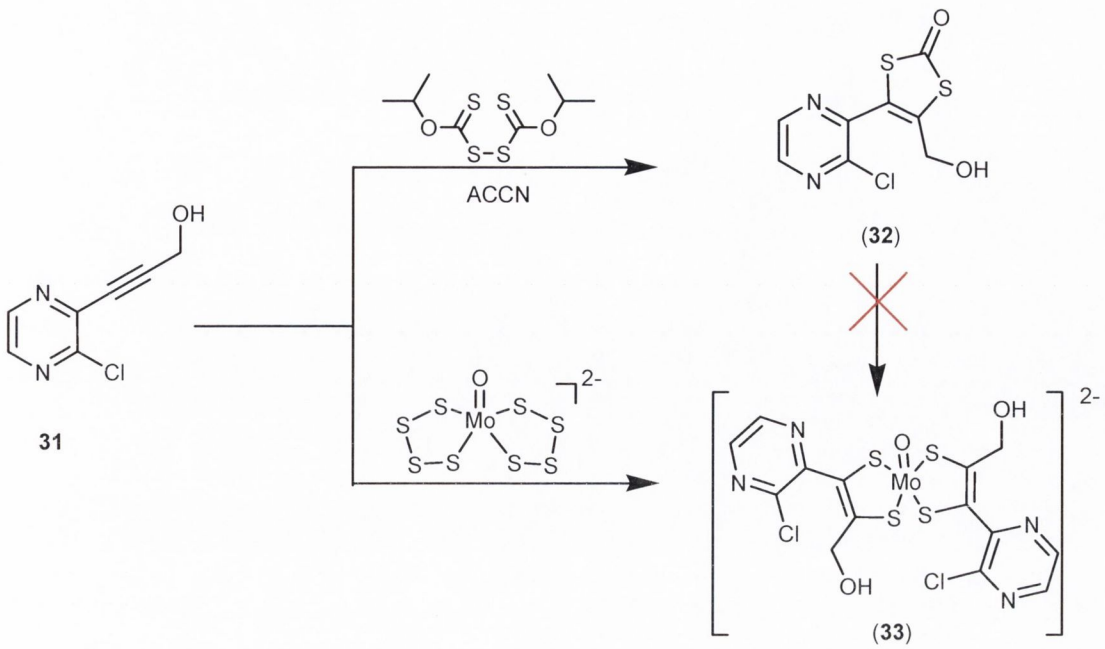

Scheme 5.4: Synthesis of open alcohol form ligand (**32**) and formation of molybdenum complex (**33**) (here only the *trans* isomer is shown) from active alkyne **31**.

Furthermore, a direct approach was utilised in which the reaction of electron deficient alkyne **31** with molybdenum oxo *bis*-tetrasulfide successfully afforded the target open alcohol form molybdenum complex **33** (Scheme 5.4). Formation of complex **33** was confirmed by spectroscopic studies. However, ESI-HRMS data indicated the presence of not only the complex **33** but also an impurity possibly related to the used molybdenum precursor which was impossible to separate. Despite of this solubility issue, the synthesis of open alcohol form molybdenum complex is still a considerable and interesting development towards the synthesis of more accurate structural synthetic model of the DMSO reductase with MPT in the open alcohol form.

Finally, it was intended to design and synthesise air stable methoxyphenyl (**37**) and pyrazine (**38**) dithiolene CpCo complexes. X-ray structural analysis of novel complexes **37** and **38** confirmed the involvement of dithiolene which coordinated to Co centre as half sandwiched cobaltadithiolene complexes, showing typical two legged piano-stool geometry (Figure 5.2). Spectroelectrochemical investigations for complexes **37** and **38** showed a rich redox chemistry, confirming a fully reversible,

one electron, redox couple for Co^{III}–Co^{II}. In addition, bulk electrolysis process further confirmed the single electron transfer involved in both complexes **37** and **38**.

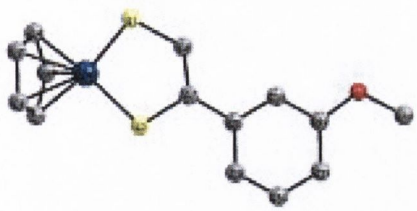

37

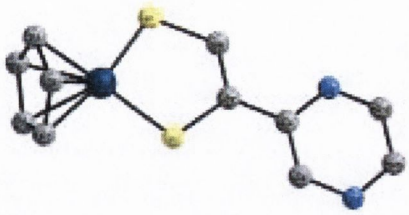

38

Figure 5.2: X-ray crystal structure of CpCo dithiolene based complexes (**37** and **38**).

However, the main motive of synthesising pyrazine dithiolene CpCo complex (**38**) was to study the protonation effect upon addition of acid to the complex and results obtained showed a shift in the redox potential of the Co centre to a more positive value. This shift can be demonstrated as a possible electronic effect which communicated from the pyrazine to cobaltadithiolene moiety upon protonation, hence modulating the redox properties of MPT towards metal centre. The data obtained from UV-Vis spectroelectrochemical studies confirmed that there are no intermediate states involved in the complexes **37** and **38** during reduction and re-oxidation processes and these processes were found to be fully reversible. Moreover, EPR spectroscopic data for Co^{II} state of both complexes are consistent with the presence of unpaired electron which is coupled to the Co (7/2) nucleus. However, reproduction of all the features in the experimental spectra of both complexes require assimilation and are still under study.

Chapter 6

Appendix

Appendix 6.1

Crystal data and structure refinement for compound 14

Empirical formula	$C_7H_6N_2S_3$
Formula weight	214.32
Temperature	108(2) K
Wavelength	0.71073 A
Crystal system	Orthorhombic
Space group	P2(1)2(1)2(1)
Unit cell dimensions	a = 5.6654(11) Å α = 90° b = 10.104(02) Å β = 90° c = 16.298(03) Å γ = 90°
Volume	933.0(3) $Å^3$
Z	4
Density (calculated)	1.526 Mg/m^3
Absorption coefficient	0.737 mm^{-1}
F(000)	440
Crystal size	0.40 x 0.10 x 0.10 mm^3
Theta range for data collection	2.50 to 31.32°
Index ranges	-8<=h<=7, -14<=k<=13,-23<=l<=23
Independent reflections	14905 / 2787 [R(int) = 0.0841]
Completeness to theta = 25.00°	99.7%
Max. and min. transmission	1.0000 and 0.6565
Refinement method	Full-matrix least-squares on F^2
Data / restraints / parameters	2787 / 0 / 127
Goodness-of-fit on F^2	0.959
Final R indices [I>2sigma(I)]	R1 = 0.0560, wR2 = 0.1227
R indices (all data)	R1 = 0.0800, wR2 = 0.1331

Appendix 6.2

Crystal data and structure refinement for compound 15

Empirical formula	$C_{13}H_{10}N_2OS_5$
Formula weight	370.53
Temperature	108(2) K
Wavelength	0.71073 A
Crystal system	Monoclinic
Space group	P21/n
Unit cell dimensions	a = 8.1317(16) Å α = 90° b = 20.856(04) Å β = 101.63(3)° c = 8.7162(17) Å γ = 90°
Volume	1447.9(5) $Å^3$
Z	4
Density (calculated)	1.700 Mg/m^3
Absorption coefficient	0.798 mm^{-1}
F(000)	760
Crystal size	0.45 x 0.30 x 0.20 mm^3
Theta range for data collection	2.74 to 41.39°
Index ranges	-10<=h<=11, -30<=k<=30,-11<=l<=12
Independent reflections	15450 / 4250 [R(int) = 0.0326]
Completeness to theta = 25.00°	98.3%
Max. and min. transmission	0.9545 and 0.8010
Refinement method	Full-matrix least-squares on F^2
Data / restraints / parameters	4250 / 0 / 191
Goodness-of-fit on F^2	1.152
Final R indices [I>2sigma(I)]	R1 = 0.0444, wR2 = 0.1434
R indices (all data)	R1 = 0.0504, wR2 = 0.1775

Appendix 6.3

Selected bond lengths and bond angles for compound 14

Selected bond lengths for 14 [Å]		Selected bond angles for 14 [°]	
C(3)-C(2)	1.530(5)	C(1)-S(2)-C(3)	98.20(19)
C(3)-S(2)	1.838(4)	C(1)-S(3)-C(2)	98.25(19)
C(2)-S(3)	1.815(4)	C(3)-C(2)-S(2)	107.6(3)
C(1)-S(1)	1.628(3)	C(3)-C(2)-S(3)	109.8(3)
C(1)-S(2)	1.757(4)	C(4)-C(3)-S(2)	111.6(3)
C(1)-S(3)	1.729(4)	C(4)-C(3)-C(2)	111.4(3)
C(5)-N(1)	1.109(5)		
C(4)-N(2)	1.410(6)		

Appendix 6.4

Selected bond lengths and bond angles for compound 15

Selected bond lengths for 11[Å]		Selected bond angles for 11 [°]	
C(9)-S(1)	1.743 (2)	C(8)-N(1)-C(1)-C(2)	175.51 (5)
C(10)-S(5)	1.752 (2)	C(7)-N(2)-C(6)-C(5)	176.70 (5)
C(9)-C(10)	1.425 (3)	S(2)-S(3)-S(4)-S(5)	76.44 (6)
N(1)-C(11)	1.379 (3)	S(1)-S(2)-S(3)-S(4)	78.04 (5)
S(1)-S(2)	2.063 (10)	S(1)-S(2)-S(3)	103.90 (4)
S(2)-S(3)	2.061 (10)	S(2)-S(3)-S(4)	104.80 (4)
S(3)-S(4)	2.055 (10)	S(3)-S(4)-S(5)	104.21 (4)
S(4)-C(5)	2.064 (10)	C(11)-O(1)-N(1)	117.59 (19)

Appendix 6.5

Crystal data and structure refinement for compound 22

Empirical formula	$C_7H_4N_2OS_2$
Formula weight	196.24
Temperature	108(2) K
Wavelength	0.71073 Å
Crystal system	Orthorhombic
Space group	*Pna2(1)*
Unit cell dimensions	a = 20.199(4) Å α = 90° b = 10.197(2) Å β = 90° c = 3.7804(8) Å γ = 90°
Volume	778.6(3) $Å^3$
Z	4
Density (calculated)	1.674 Mg/m^3
Absorption coefficient	0.626 mm^{-1}
F(000)	400
Crystal size	0.40 x 0.05 x 0.05 mm^3
Theta range for data collection	2.24 to 31.04°
Index ranges	-29<=h<=27, -14<=k<=14, -4<=l<=3
Independent reflections	6649 / 2141 [R(int) = 0.0463]
Completeness to theta = 25.00°	98.0%
Max. and min. transmission	1.0000 and 0.7837
Refinement method	Full-matrix least-squares on F^2
Data / restraints / parameters	2141 / 1 / 113
Goodness-of-fit on F^2	1.124
Final R indices [I>2sigma(I)]	R1 = 0.0497, wR2 = 0.1183
R indices (all data)	R1 = 0.0523, wR2 = 0.1213

Appendix 6.6

Crystal data and structure refinement for compound 29

Empirical formula	C11 H8 N2 O
Formula weight	184.19
Temperature	108(2) K
Wavelength	0.71073 Å
Crystal system	Monoclinic
Space group	*P2(1)/c*
Unit cell dimensions	a = 8.9081(18) Å alpha = 90°. b = 13.674(3) Å beta = 116.03(3)°. c = 8.0206(16) Å gamma = 90°.
Volume	877.9(3) $Å^3$
Z	4
Density (calculated)	1.394 Mg/m^3
Absorption coefficient	0.093 mm^{-1}
F(000)	384
Crystal size	0.40 x 0.40 x 0.35 mm^3
Theta range for data collection	2.95 to 31.21°
Index ranges	-12<=h<=10, -18<=k<=19, -11<=l<=9
Independent reflections	4993 / 2548 [R(int) = 0.0157]
Completeness to theta = 25.00°	98.3%
Max. and min. transmission	0.9969 and 0.9626
Refinement method	Full-matrix least-squares on F^2
Data / restraints / parameters	2548 / 0 / 159
Goodness-of-fit on F^2	1.114
Final R indices [I>2sigma(I)]	R1 = 0.0468, wR2 = 0.1118
R indices (all data)	R1 = 0.0491, wR2 = 0.1135

Appendix 6.7

Selected bond lengths and bond angles for compound 22

Selected bond lengths [Å]		Selected bond angles [°]	
C(3)-C(2)	1.351(4)	C(3)-C(4)-C(5)-N(2)	149.04
C(3)-S(2)	1.748(3)	C(2)-C(1)-S(1)	96.18(14)
C(2)-S(1)	1.720(3)	C(3)-C(1)-S(2)	95.64(14)
C(5)-N(1)	1.330(4)	C(1)-O(1)-S(1)	123.4(2)
C(4)-N(2)	1.340(4)		
C(3)-C(4)	1.459(4)		
S(2)-C(1)	1.771(3)		
S(1)-C(1)	1.768(3)		

Appendix 6.8

Selected bond lengths and bond angles for compound 29

Selected bond lengths [Å]		Selected bond angles [°]	
C(10)-C(11)	1.183(16)	C(6)-N(1)-C(7)	117.5(9)
C(9)-N(2)	1.470(13)	C(7)-C(8)-O(1)	122.9(10)
C(8)-N(2)	1.371(13)	O(1)-C(8)-N(2)	122.2(10)
C(8)-O(1)	1.232(14)	N(2)-C(9)-C(10)	112.5(9)
C(7)-N(1)	1.286(16)		
C(1)-N(2)	1.396(14)		
C(6)-N(1)	1.391(15)		

Appendix 6.9

Crystal data and structure refinement for complex 37

Empirical formula	$C_{14}H_{13}CoOS_2$
Formula weight	320.29
Temperature	100(2) K
Wavelength	0.71073 Å
Crystal system	Orthorhombic
Space group	*Pbca*
Unit cell dimensions	a = 22.230(14) Å α = 90° b = 8.361(5) Å β = 90° c = 28.981(18) Å γ = 90°
Volume	5387.0(6) $Å^3$
Z	16
Density (calculated)	1.580 Mg/m^3
Absorption coefficient	1.567 mm^{-1}
F(000)	2624
Crystal size	0.070 x 0.140 x 0.160 mm^3
Theta range for data collection	2.70 to 33.91°
Index ranges	-32<=h<=34, -8<=k<=12, -42<=l<=44
Independent reflections	10580 [R(int) = 0.0323]
Completeness to theta = 25.00°	98.0%
Max. and min. transmission	0.6704 and 0.7467
Refinement method	Full-matrix least-squares on F^2
Data / restraints / parameters	10580 / 0 / 327
Goodness-of-fit on F^2	1.064
Final R indices [I>2sigma(I)]	R1 = 0.0444, wR2 = 0.0881
R indices (all data)	R1 = 0.0708, wR2 = 0.0965

Appendix 6.10

Crystal data and structure refinement for complex 38

Empirical formula	$C_{11}H_9CoN_2S_2$
Formula weight	292.25
Temperature	165(2) K
Wavelength	0.71073 Å
Crystal system	Monoclinic
Space group	P 21/n
Unit cell dimensions	a = 11.912(2) Å α = 90°. b = 6.150(12) Å β = 104°. c = 15.995(3) Å γ = 90°.
Volume	1132.8 (4) $Å^3$
Z	4
Density (calculated)	1.714 Mg/m^3
Absorption coefficient	1.852 mm^{-1}
F(000)	592
Crystal size	0.41 x 0.33 x 0.075 mm^3
Theta range for data collection	1.916 to 31.368°
Index ranges	-16<=h<=16, -8<=k<=8, -23<=l<=23
Independent reflections	13030 / 3382 [R(int) = 0.0364]
Completeness to theta = 25.24°	98.9%
Max. and min. transmission	0.4455 and 0.3321
Refinement method	Full-matrix least-squares on F^2
Data / restraints / parameters	3382 / 0 / 145
Goodness-of-fit on F^2	1.196
Final R indices [I>2sigma(I)]	R1 = 0.0594, wR2 = 0.1944
R indices (all data)	R1 = 0.0696, wR2 = 0.2304

Appendix 6.11

Selected bond lengths and bond angles for complex 37

Selected bond lengths [Å]		Selected bond angles [°]	
C(6)-C(7)	1.369(3)	S(1)-C(6)-C(7)-S(2)	-1.30(2)
C(6)-S(1)	1.711(2)	C(7)-S(2)-Co(1)	106.2(7)
C(7)-S(2)	1.733(2)	C(6)-S(1)-Co(1)	105.4(7)
C(7)-C(8)	1.482(3)	C(6)-C(7)-S(2)	116.6(15)
S(1)-Co(1)	2.106(6)	S(1)-C0(1)-S(2)	91.15(2)
S(2)-Co(1)	2.114(6)		

Appendix 6.12

Selected bond lengths and bond angles for complex 38

Selected bond lengths [Å]		Selected bond angles [°]	
C(7)-C(6)	1.366(6)	S(1)-C(6)-C(7)-S(2)	-0.02(2)
C(7)-S(2)	1.724(4)	C(6)-S(1)-Co(1)	105.8(14)
C(6)-S(1)	1.709(4)	C(7)-S(2)-Co(1)	105.6(14)
C(7)-C(8)	1.471(5)	C(6)-C(7)-S(1)	118.1(3)
S(1)-Co(1)	2.109(12)	S(1)-C0(1)-S(2)	91.26(4)
S(2)-Co(1)	2.102(12)		

List of publications

The unexpected and facile molybdenum mediated formation of tri- and tetracyclic pentathiepins from pyrazine-alkynes and sulphur, **M. Zubair**, A. Ghosh, C. Schulzke, *Chemical Communications*, 2013, 49, 4343.

Synthesis, characterization, in vitro antimicrobial, and U2OS tumoricidal activities of different coumarin derivatives, S. Rehman, M. Ikram, R. J. Baker, **M. Zubair**, S. Min, E. Azad, K. Riaz, K. Mok, S-U, Rehman, *Chemistry Central Journal*, 2013, 7, 68.

Synthesis, structure and redox properties of asymmetric (cyclopentadienyl)(ene-1,2-dithiolate)cobalt(III) complexes containing phenyl, pyridyl and pyrazinyl units, James. P. Dicks, **Zubair. Muhammad**, E. Stephen Davies, C. David Garner, Carola Schulzke,3, Claire Wilson, Jonathan McMaster, *European Journal of Inorganic Chemistry*, xxxx, x. xx

Synthesis and spectroelectrochemical investigations of novel pyrazine-derived dithiolene molybdenum and tungsten complexes as models for the molybdenum cofactor, **M. Zubair**, C. Schulzke, J. McMaster, E. S. Davies, R. J. Baker, manuscript in preparation, *Dalton Transaction*, xxxx, xx.

Conferences

M. Zubair, C. Schulzke

Studies on the novel pyrazine-derived dithiolene molybdenum and tungsten complexes as a synthetic analogue to the naturally occurring molybdenum cofactor, Chemistry Colloquium, June-2012, Limerick, Ireland, **poster presentation (First prize winner)**.

M. Zubair, C. Schulzke

Synthesis and characterization of novel pyrazine-derived dithiolene molybdenum complexes as models for the pyranopterin ligand in the molybdenum cofactor,